University of Alberta

Flow Characteristics in Small Northern Streams and Nature-like Fishpasses

by

Abul Basar Mohammad Baki

A thesis submitted to the Faculty of Graduate Studies and Research
in partial fulfillment of the requirements for the degree of

Doctor of Philosophy

in

Water Resources Engineering
Department of Civil and Environmental Engineering

Fall, 2013
Edmonton, Alberta

To my parents,

Abstract

Increasingly, human activities for the societal development and quality of life can alter, disrupt or destroy aquatic habitat with varying degrees. The rising awareness and concern regarding such type of human activities on stream and riverine ecosystem have resulted in a movement towards habitat compensation to achieve no net loss in productive capacity of fish habitat. As part of a fish habitat compensation project, this thesis investigated detailed flow characteristics in small northern streams and in rock-ramp type nature-like fishpasses through field, laboratory, and numerical studies. The principal motivation for this study is to advance our understanding of flow characteristics in a rock-ramp fishpass to retrofit small streams for fish habitat connectivity and compensation.

First, the flow characteristics of a headwater stream as a fish migration corridor and the hydraulic characteristics of several headwater streams in the Northwest Territories of Canada were investigated. The analysis of stream hydrological or hydraulic flow characteristics demonstrated that some sections of the study stream for certain durations of the study period appeared to naturally provide suitable habitat for select stages of YOY (young-of-the-year) Arctic grayling, while other sections would require certain modifications and additional outlet flow arrangements. The study of hydraulic characteristics explored the nature of at-a-station hydraulic geometry and flow resistance in an unstudied geographic region of the

Northwest Territories of Canada for the future habitat assessment and predictions.

Next, detailed mean and turbulence flow characteristics generated by a staggered arrangement of boulders in a rock-ramp nature-like fishpass were investigated experimentally. The results showed that this type of fishpass can produce adequate water depth and favorable flow velocity, turbulent intensity, and turbulent kinetic energy for suitable fish passage. Some general correlations were developed for predicting the mean and turbulence flow parameters in a rock-ramp fishpass as a function of normalized discharge and streamwise distance. Moreover, a flow resistance analysis based on basic concepts for wake-interference flow regime in this fishpass has resulted in a general equation for the average velocity.

Finally, a three-dimensional Computational Fluid Dynamics (CFD) solver was used to investigate the flow characteristics in a rock-ramp nature-like fishpass under different flow conditions and geometric variables. The model was validated with experimental data and a good agreement was achieved. The findings emanating from this numerical study optimized the design of rock-ramp fishpasses.

Acknowledgements

First and foremost I offer my sincerest gratitude to my supervisor, Dr. David Z. Zhu, who has supported me throughout the course of this study with his encouragement, excellent supervision, invaluable advice and support. I also would like to express my sincere thanks to Dr. N. Rajaratnam for his valuable and kind guidance and suggestions on my research. Their strong interest and enthusiasm in this subject was very inspiring and helped to make this research possible. Also, I am very grateful for the contributions of the committee members of my PhD defense: Dr. Ana Maria da Silva (Queen's University), Dr. Bill Tonn (Department of Biological Sciences), and Dr. Evan Davies (Department of Civil and Environmental Engineering).

I am extremely grateful to Dr. Bill Tonn for his motivation and innovative ideas especially for my field studies. I am very much thankful to all hard working field crew members, including G. Courtice, M. Hulsman, B. Lunn, O. Yu, C. Cahill, and A. Erwin. I would also like to acknowledge the staff of the Environmental Department at Diavik Diamond Mine, Inc. for their help with field logistics.

I wish to thank Gregory Courtice for his invaluable help in the lab measurements. Also I would like to thanks Perry Fedun, Chris Krath, and Felipe Justo Breton for setting up the experimental arrangement at different stages of this study. Special thanks to Perry Fedun for his technical supports in the lab.

I would like to acknowledge the financial support from the Natural Sciences and Engineering Research Council (NSERC) of Canada and Diavik Diamond Mines, Inc (DDMI). This research was made possible through their grants. Also funding from the Provost Doctoral Entrance Award, University of Alberta, and my supervisor, Dr. David Zhu, are also gratefully acknowledged.

I also would like to express my sincere thanks to all of my family members for their continuous love, support and encouragement. I greatly thank my beloved wife, Masnuna Khatun, for her love, support and sacrifices to inspire me daily progress.

Above all, I am thankful to Allah the Almighty for his Grace and Mercy to make everything possible.

Table of Contents

List of Tables

List of Figures

List of Abbreviations

Acronym	Definition
ADV	Acoustic Doppler Velocimeter
CFD	Computational Fluid Dynamics
COR	Correlation Coefficient
CSF	Continuum Surface Force
CV	Coefficient of Variation
DDM	Degree Day Method
DDMI	Diavik Diamond Mines Inc.
DO	Dissolved Oxygen
FDC	Flow Duration Curves
MAE	Mean Absolute Error
MAPE	Mean Absolute Percentage Error
MF	Mean Flow
NTC	Northwest Territories of Canada
RANS	Reynolds Averaged Navier Stokes
SD	Standard Deviation
SK	Skewness
SNR	Signal-to-Noise Ratio
TSS	Total Suspended Solids

UBC	University of British Columbia
UBCM	UBC Watershed Method
VOF	Volume of Fluid
YOY	Young-of-the-Year

List of Notations

Symbol	Definition
A	total flow area across the entire cross section
A_{cv}	channel bed area considered as control volume ($A_{cv} = L_z \times B$)
A_d	direct catchment area (km^2)
A_p	projected cross sectional area of each boulder
B	width of the flume/channel
$B_{1/2}$	total lateral width of detailed measurement area
C	Chezy's C
C_f	coefficient of runoff
C_D	drag coefficient
C_L	lift coefficient
C^*	flow resistance coefficient for large scale roughness
D	boulder diameter
D_{84}	84-percentile bed material size
D_{50}	50-percentile bed material size
d	cross sectional mean water depth
E	lake evaporation
e	function of stream slope varying from 11.1-13.46 for a gravel bed river
f	Darcy-Weisbach friction factor

f_f	frequency, Hz
Fr	Froude number
F_D	drag force
F_L	lift force
F_R	resistance force
g	gravitational acceleration=9.81 m/s^2
G	force due to gravity
$G_u(w)$	power spectra of the streamwise velocity in the domain of wave number
$G_u(f)$	power spectra of the streamwise velocity in the domain of frequency
h	local water depth
H	average water depth
H_0	unregulated flow depth
H/D	submergence ratio
z/H	relative flow depth from channel bottom
i	average melting water plus rainfall intensity (mm/hr)
L	total longitudinal length of detailed measurement area
L_z	streamwise distance of the control volume
l^*	boulder height to water depth ratio (D/H)
K	turbulent kinetic energy per unit mass
K_u	coefficients of kurtosis
k	normalized turbulent kinetic energy

k_{max}	maximum normalized turbulent kinetic energy
$\bar{k}$	depth-average normalized turbulent kinetic energy
k_s	effective roughness length
m	form roughness component
N	number of boulders over a bed area, A
n	Manning's n
P	amount of rainfall
PM	daily snowmelt water
PTM	point snowmelt factor
Q	channel discharge/steam flow rate
Q_0	flow through the stream channel
Q^*	dimensionless discharge ($Q^* = Q/\sqrt{gS_0R_v^3B^2}$)
Q_b^*	net water flux
Q_{50}	50^{th} percentile flow from the flow duration curve
Q_{90}	90^{th} percentile flow from the flow duration curve
R	hydraulic radius
Re	Reynolds number
R_v	volumetric hydraulic radius ($R_v = H(1-2/3\lambda l^*)$)
R/D_{84}	relative roughness
S_0	channel slope
S_u	coefficients of skewness

s_l, s_t	boulders centre to centre distance in longitudinal and lateral directions
T	daily average temperature above 0 °C
T_a	daily average temperature recorded for each hour above freezing
T_{dewp}	dew point temperature
T_{min}	minimum temperature above freezing
T_x	ratio of T_{min} and T_{dewp}
u, v, w	time-averaged streamwise, lateral and vertical velocities
u', v', w'	fluctuating streamwise, lateral and vertical velocity components
u'_{rms}	root-mean-square velocity in streamwise direction
v'_{rms}	root-mean-square velocity in lateral direction
w'_{rms}	root-mean-square velocity in vertical direction
$\bar{u}$	depth-average streamwise velocity
u_0	unregulated water velocity
u_{avg}	streamwise average velocity in the detailed measurement area
u_{avg}*	dimensionless streamwise average velocity ($u_{avg}* = u_{avg} / \sqrt{gS_0R_v}$)
$\overline{u'_{rms}}$	depth-average streamwise turbulent intensity
U	magnitude of flow velocity, $U = \sqrt{u^2 + v^2 + w^2}$
U_{max}	maximum velocity magnitude of U
U_{max}*	dimensionless maximum velocity magnitude ($U_{max}* = U_{max} / \sqrt{gS_0R_v}$)
U_{xy}	velocity magnitude on the horizontal plane (XY)
V	cross sectional mean velocity

V_*	stream shear velocity
V_s	boulder volume
W	channel water surface width
$-\overline{u'v'}$	Reynolds shear stress in XY plane
$-\overline{u'w'}$	Reynolds shear stress in XZ plane
$-\overline{v'w'}$	Reynolds shear stress in YZ plane
$(-\overline{u'v})_{\max}$	maximum Reynolds shear stress in XY plane
$\overline{-\overline{u'v'}}$	depth-average Reynolds shear stress in XY plane
$\overline{u'_{rms}}/U_{\max}$	normalized depth-average streamwise turbulence intensity
$\overline{-\overline{u'v'}}/U_{\max}$	normalized depth-average Reynolds shear stress in XY plane
w_{W}	wave number ($2\pi f/u$)
z	distance from the channel bed
X, Y, Z	streamwise, lateral and vertical coordinate distance
$X/D, Y/D$	relative streamwise and lateral distance
ΔS	storage change based on lake level fluctuation
du/dx	streamwise velocity gradient
α	ratio of snow and water density
λ	fraction of bed area occupied by boulders ($\lambda = N(\pi D^2/4)/A$)
υ	kinematic viscosity of water taken to be 1×10^{-6} m^2/s
ρ	density of water
η	Kolmogorov length scale

ε	energy dissipation rate
φ	error in the evaluation of the water balance components
σ	Ratio between D_{84} and D_{50}
a, c, p, y, q	numerical constants
b, t, l, z, x	numerical exponents

CHAPTER 1

General Introduction

1.1 Research Background

In the last few decades, increasing human activities on stream and riverine ecosystem (construction of dams, weirs, regulators, floodgates, bridge footings, hydropower facilities, flood control and erosion control works, and artificial channels and uses of land for industries) were introduced with varying degrees for societal development and quality of life. Such human activities have negative impacts on populations of fish due to habitat fragmentation and loss of connectivity when movement is impeded by physical barriers (Lucas and Baras 2001). Fishpass structures against such barriers facilitate the upstream migration of fish as quickly as possible with a minimal amount of stress, delay, injury, or mortality (Orsborn 1987). Canada's policy on the management of fish habitat requires habitat compensation to achieve no net loss (NNL) in productive capacity regarding such type of human activities (Quigley and Harper 2006). When human activities are proposed that will result in a Harmful Alteration, Disruption & Destruction (HADD), habitat compensation, i.e., the restoration of damaged, enhancement of extant, or development of new habitat, is required to offset habitat loss and achieve NNL. Habitat compensation projects are, in essence, ecological experiments and should be conducted accordingly (Walters and

Holling 1990), with rigorous study designs that will improve scientific defensibility of habitat management decisions and advance our understanding (Scruton et al. 2005).

In recent years, a holistic ecosystem approach has led to a new concept of ecological or nature-like fishpass design over conventional fishpasses (e.g. vertical slot, Denil, weir, and culvert fishpasses). In accordance with ecological design principles, a nature-like fishpass should be able to accommodate all species living in a waterbody (Katopodis et al. 2001). Recently, they have been recognized as economically and ecologically viable alternatives to traditional conventional fishpasses, and have become of considerable interest throughout much of the world. Nature-like fishpasses are constructed with naturally occurring materials such as combinations of gravels, rocks, boulders, bamboo, wood etc. and mimic meandering patterns, cross-sections of nearby rivers, aiming to generate diverse hydraulic conditions and pathways for various size fish (Katopodis and Williams 2011). Classifications of nature-like fishpasses are based on configuration of structures, including the arrangement of boulders (DVWK 2002); they include embedded-boulder constructions, ramps with perturbation boulders, and pool-type ramps. Another classification of nature-like fishpasses is based on their locations relative to barrages (DVWK 2002); they are bottom ramps and bypass channels. In general, two kinds of nature-like fishpass designs can be distinguished: pool and riffle type and rock-ramp type (Katopodis and Williams 2011). The pool and riffle type is built in a stair-step configuration

where typically short steep reaches (riffles) connect to flat deeper reaches (pools) (*Figure 1.1b*). A rock-ramp fishpass has a continuous slope from one end to the other, comprising a series of large-sized boulders (*Figure 1.1a*).

The genesis of this study is related to proposed fish habitat compensation projects to be undertaken by Diavik Diamond Mines Inc. (DDMI) in compliance with the provisions for "no net loss" of fish habitat under Canada's Fisheries Act. Because of HADDs resulting from their mining activities in the Lac de Gras drainage basin, Northwest Territories of Canada, DDMI has proposed two fish habitat compensation projects (M-Lakes and West Island) within the basin to offset aquatic habitat loss and achieve NNL. In-stream structures will be intended to enhance inter-lake connectivity to increase the productive capacity of the small lakes to help achieve NNL in the watershed. Components of DDMI's approved habitat compensation projects included field study in the Barrenlands of Canada's southern Arctic, and detailed laboratory experiments plus computational fluid dynamics (CFD) modeling of nature-like fishpasses.

1.2 Research Motivation

The primary motivation for this study is to explore the detail flow characteristics in a rock-ramp fishpass through exploratory lab study and numerical study to retrofit small Arctic streams for fish habitat connectivity and compensation.

The Barrenlands region of Canada's Northwest Territories has an abundance of water resources, which occupy up to 30% of this northern landscape, and are often present as chains of lakes and their interconnecting outlet streams (Spence et al. 2003). In the last 50 years, Arctic regions have experienced a steady expansion in the development of their natural resources. Recent expansion of gold, base metals, and diamond mining activities in this region, and associated alterations of lakes for storage and treatment of tailings effluent, has prompted recent interest in the eco-hydrology of lake-stream systems. Research on head-water stream hydraulics and lake hydrology regarding fish habitat, especially in Northern Canada, is extremely scarce. Very few studies were carried out on open water Arctic hydrology (Spence et al. 2003; Spence and Woo 2003; Mielko and Woo 2006; and Woo and Mielko 2007) and northern fish ecology (Jones and Tonn 2004; Jones et al. 2003a&b). Furthermore, there is no literature on hydraulic geometry and flow resistance for these head-water streams. Effective protection, management, and restoration of Arctic hydrology and associated freshwater ecosystems require more knowledge concerning the characteristics of undisturbed reference sites. Motivation of field study is to assess stream habitat for the fish habitat compensation project.

This thesis studied one Arctic head-water lake and its outlet stream in order to examine the physical, hydrological, and chemical characteristics within an integrated framework of lake-stream connectivity. Also, the suitability of the stream sections was assessed for small and large young-of-the-year Arctic

grayling. Recently, hydraulic geometry and flow resistance has been employed in a range of river management activities (Ferguson 1986), to estimate the minimum flow requirements for fish passage and to assess the available fish habitat (Jowett 1998). Therefore, the present study investigated the at-a-station hydraulic geometry and flow resistance in Arctic headwater streams with large scale roughness for the future habitat assessment and predictions. Results from this study will increase our ability to predict and understand the eco-hydrological and eco-hydraulics behaviors of headwater streams in an unstudied geographic region of the Northwest Territories, Canada.

An ecosystem approach leading to nature-like fishpasses, mainly rock-ramp and pool–riffle types, was advanced in the 1990s (Katopodis and Williams 2011). The major advantages of rock-ramp type fishpass is to effectively dissipate energy, reduce flow velocity and increase water depth while providing resting places and shelters for fish. Hence, the performance of this type of fishpass showed most promising results, evaluated by Thorncraft and Harris (1996), Franklin et al. (2012), and Franklin and Bartels (2012). The hydraulics of conventional fishpasses (Rajaratnam et al. 1986; Ead et al. 2004; Liu et al. 2005; and so on) has been studied for many years; however, the same is not true for nature-like fishpasses which have limited studies. The detailed mean and turbulent flow characteristics in such nature-like fishpass facilities are still in an early phase and have not been systematically analyzed. For instance, USBR (2007), DVWK (2002), and Parasiewicz et al. (1998) provides some practical guidelines for

nature-like fishpasses and provided some examples of field applications based on critical flow criteria. Haro et al. (2008) conducted several experiments with field-scale laboratory setup for a nature-like fishpass in a perturbation boulder design. Recently, Wang and Hartlieb (2011) examined the hydraulic and geometric parameters of nature-like pool-type fishpasses via experimental and field investigations. However, some studies, particularly on simple fish habitat structures, (Shamloo et al. 2001; Tritico and Hotchkiss 2005; Strom and Papanicolaou 2007; Sadeque et al. 2008; Lacey and Roy 2008; Lacey and Rennie 2012; and Papanicolaou et al. 2012) have investigated the flow characteristics around different bluff bodies and isolated instream pebble cluster. Therefore to date, no studies to our knowledge have examined the detailed flow characteristics in rock-ramp nature-like fishpasses.

Recently, many compensation projects have elected to incorporate nature-like fishpass designs. Materials available on site are used to construct structures that simulate natural stream characteristics suitable for a variety of fish species (Katapodis et al. 2001). These structures are usually more cost-effective in remote settings than traditional designs though may sacrifice predictability as site materials vary. The motivation of lab study is to explore the flow characteristics in a rock-ramp fishpass systematically to retrofit small streams. This thesis presented a detailed investigation on the mean and turbulent flow characteristics in a rock-ramp nature-like fishpass for a staggered arrangement of boulders.

Hopefully, the outcome of this study will allow us to make potential improvements for the design and building of successful rock-ramp fishpasses.

In the past ten to fifteen years, much attention has been directed to the development of numerical models as tools to facilitate eco-hydraulic studies (Crowder and Diplas 2000, Guay et al. 2000). A typical example is the development of the Physical Habitat Simulation Method (PHABSIM, see Bovee et al. 1998), River2D (see Steffler et al. 2002), and CFD modeling for vertical slot fishpass (Lai et al. 2003; Khan et al. 2004; Khan 2006) and for stream deflectors (Salaheldin et al. 2003; Haltigin et al. 2007; Shen and Diplas 2008). The above modeling studies have demonstrated that there is great potential in using computational fluid dynamics (CFD) for representing the unknown flow fields in the nature-like fishpasses. The motivation of numerical study is to access the CFD capability for the rock-ramp type nature-like fishpasses to optimize the design. This thesis investigated the flow characteristics in a rock-ramp fishpass under different flow conditions and geometric variables (channel slopes, boulder diameters, boulder spacing, and boulder arrangements). Results from this study could play an important role in advancing our knowledge about the effect of geometric variables on mean flow characteristics to optimize the design of rock-ramp fishpasses and would be useful to both fishpass designers and fish biologists.

1.3 Research Objectives

The overall objective of this thesis is to investigate the detailed flow characteristics in a rock-ramp type nature like fishpass to retrofit small streams for habitat connectivity and compensation. The thesis is organized around the following specific objectives:

(i) To investigate the hydrological characteristics and fish suitability of an Arctic stream within an integrated framework of lake-stream connectivity.

(ii) To investigate the at-a-station hydraulic geometry and resistance to flow for headwater streams in the Northwest Territories of Canada.

(iii) To investigate the mean flow characteristics in a rock-ramp type fishpass.

(iv) To investigate the turbulence flow characteristics in a rock-ramp type fishpass.

(v) To develop computational fluid dynamics model of a rock-ramp type fishpass.

1.4 Significance of this Research

Results from field study will increase our ability to predict and understand the eco-hydrological and eco-hydraulics behaviors of head-water streams in an unstudied geographic region of the Barrenlands region of the Northwest Territories, Canada. The major contribution from field study includes:

- the hydrological characteristics with an integrated framework of lake-stream connectivity;
- the suitability of a stream as fish migration corridor based on physical, chemical, hydrological, and hydraulic aspects; and
- the nature and variability of at-a-station hydraulic geometry relationships and flow resistance of head-water streams.

Results from lab study on rock-ramp type nature-like fishpass will increase our ability

- to predict and understand the detail mean and turbulence flow characteristics systematically in a rock-ramp type fishpass structure; and
- to predict some mean and turbulence flow parameters in a rock-ramp type fishpass from some general correlations as a function of discharge and streamwise distance.

Results from numerical study confirm the CFD capability in prediction of flow field in a rock-ramp type fishpass to optimize the design.

Finally, the outcome of this study will allow us to develop potential improvements for the design and operation of rock-ramp nature-like fishpasses more generally and develop a general nature-like fishpass design guideline. The outcome of the proposed study has prospective applications in various governmental and

industrial sectors in the sense that it improves the design and operation of nature-like fishpass more generally.

1.5 Organization of Thesis

This thesis is written in paper format and composed of seven chapters including general introduction, two field studies, two experimental investigations, one numerical modeling, and general conclusions and recommendations. Chapter 1 provides research background and motivation with specific research objectives.

In Chapter 2, an Arctic undisturbed head-water stream is studied based on field measurements. The main focus is on the hydrological characteristics and fish suitability of stream within an integrated framework of lake-stream connectivity. In Chapter 3, focus is given to at-a-station hydraulic geometry and flow resistance in head-water streams with large scale roughness in Canada's Northwest Territories. The nature of at-a-station hydraulic geometry and flow resistance of these streams were examined and compared with other relevant studies.

In Chapter 4, the mean flow characteristics of a rock-ramp type nature-like fishpass with a staggered arrangement of boulders are studied in a laboratory flume at three different channel slopes (1.5, 3, and 5%) for several discharges. Some general correlations for predicting the average flow depth and velocity in a rock-ramp fishpass as a function of normalized discharge and streamwise distance are proposed. Chapter 5 investigated the turbulence characteristics that have

potential importance for fish passage in a rock-ramp fishpass for the above experimental setup. The other focuses are to develop some general correlations for predicting the average turbulent intensity, turbulent kinetic energy, and Reynolds shear stress in a rock-ramp fishpass as a function of normalized streamwise distance and to distinguish the influence of cluster of boulders (wake interference flow) versus single boulder (isolated roughness flow) on flow fields in the wake region behind the boulder.

In Chapter 6, a three-dimensional computational fluid dynamics model (ANSYS-CFX) of a rock-ramp type nature-like fishpass was used to investigate the fishpass hydrodynamics. The study analyzed the flow characteristics in a rock-ramp type fishpass under different flow conditions and geometric variables (channel slopes, boulder diameters, boulder spacings, and boulder arrangements) to optimize the design of rock-ramp fishpasses. Finally, the overall conclusions and recommendations for future work are presented in Chapter 7.

1.6 References

Bovee, K. D., Lamb, B. L., Bartholow, J. M., Stalnaker, C. B., Taylor, J., Henriksen, J. (1998). "*Stream habitat analysis using the instream flow incremental methodology*." US Geological Survey, Biological Resources Division Information and Technology Report USGS/BRD, 1998-0004.

Crowder, D. W., and Diplas, P. (2006). "Applying spatial hydraulic principles to quantify stream habitat." *River Research and Applications*, 22(1), 79-89.

Crowder, D. W., and Diplas, P. (2000). "Using two-dimensional hydrodynamic models at scales of ecological importance." *Journal of Hydrology*, 230(3-4), 172–191.

DVWK (2002). "*Fish passes-Design, dimensions and monitoring*." Published by the Food and Agriculture Organization of the United Nations in arrangement with German Association for Water Resources and Land Improvement as DVWK-Merkblatt.

Ead, S.A., Katopodis, C., Sikora, G. J., and Rajaratnam, N. (2004). "Flow regimes and structure in pool and fishways." *Journal of Environmental Engineering and Science*, 3, 379–390.

Ferguson, R. I. (1986). "Hydraulics and hydraulic geometry." *Progress in physical Geography*, 10 (1), 1-31.

Franklin, P.A., and Bartels, B. (2012). "Restoring connectivity for migratory native fish in a New Zealand stream: effectiveness of retrofitting a pipe

culvert." *Aquatic Conservation: Marine and Freshwater Ecosyst*ems, 22, 489–497.

Franklin, A. E., Haro, A., Castro-Santos, T., and Noreika, J. (2012). "Evaluation of nature-like and technical fishways for the passage of Alewives at two coastal streams in New England." *Transactions of the American Fisheries Society*, 141, 624-637.

Guay, J. C., Boisclair, D., Rioux, D., Leclerc, M., Lapointe, M., Legendre, P. (2000). "Development and validation of numerical habitat models for juveniles of Atlantic Salmon." *Canadian Journal of Fisheries and Aquatic Sciences*, 57, 2065–2075.

Haro, A., Franklin, A., Castro-Santos, T., and Noreika, J. (2008). Design and evaluation of nature-like fishways for pasage of Northeastern Diadromous fishes. Final report, Submitted to NOAA National Marine Fisheries Service Office of Habitat Conservation.

Jones, N. E., and Tonn, W. M. (2004). "Resource selection functions for age-0 Arctic grayling (Thymallus arcticus) and their application to stream habitat compensation." *Canadian Journal of Fisheries and Aquatic Sciences*, 61, 1736–1746.

Jones, N. E., Tonn, W. M., Scrimgeour, G. J., and Katopodis, C. (2003a). "Ecological characteristics of streams in the Barrenlands near Lac de Gras, N.W.T., Canada." *Arctic*, 56(3), 249-261.

Jones, N. E., Tonn, W. M., Scrimgeour, G. J., and Katopodis, C. (2003b). "Productive capacity of an artificial stream in the Canadian Arctic: assessing

the effectiveness of fish habitat compensation." *Canadian Journal of Fisheries and Aquatic Sciences*, 60, 849–863.

Jowett, I.G. (1998). "Hydraulic geometry of New Zealand rivers and its use as a preliminary method of habitat assessment." *Regulated Rivers-Research & Management*, John Wiley and Sons, 14, 451–466.

Katopodis, C., Kells, J. A., and Acharya, M. (2001). "Nature-like and conventional fishways: alternative concepts?" *Canadian Water Resources Journal*, 26(2), 211-232.

Katopodis, C., and Williams, J. G. (2011). "The development of fish passage research in a historical context." *Ecological Engineering*, 48, 8-18.

Khan, L. A. (2006). "A three-dimensional computational fluid dynamics (CFD) model analysis of free surface hydrodynamics and fish passage energetics in a vertical-slot fishway." *North American Journal of Fisheries Management*, 26, 255–267.

Khan, L. A., Wicklein, E. A., Rashid, M., Ebner, L. L., Richards, N. A. (2004). "Computational fluid dynamics modeling of turbine intake hydraulics at a hydropower plant." *Journal of Hydraulic Research*, 42, 61–69.

Lacey, R. W. J., and Rennie, C. D. (2012). "Laboratory investigation of turbulence flow structure around a bed mounted cube at multiple flow stages." *Journal of Hydraulic Engineering*, 137(1), 71-84.

Lacey, R. W. J., and Roy, A. G. (2008). "The spatial characterization of turbulence around large roughness elements in a gravel-bed river." *Geomorphology*, 102, 542-553.

Lai, Y. G., Weber, L. J., and Patel, V. C. (2003). "Nonhydrostatic three-dimensional model for hydraulic flow simulation, I. formulation and verification." *Journal of Hydraulic Engineering*, 129, 196–205.

Liu, M., Rajaratnam, N., and Zhu, D. Z. (2005). "Mean flow and turbulence structure in vertical slot fishways." *Journal of Hydraulic Engineering*, 132(8), 765–777.

Lucas, M. C., and Baras, E. (2001). "*Migration of Freshwater Fishes*." Blackwells, Oxford.

Mielko, C., and Woo, MK. (2006). "Snowmelt runoff processes in a headwater lake and its catchment, subarctic Canadian shield." *Hydrological Processes*, 20, 987–1000.

Orsborn, J. F. (1987). "*Fishways-historical assessment of design practices*." In: M. J. Dadswell, R. J. Klauda, C. M. Moffitt, R. L. Saunders, R. A. Rulifson, and J. E. Cooper, (eds), Common strategies of anadromous and catadromous fishes, American Fisheries Society, Symposium 1, Bethesda, Maryland.

Papanicolaou, A. N., Kramer, C. M., Tsakiris, A. G., Stoesser, T., Bomminayuni, S., and Chen, Z. (2012). "Effects of a fully submerged boulder within a boulder array on the mean and turbulent flow fields: Implications to bedload transport." *Acta Geophysca*, 60(6), 1502-1546.

Parasiewicz, P., Eberstaller, J., Weiss, S., and Schmutz, S. (1998). "*Conceptual Guidelines for Nature-like Bypass Channels*." In: M. Jungwirth, S. Schmutz, and S. Weiss, (eds), Fish Migration and Fish Bypasses, Oxford: Fishing News Books, Blackwell Science Ltd, 348-362.

Quigley, J. T., and Harper, D. J. (2006). "Effectiveness of fish habitat compensation in Canada in achieving no net loss." *Environmental Management*, 37(3), 351-366.

Rajaratnam, N., Van der Vinne, G., and Katopodis, C (1986). "Hydraulics of vertical slot fishways.' *Journal of Hydraulic Engineering*, 112(10), 909–927.

Sadeque, M. A. F., Rajaratnam, N., and Loewen, M. R. (2008). "Flow around cylinders in open channels.' *Journal of Engineering Mechanics*, 134(1), 60-71.

Salaheldin, T. M., Imran, J. I., and Chaudhry, M. H. (2003). "Numerical modeling of three-dimensional flow field around circular piers." *Journal of Hydraulic Engineering*, 130 (2), 91-100.

Scruton, D. A., Clarke, K. D., Roberge, M. M., Kelly, J. F., and Dawe, M. B. (2005). "A case study of habitat compensation to ameliorate impacts of hydroelectric development: effectiveness of re-watering and habitat enhancement of an intermittent flood overflow channel." *Journal of Fish Biology*, 67, 244–260.

Shamloo, H., Rajaratnam, N., and Katopodis, C (2001). "Hydraulics of simple habitat structures." *Journal of Hydraulic Research*, 39(4), 351–366.

Shen, Y., and Diplas, P. (2008). "Application of two- and three-dimensional computational fluid dynamics models to complex ecological stream flows." *Journal of Hydrology*, 348, 195-214.

Spence, C., Rouse, W. R., Worth, D., and Oswald, C. (2003). "Energy budget processes of a small northern lake." *Journal of Hydrometeorology*, 4, 694-701.

Spence, C., and Woo, MK. (2003). "Hydrology of a subarctic Canadian shield: soil-filled valleys." *Journal of Hydrology*, 279, 151–166.

Steffler, P., Ghanem, A., and Blackburn, J. (2002). "*River2D Version 0.90*." University of Alberta, Fisheries and Oceans, Canada, and United States Geological Survey.

Strom, K.B., and Papanicolaou, A. N. (2007). "ADV measurements around a cluster microform in a shallow mountain stream." *Journal of Hydraulic Engineering*, 133(12), 1379-1389.

Thorncraft, G. A., and Harris, J. H. (1996). "Assessment of rock-ramp fishways." NSW Fisheries Research Institute and the Coorperative Research Centre for Freshwater Ecology, Report for NSW Environment Protection Authority.

Tritico, H. M., and Hotchkiss, R. H. (2005). "Unobstructed and obstructed turbulent flow in gravel bed rivers." *Journal of Hydraulic Engineering*, 131(8), 635-645.

U.S.B.R. (2007). "*Rock-ramp Design Guidelines*." U.S. Department of the Interior Bureau of Reclamation Technical Service Center Denver, Colorado, USA.

Walters, C. J., and Holling, C. S. (1990). "Large-scale management experiments and learning by doing." *Ecology*, 71, 2060-2068.

Wang, R.W., and Hartlieb, A. (2011). “Experimental and field approach to the hydraulics of nature-like pool-type fish migration facilities.” *Knowledge and Management of Aquatic Ecosystems*, 400, 05.

Woo, MK., and Mielko, C. (2007). “An integrated framework of lake-stream connectivity for a semi-arid, subarctic environment.” *Hydrological Processes*, 21, 2668–2674.

(a) (b)

Figure 1.1 Photographs of (a) rock-ramp type (DVWK 2002) and (b) pool-weir type nature-like fishpass (photo credits: Dalei Chen).

CHAPTER 2

The Hydrological Characteristics of a Stream within an Integrated Framework of Lake-Stream Connectivity in the Lac de Gras Watershed, N.W.T., Canada*

2.1 Introduction

The Barrenlands region of Canada's Northwest Territories has an abundance of water resources, which occupy up to 30% of this northern landscape, and are often present as chains of lakes and their interconnecting outlet streams (Spence et al. 2003). This landscape is characterized by low topographic relief, poorly integrated drainages, continuous permafrost, and abundant small, shallow lakes. The hydrological regime of this terrain has been described as low-arctic nival, distinguished by long, cold winters when processes are relatively dormant, brief spring snowmelt periods when high stream flow and widespread flooding are enhanced by the frozen ground, and by short summers with low stream flow (Woo 1990). Although abundant, Arctic and subarctic freshwater ecosystems and their hydrology are among the least studied and most poorly understood in North

*The content of this chapter has been published as: Baki et al. (2012a). "The Hydrological Characteristics of a Stream within an Integrated Framework of Lake-Stream Connectivity in the Lac de Gras Watershed, N.W.T., Canada." *Canadian Journal of Civil Engineering*, 39(3): 279-292.

America (Schindler 2001). Although the hydrology of this region is poorly known, field observations suggest that lakes typically undergo large seasonal volume fluctuations due to the combined influence of their shallow depth, extreme spring flooding, and intense evaporation during arid summers (Gibson et al. 1994).

In the last 50 years, Arctic regions have experienced a steady expansion in the development of their natural resources. Recent expansion of gold, base metals, and diamond mining activities in the region, and associated alterations of lakes for storage and treatment of tailings effluent, has prompted recent interest in the eco-hydrology of lake-stream systems. Research on stream hydraulics, hydrology, and water quality regarding fish habitat, especially in northern Canada, is extremely scarce. The very few studies on open water hydrology of northern Canadian lakes and streams include subarctic work by Spence et al. (2003), Spence and Woo (2003), Mielko and Woo (2006), and Woo and Mielko (2007). More specifically, published research on the suitability of lake-stream networks as they relate to northern fish ecology and habitat on the Barrenlands tundra is limited to Jones and Tonn (2004) and Jones et al. (2003a&b). Despite this recent progress, effective protection, management, and restoration of Arctic hydrology and associated freshwater ecosystems require more knowledge concerning the characteristics of undisturbed reference sites. As meteorological data are scarce and field measurements are very expensive, tedious, and time consuming in northern

Canada, there is a growing need to develop and use hydrological predictive models as a management tool.

Diversity is a key characteristic of any productive in-stream habitat (Wesche 1985). Considering the importance of physical, chemical, hydrological, and hydraulic aspects of streams to fish, it is imperative that the proper blend of stream discharge, water depth, water velocity, water quality and substrate types be present if a stream is to sustain or act as a migration corridor for fish. Here, we studied an outlet stream connecting a headwater lake to Lac de Gras to examine the physical, chemical and hydrological characteristics within an integrated framework of lake-stream connectivity. Specifically, the objectives of this study were to measure the flows in the stream, investigate the hydrological characteristics of the stream including the relationship between water balance of the lake and the flow conditions of the outlet stream, and finally, to examine the suitability of the stream as a fish migration corridor based on stream geometry, stream flow characteristics, stream water temperature and stream water quality. Our study is based on summer 2009 and 2010 field data. Also, we used index models to predict stream flow. Results from this study will increase our ability to predict and understand the eco-hydrological behaviour of headwater outlet streams that will assist in the design of fish habitat manipulation projects. Our findings will also increase our knowledge of eco-hydrology in the Barrenlands region of the Northwest Territories.

The genesis of this study is related to the proposed fish habitat compensation projects to be undertaken by Diavik Diamond Mines Inc. (DDMI) in compliance with the provisions for "no net loss" of fish habitat under Canada's Fisheries Act. DDMI has proposed compensation projects that seek to increase the habitat quality of small lake-outlet streams and to improve the connectivity among small lakes in the greater Lac de Gras watershed. The proposed projects will modify stream habitat through installation of instream deflector berms, channelization of the stream channels, development of a step pool series to allow fish passage over a cascade, and creation of instream fish spawning habitats. The ultimate goal of these modifications is to improve fish migration among lakes, and to provide spawning and nursery habitats, especially for Arctic grayling, which represents an important component of the lake and stream fish communities in the Lac de Gras watershed (Golder Associates Ltd. 2001, 2004; Jones et al. 2003b).

2.2 Background and Field Techniques

The study area is located in the Northwest Territories of Canada, near the DDMI mine site, which is located on an island in Lac de Gras (64° 30' N, 110° 16' W) approximately 320 km northeast of Yellowknife in an area commonly referred to as the Barrenlands. The Barrenlands region is dominated hydrologically by a large snowmelt freshet followed by a gradual drying of the landscape. Barrenland streams flow over folded rock and glacial features, creating highly irregular drainage patterns, but occasionally follow trellis and dendritic configurations for

short distances having a low sinuosity and large scale roughness (>50% large boulder) (Jones et al. 2003a). The climate of this study area is semi-arid with 200-300 mm precipitation annually, 50% of which falls as snow (Jones et al. 2003a). The mean annual temperature is approximately –12 °C with a summer maximum of 27 °C and winter minimum of –54 °C (Environment Canada 1991). Ice break-up on the smaller lakes begins in late-May when daytime temperatures rise above 0 °C. The ice-free season of small lakes typically extends from late June to late-September. Following spring runoff, evaporation from lakes gradually lowers lake levels, stream flows diminish, and surface flow is lost in many small streams.

The study site was located near the mine on West Island (WI). The WI lake is a headwater lake with a single outlet stream, the West Island Stream (WIS). WIS flows 420 m from WI lake (at 423.2 m above sea level) before emptying into Lac de Gras (at 415.7 m above sea level) (Golder Associates Ltd. 2004) (*Figure 2.1a*). Data were collected during summers 2009 and 2010, from the first week in June to the last week in August. For this baseline survey, we identified the surface outlet of the study lake and the direct runoff area into the lake, measured the length of the stream along the thalweg, and selected several sites for stream flow measurement. Four cross sections in WIS (XS-1, XS-2, XS-3 and XS-4) were chosen for hydraulic measurements and the selected stream cross sections were located, respectively, 18.0, 248.8, 291.6, and 401.0 m downstream from the most upstream point of WIS (*Figure 2.1*). The number of riffles and pools were identified during the baseline inspection of the stream by walking along the

thalweg and observing patterns in the water surface and changes in the bed elevation. The stream has a pool-riffle sequence, is narrow (median=1.8m; *Table 2-1*), and the channel is shaded by riparian shrubs. In mid June 2010, a detailed survey of stream bathymetry was conducted using a Total Station (Model: Leica TC407). Stream bed materials were sampled by the random selection "pebble count" method, using a total of 100 particles in three transects (upstream, middle and downstream) along the stream (Wolman 1954). In this method, the investigator measures the intermediate dimension of particles encountered every step while walking through the stream, taking care to sample the entire site equally. Size distribution of the stream bed material from three transects was plotted as cumulative percentage frequency curves and the D_{50} and D_{84}, which is exceeded by 50% and 84%, respectively; percentile values were subsequently extracted. The streambed consisted of a mix of clay, grass, gravel, cobble, and boulders. Many downed shrubs and small pieces of woody debris were in the channel, and the stream banks had exposed roots and grass throughout.

Wetted width was measured perpendicular to flow across the stream. To obtain the stream discharge, each transect was divided into at least ten cells; additional cells were added wherever the stream width exceeds 3m. Velocity measurements were taken using a Marsh-McBirney current meter (Model: 2000 Flo-Mate) at 0.6 of depth (Harrelson et al. 1994) over 20 seconds at each cell. Discharge for each cell was calculated by multiplying the depth at midpoint by the width of the cell by the velocity. Total stream discharge is the sum of each cell. The stream

discharges at cross sections XS-1, XS-2, XS-3, and XS-4 were measured on several days at various stages to develop rating curves for both years. Mini-Diver dataloggers (Schlumberger Water Services) were installed for continuous water level recoding at XS-1 and XS-3 during July-October 2009, and at XS-1, XS-3, and XS-4 from June to October 2010. The Divers measured water levels at a frequency of 5 and 15 minutes during 2009 and 2010, respectively. Using the rating curves, recorded water level was used to convert water level into continuous stream discharges for those sections.

The flow hydrographs were constructed from the daily mean discharge at XS-1 and XS-3 during 2009, and XS-1, XS-3, and XS-4 during 2010, as continuous water level recording occurred at those sections. Traditionally, hydrological flow indices or exceedance percentiles are used to provide recommendations on flow for base flows and instream conditions for the planning of water resource development (Pyrce 2004). Here, we used Q_{50} discharge (50^{th} percentile from the flow duration curve) as the base flow indicator in the flow hydrographs. Next, we calculated the timeframe in total number of days that had the corresponding Q_{50} flow in each hydrograph during 2010 only, as flow data for 2009 were unavailable for the full duration of the summer. Records of daily mean discharge were also used to calculate the average unit yield (litre/s/km^2) and flow duration curves (FDC) of the different cross sections. Average unit yield of stream is the average discharge (litre/s) per unit of the corresponding total drainage area (km^2). Flow duration curves are cumulative frequency distributions that show the percentage

of time that a specified discharge is equaled or exceeded during a period of interest. These curves are usually used to demonstrate the stream's low flow potential. The mean flow (MF) and median flow (Q_{50}) express the central tendencies of the flow; Q_{90} are the values of flow equaled or exceeded 90% of the time; skewness (SK) and coefficient of variation (CV), express the second and third moments of the distribution of data, used for comparisons of flow variability (McMahon 1982). SK is simply calculated as MF divided by Q_{50}, and CV is the standard deviation divided by MF following Clausen and Biggs (2000). Also, the ratio between the 90% and 50% flow values was used as an index of low stream flow as compared with the median discharge.

In 2009, the lake water level of WIL was recorded manually using a vertical staff gauge. In 2010, however, lake water level of WIL was recorded automatically at 15-min intervals using Mini-Diver dataloggers. To assess the suitability of summer stream temperatures for cold-water fish species, stream-temperature data were collected at three sites (upstream, middle, and downstream) in WIS. In 2009, temperature dataloggers set to record at 20-min intervals were installed during the second week of June and retrieved in mid-August. In 2010, temperature dataloggers set to record at 30-min intervals were installed in the second week of June and retrieved in the last week of August.

A HydroLab was used to measure conductivity, pH, and dissolved oxygen (DO) at the discharge measurement cross sections of the stream for both years. Clean

500 ml plastic jars were used to collect water samples from the flow measurement locations of the stream for analysis of total suspended solids (TSS); all samples were processed and analyzed according to standard procedures.

Daily rainfall, hourly net solar radiation, air temperature, and wind speed data were collected from the DDMI meteorological station located at the mine's airstrip. Evaporation was calculated daily by the Priestley and Taylor (1972) method for the water surface of the lake, using net radiation and air temperatures, and an average α value of 1.26 (Eaton et al. 2001). Based on the daily recorded rainfall, estimated evaporation, observed lake water level, and measured lake outlet flow (stream discharge), the water balance of WIL (expressed in m^3/day) during the open-water season for both years was predicted using the following equation:

$$\Delta S = P - E - Q_o + Q_b^* + \varphi \qquad (2.1)$$

Here, direct measurements were made of rainfall on the lake area (P), storage change based on lake level fluctuation (ΔS), flows through the stream channel (Q_o), while lake evaporation (E) was calculated by the Priestley and Taylor method using measured variables; Q_b^* is the net flux of water delivered to or leaked from the lake via overland or subsurface flows from the direct catchment area, and φ is the error in the evaluation of the water balance components. Unfortunately, Q_b^* and φ cannot be assessed independently. We can estimate Q_b^* as a residual term in Eq. (2.1) if we assume that φ is small relative to the magnitude of various components of the water balance. Fluctuations of lake

storage relative to outflow threshold was investigated for the study lake using the observed lake water levels and recorded stream discharges in relation to the corresponding water balance.

Finally, the stream's physical (stream slope, substrate, and number of pools & riffles), hydrological (flow pattern, base flow, and water temperature), hydraulic (water depth and velocity), and chemical (pH, dissolved oxygen, conductivity, and total suspended solids) parameters during 2009 and 2010 were used to examine the stream's suitability to function as a corridor for fish migration (i.e., to function as a fishway). To do this, we examined the stream's present characteristics and compared them to the conditions required for the major life stages of Arctic grayling.

2.3 Results

2.3.1 Stream Physical Characteristics

The morphological information pertaining to the study stream system includes direct catchment area (30.08 ha), lake area (13.65 ha), maximum lake water depth (12.0 m), stream length (420.0 m), stream substrate composition (D_{84}= 220 mm and D_{50}= 26 mm), number of pools (10) and riffles (9), and stream longitudinal slope (1.88%) (*Figure 2.1b*). Table 2-1 shows the physical characteristics of the study stream with median and standard deviation (SD) for the 2009 and 2010 field data. Overall, the cross sectional average bankfull width ranged from 0.75 to 3.33

m, the cross sectional bankfull depth ranged from 0.07 to 0.27 m, the width/depth ratio ranged from 4.6 to 14.4, and, the relative submergence d/D_{84} (d/D_{50}) ranged from 0.34 to 1.22 (2.86 to 10.31), where d is the cross sectional average water depth. The outlet of this stream flows into Lac de Gras in the form of a cascade (about 40 m in length), which has a slope of approximately 20 % (*Figure 2.1b*).

2.3.2 Stream Flow

The hourly average water level and discharge at two sections (XS-1 and XS-3) between the third week of July and second week of August, 2009 are shown in Figure 2.2. It is apparent that maximum discharge occurs at the start of the monitoring period, and stream flow declined almost to zero by the end of the study period. The hourly average water level and discharge at three sections (XS-1, XS-3, and XS-4) between the first week of June and last week of August, 2010 are shown in Figure 2.3. Following maximum discharge during the first week of July, stream flow declined to almost zero by the end of July, except at XS-1. Based on the measured and estimated flow data, the statistical values of discharge, velocity, and water depth in W1S during 2009 and 2010 are summarized in Table 2-2.

For 2010, but not in 2009, the continuous water level and discharge data encompassed the early freshet. In flow hydrographs during 2009 (*Figure 2.2*), there are several fluctuating discharges over the study period due to several

rainfall events as manifested by components of rainfall distribution in the water balance analysis (*Figure 2.7*). In 2010, the flow hydrographs (*Figure 2.3*) contain three significant peaks due to snow melt from increasing temperature (*Figure 2.6*) as well as intense rainfall in the first week of July (*Figure 2.7*). The differences in maximum and minimum stream discharges (*Table 2-2*) indicate that seasonal variation in mean daily discharge is extremely high. The average discharge was 0.0025 and 0.0027 m^3/s at XS-1 and XS-3 over the study period in 2009. In 2010, it was 0.0089, 0.0118 and 0.0589 m^3/s over the study period at XS-1, XS-3, and XS-4, respectively. This indicates that the variations of discharge tend to increase along the stream thalweg distance from upstream to downstream. The measured maximum cross sectional velocities also follow the same increasing trend along the stream thalweg distance from upstream to downstream, with the exception of XS-3 in 2009 (*Table 2-2*).

By enlisting flow statistics from historical stations at the Ekati Diamond mine and Water Survey of Canada stations near Lac de Gras, Golder Associates (2004) categorized flows with respect to the relative magnitude of peak flow within channels from very low (less than 0.075 m^3/s) to very high (greater than 0.50 m^3/s). According to this classification, flow conditions in all sections were very low in 2009, i.e., at values expected to be exceeded at least 4-5 times out of every 5 years (*Table 2-2*). In 2010 (*Table 2-2*), the flow conditions at XS-1 and XS-2 were very low; at XS-3 they were average (expected to be exceeded at least 2-3 times out of every 5 years); and at XS-4 they were high (expected to be exceeded

at least 1-2 times out of every 5 years). Ekati (2009) estimated the maximum and minimum unit yields (l/s/km^2) ranged about 1-275, 0.2-215, and 1-120 l/s/km^2 from the measured flow data of Vulture-Polar, Cujo, and Counts streams, respectively from 1997 to 2008 in the Koala watershed within the Lac de Gras region (*Figure 2.4*). In our study area, the average unit yields for WI stream in 2009-2010 were about 8 and 40 l/s/km^2, respectively (*Figure 2.4*).

2.3.3 Flow Duration Curve

A flow duration curve (FDC), shown in Figure 2.5, is one of the most informative means of displaying the complete range of stream discharges, from low flow to high flow events. The median flow (Q_{50}) was highest at XS-1 during 2009 and 2010. Q_{90}, a streamflow exceeded 90% of the time, was highest at XS-3 and XS-1 during 2009 and 2010, respectively. This value indicates how much water is available most of the time, and indicates the minimum flow to protect the stream (Petts et al. 1997); it also serves as a threshold to help identify extremely low flows (Allan and Castillo 2007). The suitability for benthic and other communities in a stream is reflected in low values of CV and Skewness (Clausen and Biggs 2000). As can be seen from Table 2-3, the low flow variations in XS-1 during 2010 would produce suitable environments for these communities, whereas the high flow variations in streams XS-1 and XS-3 during 2009 and XS-3 and XS-4 during 2010 would probably present challenging environments. The ratio between the 90% and 50% flow values provides an index of low stream flow as compared

with the median discharge, enabling comparisons between streams with different magnitudes of flow. The highest ratios (Q_{90}/Q_{50}>0.1), found at XS-3 during 2009 and XS-1 during 2010 (*Table 2-3*), indicate reliable low flows that are closer to the 50% flow value. The smallest ratios (Q_{90}/Q_{50}<0.1), found in the cross sections XS-1 in 2009, and XS-3 and XS-4 in 2010, reflect very low flows that are consistently small compared with the stream's medium discharge.

2.3.4 Stream Temperature

The average water temperatures during 2009 in the upstream, middle, and downstream sections of WIS were 10.88 and 12.70, 8.91 and during 2010 were 11.00, and 8.29 and 11.35 °C, respectively (*Figures 2.6*). The average stream temperatures in 2010 were warmer than 2009. The 7-day moving average of daily maximum and minimum temperatures were compared with daily average temperatures for both years in Figures 2.6, which also show the date at which the 7-day moving average of daily minimum temperature exceeded 4 °C. In the downstream section, the distinctions of 7-day moving average of the daily maximum and minimum downstream water temperature during 2010 were especially high from mid-July to the end of the study period during 2010 (*Figure 2.6c*): in this cross section the water depth was very shallow within that time period and there was a strong effect of direct sunlight. The 7-day moving average of the daily minimum stream temperature at all sections of WIS was greater than 4 °C from the last week of June in 2009 and from mid-June in 2010, resulting in

above 4°C temperatures approximately 74 and 85 % of the time, respectively. The water temperatures in the downstream and middle sections of WIS were lower than that of the upstream section for both years, which may have been due to the effect of additional groundwater discharge to the stream (Baevsky 1991). Based on temperature data collected from 16 streams during 1998-2001, Jones et al. (2003b) found that the average daily stream water temperatures often reached 14 °C, where daily averages during the 2009 and 2010 summer typically ranged between 10 and 15 °C in our study area.

2.3.5 Water Quality

Table 2-4 shows the chemical characteristics of the study stream at each discharge measurement cross section, with median and standard deviation (SD) during 2009 and 2010. Stream water pH ranged from 5.1 to 8.8 (6.7 ± 1.3; median ± SD), dissolved oxygen (DO) ranged from 4.3 to 10.4 mg/ liter (7.4 ± 2.0 mg/ liter), conductivity ranged from 14.9 to 31.0 ms/cm (23.2 ± 4.6), and total suspended solids (TSS) ranged from 2 to 7 mg/ liter (3.4 ± 1.7) over the study period. The stream temperature, pH, and DO values on 31 July, 2009 were generally lower than those on 8 August, 2010 (*Table 2-4*). The water quality data in the study stream are comparable with values in Jones et al. (2003a) from the same region, where the average values of pH, DO, conductivity and TSS were 6.78, 9.8 mg/ liter, 14.3 ms/cm, and 1.78 mg/ litre, respectively. The DO levels in cross sections

XS-2 and XS-4 in 2010 were less than 6.0 mg/litre as they were affected by groundwater contributions, which have a lower DO level.

2.3.6 Lake Water Balance

Lake water balance during the open-water season for both years permits an evaluation of how various hydrologic components influence lake storage capacity. For the 2009 and 2010 study periods, total lake evaporation was 160 mm (3.57 mm/day) and 232 mm (4.47 mm/day), respectively. Figure 2.7 is a plot of the daily values of water balance components in m^3/day for our lake during 2009 and 2010, and Table 2-5 provides their total magnitudes for the study period. For 2009, ΔS (i.e., storage change based on lake level fluctuation) were plotted based on several days of manually observed lake water levels. During the spring freshet, there was a large water influx (positive Q_b^*) derived from snowmelt on the basin slopes, and it was mainly the overland and subsurface contributions that raised the lake storage. After the melt period, Q_b^* became negative, suggesting that there was a continuous groundwater loss from the lakes and continuous lake water level drop.

2.3.7 Lake Storage and Stream Flow

During the spring freshet, fast delivery of water from the basin slopes enables a rapid increase in lake storage, permitting a quick rise of lake level above the outlet

threshold to produce outflow. During this period, a large amount of overland flow can be generated that may overwhelm the stream channel receiving the lake outflow (*Figure 2.8*). After the snow has melted, evaporation will cause a net drawdown in lake levels, eventually leading to an outflow that is confined to the stream channel. Field information can be combined with a water balance analysis to relate lake storage to outflow. The lake threshold is normally the lowest point along the perimeter of the lake where outflow occurs through the outlet stream. The lake water level declined to the threshold levels after the first and last weeks of August in WIL during 2009 and 2010, respectively (*Figure 2.9*), although some downstream sections still had some flow due to the subsurface contribution as discussed earlier.

2.4 Discussion

The historical climate data (June, July and August, 1998 to 2008) obtained from the Ekati station of the Meteorological Service of Canada, and the Polar station of EKATI Diamond Mine (EKATI 2009) (approximately 40 km north of the study site) indicate that air temperatures in 2009 and 2010 were average and well below average, respectively. Because the seasonal precipitation in 2009 and 2010 was less than all previous values, conditions during our 2009 and 2010 study were exceptionally dry for the Lac de Gras region (*Figure 2.10*). Generally, all Barrenland streams originate as lake outlets, and our analysis indicates that the WIS study stream has diverse physical characteristics, including gross slope,

stream width, bankfull depth and substrate composition, all of which are similar to the stream characteristics described by Jones et al. (2003a) in the same region. Based on stream morphology type (step-pool), bed material size (boulder dominant) and width/depth ratio (about 10), our study stream can be classified as a small stream (Hogan and Ward 1997) with steep slope, shallow depth and contracted width. The stream longitudinal slope varies from flat, to average (2%), to steep (20%) slopes at the upstream, midstream, and downstream sections, respectively. According to the stream roughness classification of Bathurst (1985), the stream conditions indicate large-scale roughness (d/D_{84}<1.2), as large boulders protrude through the surface of the flow in much of the flow range.

2.4.1 Stream Flow Measurements

The flow data encompassed the early freshet in 2010, but not in 2009. The stream flows in most cross sections were at a maximum during the first week of July, though these flows were still relatively low during 2009, and varied from very low to high during 2010 when compared with Golder Associates' classification (Golder Associates 2004). In summer 2009, the average unit yield for our study stream was comparable to that of Counts stream, but well below Vulture-Polar and Cujo streams. In contrast, during summer 2010, the average unit yield for our study stream was comparable to both Vulture-Polar and Cujo streams and exceeded that for the Counts stream. However, it is important to note that the drainage areas of Vulture-Polar (7.17 km^2), Cujo (2.90 km^2), and Counts (4.25

km^2) streams are respectively about 22, 9, and 13 times greater than our direct catchment area (0.32 km^2). Based on the hydrograph trends of selected cross sections in the study stream, it is apparent that the stream experienced a few peak flows over the month of June and then flow declined sharply. A review of the hydrograph characteristics for smaller basins suggests that the peak flow periods are generally short in duration (i.e., on the order of a few hours). Importantly, the flows tend to decline quite rapidly with maximum daily flows being in the order of 50% of the peak flow of the hydrograph, and maximum weekly flows found to be in the order of 15% of the peak instant of the hydrograph. The stream discharge and maximum cross sectional velocity changed from very low to very high as water flowed from upstream to downstream due to the additional contributions of meltwater from the larger drainage area, as well as from subsurface groundwater. The contribution of subsurface groundwater to the downstream sections is also obvious in the variation of stream water temperature.

2.4.2 Stream Flow Analysis

Flow duration curves: The median flow (Q_{50}) is a guideline to protect and conserve aquatic biota (U.S. Fish and Wildlife Service 1981) and guides aquatic baseflow policy for water resources planning and management (Ries and Friesz 2000). The Q_{50} flow exists in our study stream only about 43% of the total study period in 2010 (*Table 2-6*); this is uncommon compared to the general stream flow system, and could be due to the extreme flow variation. The flow duration

curves suggest that the highest ratios, between 90% and 50% flows for some cross sections, indicated reliable low flows that are closer to the 50% flow value, but that smaller ratios elsewhere reflected very low flows that were consistently low when compared to the associated stream's medium discharge. The flow duration curves also suggest that the low flow variations in a single cross section during 2010 should provide suitable environments for benthic and other aquatic communities, whereas higher flow variations in the remaining cross sections could result in stressful environment.

Lake water balance and lake outlet flow: The estimated evaporation rates in our water balance computation are comparable to the values found by Mielko and Woo (2006) of 3.3 mm/day for May to August 2004 and by Woo and Mielko (2007) of 4.8 mm/day in June 2004. Regarding rainfall, Jones et al. (2003a) estimated about 0.96, 1.96, and 1.28 mm/day average rainfall during summer (June to August) in 1998, 1999, and 2000, respectively. Also, Spence et al. (2003) recorded average rainfall of about 1.27 and 1.3 mm/day during 1999 and 2000 (June to September) respectively, at Skeeter Lake, located approximately 250 km west of our study area. In our study area, for the open water period from 1 July to 14 August 2009 (25 June to 15 August, 2010), total rainfall was about 2.51 (1.03) mm/day, which was less than the evaporation rate of 3.57 (4.47) mm/day, which led to a net drawdown of the lake level. Water balance calculations indicate that a given lake can be recharged in the same year by slope runoff from the direct catchment area as was apparent during 2010; but, groundwater loss in other years

through subsurface conditions was apparent during 2009. Woo and Mielko (2007) also estimated similar overland and subsurface contributions as well as continuous groundwater loss. Likewise, Spence et al. (2003) assumed 0.5 mm/day groundwater loss to estimate the water budget of Skeeter Lake. Despite the bedrock structure, seepage loss is highly plausible because rock fractures can be effective conduits to convey water (Thorne et al. 1999) in our study area. The ratio of a lake's total loss ((evaporation, plus outflow, plus groundwater loss) to its recharge (rainfall, plus inflow)) was 1.45 during 2009 and 1.6 during 2010 (*Table 2-5*). As a result, the summer water balance in our study area caused drawdown of lake level to below the threshold levels that ultimately lead to periods of zero outflows.

Snowmelt modeling for stream flow prediction: Snowmelt can be modeled to estimate the stream flow for our small watershed. However, due to the remote location, the availability of detailed meteorological data restricts the accuracy of any model. Snowmelt models range from the sophisticated, data intensive surface energy model to the rather simple index models. The choice of model is generally based on the availability of data, how the results will be used, and possibly the conditions that prevail (Kane et al. 1997). This paper has made an attempt to predict the stream flow using the index models for snowmelt and rational methods for stream discharge. Data for the index models consisted entirely from meteorological inputs of daily maximum/minimum temperature and rainfall. In terms of index models, the Degree day method (DDM) and U.B.C. Watershed

Method (UBCM) (Quick and Pipes 1977) were used. Previously, the DDM was used by Kane et al. (1997) in an Arctic region where it worked well for average conditions, and the UBCM was originally used for daily stream flow forecasting on the Fraser River system in British Columbia, Canada.

According to Timoney et al. (1992) and a snowpack density distribution map produced by Environment Canada, in our study area we can assume the snow pack density to be 175 kg/m^3. In the DDM method ($M=aT_a$), the ratio of snow and water density, a = 0.175 and temperature (T_a) was used as the daily average temperature recorded for each hour above freezing. In the UBCM method, the first step is to calculate T_x from the ratio between minimum temperature above freezing and reference dewpoint (T_{min}>freezing temperature/T_{dewp}), then calculate T from daily average temperature above 0 °C, T_x, T_{min}, and daily temperature range using (T=$T_{daily\ avg.}$> 0 °C + T_x * ($T_{daily\ tem\ range}$ / XT + T_{min}>freezing temp.)), and finally calculate daily snowmelt (PM)=PTM * T, where, T_{dewp}= reference dewpoint (used a value of 3.5 °C), XT is a constant with a usual value of 6.0, PTM is the point snowmelt factor with a usual value of 3.5 mm/°C, and PM=daily snowmelt water (mm). Then, for the stream discharge, we have used the Rational method. In this method, $Q=0.28C_fiA_d$, where, Q=design discharge (m^3/s), C_f= dimensionless coefficient of runoff (we have used 0.11), i=average melting water plus rainfall intensity (mm/hr), and A_d=direct catchment area (km^2).

For this analysis, we used the Yellowknife weather station's (Environment Canada) meteorological data for 2010. Although Yellowknife is approximately 320 km southwest from our study area, due to the lack of complete daily meteorological data from the nearest weather stations, its weather station provides the best available data. It was assumed that the evaporation and subsurface contribution in the lake from the snowmelt water are equal and opposite to each other, and the lake open water season evaporation is equal and opposite to the subsurface contribution into the stream flow; consequently, we overlooked the evaporation and subsurface contribution and groundwater loss parts for the whole season. From field observation, it was approximated that all snow melted prior to 24 June, 2010. From 1 May to 24 June the main source of water was snowmelt and rainfall, following this time (24th June to the end August) the only source of water was rainfall. The predicted and recorded stream flow during 2010 at XS-3 of our study stream is shown in Figure 2.11.

Comparing the model results to the recorded data, it is evident that the performance of both models-especially considering the prevailing field conditions as well as our minimal expectations - are reasonably good in terms of the total volume, but both models were unable to accurately predict recorded flows and capture the peak stream flows. Under-predictions within these models are due to some restrictions, such as hydrological assumptions, ignoring the catchment characteristics, sparse data from a remote weather station, and huge overland flow during the melting period (section 3.7). Flows in the stream increase by orders of

magnitude over a relatively short period of time when snow that has been accumulating for seven to nine months finally melts. The reality is that any type of field measurements, like stream flow measurements, in northern Canada is very expensive, tedious, and time consuming, but meteorological data are available for about 10 to 20 years. So, using the model it is possible to approximate the past 10 to 20 years of stream flows from the meteorological records. In the future, it is recommended that these stream flow predictions from a complete model using detailed data be used for any hydrologic assessment in this watershed region.

2.4.3 Stream Connectivity for Fishpass

Barrenland streams are used mainly for spawning and subsequently as nursery habitat for young-of-the-year (YOY) Arctic grayling, whereas the numerous lakes in the region are used by all ages and species of fish for overwintering (Jones et al. 2003b). To provide complete stream connectivity, no matter how large or small the stream, requires the proper range of flows through a suitable channel configuration (Wesche 1985). The existing stream gross slope (2%) might be fitting for fish migration, but the presence of flat slope at upstream section and cascades with a slope of about 20% at the lower part of the stream, present probable fish barriers (Golder Associates Ltd., 2004). Therefore, the upstream section needs some modifications for a defined channel with consistent slope and the downstream section should retrofit by a fishpass structure to control slopes and flows creating hydraulic characteristics more suitable to fish passage. Stream

bottom substrate size is directly related to water velocity, with larger materials (e.g., rubble, boulder) associated with faster currents, and smaller materials (e.g., silt, sand) associated with slower currents (Wesche 1985). The response shapes of the habitat suitability index graph for Arctic grayling in a coldwater region indicated that the probabilities of habitat use were maximal at bottom substrates with 1.0 to 20.0 cm diameters (Hubert et al. 1985). The predominant substrate class in our stream varied from gravel to boulder where D_{84}= 22 cm and D_{50}= 2.6 cm, providing high quality spawning habitat. A pool-riffle sequence in streams is important in providing cover, resting, and food-producing areas (Wesche 1985). Arctic grayling are found almost exclusively in pools and seldom in riffles unless there are flow refuges (e.g., boulders) in the riffles. Our WIS study stream consisted of riffles and pools in sequence, which is advantageous for fish by providing cover and both resting and food-producing areas.

The analysis of flow duration curves indicate that the low flow variations in XS-1 during 2010 would produce suitable environments for benthic and other communities in a stream, whereas the high flow variations in streams XS-1 and XS-3 during 2009 and XS-3 and XS-4 during 2010 would probably produce stressful environments. For fish migration, the base/minimum flow is an essential matter. In our study stream, Q_{50} flows existed only about 43% of the total study period in 2010, and for the rest of the study period flows were considered sub-optimal for fish migration. To enhanced connectivity and optimize performance, the stream outlet could be controlled to eliminate the initial unconfined peak

discharge; discharges are minimized while flow depth and storage retention is maximized; creating flows suitable to fish migration for longer duration.

Water depth of a stream influences the photosynthetic production of periphytic invertebrate food by regulating the light intensity reaching the substrate. Velocity is also an important parameter in determining distributional patterns of aquatic invertebrates. Increased water velocities increase the exchange rate between the organism and its water supply, thereby promoting respiration and food acquisition. Jones and Tonn (2004) developed resource selection curves for small and large YOY Arctic grayling in natural Barrenlands streams close to our study area. The response shapes for water depth and water velocity indicated that the probabilities of habitat use were maximal at 13 cm and 2 cm/s for small Arctic grayling, and at 58 cm and 10 cm/s for large Arctic grayling, respectively. During our study periods 2009 and 2010, the average maximum depth at several of the cross sections was 12.0-25.0 cm, representing adequate depth for the smallest Arctic grayling, but sub-optimal depths for large YOY (*Table 2-2*). Other cross sections had average highest depths less than 10.0 cm for both years and would thus be sub-optimal for both sizes of Arctic grayling (*Table 2-2*). Based on the maximum cross sectional velocity, the cross sections XS-2 and XS-4 during the first week of July 2009, and XS-2, XS-3 and XS-4 during middle of June 2010, were suitable for both size-classes of Arctic grayling. In contrast, XS-3 during the first week of July 2009, and XS-1 during the middle of June 2010, was only suitable for small Arctic grayling. In 2009, XS-1 was not suitable for either size of

YOY Arctic grayling. At the end of our study period, however, all the cross sections failed to maintain the target velocity (<0.1 cm/s in 2009 and <0.7 cm/s in 2010) required for even small Arctic grayling.

Water temperature plays an important role in regulating the migratory timing and enroute survival of adult salmonids (Macdonald et al. 2000). Water temperature influences the growth of fish both directly, through physiological processes, and indirectly by affecting rates of energy flow and nutrient dynamics (Jones et al. 2003b). Here, 4 °C is assumed as a critical temperature, as stream temperatures below 4 °C (but higher than 0 °C) are considered favorable for upstream migration by mature adults (Falk et al. 1982), and above 4 °C (but less than 11 °C) are considered suitable for spawning of Arctic grayling (Tack 1972). The 7-day moving average of the daily minimum stream temperature at upstream, middle and downstream sections of WIS reached 4 °C during the last week of June in 2009 and mid-June in 2010 (*Figure 2.6*). So, the stream temperature was conducive to upstream migration until the last week of June in 2009 and mid-June in 2010; temperature appears to be suitable for Arctic grayling spawning in the remainder of the time. We have considered the 7-day moving average of the daily minimum rather than average and maximum temperatures, as after this period the stream temperature is above 4 °C for the entire day and night. To better understand the lifecycle of Arctic grayling in the cold water region, the seasonal movements of Arctic grayling fry, juveniles, and adults in small Alaskan streams in relation to the flow and ice regimes is illustrated in Figure 2.12 adapted from

Stewart et al. (2007). Where, the movements occur later in the spring and earlier in the fall, they serve to illustrate the general pattern of movements in response to flow and ice conditions, with the exceptions that in some streams spawners migrate upstream under the ice and fry may extend their stream residence (Deleray 1991).

Water quality is also an important component of stream fish habitat. The response shapes of habitat suitability index graphs for Arctic grayling in coldwater regions indicated that the probabilities of habitat use were maximal at 6 to 12 mg/liter of DO (Hubert et al. 1985), where the average DO in our study stream for both years was 7.4 mg/liter. Also, for general fish habitat, a low pH value (less than 5) indicates acidic conditions; a high pH (greater than 9) indicates alkaline conditions. Many biological processes, such as reproduction, cannot function in acidic or alkaline waters. Total suspended solids less than 25 mg/liter should not be harmful to fish or fish habitat (DFO & DOE 1983). Results indicate that stream water quality in both years (*Table 2-4*) is indicative of high quality fish habitat.

2.5 Summary and Conclusions

The existing pool-riffle sequence stream with its steep slope (gross slope about 2%) and gravel/boulder bed substrate (D_{84} varied from 2.6 to 22 cm) could provide a corridor with high quality habitat suitable for fish migration, but the presence of cascades and scarcity of water most likely present fish barriers

regardless of the remaining instream habitat characteristics. The flow hydrographs, encompassing the early freshet during 2010, demonstrated that stream discharges were maximal in most of the cross sections during the first week of July, and subsequently declined to zero during August, and that median flows existed only about 43 % of the total study period during the exceptionally dry summer of 2010 in the Lac de Gras region. The flow conditions changed from very low to high as water flowed from upstream to downstream due to the additional contributions of meltwater from the larger drainage area as well as subsurface groundwater. High ratios between 90% and 50% flow from flow duration curves indicated reliable low flows in some cross sections of streams, but smaller ratios elsewhere reflected very low flows that were quite small compared to the streams' medium discharge. The lower part of WIS was cooler than the upper-most section of WIS, and the stream temperatures reached 4 °C in all sites during the last week of June in 2009 and mid-June in 2010, resulting in above 4 °C temperatures approximately 80% of the time for both years. Water balance calculations show continuous summer evaporation in addition to groundwater loss, which caused the lake level to decline below threshold levels, ultimately leading to periods of zero outflow. This resulted in an inability to re-establish flow connectivity among the lake and stream due to insufficient rainfall in both years. The attempt to predict the stream flow using the index models for snowmelt and rational methods for stream discharge proved quite satisfactory considering the prevailing field conditions as well as our minimal expectations.

Based on resources selection curves (Jones and Tonn 2004) and seasonal movements (Stewart et al. 2007) for small and large YOY Arctic grayling , the study stream would be suitable for both small and large YOY Arctic grayling at the beginning of the summer, but decline to sub-optimal conditions by mid-August, based on depth (habitat maximal at 13 cm for small and 58 cm for large grayling) and velocity (habitat maximal at 2 cm/s for small and 10 cm/s for large grayling). The stream temperatures (0 to 4 °C) in our study area appeared conducive to upstream migration up to the end and middle of June in 2009 and 2010, respectively, after which increased temperatures (4 to 11 °C) may encourage spawning in Arctic Grayling. Finally, the stream exhibited the water quality necessary for high quality fish habitat. Overall, some sections of the study stream for certain durations of the study period (entire June) appeared to naturally provide suitable habitat for select stages of YOY Arctic grayling, while other sections could provide suitable habitat after certain modifications (creating a defined channel with consistent slope and fishpass structures) and additional outlet flow arrangements or by controlling the stream outlet (discharges are minimized while flow depth and storage retention is maximized) are achieved through the fish habitat compensation project. Overall, this study gives an account of the in-depth eco-hydrologic behavior of an outlet stream in the Barrenlands region of the Northwest Territories, Canada.

2.6 References

Allan, J. D., and Castillo, M. M. (2007). "*Stream ecology: structure and function of running waters*." Published by Springer, Second edition, Dordrecht, Netherlands, pp. 24.

Baevsky, Y. H. (1991). "Physical and water-quality characteristics affecting trout-spawning habitat in the Quashnet River, Cape Cod, Massachusetts: U.S." Geological Survey Water-Resources Investigations Report 91-4045, pp.21.

Bathurst, J. C. (1985). "Flow resistance estimation in mountain rivers." *Journal of Hydraulic Engineering*, *ASCE*, 111, 625–641.

Clausen, B., and Biggs, B. J. F. (2000). "Flow variables for ecological studies in temperate streams: groupings based on covariance." *Journal of Hydrology*, 237,184–197.

Deleray, M. A. (1991). "Movement and utilization of fluvial habitat by age-0 Arctic grayling, and characteristics of spawning adults, in the outlet of Deer Lake, Gallatin County, Montana." M.Sc. Thesis, Montana State University, Bozeman, Montana.

Department of Fisheries and Oceans and Environment Canada, (1983). "A rationale for standards relating to the discharge of sediments into Yukon streams from placer mines." Interdepartmental Committee on Placer Mining, New Westminster, B.C., pp.24.

Eaton, A. K, Rouse, W. R, Lafleur, P., Marsh, P., and Blanken, P. D. (2001). "Surface energy balance of the western and central Canadian subarctic:

variations in the energy balance among five terrain types." *Journal of Climate,* 14, 3692–3703.

Ekati. (2009). "Report on 2008 aquatic effects monitoring program appendix A: Evaluation of Effects." Submitted to BHP Billiton Diamonds Inc., Yellowknife, Northwest Territories, Canada.

Environment Canada. (1991). "Canadian climate normals: 1961–1990." Ottawa. http://www.msc smc.ec.gc.ca/climate/climate_normals/index_e.cfm.

Falk, M. R., Roberge, M. M., Gillman, D. V., and Low, G. (1982). "The Arctic grayling, *Thymallus arcticus* (Pallas), in Providence Creek, Northwest Territories, 1976-79." Canadian Manuscript Rep. Fish. Aqua. Sci., Western Region, Dept. Fish. Oceans, Winnipeg, Manitoba R3T2N6, pp.27.

Gibson, J. J., Edwards, T. W. D., and Prowse, T. D. (1994). "Evaporation in the north: overview of quantitative studies using stable isotopes." Mackenzie Basin Impact Study (MBIS), Interim Report No. 2, S. J. Cohen (Editor), Yellowknife, N.W.T., pp. 138-150.

Golder Associates Ltd. (2001). "Conceptual design and compensation work plan for the fish habitat compensation program." Submitted to Diavik Diamond Mines Inc., Lac de Gras, Northwest Territories, Canada.

Golder Associates Ltd. (2004). "Report on stream fish habitat design for the West Island stream at the Diavik Diamond Mine." Submitted to Diavik Diamond Mines Inc., Calgary, Alberta, Canada.

Harrelson, C. C., Rawlins, C. L., and Potyondy, J. P. (1994). "Stream channel reference sites: an illustrated guide to field technique." Gen. Tech. Rep. RM-

245. Fort Collins, CO: U.S. Department of Agriculture, Forest Service, Rocky Mountain Forest and Range Experiment Station, pp.61.

Hogan, D. L., and Ward, B. R. (1997). "*Watershed Geomorphology and Fish Habitat.*" Chapter 2 in P. A. Slaney and D. Zalkodas [eds.] Fish habitat rehabilitation procedures. Province of B. C., Ministry of Environment, Lands, and Parks, and Ministry of Forests. Watershed Restoration Technical Circular No. 9.

Hubert, W. A., Helzner, R. S., Lee, L. A., and Nelson, P. C. (1985). "Habitat suitability index models and instream flow suitability curves: Arctic grayling riverine populations." U.S. Fish Wild1ife Service, Report 82(10.110), pp.34.

Jones, N. E., and Tonn, W. M. (2004). "Resource selection functions for age-0 Arctic grayling (Thymallus arcticus) and their application to stream habitat compensation." *Canadian Journal of Fisheries and Aquatic Sciences*, 61, 1736–1746.

Jones, N. E., Tonn, W. M., Scrimgeour, G. J., and Katopodis, C. (2003a). "Ecological characteristics of streams in the Barrenlands near Lac de Gras, N.W.T., Canada." *Arctic*, 56(3), 249-261.

Jones, N. E., Tonn, W. M., Scrimgeour, G. J., and Katopodis, C. (2003b). "Productive capacity of an artificial stream in the Canadian Arctic: assessing the effectiveness of fish habitat compensation." *Canadian Journal of Fisheries and Aquatic Sciences*, 60, 849–863.

Kane, D. L., Gieck, R. E., and Hinzman, L.D. (1997). "Snowmelt modeling at small Alaskan Arctic watershed." *Journal of Hydrologic Engineering*, 2(4), 204-210.

Macdonald, S., Foreman, M., Farrell, T., Williams, I., Grout, J., Cass, A., Woodey, J., Enzenhofer, H., Clarke, C., Houtman, R., Donaldson, E., and Barnes, D. (2000). "The influence of extreme temperatures on migrating Fraser River sockeye salmon during the 1998 spawning season." Canadian Technical Report of Fisheries and Aquatic Sciences, No. 2326.

McMahon, T. A. (1982). "World hydrology: does Australia fit?." In hydrology and water resources symposium, Institution of Engineers, Melbourne, pp.1-7.

Mielko, C., and Woo, MK. (2006). "Snowmelt runoff processes in a headwater lake and its catchment, subarctic Canadian shield." *Hydrological Processes,* 20, 987–1000.

Petts, G. E., Bickerton, M. A., Crawford, C., Lerner, D. N., and Evans, D. (1997). "Flow management to sustain groundwater-dominated stream ecosystems." *Hydrological Processes*, 13, 497-513.

Priestley, C. H. S., and Taylor, R. J. (1972). "On the assessment of surface heat flux and evaporation using large scale parameters." *Monthly Weather Review*, 100, 81–92.

Pyrce, R.S. (2004). "Hydrological Low Flow Indices and their Uses." WSC Report No.04-2004, Watershed Science Centre, Peterborough, Ontario, pp. 33.

Quick, M. C., and Pipes, A. (1977). "U.B.C. watershed model." *Hydrological sciences Journal*, 22(1), 153-161.

Ries, K.G., and Friesz, P.J. (2000). "Methods for estimating low-flow statistics for Massachusetts streams." U.S. Geological Survey Water-Resources Investigations Report, pp. 4135.

Schindler, D. W. (2001). "The cumulative effects of climate warming and other human stresses on Canadian freshwaters in the new millennium." *Canadian Journal of Fisheries and Aquatic Sciences*, 58, 18-29.

Spence, C., Rouse, W. R., Worth, D., and Oswald, C. (2003). "Energy budget processes of a small northern lake." *Journal of Hydrometeorology*, 4, 694-701.

Spence, C., and Woo, MK. (2003). "Hydrology of a subarctic Canadian shield: soil-filled valleys." *Journal of Hydrology*, 279, 151–166.

Stewart, D. B., Mochnacz, N. J., Reist, J. D., Carmichael, T. J., and Sawatzky, C. D. (2007). "Fish life history and habitat use in the Northwest Territories: Arctic grayling (Thymallus arcticus)." Canadian Manuscript Report of Fisheries and Aquatic Sciences 2797.

Tack, S. L. (1972). "Distribution, abundance and natural history of the Arctic grayling in the Tanana River drainage." Alaska Department of Fish Game. Federal Aid in Fish Restoration, Annual Repeport of Progress, 13(F-9-5), pp.34.

Thorne, G., Laporte, J., and Clarke, D. (1999). "Water budget of an upland outcrop recharge area in granitic rock terrane of southeastern Manitoba,

Canada." Proceedings of the twelfth International Northern Research basins symposium and workshop. Reykjavik, Iceland, August 23–37, pp. 317–330.

Timoney, K., Kershaw, G. P., and Olesen, D. (1992). "Late winter snow-landscape relationships in the subarctic near Hoarfost River, Great Slave lake, Northwest territories, Canada." *Water Resources Research*, 28(7),1991-1998.

U.S. Fish and Wildlife Service, (1981). "Interim regional policy for New England stream flow recommendations." Region 5 of U.S. Fish and Wildlife Service, Newton Corner, M A.

Wesche, T. A. (1985). "*Stream channel modifications and reclamation structures to enhance fish habitat*." In: The Restoration of Rivers and Streams: Theories and Experience, Butterworth Publishers, Boston.

Wolman, M. G. (1954). "A method of sampling coarse bed material." *Transactions-American Geophysical Union*, 15, 951-956.

Woo, MK. (1990). "*Permafrost Hydrology."* In: Northern Hydrology: Canadian Perspectives, T. D. Prowse and C. S. L. Ommanney, (Editors), NHRI Science Report No. 1, National Hydrology Research Institute, Environment Canada, Saskatoon, Saskatchewan, pp. 63-76.

Woo, MK., and Mielko, C. (2007). "An integrated framework of lake-stream connectivity for a semi-arid, subarctic environment." *Hydrological Processes*, 21, 2668–2674.

Table 2-1 The physical characteristics of the study stream during the years 2009 and 2010.

Year	X-section	Bankfull width (m)	Bankfull depth (m)	Width:Depth	d/D_{50}	d/D_{84}
2009	XS-1	3.33	0.26	12.84	9.98	1.18
	XS-2	0.75	0.15	5.03	5.73	0.68
	XS-3	1.87	0.14	13.19	5.46	0.65
	XS-4	1.07	0.07	14.35	2.86	0.34
2010	XS-1	3.27	0.25	13.25	9.50	1.12
	XS-2	1.35	0.17	8.16	6.38	0.75
	XS-3	1.88	0.16	12.04	6.00	0.71
	XS-4	1.23	0.12	10.25	4.6	0.55
Median	-	1.84	0.16	11.14	6.3	0.75

Table 2-2 Summary statistics of stream hydraulics at all cross sections during 2009 (July-August) and 2010(June-August) study period (dates in parentheses represent the date of occurrence).

Year	Parameter	Statistic	XS-1	XS-2	XS-3	XS-4
2009	Discharge* (m^3/s)	Max	0.01 (July 1)	0.0163 (July 1)	0.013 (July 1)	0.0121 (July 1)
		Min	0 (Aug 8)	-	0.0014 (Aug 14)	-
	Velocity** (cm/s)	Max	1.0 (July 1)	11.09 (July 1)	4.0 (July 1)	13.08 (July 1)
		Min	0 (Aug 8)	-	-	-
	Depth (cm)	Max	33.0 (July 1)	16.60 (July 1)	24.50 (July 1)	9.30 (July 1)
		Min	16.10 (Aug 8)	-	11.70 (Aug 14)	-
2010	Discharge (m3/s)	Max	0.0274 (July 2)	0.0588 (June 17)	0.2797 (June 6)	0.3745 (July 2)
		Min	0.0008 (Aug 29)	0.0006 (Aug 6)	0 (Aug 31)	0 (Aug 22)
	Velocity** (cm/s)	Max	2.95 (June 17)	19.17 (June17)	24.51 (June 5)	46.10 (June 19)
		Min	0.39 (Aug 8)	0.69 (Aug 6)	0.29 (Aug 8)	-
	Depth (cm)	Max	36.19 (July 2)	46.0 (June 17)	32.45 (June 6)	20.61 (July 2)
		Min	15.39 (Aug 29)	21.0 (Aug 6)	Dry (Aug 31)	Dry (Aug 22)

* Based on direct measured data as continuous data were not collected prior to July 18, 2009

** Maximum and minimum velocity based on measured data

Table 2-3 The estimated values of Q_{50} and Q_{90} for different cross sections of WIS in 2009 and 2010.

Year	X-section	Mean flow (m^3/s)	Median flow (Q_{50}) (m^3/s)	Q_{90} (m^3/s)	Skewness	Coefficient of Variation	Q_{90}/Q_{50}
2009	XS-1	0.0025	0.0020	0.0002	1.270	0.980	0.090
	XS-3	0.0027	0.0018	0.0015	1.510	0.970	0.830
2010	XS-1	0.0108	0.0100	0.0020	1.080	0.640	0.200
	XS-3	0.0153	0.0060	0.00001	2.560	1.760	0.002
	XS-4	0.0590	0.0110	0.00001	5.362	1.550	0.001

Table 2-4 Measured chemical characteristics at the discharge measurement cross sections of the stream during 2009 and 2010.

Date	X section	pH	DO (mg/ liter)	Conductivity (ms/cm)	TSS (mg/ liter)
31st July 2009	XS-1	6.3	10.4	19.4	2.0
	XS-2	5.1	7.2	24.3	2.0
	XS-3	5.4	7.9	24.3	4.0
	XS-4	5.5	8.3	23.4	7.0
8th August 2010	XS-1	8.6	9.4	14.9	3.0
	XS-2	7.6	5.4	31.0	3.0
	XS-3	7.7	6.6	24.3	4.0
	XS-4	7.5	4.3	23.8	2.0

Table 2-5 Water balance (in m^3/day) of the study lake in 2009 and 2010. R, Q_i, Q_o, and ΔS were measured, E was calculated from meterological data, and Q_b* was determined by difference calculation.

Year	Period	P (m^3/day)	E (m^3/day)	Measured Q_o (m^3/day)	Observed ΔS (m^3/day)	Q_b^* (m^3/day)
2009	July 1 to August 14	804	487	220	-364	-461
2010	June 25 to August 15	330	610	718	-197	801

Table 2-6 The total number of days that the daily discharge is greater than the 50th percentile (Q_{50}) of the daily discharge during 2010.

Year	X-section	Total days	% of total duration
2010	XS-1	39	46
	XS-3	38	44
	XS-4	33	40

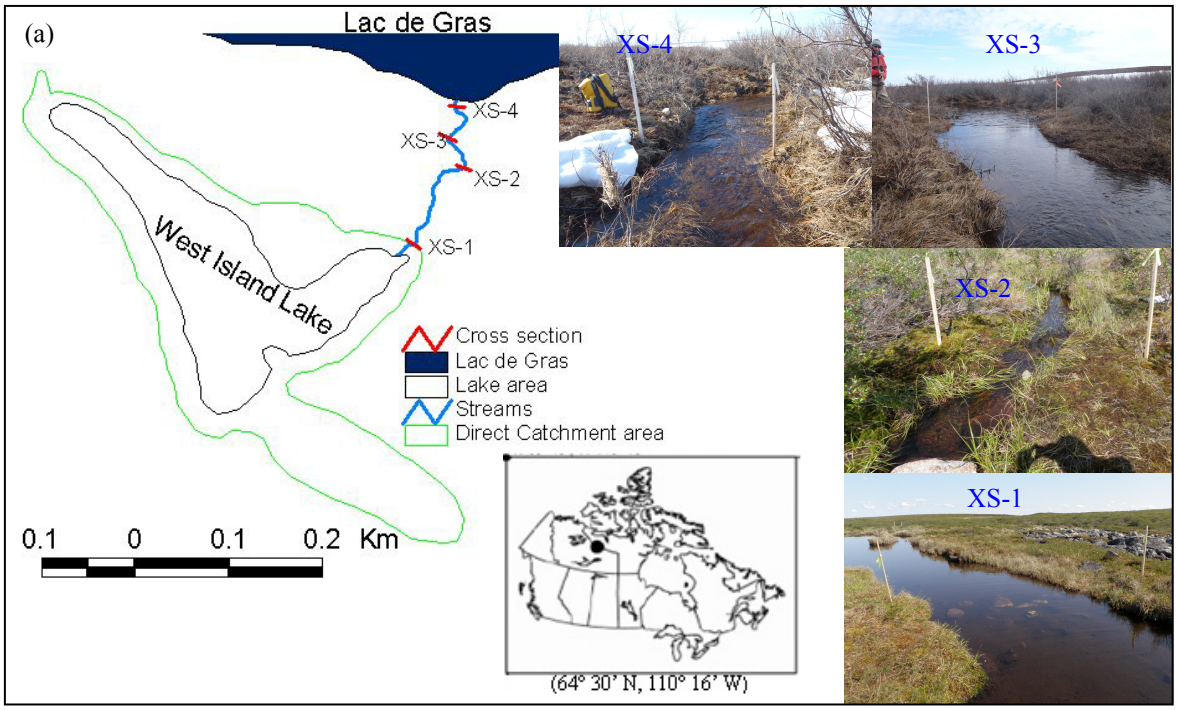

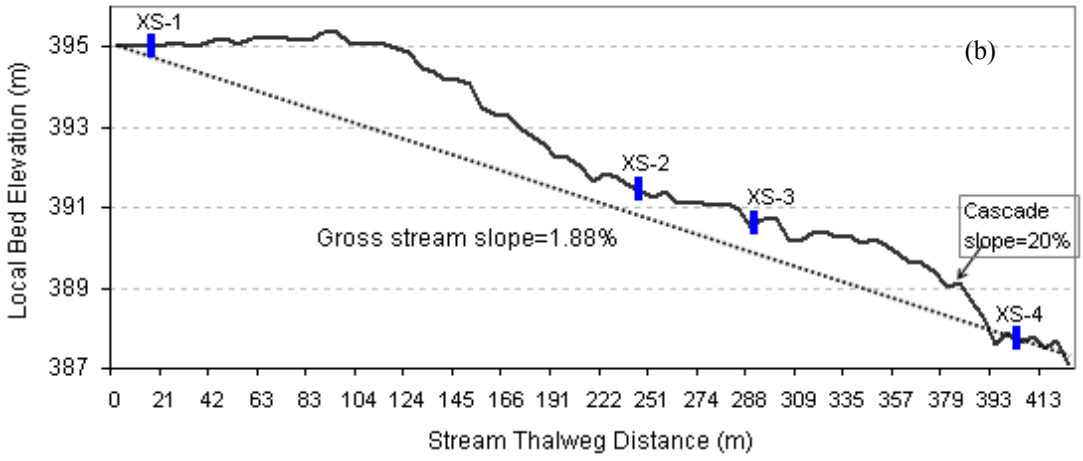

Figure 2.1 (a) West Island study site with photos of the four stream cross sections and (b) the bed profiles of the study stream showing the cross sections and cascade locations.

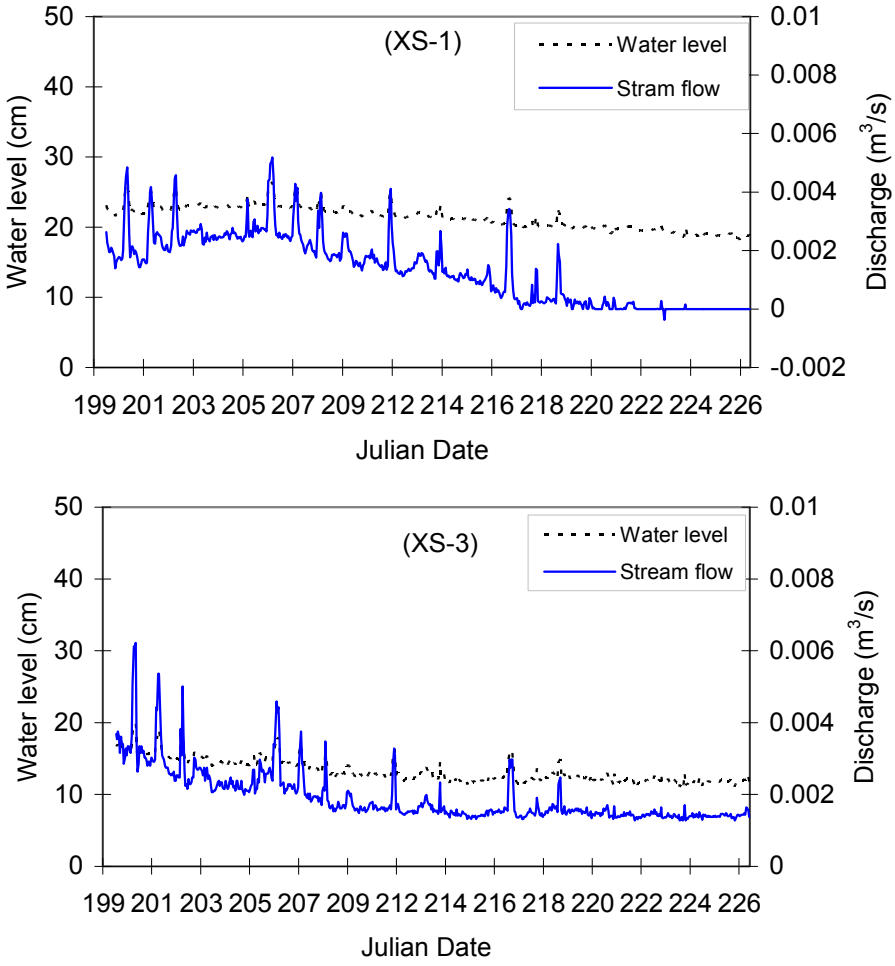

Figure 2.2 The hourly average water level and discharge at sections XS-1 and XS-3 during 2009.

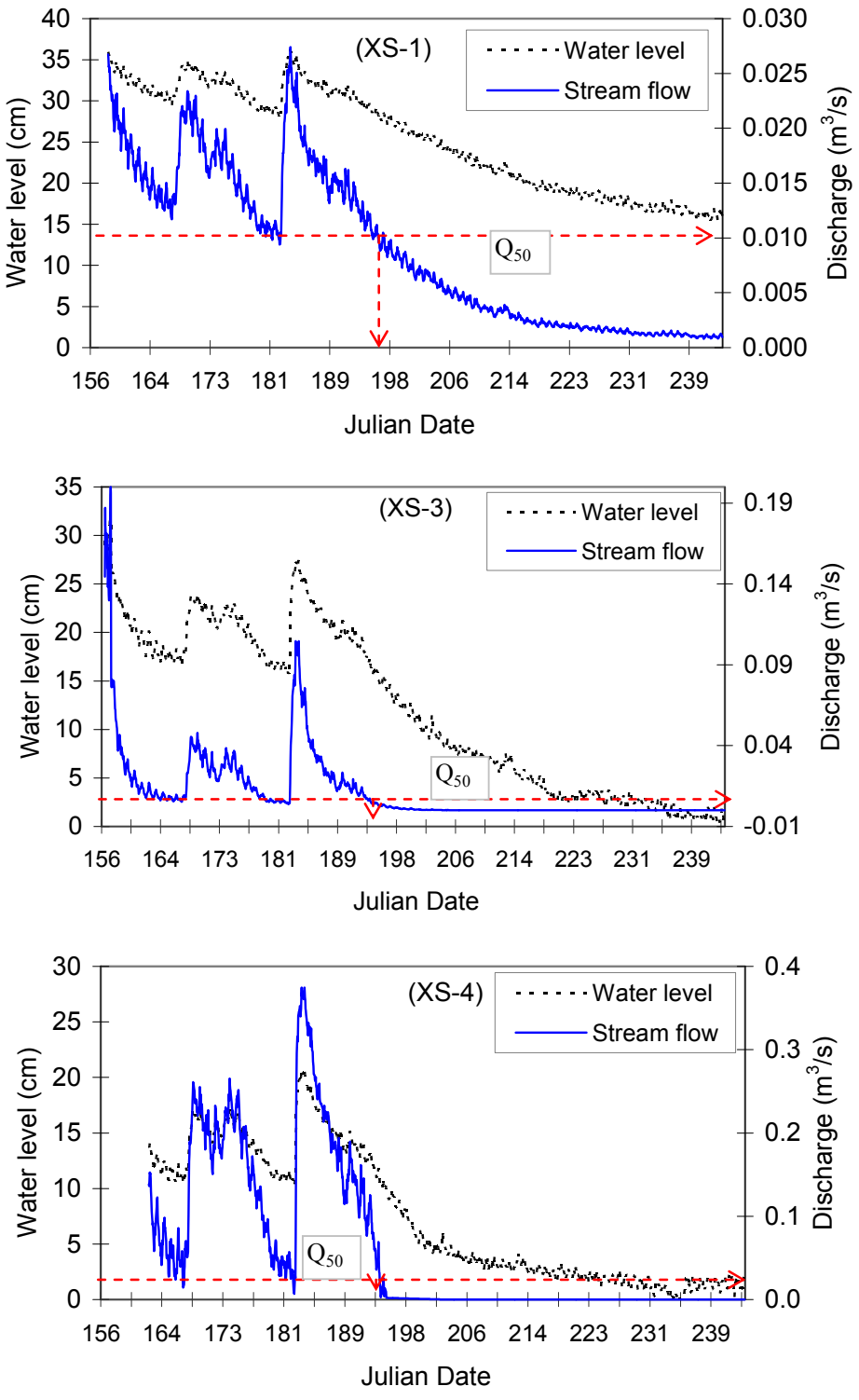

Figure 2.3 The hourly average water level and discharge at sections XS-1, XS-3, and XS-4 during 2010, showing the Q_{50} discharge level (arrow sign indicates the date up to which the corresponding Q_{50} flows exist).

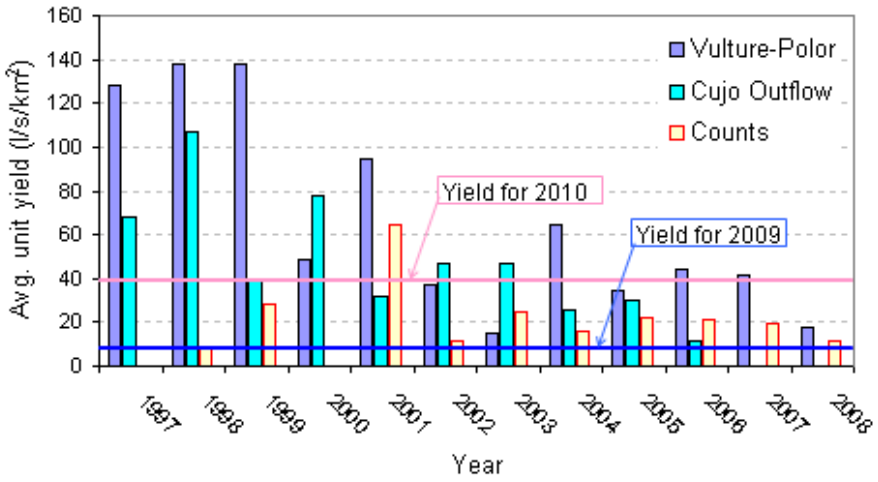

Figure 2.4 The variation of average unit yield (l/s/km^2) of Vulture-Polar, Cujo, and Counts outflow streams from 1997 to 2008 in the Koala watershed and from our study stream during 2009 and 2010 (indicated by blue and red lines, respectively).

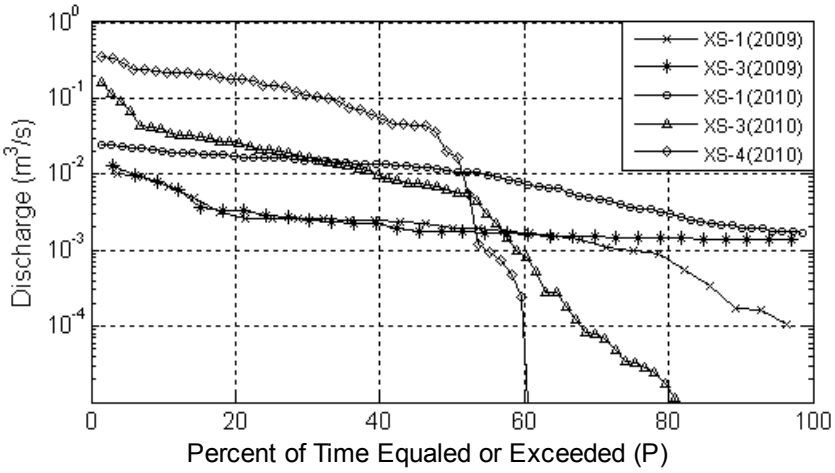

Figure 2.5 The FDC for different sections of WIS during 2009 and 2010.

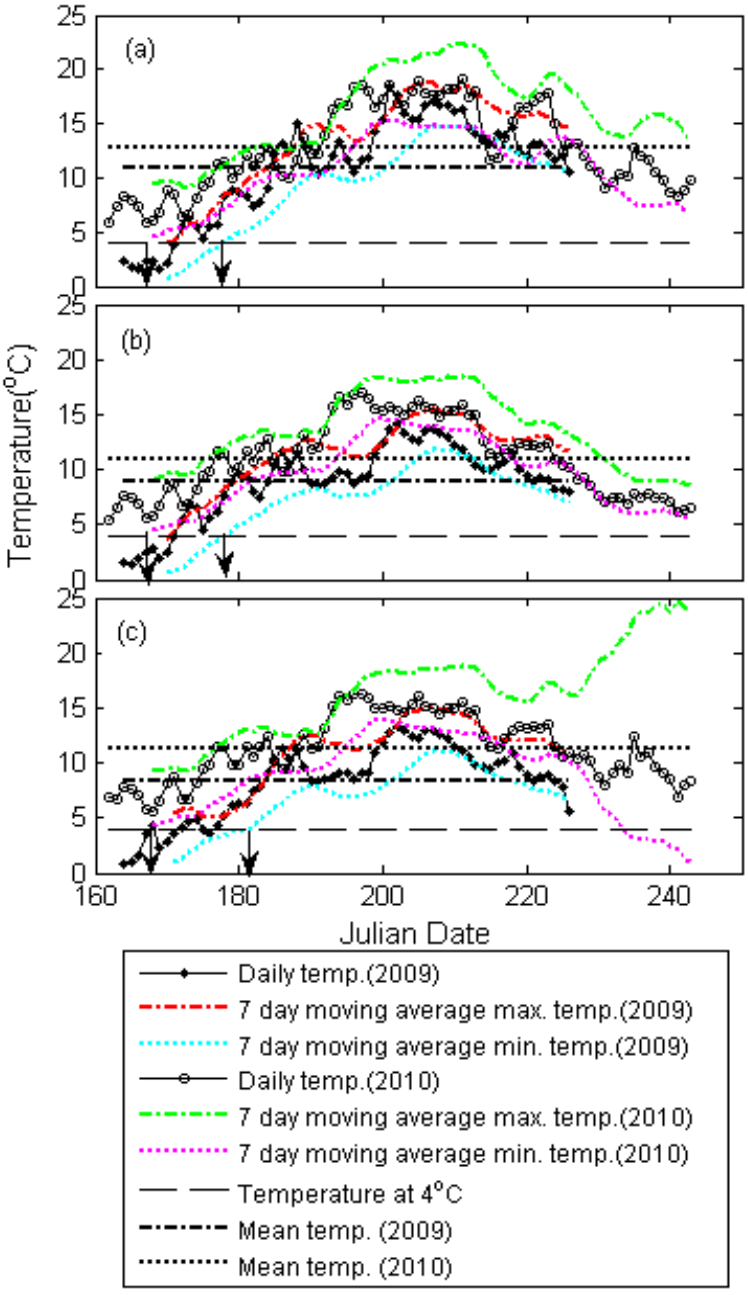

Figure 2.6 The comparison of stream temperatures in the WIS: (a) Upstream, (b) Middle, and (c) Downstream sections during June to August 2009 and 2010 (arrow sign indicates the date at which the 7-day moving average of daily minimum temperature rises above 4 °C).

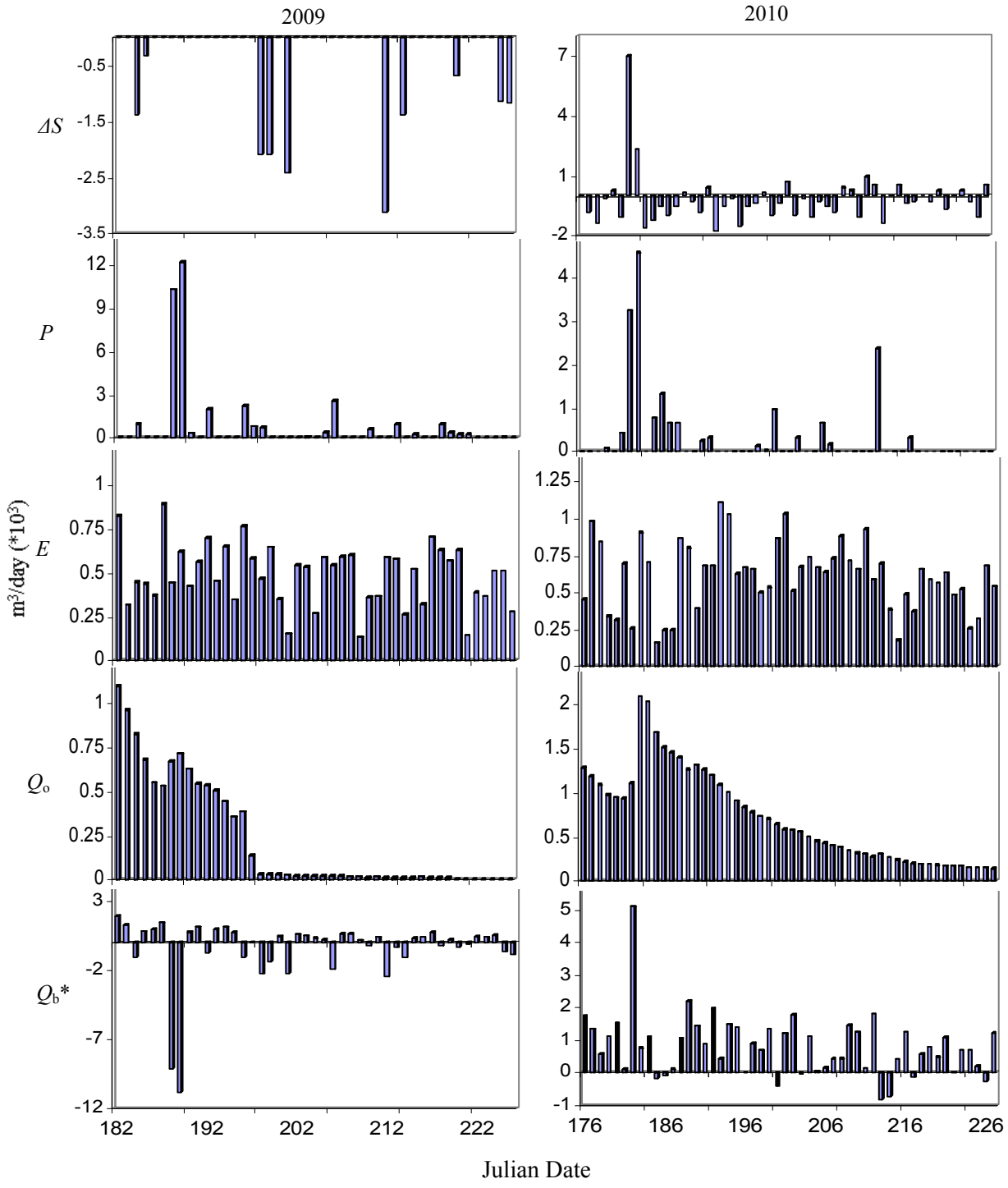

Figure 2.7 Daily variation of water balance components in m^3/day of our study lake during 2009 and 2010.

Figure 2.8 Overland flow during snow melt period (second week of June) in WIS.

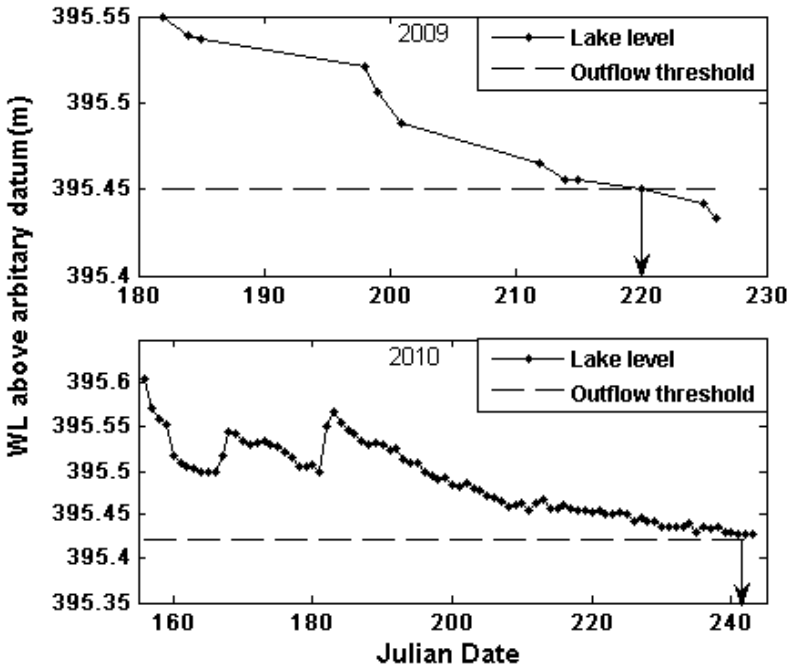

Figure 2.9 Fluctuations of lake storage relative to outflow thresholds for 2009 and 2010 (arrow sign indicates the date at which the corresponding stream flow equaled zero).

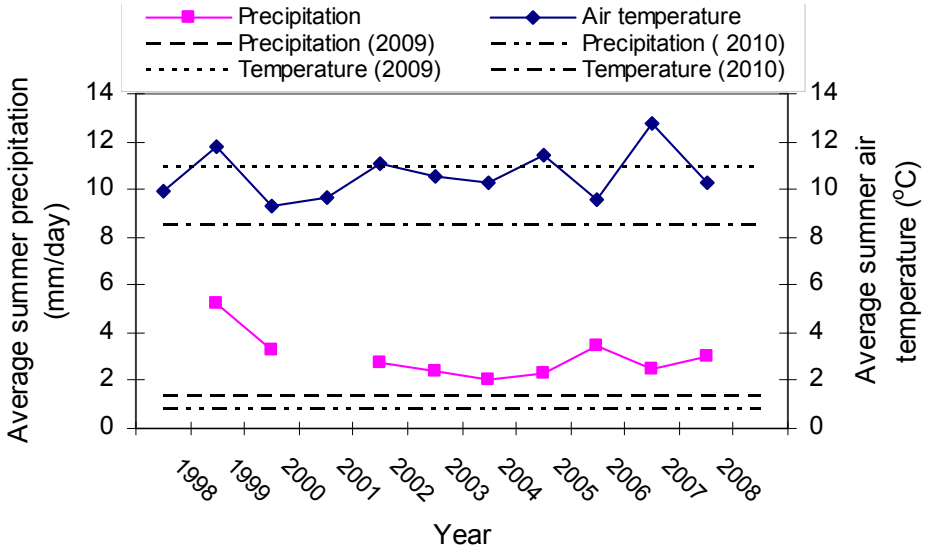

Figure 2.10 The yearly variation of average air daily temperature and precipitation during the summer period, 1998-2008, compared to the DDMI meteorological station data for the same period in 2009 and 2010.

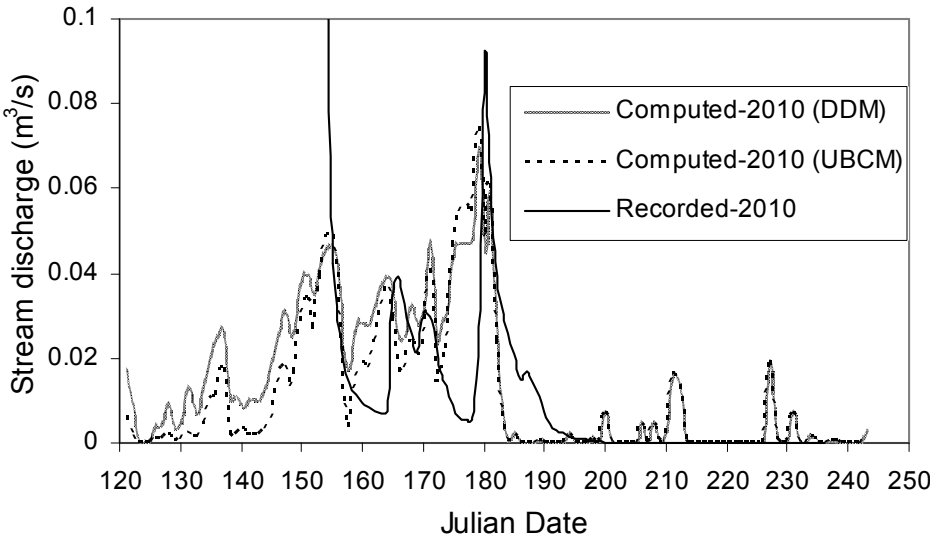

Figure 2.11 The predicted and recorded stream flow during 2010 at XS-3.

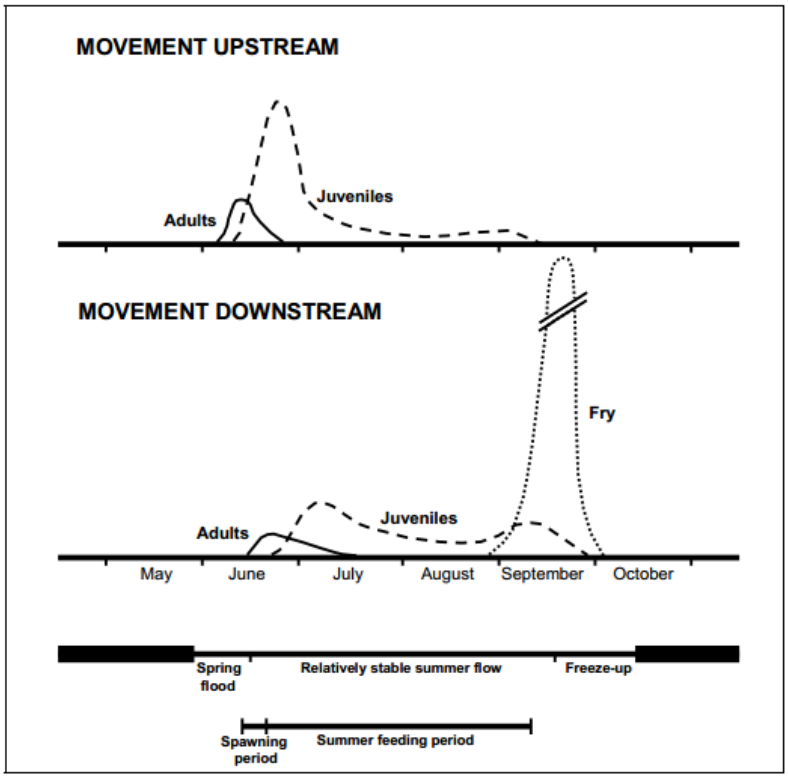

Figure 2.12 Schematic diagram of Arctic grayling movements in small Alaskan streams (adapted from Stewart et al. 2007).

CHAPTER 3

Hydraulic Geometry and Resistance to Flow in Headwater Streams in the Northwest Territories, Canada*

3.1 Introduction

The term 'hydraulic geometry' (downstream and at-a-station) quantitatively describes the relationship among principal hydraulic variables of river width, depth, and velocity with changing discharge. Downstream hydraulic geometry deals with spatial variations in channel properties at a reference discharge (Knighton 1998). At-a-station hydraulic geometry deals with temporal variations in flow variables as discharge fluctuates at a cross section (Knighton 1998). A number of hydraulic geometry studies have been reported since the classic work of Leopold and Maddock (1953). These include studies of at-a-station hydraulic geometry on large and lowland rivers by Ponton (1972) and Park (1977), and small and steep streams with low flow by Wolman (1955), Knighton (1975, 1998), Castro and Jackson (2001), Lee and Ferguson, (2002), and Reid et al. (2010). The hydraulic geometry technique is applied worldwide (Park 1977) to determine the degree to which rivers respond to different sets of imposed constraints in varied geographic settings (Reid et al. 2010). Hydraulic geometry

*The content of this chapter has been published as: Baki et al. (2012b). "Hydraulic Geometry and Resistance to Flow in Small Headwater Streams in the Northwest Territories, Canada." *Canadian Journal of Civil Engineering*, 39(12): 1252-1263.

has been employed in a range of river management activities (Ferguson 1986). Recent applications estimate minimum flow requirements for fish passage and assess available fish habitat (Jowett 1998).

In contrast with hydraulic geometry, flow resistance describes the mechanism in streams by which physical shape and bed roughness of the channel control flow depth, width, and velocity. Bathurst (1993) suggests total resistance is composed of three primary components: (i) boundary, (ii) channel, and (iii) free surface resistance. Boundary resistance is caused by protrusion of individual grains (grain resistance) from the bed into the flow and the pressure differences over bed forms (form resistance). Channel resistance is associated with undulations in the channel bed and banks as well as alterations in channel plan form and cross-sectional shape. Free surface resistance is caused by disruptions in water surface by waves and abrupt changes in gradients (e.g. hydraulic jumps) (Bathurst 1993). Theoretical aspects of open channel flow resistance are documented by Leopold et al. (1960) and Bathurst (1982). Flow resistance under low flow conditions in mountain streams have been studied where various equations and modifications of resistance coefficients have been proposed (Bathurst et al. 1981; Jarrett 1984; Bathurst 2002; Reid and Hickin 2008). For high-gradient boulder-bed streams, there is no satisfactory flow resistance equation and no single unified means for quantifying the wide variation in resistance (Bathurst 1985). Bathurst (2002) discusses the requirement of flow resistance relationships for "flood routing, prediction of flow depths and velocities for design floods, channel flood capacity

estimation and the indirect estimation of flood discharges by the slope-area technique."

The Northwest Territories of Canada occupy an area of 1.35 million km^2, 13.5% of the total land area of Canada (Statistics Canada 2005). This region is densely populated with shallow lakes and their interconnecting streams; the landscape is characterized by low topographic relief, poorly integrated drainages, and continuous permafrost (Jones et al. 2003). Many chains of lakes and interconnecting streams have been formed to comprise 21% of the landscape as a result of extensive glacial activity in conjunction with relatively low (approximately 50 m) topographical relief (Jones et al. 2003). The hydrological regime of these streams is described by long cold winters where processes are relatively dormant due to fully frozen streams, brief spring snowmelt periods with high stream flow, and short summers with low stream flow (Woo 1990). Despite their abundance, there is no literature on hydraulic geometry and flow resistance for these intermittent head-water streams. There are limited studies on hydrological and ecological characteristics of Canada's northern lakes and streams (Jones et al. 2003 and Jones and Tonn 2004).

Motivation of this study is to assess stream habitat for a fish habitat compensation project. Focus is given to at-a-station hydraulic geometry and flow resistance in head-water streams with large scale roughness in Canada's Northwest Territories. The purpose of this study is to investigate the nature of at-a-station hydraulic

geometry of these intermittent headwater streams; define a set of hydraulic geometry relationships in an unstudied geographic area; examine the nature of flow resistance of these streams with large scale roughness; and compare our results with other relevant studies. Therefore, this study addresses a general question: what is the nature of at-a-station hydraulic geometry and flow resistance in head-water streams of the Barrenlands? Results from this study will increase our ability to understand the nature and variability of at-a-station hydraulic geometry relationships and flow resistance in an unstudied geographic region of the Northwest Territories, Canada.

3.2 Study Area and Sites Selection

The study area is located in the Northwest Territories of Canada, centered at the Diavik Diamond Mines, Inc. (DDMI) mine site (64° 30' N, 110° 16' W), in the greater Lac de Gras watershed, approximately 320 km northeast of Yellowknife, in an area commonly referred to as the Barrenlands (*Figure 3.1*). Four sites comprised of a total six streams were selected for this study. All study sites were located around the mine site, which included: West Island (WI), which has a single stream (WIS); Reference Two (R2), which has a single stream (R2S); Mainland (M), which has two streams (M1S and M2S); and Reference Six (R6), which has two streams (R6S1 and R6S2) (*Figure 3.1*). Photographs of study streams during summer 2010 are presented in Figure 3.2. These four sites are located within the same watershed, which minimizes "variability of stream

channel geometry produced by the governing controls of watershed geology, glacial history and hydrology" as discussed by Reid (2005).

Study sites were chosen based on their similar geophysical characteristics after an extensive reconnaissance survey. Several features of the study sites make them well suited to the study of hydraulic geometry and flow resistance. (1) Head-water streams: each stream is the outlet from a head-water lake of similar size. Direct catchment area of each lake ranges from 8.5 to 48.0 ha with a mean of 22.9 ha (*Table 3-1*). (2) Steep slopes: all streams have steep bed slopes ranging from 1.0 to 2.2% with a mean of 2% (*Table 3-1*). Bathurst (2002) characterized that the bed slopes for the steep mountain streams ranged from 0.1 to 5%. (3) Narrow streams: average bankfull width varies from 2.6 to 3.7 m with a mean of 3.0 m. (4) Large-scale roughness: bottom substrate of all streams cover a wide range of grain sizes from silt to boulders (0.0625 to 256 mm). The relative submergence d/D_{84} ranges from 0.5 to 1.3, with a mean value of 0.8, where d is the cross sectional mean water depth and D_{84} is the 84-percentile bed material size. According to the stream roughness classification (Bathurst, 1985), study stream characteristics indicate large-scale roughness ($d/D_{84}<1.0$). In all study streams, few cross sections have boulders protruding through the water surface. Most cross sections have fully submerged boulders acting as large scale roughness elements that are partly imbedded in soil (*Figure 3.2*). Majority of detailed study cross sections consist of very few to no submerged boulders at all. (5) Morphology: streams have similar morphologies that vary from plane bed to cascades, including pool-riffle

sequences. Many drowned shrubs and small pieces of woody debris are in the channels, and stream banks are stable having exposed roots and grass throughout. Finally, (6) flow hydrograph: all streams have similar flow variation over summer periods. Snow pack melts rapidly during freshet, creating a large peak in discharge and then a sudden decline in flow (*Figure 3.3*). Stream discharge ranges over two orders of magnitude, from 0.0025 to 0.11 m^3/s, indicating seasonal variation in mean daily discharge is moderately high, ranging from 25 to 90 times of minimum summer flows at all sites.

3.3 Study Methods

3.3.1 Field Measurements

Data were collected from June to August 2010. A total of nine cross sections (four in WIS (XS-1, XS-2, XS-3 and XS-4, and one in each of R2S, M1S, M2S, R6S1, and R6S2) were chosen for detailed study. Sections were selected from a stream reach that was readily and safely accessible and provided a representative section of the entire natural stream. At each cross section, discharge was measured over multiple days (5 to 11) at various stages, altering from maximum to minimum, using the area-velocity method (Linsley et al. 1982). Water surface width (*W*) was measured using a surveyor's tape stretched perpendicular to flow across the stream. Each transect was divided into at least ten cells; additional cells were added wherever stream width exceeded 2.0 m. Measurements of flow depth were taken using a metre stick at 10 or more equally spaced locations along the width

of the cross section. As channels were relatively narrow (bankfull width ranging from 2.64 to 3.67 m) any significant deviations from uniform depth (i.e. large boulders) had multiple measurements taken over the irregularity. Each measurement represented at most 10% of the channel bed. Velocity measurements were taken using a Marsh-McBirney (Model 2000 Flo-Mate) current meter. Measurements of velocity were taken at 0.6 of the depth from surface, over 20 seconds at each cell. Discharge for each cell was calculated by multiplying midpoint depth by cell width by velocity. Total stream discharge (Q) is the sum of each cell discharge. Total flow area (A) across the entire cross section was obtained from summing individual cell areas. Finally, cross sectional mean water depth (d) was calculated from $(d = A/W)$ and cross sectional mean velocity (V) was calculated from $(V = Q/A)$. Assuming a rectangular shape, hydraulic radius (R) was calculated from $R = A/(2d + W)$.

A Total Station (Model, Leica TC407) was used to conduct a detailed survey of stream bathymetry. Stream water surface slope was measured by trigonometric levelling along each flow measurement cross section, considering 10.0 m reaches to a distance of 5.0 m on each side of the section. Stream gross bed slope was determined considering the entire stream length. Water surface slope was used rather than channel gross bed slope as each stream comprised of one or more cascades which produce higher energy gradients compared to gross bed slope. Stream bed materials were sampled by the random selection "pebble count" method, using a total of 100 particles in each transect (number of transects based

on stream length) along the stream (Wolman 1954). This method requires the investigator to measure the intermediate dimension of particles encountered every step while walking through the stream, taking care to sample the entire site equally. Size distribution of stream bed material was plotted as cumulative percentage frequency curves; D_{84} values were subsequently extracted. The bed particle size distribution of West Island stream (WIS) based on "pebble count" method is shown in Figure 3.4 and may be representative of all sites. The distribution curve is more flat and uneven due to a wide range of particle sizes in the stream bed. This bed condition is considered as gap-graded boundary materials (Holtz and Kovacs 1981). The grain-sorting coefficient (Millar 1999), $\sigma = D_{84} / D_{50}$, is about 11, indicating a poorly sorted bed. For a natural gravel bed river, the average value of σ is about 2 (Bathurst 1985).

Measurement uncertainties in all field-based studies lead to prediction uncertainties. Calculation of hydraulic geometry and resistance to flow requires direct measurement of water surface width, water depth, point velocity, stream discharge, water surface slope, and bed materials. Each measurement is subject to error. As the streams are very narrow, the maximum error associated with water surface width measurement is 1.5% on both banks. Maximum measurement error associated with shallow water depth is ±5%; the sum of ±1% error due to water surface waves, ±2.5% due to soft and uneven streambeds, and ±1.5% due to inclination of the vertical stick (10º for 20.0 cm deep cross-section). Point velocity measurement errors are mainly associated with alignment of the instrument and

unsteadiness of meter reading. According to the flow meter manufacturer, if the instrument is aligned at an angle of 10º from flow direction, error is ±1.5% of actual velocity (Marsh-McBirney 1990). Three velocity readings were recorded at each point over 3×20 seconds to avoid unsteady meter readings and point velocity was calculated as the average of the three measurements. The accuracy level of a Marsh-McBirney current meter is ±2% (Marsh-McBirney 1990). Cumulatively, these errors lead to a maximum error of ±5%. Therefore, measurements of stream discharge using classical area-velocity methodology interrelated with water surface width, water depth, and point velocity, may introduce an error of 10 to 15%. Water surface slope measurement errors are mainly associated with the true location of the reflector rod at water level. Accurate elevations were ensured by placing the rod on a stable surface adjacent to the water level. The accuracy level of the Total Station (Model, Leica TC407) is 2-5mm/km. Measurements were taken within 0.5 km of the total station, resulting in an error of approximately 1 to 2% for water surface slope. Bed material size measurement is more difficult for boulder-bed streams by pebble count. Unfortunately, no information is currently available regarding the accuracy of the pebble count method to achieve a prescribed level of accuracy. Error in measuring bed material size was estimated by the method of Hey and Thorne (1983) to be ±15%. According to Reid (2005), in many field-based geomorphic studies, variability in site conditions is larger than measurement error; selecting a fully representative range of field sites for all process variability is more important than minimizing measurement error. Knighton (1977) explains consistency in sampling procedures will usually result

in minimal measurement error, contributing only a small amount of scatter about regression lines.

3.3.2 Hydraulic Geometry

According to power function theory (Leopold and Maddock 1953), assuming that river flow is steady and uniform, at-a-station hydraulic geometry relationships may be fitted to power laws as:

$$W = aQ^b \tag{3.1}$$

$$d = cQ^t \tag{3.2}$$

$$V = pQ^l \tag{3.3}$$

Where W, d, and V are top width, mean depth, and mean velocity, respectively; a, c, and p are numerical constants and b, t, and l are numerical exponents. To satisfy the continuity equation for rectangular channels, the sum of exponents b, t, and l, as well as the product of constants a, c, and p, should equal 1.0, while the product of W, d, and V should equal Q. These relationships have been shown to hold through ranges of discharge (Roy et al. 1988) up to the bankfull stage.

At-a-station hydraulic exponents were calculated by performing linear regression on the logarithm of flow versus logarithms of water surface width, depth, and velocity at all nine cross sections for each measurement of stream discharge. Finally, based on the mean average of regression coefficients a, c, and p and exponents b, t, and l, a set of hydraulic geometry relationships were developed.

3.3.3 Flow Resistance

Flow resistance may be quantified by the Darcy-Weisbach friction factor *f*, Manning's *n*, and Chézy's *C*:

$$v/v_* = (8/f)^{1/2} = R^{1/3}/(gn^2) = (C^2/g) \tag{3.4}$$

where, $V_* = \sqrt{gRS_0}$ is the bed shear velocity, *g* is the gravitational acceleration, *R* is the hydraulic radius, and S_0 is the channel slope. These classic equations implicitly account for the boundary shear stress (Jordanova 2008). Therefore, at low flow conditions where flow depths are greater than the size of roughness elements, resistance is dominated by form drag due to pressure differences over bed forms (Jordanova 2008).

Keulegan (1938) integrated the logarithmic velocity profile for a turbulent boundary layer and applied it over the entire cross section. He suggested that the logarithmic form of flow resistance based on the correlation of Darcy-Weisbach f can be related to the roughness length (k_s) through the equation:

$$\sqrt{\frac{1}{f}} = 2.03\log\left(\frac{12.2R}{k_s}\right) \tag{3.5}$$

In this equation, the effective roughness length (k_s) is usually equal to D_{50} (the median size of bed materials) during the absence of form resistance for well-sorted sediment (Reid and Hickin 2008). In gravel bed rivers for setting $k_s = D_{50}$, the above equation estimates lower values of flow resistance (Millar 1999). For natural streams where the bed is composed of poorly sorted boundary materials

and both grain and form roughness components are present, skin resistance to flow is enhanced by form drag on larger clusters. k_s may then be expressed as a function of bed material size, $k_s = mD_*$, where *m* represents the form roughness component of the system (Bray 1982) and D_* is often set as D_{50} or D_{84} (84-percentile bed material size) of the size distribution. Here, D_* was set as D_{84} rather than D_{50} as Bathurst (2002) proposed that "relative submergence based on D_{84} is an excellent primary predictor of the resistance function $\sqrt{1/f}$". The resistance function is inversely related to relative roughness area, which is the ratio between total cross sectional area to projected boulder area (Bathurst 1985). Hey (1979) by empirical study and Wiberg and Smith (1991) by theoretical analysis observed that D_{84} is the dominant sediment length scale for flow over non-uniform bed material. In mountainous settings, Millar (1999) concluded that form resistance dominates shear-friction resistance, contributing up to 90% of total resistance. After 1938, researchers suggested different forms (logarithmic, power, numerical, etc.) of flow resistance equations for different situations. Subsequent to Keulegan, Hey (1979) proposed a modified equation based on D_{84}:

$$\sqrt{\frac{1}{f}} = 1.987 \log\left(\frac{eR}{3.5D_{84}}\right) \tag{3.6}$$

Where *e* is the function of stream slope varying from 11.1-13.46 for a gravel bed river having slopes of up to 2%. The modified equation of Keulegan by Thompson and Campbell (1979) is:

$$\sqrt{\frac{1}{f}} = 2.03 \log\left(\frac{12.2R}{2.37D_{84}}\right)\left(1 - \frac{0.237D_{84}}{R}\right) \tag{3.7}$$

The additional term in this equation allows for drag on large obstacles which partly block flow. Bathurst (1985) derived a more suitable empirical equation for mountain streams:

$$\sqrt{\frac{1}{f}} = 1.987 \log\left(\frac{R}{D_{84}}\right) + 1.414 \tag{3.8}$$

Beyond the above semi-logarithmic law, Bathurst (2002) proposed the power law of flow resistance for mountain rivers with $d/D_{84}<11$ and $S_0>0.8\%$:

$$\sqrt{\frac{1}{f}} = 1.1\left(\frac{d}{D_{84}}\right)^{0.93} \tag{3.9}$$

where d is the mean flow depth (approximately equal to hydraulic radius for typical mountain river cross sections).

Initially, flow resistance was calculated using Eq. 3.4 from primary flow-variables and water surface slope for each cross section, which yield 71 individual estimates of both f and n. To complete this analysis, the stream hydraulic radius (R) was used, as resistance is strongly dependent on it. R may be approximated by flow depth (Bathurst 2002). Relationships between resistance coefficients (Manning's n and Darcy-Weisbach f) and relative roughness (R/D_{84}) in our study sites were analyzed using power equations:

$$n = y(R/D_{84})^z \tag{3.10}$$

$$f = q(R/D_{84})^x \tag{3.11}$$

where y and q are numerical constants and z and x are numerical exponents. Power equations were proposed for estimating Darcy-Weisbach f and Manning's

n at different relative roughness. Variation of $\sqrt{1/f}$ with relative roughness (R/D_{84}) was compared with logarithmic laws (Eqs. 3.6, 3.7, and 3.8) and Bathurst's (2002) proposed power law (Eq. 3.9). Individual site/cross sections were adjusted with variation of form roughness component (m) values in Keulegan function curves.

3.4 Results and Discussion

3.4.1 Hydraulic Geometry

At-a-station hydraulic geometry relationships, derived from 9 individual sets of field data, reveal that water-surface width (W), mean water depth (d), and mean flow velocity (V) all increased with increasing discharge at all sections. These relationships are described by positive exponents, where mean water surface width exponent (b) varies from 0 (M1S, no change in width) to 0.40 (R6S1) and has a mean value of 0.14 (*Table 3-2*). The mean water depth exponent (t) ranges from 0.10 (R6S1) to 0.27 (XS-3), is less variable than the width exponent, and has a higher mean value of 0.17 (*Table 3-2*). Minimum width and depth exponents in M1S and R6S1, respectively, indicate that water surface width and depth do not vary significantly with discharge. Velocity exponent (l) ranges from 0.43 (XS-4) to 0.85 (M1S), has a mean value of 0.65, and distribution is symmetric about the mean. Mean values of the velocity exponent are greater than mean width and depth exponents combined. Therefore, mean velocity increased faster with discharge than with width or depth at each field site. In all study cross sections,

the velocity exponent (l) exceeded the width exponent (b) and mean depth exponent (t), and is greater than the sum of b and t in 7 out of 9 study cross sections (*Figure 3.5*) demonstrating the dominant role of velocity in accommodating changing discharge in headwater streams. This is in contrast to the general pattern of at-a-station hydraulic geometry for lowland rivers, and consistent with expectations for steep shallow streams (Lee and Ferguson 2002). Depth exponents (t) are greater than width exponents (b) in six out of nine cross sections (*Figure 3.5*), indicating that a decreasing width/depth ratio is positively correlated with discharge (Reid et al. 2010) thus channel cross sectional shapes are characterized as trapezoidal or parabolic (Leopold and Maddock 1953). As expected, this condition corresponds to XS-1, XS-3, XS-4, M2S, and R2S cross sections where banks are relatively resistant to erosion (Rhodes 1977). The remaining three cross sections (XS-2, R6S1, and R6S2) had $t<b$, indicating that width/depth ratio increases with increasing discharge and thus channel cross sectional shapes are characterized as convex downwards. In M1S, ratio of water surface width to depth decreases with increasing discharge at a rate faster than other sections, because $b=0$ and $t+l \cong 1.0$ (Ferguson 1986). This condition represents a rectangular cross section due to the presence of cut at both banks.

Power curves fit the data quite well throughout the data range at each cross-section, as reflected in the R^2 values. For width, R^2 values range from 0.35 to 0.94, with a mean value of 0.83; only one section had an R^2 value of 0.35 and the remainder of sections had $R^2 > 0.77$ (*Table 3-2*). For mean water depth, R^2 values

ranged from 0.46 to 0.94, with a mean value of 0.85; in 6 out of 9 cross sections R^2 is > 0.90. For velocity, R^2 ranges from 0.89 to 1.0, with a mean value of 0.97. Relationships presented include well established correlation because Q, by definition, is dependent of W, d, and V. A well established relationship can yield correlations of 0.70 (Schlager et al. 1998) and for random data as high as 0.90 (Benson 1965). The exponents of relationships show a reasonable discrepancy based on standard error, which ranges from 2 to 5% of the mean. Mean average of regression coefficients *a, c*, and *p,* and exponents *b*, *t*, and *l*, result in the following proposed regression stream geometry equations in the study area:

$$W = 3.12Q^{0.14} \tag{3.12}$$

$$d = 0.34Q^{0.17} \tag{3.13}$$

$$V = 0.95Q^{0.65} \tag{3.14}$$

The definition of volumetric flux requires the product of mean width, depth, and velocity to be equal to discharge. With these proposed relationships, the product of coefficients is 1.0, and the sum of exponents is 0.96.

The mean (range) of exponents of water suface width, depth, and velocity are 0.14 (0-0.40), 0.17 (0.10-0.27) and 0.65 (0.45-0.85), respectively (*Table 3-2*). Mean values of width, depth, and velocity exponents at the sites are lower (except Wolman (1955) and Knighton (1975)), much lower (about two times), and higher than reported mean values in Table 3-3, respectively. Considering mountain streams (Miller1958; Coates1969; Ponton1972; and Reid et al. 2010), their mean values of width/depth and velocity exponents are higher and lower than those

found in the study sites, respectively. Normally, a small stream generated from a small drainage area produces lower values of width and depth exponents (Klein 1981) which result in an increased magnitude of the velocity exponent due to flow continuity. The range of exponents derived by Park (1977) from a set of worldwide rivers (*Table 3-3*) enclosed the range of width and depth exponents in the study area, indicating study exponents are highly variable in the global context. The range of water suface width exponents in the study area is similar to the 0.05-0.45 found by Reid et al. (2010) for mountains streams. Similarly, the range of mean water depth exponents is only comparable with the range (0.19-0.36) found by Lee and Ferguson (2002) in small step-pool streams (*Table 3-3*). This range is relatively constricted in the study area compared to the extensive ranges 0.09-0.47, 0.26-0.63, and 0.06-0.73 found by Reid et al. (2010) for mountain streams, by Knighton (1975) for braided rivers, and by Park (1977) for world wide analysis, respectively. The range of velocity exponents is very similar to the 0.50-0.87 found by Beven et al. (1979) in small steep reaches and 0.51-0.84 found by Lee and Ferguson (2002) in small step-pool streams. This range is dissimilar with 0.17-0.84 found by Reid et al. (2010) in mountain streams and 0.07-0.71 by Park (1977) for world wide analysis. In the Lac de Gras region however, the glaciation processes would predominate in producing major features of topography and drainage patterns.

3.4.2 Flow Resistance

In the study area, the Darcy–Weisbach f ranges from 1.0 to 267 with a mean value of 45, and Manning's n ranges from 0.085 to 1.37 with a mean value of 0.45. Both ranges excluded some extreme values of f and n corresponding to extremely small depths. At shallow depths, flow is forced to wander over and between the larger bed elements (Reid and Hickin 2008) and flow resistance may be extreme "as a result of boulder drag, wake vortices, local hydraulic jumps and jetting of flow" (Judd and Peterson 1969), which violate the uniform flow assumptions often made in hydraulic analysis. Uniform flow is defined where flow depth is equal at every channel cross section. This condition is less applicable in steep streams at low flow (Reid 2005). The range of resistance values in the study area are comparable to those reported by Reid and Hickin (2008) in a mountain stream with flow that ranged from 0·0006 to 5·52 m^3/s and relative roughness (R/D_{50}) from 0·27 to 3·30. These values for Darcy–Weisbach f and Manning's n were 0.29 to 12700 and 0.05 to 7.95, respectively. Bathurst (1982) reported that boulder-bed streams typically have Manning's n values that range from 0·04 to 0·2, and Marcus *et al.* (1992) reported n values that ranged from 0·056 to 0·183 for 20 cross sections in which stream discharge varied between 0·16 and 1·39 m^3/s. At the study sites, very high flow resistance is attributed to the presence of large bed materials, drowned shrubs, small pieces of woody debris, exposed roots, vegetation, and irregularities in the longitudinal profile of the bed that may add secondary sources of resistance in these environments (Lee and Ferguson 2002).

Variation of resistance coefficients with relative submergence: The relationships between resistance coefficients and relative roughness (R/D_{84}) signify that flow resistances vary significantly with relative submergence in all sites. It is evident that flow resistance became extreme at low values of relative submergence in all cross sections due to the violation of uniform flow assumptions. Power relationships show a consistent trend of decreasing resistance to flow with increasing values of relative submergence, which result in negative exponents found within power equations. Negative exponents *z* and *x* of Manning's *n* and Darcy-Weisbach *f* range from -0.26 to -5.34 (-2.59 ± 1.81; mean ± standard deviation) and -0.86 to -11.08 (-5.52 ± 3.63), respectively (*Table 3-4*), excluding M1S. The constant values of water surface width in M1S affect regression coefficients and exponents of these power equations. Another consistency evident is the generally good agreement between power equations and the data at each section, as calculated in R^2 terms. For Darcy-Weisbach f , R^2 values range from 0.75 to 0.98 with a mean value of 0.85 (*Table 3-4*). Similarly, for Manning's *n* these values range from 0.72 to 0.98 with a mean value of 0.81 (*Table 3-4*).

Variation of $\sqrt{1/f}$ with relative submergence: Values of $\sqrt{1/f}$ obtained from field measurements are plotted against relative submergence *(R/D_{84})* in Figure 3.6. To test the validity of Eqs. 3.6, 3.7, 3.8, and 3.9 for our study area, relationships between $\sqrt{1/f}$ and log *(R/D_{84})* are examined. $\sqrt{1/f}$ is used instead of the simple coefficient *f*, because it is more convenient when considering semi-logarithmic resistance equations and it equals the dimensionless velocity given by the ratio of

mean velocity to shear velocity (Bathurst 1985). R6S1 and R6S2 stream data show a defined and approximately linear trend, while other sites have more scatter. All data points fall below the line of Eq. 3.8, as well as lines of Eqs. 3.6, 3.7, and 3.9, except for data from R6S1 and R6S2 streams. Data from R6S1 and R6S2 streams provide a good fit with the curves of Eqs. 3.6, 3.7, and 3.9, where water surface slopes were higher (>2%).

Fits to individual sections using Keulegan Function: Improvement in relationships of estimated Darcy-Weisbach resistance coefficients and consequent relative roughness are fitted with Keulegan function curves that vary values of *m* separately for each section (*Figure 3.7*). For the study sites, best-fit values of *m* averaged 4.30 and were mostly between 2.55 to 4.75, only higher (>5.0) in XS-1, M1S, and R2S. From the literature, *m* values were found to be in the range of (2.0-3.50) reported by Thompson and Campbell (1979), Hey (1979), Bray (1982), and Bathurst (1985) for gravel bed rivers with slopes up to 2%; ranged from (1.10-3.50) as reported by Lee and Ferguson (2002) for steep streams with step-pool morphology; and (2.70-5.40) as reported by Reid (2005) with a mean value of 3.60. Most sites have *m* values within the range found by the previous studies (Thompson and Campbell 1979; Hey 1979; Bray 1982; Bathurst 1985; and Lee and Ferguson 2002). The *m* values for XS-2, XS-4, R2S, R6S1, and R6S2 are within the range found from the most similar study by Reid (2005). Only XS-1 and M1S have *m* values that exceed the above limits, where water surface slopes were lower (<0.5%). For the entire data set, when $m=1$ all data are plotted above

the function curve as roughness length is dependent on median grain size alone ($k_s = D_{50}$). According to Millar (1999), the offset between the data and curve for *m=1* is an expression of form resistance in the system. For the mean *m* value of 4.30, the Keulegan function curve does not fit well and scatter with the complete data set, likely due to section-to-section differences of resistance.

3.5 Summary and Conclusions

This study investigates the post runoff at-a-station hydraulic geometry and resistance to flow for head-water streams in the Northwest Territories of Canada. These streams are characterized by a steep slope, shallow depth, narrow width, large-scale roughness, and high seasonal discharge variability. For these systems, the following summary can be drawn: (1) power functions describe at-a-station hydraulic geometry relationships very well, the velocity exponent (*l*) exceeded the width exponent (*b*) and mean depth exponent (*t*) at all sections, and is greater than the sum of *b* and *t* in 7 out of 9 study cross sections demonstrating the dominant role of velocity in accommodating changing discharge in headwater streams; (2) depth exponents are greater than width exponents in 6 of 9 cross sections, indicating that width/depth ratio decreased with increasing discharge having trapezoidal/parabolic cross-sectional shapes, while the remaining three sections had increasing width/depth ratios with increasing discharge having convex cross-sectional shapes; (3) a well-defined fit between power functions and the data sets at each cross-section were reflected in R^2 values with means of 0.83, 0.85, and

0.97 for water surface width, mean depth, and mean velocity, respectively; (4) mean values of width, depth, and velocity exponents (0.14, 0.17, and 0.65, respectively) in our sites are lower, much lower, and higher than those typically reported in the literature which varied from 0.20 to 0.49, 0.20 to 0.41, and 0.13 to 0.55 for the braided rivers, mountain, and steep-pool streams, respectively; (6) with high stream discharge variability, the Darcy–Weisbach f ranges from 1.0 to 267 with a mean value of 45, and Manning's n ranges from 0.085 to 1.37 with a mean value of 0.45; (7) power relations of resistance to flow with relative submergence at all sites show a consistent trend of decreasing resistance to flow with increasing values of relative submergence, providing negative exponents in power equations that are also reflected by good agreement between the power relation and the data as calculated in the R^2 term; (8) variations of $\sqrt{1/f}$ against relative submergence (R/D_{84}) in the study sites reveal that all data fall below the line of logarithmic and power law (flow resistance) equations, having a more scattered format except for two sites that show an approximately linear trend; (9) Keulegan logarithmic curves describe reach resistance data well where the best-fitted m (form roughness component) values range from 2.55 to 4.75 with a mean value of 4.30, where most of the sites have m values within the range found by previous researchers.

The primary flow variables (water surface width, mean depth, and mean velocity) can be determined from well defined at-a-station hydraulic geometry relationships with a minimum of observational data. These relationships are only applicable to

flows within a similar range found in the study streams. Power equations between flow resistance and relative submergence at individual cross sections plus Keulegan function curves fitted for each section separately describe hydraulic relations very well. Governing conditions in these settings may be variable and therefore these relationships may not be extrapolated to bankfull conditions or transferable to other streams. As stream geometry is transient in nature, at-a-station relationships may be required at each time period and cross-section of interest.

3.6 References

Bathurst, J. C. (1982). "*Flow resistance in boulder-bed streams*." In Gravel-Bed Rivers: Fluvial Processes, Engineering and Management, R. D. Hey, J. C. Bathurst, and C. R. Thorne (eds.), Wiley, Chichester, 443–465.

Bathurst, J. C. (1985). "Flow resistance estimation in mountain rivers." *Journal of Hydraulic Engineering*, ASCE, 111(12), 625–641.

Bathurst, J. C., (1993). "*Flow resistance through the channel network*." In: K. Beven and M. J. Kirkby (Eds.), Channel Network Hydrology, Wiley, Chichester, 69–98.

Bathurst, J. C. (2002). "At-a-site variation and minimum flow resistance for mountain rivers." Journal of Hydrology, 269, 11–26.

Bathurst, J. C., Li, R. M., and Simons, D. B. (1981). "Resistance equation for large-scale roughness." *Journal of Hydraulic Engineering*, ASCE, 107 (12), 1593-1613.

Benson, M. A. (1965). "Spurious correlation in hydraulics and hydrology." *Journal of the Hydraulics Division,* ASCE, 91 (4), 35–42.

Beven, K., Gilman, K., and Newson, M. (1979). "Flow and flow routing in upland channel networks." *Hydrological Sciences Bulletin*, Taylor & Francis, 24, 303-325.

Bray, D. I. (1982). "*Flow resistance in gravel-bed rivers*." In Gravel-Bed Rivers, R. D. Hey, J. C. Bathurst, and C. R. Thorne (eds). Wiley, Toronto, 109–132.

Castro, J. M., and Jackson, P. L. (2001). "Bankfull discharge recurrence intervals and regional hydraulic geometry relationships: patterns in the Pacific Northwest, U.S.A." *Journal of the American Water Resources Association*, 37,1249–1262.

Coates, D. R. (1969). "Hydraulic geometry in a glaciated region." *Transactions, American Geophysical Union,* AGU, 50, 149.

Ferguson, R. I. (1986). "Hydraulics and hydraulic geometry." *Progress in physical Geography*, 10 (1), 1-31, doi: 10.1177/030913338601000101

Hey, R. D. (1979). "Flow resistance in gravel-bed rivers." *Journal of the Hydraulics Division*, ASCE, 105(4), 265–279.

Hey, R. D., and Thome, C. R. (1983). "Accuracy of Surface Samples from Gravel Bed Material." *Journal of Hydraulic Engineering*, ASCE, 109(6), 842-851.

Holtz, R. D., and Kovacs, W. D. (1981). "*An introduction to geotechnical engineering*." Prentice Hall, Inc., Englewood Cliffs, N.J.

Jarrett, R. D. (1984). "Hydraulics of high-gradient streams." *Journal of Hydraulic Engineering,* ASCE, 110(11), 1519–1539.

Jordanova, A. J. (2008). "*Low flow hydraulics in rivers for environmental applications in South Africa*." Unpublished Ph. D. Thesis, University of the Witwatersrand, Johannesburg, South Africa.

Jowett, I. G. (1998). "Hydraulic geometry of New Zealand rivers and its use as a preliminary method of habitat assessment." *Regulated Rivers-Research & Management,* John Wiley and Sons, 14, 451–466.

Jones, N. E., Tonn, W. M., Scrimgeour, G. J., and Katopodis, C. (2003). "Ecological characteristics of streams in the Barrenlands near Lac de Gras, N.W T., Canada." *Arctic*, 56(3), 249-261.

Jones, N. E., and Tonn, W. M. (2004). "Resource selection functions for age-0 Arctic grayling (Thymallus arcticus) and their application to stream habitat compensation." *Canadian Journal of Fishes and Aquatic Science*, 61, 1736–1746.

Judd, H. E., and Peterson, D. F. (1969). "Hydraulics of large bed element channels." Report No. PRWG17-6, Utah Water Research Lab., Utah State University, Logan, Utah.

Keulegan, G. H. (1938). "Laws of turbulent flow in open channels." *Journal of Research of the National Bureau of Standards*, 21, 707–741.

Klein, M. (1981). "Drainage area and the variation of channel geometry downstream." *Earth Surface Processes and Landforms*, 6, 589-593.

Knighton, A. D. (1975). "Variations in at-a-station hydraulic geometry." *American Journal of Science*, 275, 186–218.

Knighton, A. D. (1977). "*Short-term changes in hydraulic geometry.*" In River Channel Changes, K. J. Gregory (Ed.), Wiley-Interscience, Chichester, 101-119.

Knighton, A. D. (1998). "*Fluvial Form and Processes*." Oxford University Press Inc., New York.

Lee, A. J., and Ferguson, R. I. (2002). "Velocity and flow resistance in step-pool streams." *Geomorphology*, 46, 59-71.

Leopold, L. B., Bagnold, R. A., Wolman, M. G., and Brush, M. B. (1960). "Flow Resistance in Sinuous or Irregular Channels." United States Geological Survey Professional Paper 282-D, 111–134.

Leopold, L. B., and Maddock, Jr. T. (1953). "The hydraulic geometry of stream channels and some physiographic implications." U. S. Geological Survey Professional Paper 252, U. S. Government Printing Office, Washington, DC.

Linsley, R. K., Kohler, M. A., and Paulhus, J. L. H. (1982). "*Hydrology for Engineers*." McGraw Hill, New York.

Marsh-McBirney, (1990). Model 2000: Installation and Operations Manual. Marsh-McBirney Inc., 4539 Metropolitan Court, Frederick, Maryland.

Marcus, W. A., Roberts, K., Harvey, L., and Tackman, G. (1992). "An evaluation of methods for estimating Manning's n in small mountain streams." *Mountain Research and Development, International Mountain Society*, 12, 227–239.

Millar, R. G. (1999). "Grain and form resistance in gravel-bed rivers." *Journal of Hydraulic Research*, 37, 303–312.

Miller, J. P. (1958). "High mountain streams: Effect of geology on channel characteristics and bed material." New Mexico Bureau of Mines and Mineral Resources, Memo 4, Socorro, New Mexico.

Park, C. C. (1977). "World-wide variations in hydraulic geometry exponents of stream channels: an analysis and some observations." *Journal of Hydrology*, 33, 133–146.

Ponton, J. R. (1972). "*Hydraulic geometry in the Green and Birkenhead Basins, British Columbia.*" In: O. H. Slaymaker and H. J. McPherson (Eds.), Mountain Geomorphology: Geomorphological Processes in the Canadian Cordillera. Tantalus Research Ltd., Vancouver, BC, 151–160.

Reid, D. E. (2005). "*Low-flow hydraulic geometry of small, steep streams in southwest British Columbia.*" Unpublished M.Sc.Thesis, Simon Fraser University, Burnaby, BC, Canada.

Reid, D. E., and Hickin, E. J. (2008). "Flow resistance in steep mountain streams." *Earth Surface Processes and Landforms*, 33, 2211–2240.

Reid, D. E., Hickin, E. J., and Babakaiff, S. C. (2010). "Low-flow hydraulic geometry of small, steep mountain streams in southwest British Columbia." *Geomorphology*, Elsevier, 122, 39-55.

Rhodes, D. D. (1977). "The b-f-m diagram: Graphical representation and interpretation of at-a-station hydraulic geometry." *American Journal of Science*, 277, 73-96.

Roy, A. G., Roy, R., and Bergeron, N. (1988). "Hydraulic geometry and changes in flow velocity at a river confluence with coarse bed material." *Earth Surface Processes and Landforms*, 13, 583-598.

Schlager, W., Marsal, D., Van der Geest, P. A. G., and Sprenger, A. (1998). "Sedimentation rates, observation span, and the problem of spurious correlation." *Mathematical Geology*, SpringerLink, 30, 547–556.

Statistics Canada, (2005). Natural Resources Canada, GeoAccess Division, http://www.statcan.gc.ca/tables-tableaux/sum-som/l01/cst01/phys01-eng.htm

Thompson, S. M., and Campbell, P. L. (1979). "Hydraulics of a large channel paved with boulders." *Journal of Hydraulic Engineering*, ASCE, 17, 341–354.

Wiberg, P. L., and Smith, J. D. (1991). "Velocity distribution and bed roughness in high-gradient streams." *Water Resources Research*, AGU, 27(5), 825–838.

Wolman, M. G. (1954). "A method of sampling coarse bed material." *Transactions-American Geophysical Union*, AGU, 15, 951-956.

Wolman, M. G. (1955). "The natural channel of Brandywine Creek Pennsylvania." Geological Survey Professional Paper 271, U. S. Government Printing Office, Washington, DC.

Woo, M. K. (1990). "*Permafrost Hydrology*." In: Northern Hydrology: Canadian Perspectives, T. D. Prowse and C. S. L. Ommanney, (Eds.), NHRI Science Report No. 1, National Hydrology Research Institute, Environment Canada, Saskatoon, Saskatchewan, 63-76.

Table 3-1 Morphological characteristics of the study streams during summer 2010 in the Lac de Gras watershed, NWT.

Stream	Catchment Area (ha)	Length (m)	Bankfull width (m)	Gross Slope (%)	D_{84} (mm)	X-section	Water surface slope (%)	Average depth (m)	d/D_{84}
WIS	32.08	415.0	2.65	1.8	220	XS-1	0.43	0.25	1.12
						XS-2	1.35	0.17	0.76
						XS-3	1.54	0.16	0.71
						XS-4	1.48	0.11	0.51
M1S	23.81	50.0	3.67	2.0	200	-	0.28	0.26	1.30
M2S	9.06	27.5	3.00	1.5	220	-	1.11	0.11	0.52
R2S	48.32	103.0	3.32	1.0	220	-	0.40	0.17	0.79
R6S1	15.84	108.0	2.73	1.5	215	-	2.69	0.15	0.71
R6S2	8.42	177.0	2.64	2.2	225	-	2.23	0.13	0.57
Mean	22.92	146.8	3.00	1.8	217		1.28	0.17	0.78

Table 3-2 At-a-station hydraulic geometry coefficients and exponents at the study sites in the Lac de Gras watershed, NWT.

Stream name	X-section	No. of Obs.	Water surface width $W = aQ^b$			Mean depth $d = cQ^t$			Mean velocity $V = pQ^l$		
			a	b	R^2	c	t	R^2	k	l	R^2
W1S	XS-1	8	4.63	0.08	0.88	0.61	0.21	0.94	0.36	0.71	0.99
	XS-2	10	2.75	0.18	0.94	0.25	0.10	0.90	1.48	0.72	1.00
	XS-3	6	3.00	0.11	0.90	0.47	0.27	0.92	0.71	0.62	0.99
	XS-4	11	1.32	0.10	0.35	0.16	0.15	0.91	0.89	0.43	0.99
M2S	-	11	2.89	0.14	0.93	0.36	0.21	0.96	0.96	0.67	0.99
R2S	-	9	3.04	0.09	0.77	0.29	0.14	0.85	1.13	0.83	0.99
R6S1	-	8	3.36	0.40	0.93	0.19	0.11	0.46	1.55	0.53	0.97
R6S2	-	8	3.61	0.30	0.93	0.31	0.24	0.92	0.90	0.45	0.97
M1S	-	6	3.50	0	-	0.41	0.10	0.76	0.58	0.85	0.89
	Mean		3.12	0.14	0.83	0.34	0.17	0.85	0.95	0.65	0.97

Table 3-3 Comparison of the at-a-station hydraulic geometry exponents to other studies.

Study	Type of Rivers/ steams	No. of Obs.	Width exponent (b)		Depth exponent (t)		Velocity exponent (l)	
			Range	Mean	Range	Mean	Range	Mean
Our study	-	9	0-0.40	0.14	0.10-0.27	0.17	0.43-0.85	0.65
Wolman (1955)	Brandywine Creek river	7	0.00-0.08	0.04	0.32-0.46	0.41	0.46-0.69	0.55
Miller (1958)	High mountain streams	-	-	0.38	-	0.25	-	0.39
Coates (1969)	Streams in the Appalachain Plateau	18	-	0.36	-	0.20	-	0.48
Ponton (1972)	Cost mountain streams of BC	-	-	0.21	-	0.32	-	0.50
Knighton (1975)	Braided River Bollin-Dean	12	0.01-0.33	0.11	0.26-0.63	0.40	0.24-0.68	0.50
Park (1977)	World wide analysis	139	0.00-0.59	-	0.06-0.73	-	0.07-0.71	
Castro and Jackson (2001)	Pacific Northwest streams	76	-	0.49	-	0.38	-	0.13
Lee and Ferguson (2002)	Steep-pool streams	5	0.17-0.21	-	0.19-0.36	-	0.51-0.84	-
Reid et al. (2010)	Mountain streams of BC	61	0.05-0.45	0.20	0.09-0.47	0.29	0.17-0.84	0.51

Table 3-4 At-a-station Darcy-Weisbach and Manning resistance coefficients and exponents for the power equations at the study sites, Lac de Gras watershed, NWT.

Stream name	X-section	No. of Obs.	Manning's n $n = y(R/D_{84})^z$			Darcy-Weisbach f $f = q(R/D_{84})^x$		
			y	z	R^2	q	x	R^2
W1S	SX-1	8	1.34	-2.70	0.81	23.23	-5.73	0.83
	SX-2	10	0.02	-5.34	0.98	0.07	-11.08	0.98
	SX-3	6	0.26	-1.50	0.78	8.72	-3.34	0.81
	SX-4	11	0.13	-0.26	0.75	2.33	-0.86	0.89
M2S	-	11	0.11	-2.43	0.91	1.62	-5.20	0.92
R2S	-	9	0.72	-5.06	0.74	0.67	-10.45	0.75
R6S1	-	8	0.03	-2.43	0.79	0.12	-5.18	0.81
R6S2	-	8	0.09	-1.01	0.72	1.03	-2.34	0.78
M1S	-	6	4.70	-8.77	0.96	2957.70	-17.87	0.96
	Mean		0.34	-2.59	0.81	4.72	-5.52	0.85

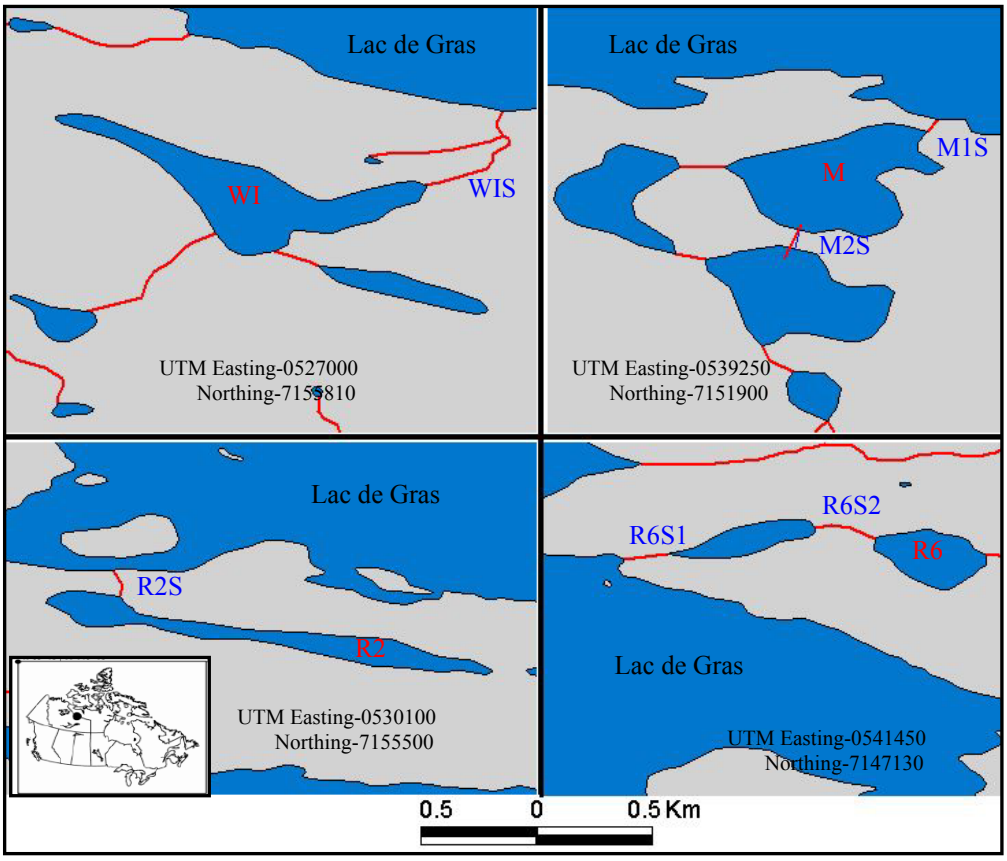

Figure 3.1 The location of the study area with four sites comprising a total of six streams in the Northwest Territories, Canada.

Downstream view of WIS at XS-1

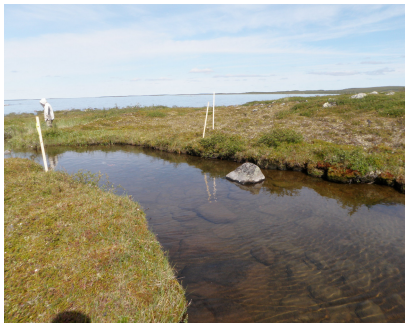

Downstream view of M1S

Upstream view of R6S1

Upstream view of M2S

Upstream view of R6S2

Downstream view of WIS at XS-4

Upstream view of R2S

Figure 3.2 Some photographs of study streams during summer 2010.

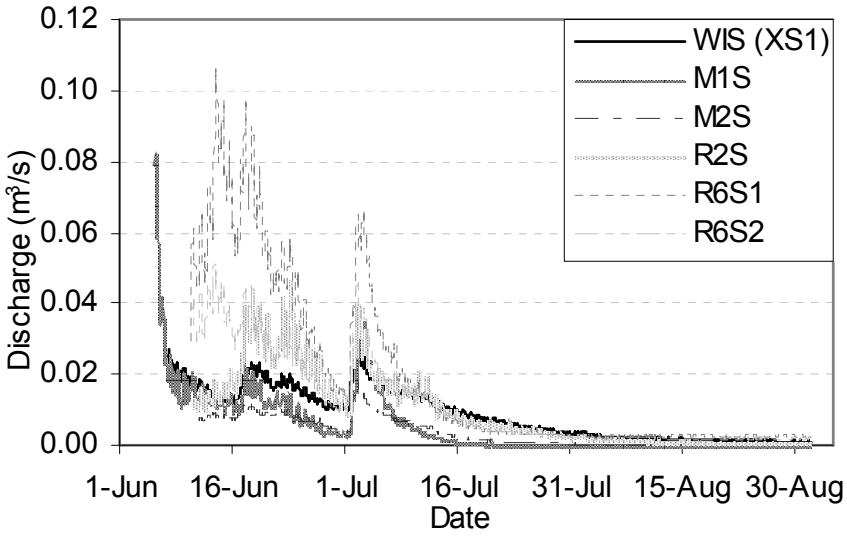

Figure 3.3 The variation in discharge over the study period in summer 2010 at all study sites in the Lac de Gras watershed, NWT. Discharge was calculated from recorded continuous water level and developed rating curves for all sites. (Note: The purpose of these rating curves in this paper were used to calculate the hydrograph pattern merely for qualitative purposes only and not for the calculation of hydraulic geometry and flow resistance.)

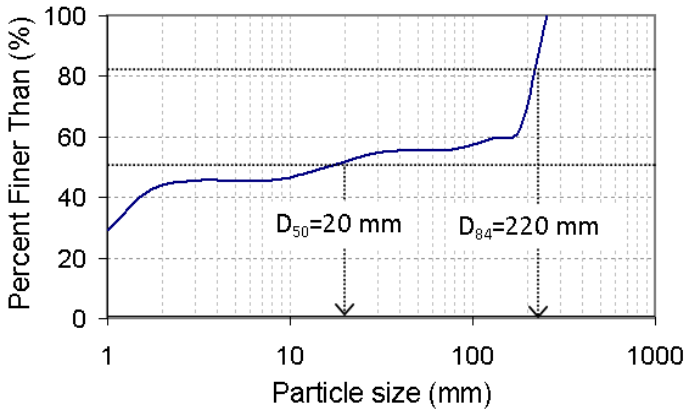

Figure 3.4 The bed particle size distribution of West Island stream (WIS).

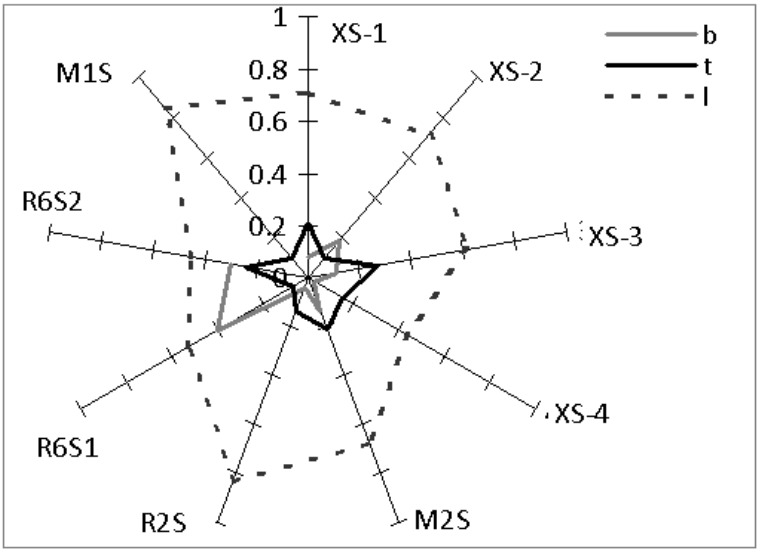

Figure 3.5 Radar plot of the hydraulic geometry exponents *b, t*, and *l* in the study area, Lac de Gras, NWT.

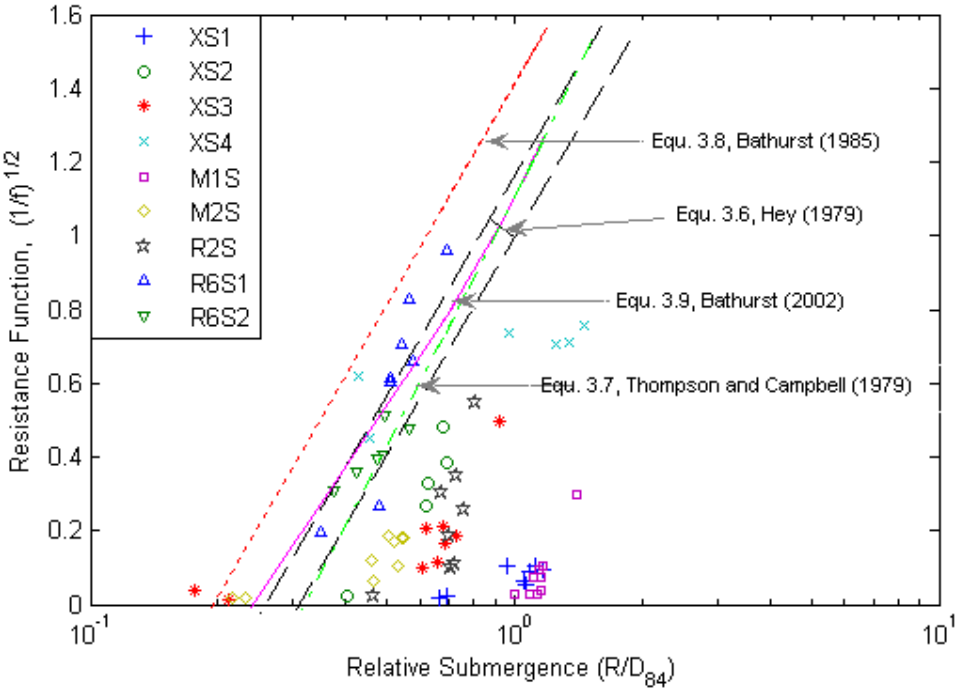

Figure 3.6 The Keulegan-style semi-logarithmic plot of $\sqrt{1/f}$ against relative submergence with individual cross sections distinguished.

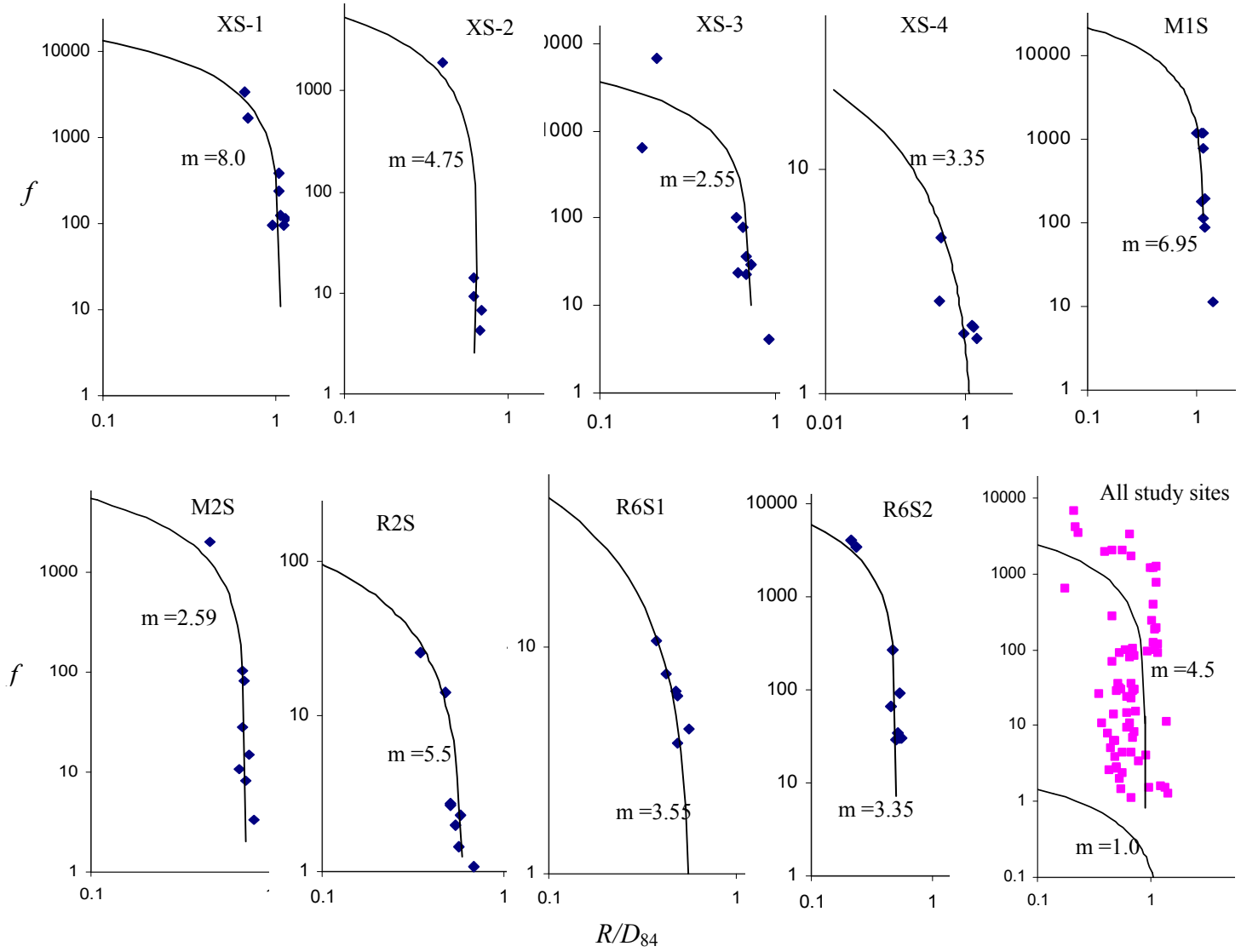

Figure 3.7 Keulegan function curves fitted to the Darcy-Weisbach resistance coefficient f versus relative roughness R/D_{84} data at individual cross sections and at all sites from the Lac de Gras watershed, NWT.

CHAPTER 4

Mean Flow Characteristics in a Rock-Ramp Type Fishpass*

4.1 Introduction

In recent years, a holistic ecosystem approach has led to a new concept of ecological or nature-like fishpass design. In accordance with ecological design principles, a nature-like fishpass should be able to accommodate all species living in a waterbody (Katopodis et al. 2001). Nature-like fishpasses which mimic natural stream characteristics have been developed, typically use natural materials, and provide suitable passage conditions for a wide variety of fish species and other aquatic organisms (Katopodis and Williams 2011). In many cases nature-like fishpasses have become the preferred choice for low-head barriers, if sufficient space is available for their construction. Classifications of nature-like fishpasses are based on configuration of structures, including the arrangement of boulders (DVWK 2002); they include embedded-boulder constructions, ramps with perturbation boulders, and pool-type ramps. Another classification of nature-like fishpasses is usually site-specific (DVWK 2002); they are bottom ramps and bypass channels.

*The content of this chapter has been accepted as: Baki et al. (2013a). "Mean Flow Characteristics in a Rock-Ramp Type Fishpass." *Journal of Hydraulic Engineering, ASCE*, http://dx.doi.org/10.1061/(ASCE)HY.1943-7900.0000816.

In general, two kinds of nature-like fishpass designs can be distinguished: pool and riffle type and rock-ramp type (Katopodis and Williams 2011). The pool and riffle type is built in a stair-step configuration where typically short steep reaches (riffles) connect to flat deeper reaches (pools). A rock-ramp fishpass has a continuous slope from one end to the other, with a series of large boulders protruding from the bed of the ramp. At peak discharges boulders are submerged, while at non-peak discharges they are emergent. For all flow conditions these boulders provide resting places for fish swimming upstream.

An important application of the hydrodynamics around in-situ large roughness elements is to establish relationships between roughness elements and the fish habitat (Lacey and Roy 2008). It is well recognized that localized, complex, small and meso-scale flow patterns created by stream flow obstructions are of biological importance and provide favorable habitat for many aquatic species (Crowder and Dipla 2006). In terms of instream habitat function, obstacles such as boulders have been positively correlated with fish density (van Zyll de Jong et al. 1997). Rocks, either isolated or placed in a series of clusters, are considered the simplest fish habitat structure in use. Model simulations and field observations suggest that the localized energy gradients and velocities surrounding boulders create essential components of aquatic habitat, such as flows suitable to fish resting and feeding (Crowder and Diplas 2000). Similarly, boulders and clusters of rocks create low shear stress zones that play an important role in determining the diversity of periphyton and invertebrates in a stream (Biggs et al. 1997). Therefore, the local

flow patterns induced by boulders and other meso-scale obstructions are critical features for enhancing fish and benthic habitat.

The advantages of rock-ramp fishpasses are that they effectively dissipate energy, reduce flow velocity and increase water depth while providing resting areas and shelters for fish. Reducing velocity and increasing depth are directly correlated to improved upstream fish migration. The performance of this type of fishpass was previously evaluated (Franklin et al. 2012; Franklin and Bartels 2012) and showed most promising results. Rock-ramp fishpasses have been found successful based on passage and attraction efficiency of attempting fishes (Thorncraft and Harris, 1996). They have been reported to increase species richness (mean increase 80%) and total fish density (mean increase 45%) upstream of a culvert (Franklin and Bartels 2012), and pass 94% of the fish that made passage attempts (Franklin et al. 2012). By comparison, a step-pool bypass type fishpass passed only 40% of the attempting fish and a technical pool-weir fishpass exhibited poor entry and poor passage for the fish (Franklin et al. 2012).

The hydraulics of the streams with large-scale roughness has been studied for many years (Bathurst 1985 and 2002; Smart et al. 2002; Ferro 2003; Pagliara et al. 2008 and others). These studies have shown that the flow resistance law is strongly affected by the geometry of the large-scale roughness elements. Jordanova (2008) conducted several experiments with hemisphere to investigate the effect of different geometries (size, arrangement, and concentration) on the

flow resistance coefficient. Papanicolaou et al. (2012) studied (experimentally and numerically) mean and turbulent flow fields within an array of fully submerged, isolated, and immobile boulders with implications for bedload transport. The hydrodynamics associated with surface mounted blocks, cylinders, and hemispheres were experimentally studied by Martinuzzi and Tropea (1993), Shamloo et al. (2001), Sadeque et al. (2008), and Lacey and Rennie (2012). In terms of field measurements, relatively few studies (Tritico and Hotchkiss 2005; Strom and Papanicolaou 2007; and Lacey and Roy 2008) have investigated the flow characteristics around isolated instream pebble clusters in gravel bed rivers. Those studies on different bluff bodies or isolated pebble clusters provided sufficient details on the flow depth versus wake structure relationships. Their applicability is limited to flow resistance, bedload transport, and detailed wake flow fields, and is inadequate for fish habitat characterization.

The hydraulics of conventional fishpasses (Rajaratnam et al. 1986; Ead et al. 2004; Liu et al. 2005; etc.) have been studied for many years. In contrast with conventional fishpasses, the flow characteristics in nature-like fishpasses are still in an early phase of study and have not been systematically analyzed. For example, USBR (2007) provides practical guidelines for design and construction of fish ramps. DVWK (2002) included a chapter with useful guidelines for nature-like fishpasses and provided some examples of field applications. Parasiewicz et al. (1998) reviewed the design basis of nature-like bypass channels based on Australian experience. Haro et al. (2008) conducted several experiments with

field-scale laboratory setup for a nature-like fishpass in a perturbation boulder design. Wang and Hartlieb (2011) examined the hydraulic and geometric parameters of nature-like pool-type fishpasses via experimental and field investigations. These studies have provided only some general guidelines based on critical velocity criteria and have limited analysis on flow characteristics.

There appears to be no literature studying the flow characteristics of natural rock-ramp fishpasses with respect to fish habitat characterization. Although the flow characteristics will vary for different geometric conditions, especially the arrangements of boulders, in a rock-ramp type fishpass, this paper presents a detailed investigation on the mean flow characteristics in a rock-ramp fishpass for a staggered arrangement of boulders. In this study, natural rocks (boulders) were used in three different slopes of 5, 3, and 1.5% in a rectangular flume, for different flow conditions. The purpose of this study was (i) to investigate the detailed mean flow characteristics, specifically the water surface profiles and velocity fields in a rock-ramp fishpass; (ii) to develop some general correlations for predicting the average flow depth and velocity in a rock-ramp fishpass as a function of normalized discharge and streamwise distance; (iii) to quantify the nature of flow resistance in a rock-ramp fishpass; finally (iv) to discuss the applicability of hydraulics induced in a rock-ramp fishpass with a relationship to fish passage. Results from this study will increase our ability to predict and understand the possible effects of flow structure on fish passage and would be useful to both fishpass designers and fish biologists.

4.2 Experimental Program

A rock-ramp fishpass was installed in a rectangular flume with width, height, and length being 0.92 m, 0.61 m, and 8.89 m, respectively (*Figure 4.1a*). The flume was connected to a head tank with a streamlined bottom and stilling arrangements to provide a smooth flow entrance. One pump was used to supply the head tank from the laboratory sump and the discharge was measured by means of a magnetic flow meter installed in the supply line. As nature-like fishpasses are normally used for slopes up to 5%, the flume was adjusted to have three different longitudinal slopes of 5, 3, and 1.5%.

The rock-ramp design consists of a staggered arrangement of isolated natural boulders of spherical shape that were placed throughout the length of the flume (*Figure 4.1a & b*). The boulders were glued to the ramp bottom with silicone. Note that the boulder stability due to the hydrodynamic forces in a rock-ramp type fishpass under the nature of field conditions is discussed in Appendix A. A total of fifty-eight boulders were used in this experiment, where the boulder diameter (D) in all directions ranged from 12 to 16 cm, with an equivalent diameter of 14 cm. These boulders were chosen to be as uniform in shape as possible. Isolated boulders were arranged in 23 rows alternating between two and three boulders per row, and resulting in a total of 11 cells, as shown in Figure 4.1a. DVWK (2002) recommended that the centre to centre distance between two boulders along longitudinal (s_l) and transverse (s_t) directions should be 2 to 3 times the boulder

diameter. Considering the flume width and boulder diameter of this experimental setup, (s_l) and (s_t) were set to 37.5 cm or 2.68D. This spacing resulted in an aerial density of about 15%, which established a wake-interference flow (Morris 1954), where the roughness elements are placed sufficiently close together so that the wake generated by each element is not completed before the next element is encountered. In mountain streams, a density less than 10% produces isolated roughness conditions (see Papanicolaou et al. 2012).

The detailed measurement area was selected from cell 6, which is within the uniform flow zone (details below), having a length L=75 cm (5.36D) in the X direction and half flume width $B_{1/2}$=46 cm (3.28D) in the Y direction (*Figure 4.1c*). Longitudinally, it started at a distance X= 409 cm from the most upstream section and extended up to X= 484 cm, and laterally it extended from sidewall to centre line, indicated in Figure 4.1a. A total of fifteen sets of experiments were conducted at different flow rates and channel slopes of 5, 3, and 1.5%, see Table 4-1. For the 5% slope, measurements were taken at each grid point (*Figure 4.1c*), with grid spacing between two points in the streamwise (X) and lateral (Y) directions of 4 to 6 cm and 7.5 to 10.5 cm, respectively. For the 3 and 1.5% slopes, the measurements were conducted at each grid point only along the centre line of the flume in the detailed measurement area (*Figure 4.1c*); assuming that the reach average water depth and velocity can be approximated from that of centre line in the flume (discussed later). For all sets of experiments, the spacing

between two measuring points in the vertical (Z) direction varied from 1 to 2 cm depending on flow conditions.

The submergence ratio *(H/D)*, where *H* is the average water depth along the centre line of the flume in the detailed measurement area, varied from 0.84 to 1.11 for the 5% slope, 0.88 to 1.26 for the 3% slope and 0.77 to 1.60 for the 1.5% slope (*Table 4-1*). The Froude number $(Fr = u_{avg} / \sqrt{gH})$ and Reynolds number $(\mathrm{Re} = u_{avg} H / \upsilon)$, for all experimental runs, (where u_{avg} is the average streamwise velocity at all measurement points in the detailed measurement area and υ is the kinematic viscosity of water) varied from *Fr*=0.39 to 0.78 and *Re*=63,000 to 192,000 respectively (*Table 4-1*).

The fluctuating water level at each point was measured using a point-gauge, and two readings were obtained for the maximum and minimum observed depths. For the 5% slope, an Acoustic Doppler Velocimeter (SonTek 10MHz ADV) was used to measure the three-dimensional instantaneous velocity fields for flow rates of 60, 75, and 100 L/s. At a flow rate of 125 L/s, the ADV was unable to provide good quality data (discussed later) due the extreme turbulence and air entrainment in the flow. Hence, a yaw probe, made and calibrated by Rajaratnam and Muralidhar (1968), was used to measure the two-dimensional mean velocity fields. For the 3% and 1.5% slopes, a Vectrino Plus (Nortek) was used to measure the three-dimensional instantaneous velocity fields.

The ADV velocity measurements were recorded at 25 Hz (with ADV) and 100 Hz (with Vectrino Plus) for a sampling period of 180s for each point. Preliminary tests were conducted to define the ADV sampling period needed for an accurate determination of the mean velocity. Tested sampling periods ranged from 30 to 300s. It was found that velocity became almost constant for sampling periods greater than 60s, therefore a sampling time of 180s was considered to be adequate for the determination of mean velocities. For all sets of experiments, the average correlation coefficients (COR) varied from 55 to 71% and the average signal-to-noise ratios (SNR) varied from 41 to 61 dB. SonTek recommends that COR and SNR values should be greater than 70% and 15 dB, respectively, for reliable turbulence measurements. But for mean velocity measurements, COR values as low as about 30% and SNR values as low as about 5 dB can be used (SonTek 1997). Also Martin et al. (2002) found that for turbulent flows, data filtered with a minimum correlation of 40% could be used to determine average velocities if at least 70% of the data were retained after filtering. In recognition of this, the raw data were filtered to eliminate poor signals based on a filtering scheme of SNR≥30 dB and COR ≥55%, and spikes were eliminated using the method of Goring and Nikora (2002) prior to the calculation of the mean velocities.

The location of the cell of velocity measurement was chosen based on the presence of uniform flow. In this study, the flow is considered uniform when the gross or average flow pattern remains constant with downstream distance. Figure 4.2 shows the longitudinal water surface profiles for the 5% slope along the centre

line of the entire flume length for 45, 60, and 100 L/s flow rates. In each cell, the water surface profile consists of two drops and two peaks. The water surface varied in a regular repetitive cycle throughout the length of the flume, except most upstream and downstream zones. Thus, the water depth appeared to remain invariant and the flow was fully developed. So, the detailed measurement area was selected from cell 6, which is within the hydraulically uniform flow zone.

Several supplementary experiments were conducted to investigate the effect of varying boulder size on the normalized water surface profiles and on the generalized relationship between discharge and average flow depth. Those experiments were performed in a different flume, 9.6 m long, 0.40 m wide and 0.6 m height. The test section consisted of a 2.0 m long and 0.40 m wide channel, formed using 20 cm thick plywood, placed on 2.6 and 5% slopes. Similar to the original rock-ramp, an array of spherical obstacles (pebble gravel) having an equivalent diameter of 2.35 cm (approximately 1/6 of the boulder diameter) was placed throughout the 2.0 m long test channel bottom section with glue. The centre to centre distance between two pebbles in the longitudinal (Δx) and lateral (Δy) directions was approximately 6.30 cm (2.68*D*). A total of ten supplementary experiments were conducted where the submergence ratio (*H/D*) varied from 0.99 to 1.30 for the 2.6% slope and 0.74 to 1.24 for the 5% slope. Table 4-2 summarizes the details of these experiments.

4.3 Results and Discussions

4.3.1 Water Surface Profiles

One of the major advantages of a rock-ramp fishpass is that it provides adequate flow depth to upstream migrating fish. Table 4-3 shows the effect of boulders on flow depth in the rock-ramp fishpass in all experiments. The ratios between regulated (with boulders) and unregulated (without boulders) average flow depth varied from 2.4 to 3.4. Herein, the unregulated average flow depth was calculated using the Manning's equation (where n=0.012 for smooth steel bottom) and the regulated average water depth was the measured water depth. This ratio decreased with increasing flow rates because water overtopped the boulders at higher flow rates. Therefore, a significant flow depth augmentation, of approximately 3 times, has occurred in the rock-ramp fishpass. That is achievable for the highest values of flow resistance associated with intermediate densities of the boulders (Hassan and Reid 1990) while developing the wake-interference flow as well as for the blockage effect.

Figure 4.3 shows the water depth (average of maximum and minimum measured depths at each point by point-gauge) contours in the detailed measurement area for the 5% slope under different flow conditions. The contour maps are almost identical for all flow conditions and reveal the occurrence of maximum depth immediately upstream of each boulder due to the obstruction and low flow depth behind each boulder due to expansion of flow area. The variation in flow depth was found to increase as the discharge increased up to $H/D = 1.0$ when

separated flow reconnected downstream of the boulder and then decreased for $H / D > 1.0$ as water surface rose above the boulder tops. Therefore, the repetitive pattern of higher and lower depths formed a relatively deeper pathway through the fishpass. The average water depth in the detailed measurement area was about 11.8, 13.0, 14.1, and 15.4 cm for flow rates 60, 75, 100, and 125 L/s, respectively. The corresponding average water depth only along the centre line of the flume in the detailed measurement area was about 11.7, 12.9, 14.2, and 15.5 cm, respectively. Given the absolute difference between area averaged and centre line averaged is less than 1%. So the area averaged water depth can be approximated from that of centre line in the flume.

Figures 4.4 shows the variation of longitudinal water surface profiles along the centre line of the flume for the 5, 3, and 1.5% slopes. In each cell, the water surface rises and falls as flow approaches upstream and downstream of the boulders, which generated two complete cycles. It is apparent that the fluctuation of water level from the mean values decreased with decreasing channel slopes, which is more evident for the 1.5% slope under 160 L/s flow rate. At each channel slope, it is also evident that the locations of peaks and drops in water surface profiles shifted downwards for higher flow rates, especially for $H / D \geq 1.6$.

The average water depth along the centre line of the flume varied from 11.75 to 15.5 cm as the flow rate varied from 60 to 125 L/s, from 12.3 to 17.6 cm for the flow rate from 45 to 120 L/s, and from 10.8 to 22.4 cm for the flow rate from 25

to 160 L/s for the 5, 3 and 1.5 % slopes, respectively. The corresponding flow depth (>11 cm) in this experimental fishpass can provide adequate depth for fish passing, and more adequate (>44 cm) in the prototype fishpasses assuming 1:4 undistorted scale model. From the literature, Reiser and Bjornn (1979) mentioned that "Fish could successfully pass any stream reach of reasonable length if the depth was greater than 12 cm when substrate particles averaged larger than 7.6 cm in diameter, or if the depth was greater than 9 cm when particles were less than 7.6 cm. In general, the water was at least deep enough to cover the fish during spawning; large salmon required 15-35 cm and smaller trout 6-10 cm".

The normalized water surface profiles along the centre line are shown in Figure 4.5(a) in the form of h/H against X/D, where h is the local water depth. It appeared that for all slopes and flow conditions, one mean trend line could be drawn through the data points. The normalized water surface profiles for all supplementary experiments are plotted in Figure 4.5(b) with the projected trend line from Figure 4.5(a). The supplementary experimental points for the 2.6 and 5% slopes follow the trend line with some degree of scatter especially for higher submergence ratios. With increasing submergence ratio, the peaks and drops in water surface profiles shifted downwards from the corresponding peaks and drops of the trend line. This was possibly because at higher submergence ratios the flow pattern did not follow the flow characteristics that occurred in wake-interference flow due to the development of skimming flow over the tops of the boulders (Peterson and Mohanty 1960).

The normalized discharge and average flow depth were correlated to develop a simple empirical relation for predicting the average flow depth in a rock-ramp fishpass. The correlations were developed between the dimensionless discharge ($Q^* = Q/\sqrt{gS_0 R_v^{\,3} B^2}$) and the submergence ratio (*H/D*). Herein, *g* is the acceleration due to gravity, S_0 is the channel slope, *B* is the channel width, and R_v is the volumetric hydraulic radius defined for a wide channel as the volume of overlying water per unit plan area of the bed (Smart et al. 2002; Jordanova 2008). The volumetric hydraulic radius is defined as $R_v = H(1-2/3\lambda l^*$, where λ is the area concentration of boulders, $\lambda = N(\pi D^2/4)/A$, which is the fraction of the bed area occupied by boulders, with *N* being the number of boulders over a bed area (*A*). l^* is the boulder height to average flow depth ratio, $l^* = D/H$. Here, the volumetric hydraulic radius was preferred essentially for minimizing the integrated effect of boulder diameter and arrangement (spacing and density). Figure 4.6 showed that *Q** is mainly a linear function of submergence ratio (*H/D*) with a good agreement of all data points for all experiments. The following equation may be written to describe the fitted line as:

$$\frac{H}{D} = 0.345Q^* \qquad (R^2=0.89) \tag{4.1}$$

The results of all supplementary experiments in the form of *Q** versus *H/D* are also plotted in Figure 4.6 to show the effect of boulder size (scaling down) on the above relationship. It was found that all supplementary experimental points

agreed well with the fitted line especially for $H / D \leq 1.2$, beyond that limit data points deviated. The probable reasons for this difference are the decreased influence of the individual boulders on resistance with increased depth. The surface area of one pebble in the supplementary experiment is about 35 times smaller than that of a boulder. At higher flow rates ($H / D \geq 1.2$), the flow skimming over the pebbles and the rate of increase of average water depth with increasing flow rates substantially declined.

This relationship in Eq. (4.1) is a curve-fit of all the experimental data and competent to estimate average flow depth for any specific discharge in this rock-ramp fishpass structure. It is recommended to verify this relationship for different arrangements and densities of boulders.

4.3.2 Velocity Field

The rock-ramp fishpass reduced mean flow velocity and increased shelter that fish can find as they ascend. Ascending fish find refuge in the flow wake of the boulders (DVWK 2002). A significant velocity reduction occurred between the unregulated and regulated average velocities (Table 4-3). The unregulated average velocity, u_0, was calculated from the Manning's equation. The regulated average velocity, u_{avg}, was the streamwise mean velocity for the 5% slope. For the 3 and 1.5% slopes, it was approximated from the centre plane in the detailed measurement area, as the results for 5% slope evidenced that u_{avg} along the centre

plane were about 10% higher than in the detailed measurement area. The velocity reduction varied from 61-71% for the 5% slope, 59-66% for the 3% slope, and 54-63% for the 1.5% slope (Table 4-3). It is expected that the reduction in velocity decreases with increasing flow rate as well as with decreasing slope. Therefore, a significant reduction of flow velocity of about 64% occurred in the studied rock-ramp fishpass.

A general relationship, similar to a depth-discharge relationship, was also found between the dimensionless discharge, Q^*, and the dimensionless maximum velocity magnitude, $U_{\max}^* = U_{\max} / \sqrt{gS_0R_v}$, and streamwise average velocity, $u_{avg}^* = u_{avg} / \sqrt{gS_0R_v}$. Herein, U_{max} is the maximum flow velocity magnitude of U at one flow rate. The magnitude of flow velocity, U, was calculated by $U = \sqrt{u^2 + v^2 + w^2}$ for the ADV, and by $U = \sqrt{u^2 + v^2}$ for the yaw probe at all measurement points along the centre line of the flume in the detailed measurement area. Herein, u, v, and w are the time-averaged streamwise, lateral and vertical velocities, respectively. The contributions of vertical velocity immediately upstream/downstream of each boulder are relatively strong, as has been shown in previous studies (Shamloo et al. 2001; Sadeque et al. 2008; Lacey and Rennie 2012); this vertical component cannot be captured with yaw probe. Figures 4.7a and 4.7b show the generalized linear relationship between Q^* and $U_{\max}^*$, as well as u_{avg}^*. For the best fitted lines, the equations are as follows:

$$U_{\max}^* = 1.504Q^* \qquad (R^2=0.90) \tag{4.2}$$

$$u_{avg}* = 1.047Q* \qquad (R^2=0.80) \tag{4.3}$$

These linear relationships are also curve-fits of all the experimental data and can be used to estimate maximum/average velocity for any specific discharge.

To verify the applicability of Eq. (4.2) for field-scale, data sets for perturbation boulder design in a rock-ramp fishpass by Harao et al. (2008) in the form of $Q*$ and $U_{\max}*$ are also plotted in Figure 4.7a. Herein, the boulder sizes were estimated from the photos having 85 cm of diameter and 115 cm of height (assuming in cylindrical shape) and the average water depth (H) was estimated using Eq. (4.1). It was found that all large-scale data points agreed with the fitted line with certain degree of scatter which is probably due to the boulders shape effect and the nature of field conditions. Therefore, the proposed Eq. (4.2) is quite reasonable with field-scale data sets.

Normalized profiles of streamwise mean velocity (u/U_{max}) over the flow depth (z/H) were analyzed for different flow rates and slopes to examine the variation of the velocity magnitude along the centre line of the flume (*Figure 4.8*). Figure 4.9 illustrates the u velocity gradient in the streamwise direction, du/dx, near the bed (at z=1.0 cm) along the centre line of the flume. From the velocity profiles, three different regions were easily identified along the centre line: downstream of boulders; intermediate region; and upstream of boulders. Downstream of the boulders (X/D=1 to 2), the velocity profiles were more irregular over the entire flow depth. In this region, Papanicolaou et al. (2012) found maximum deviations

of the measured velocity profiles from the logarithmic profile. Near the bed, the flow accelerated at higher-gradients ($du/dx > 3s^{-1}$) between locations *X/D*= 1 to 2. Also no reverse velocity was observed near the bed in this region, which is contrary to previous results (Shamloo et al. 2001; Ferro 2003; Sadeque et al. 2008). It is also important to note that the velocity profiles excluded the measurements at *X/D*<1.

The flows in the wake gradually overcome the disturbance caused by the boulders. Moving further downstream and away from the wake region, in the intermediate region (*X/D*=2 to 3), the velocity profiles started to develop at lower-gradients ($du/dx \leq 2s^{-1}$) near the bed. In this region, there are still some deviations of velocity profiles from the logarithmic profile. The profiles reached their maximum values and the variation of velocity magnitude over the entire flow depth was relatively small (less than 5 to 20%) for all experiments. The du/dx near the bed is predominantly negative between locations *X/D*=3 to 4, reconfirming the observed flow deceleration as it approaches the boulder (*Figure 4.9*). In this region, the velocity profiles in the inner layer were found to deviate increasingly from the logarithmic profile.

The spatially distributed normalized velocity in the horizontal XY plane at *z*=4 cm, $U_{xy}/U_{\max}$, and their directions for the 5% slope under different flow conditions are presented in Figure 4.10. Herein, U_{xy} is the velocity magnitude in the horizontal plane (XY). The distributions of velocity patterns were similar for

all flow conditions (60, 75, 100, and 125 L/s), except their magnitude. There are clear regions of reduced velocities downstream of the boulders which provide a large potential resting zone for fish migration. Some preferred paths (with velocity magnitude ranging from 1 to 50 cm/s) and resting areas (with velocity less than 20 cm/s) may be found by fish. Upstream of boulders, the velocity vectors deflected towards two sides and their magnitude increased approaching the body to compensate for the reduction of the velocity along the centre line of boulders. Downstream, however, the velocity vectors converged towards the centre line of the boulder and their magnitude decreased along the downstream distances because of the increasing velocity along the centre line of boulders.

An investigation was carried out to understand the detailed velocity fields and their directions in the vertical plane (XZ) through velocity vectors. Figure 4.11 shows the velocity vectors along the central vertical plane for the 5, 3 and 1.5% slopes under different flow conditions. From the velocity vectors in the vertical planes, three different regions could be clearly distinguished: upstream of the boulders, intermediate region, and downstream of the boulders (wake region). Downstream of the boulders, the wake region was prominent and its length was about 2*D* for all flow rates and slopes. This length is similar with Shamloo et al. (2001) for a hemisphere but is quite different from 1*D* to 1.5*D* given by Tritico and Hotchkiss (2005) for emerged boulders in a natural channel and 1.5*D* by Papanicolaou et al. (2012) for fully submerged boulders. In the intermediate region there was an approximate uniform distribution of velocity patterns over the

entire water depth for a short distance between converged and diverged velocity vectors along and from the centre line of boulders, respectively. In this region, the maximum magnitude of velocity vectors occurred. Upstream of boulders, the approach velocity towards the boulders started to decelerate and there was a certain influence of a vertical velocity component. The maximum magnitude of the velocity vectors varied from 0.80 to1.10, 0.75 to 1.04, and 0.64 to 1.12 m/s for the 5, 3, and 1.5% slopes for flow rates from 60 to 160 L/s, respectively. The corresponding prototype maximum velocity (for a 1:4 undistorted scale model) will vary from 1.6 to 2.2, 1.5 to 2.0, and 1.3 to 2.2 m/s, respectively, which is typically be less than the burst swim velocity of different fishes. Burst swimming speeds of Salmonid fishes (2.3–8.1 m/s) can be maintained for 15s at the low end of their range or for 6s at the high end of the range (Powers et al. 1986). Therefore, Salmonid would be able to ascend this fishpass even in prototype easily and would be able to swim through multiple cells without resting.

To understand the variation of depth-average velocity with downstream distance along the centre line of the flume, the normalized depth-average streamwise velocity ($\bar{u}/U_{max}$) is plotted against *X/D* in Figure 4.12 for all the experiments. It is interesting to observe that all the experimental results fall in a narrow band of constant width, and the variation of depth-average streamwise velocity follows a generalized trend line. Though, this relation will depend on the spatial arrangement, not just the density, of the boulders, this variation could be described by a mean line and its equation is

$$\frac{\bar{u}}{U_{\max}} = -0.086\left(\frac{X}{D}\right)^2 + 0.558\left(\frac{X}{D}\right) - 0.071 \qquad (R^2=0.995) \tag{4.4}$$

The lowest values of $\bar{u}$ (about 40% of U_{max}) downstream of a boulder increased rapidly in the downstream direction with *X/D* and attained its peak (about 80% of U_{max}) in the intermediate region and then gradually leveled off (about 70% of U_{max}) with *X/D* approaching the boulder.

4.3.3 Flow Resistance

Conventionally, flow resistance equations such as Darcy-Weisbach, Manning, and Chézy implicitly assume the dominant resistance to be boundary shear stress. Such equations are inherently unsatisfactory for low flow conditions, where the size of roughness elements is comparable to the flow depth, and resistance is dominated by form drag (Bathurst 2002). The preliminary results of this study revealed that the force due to skin friction is approximately 4% of drag force, reflecting the minimal contribution of the total forces. Similarly, Potter and Wiggert (2010) also reported that 95% of the drag is due to form drag and only 5% is due to skin drag for a single smooth sphere in a cross flow. It is hereafter assumed that the drag associated with the boulders is dominant and skin friction is negligible, and the resisting force due to form drag of *N* independent boulders in the channel bed is

$$F_D = \frac{1}{2} C_D \rho u_{avg}^2 N A_p \tag{4.5}$$

where, A_p is the projected cross-sectional area of each individual boulder, C_D is the drag coefficient, and N is the number of boulders. The streamwise weight component of the water mass over a bed area, $A\ (=L_z \times B)$, is given by

$$WS_0 = \rho g S_0 (BHL_z - N(\pi D^3 / 6)) / A \tag{4.6}$$

where, W is the weight of water, L_z is the streamwise distance of a control volume having 1.5 cells, B is the channel width. Simplifying Eq. (4.6) we get,

$$WS_0 = \rho g S_0 H(1 - 2/3\lambda l^*) \tag{4.7}$$

For uniform flow, the drag force will balance the streamwise weight component of the water mass. Now equating and simplifying Eqs. (4.5) and (4.7), with $R_v = H(1 - 2/3\lambda l^*)$ we get,

$$u_{avg} = \sqrt{\frac{2g}{C_D N A_p}} \sqrt{S_0} \sqrt{R_v} \tag{4.8}$$

Now, let $C^* = \sqrt{\frac{2g}{C_D N A_p}}$, where C^* is the flow resistance coefficient for large-scale roughness, which is comparable to Chézy coefficient, then Eq. (4.8) can be written as

$$u_{avg} = C^* \sqrt{R_v} \sqrt{S_0} \tag{4.9}$$

Eq. (4.9) is superficially similar to the Chézy equation. However, in this case the inclusion of the volumetric hydraulic radius R_v is dominated by the form drag rather than skin friction is balanced by the drag while the hydraulic radius in the Chézy equation arises from the resisting shear force at the boundary.

From Eq. (4.8), average velocity (u_{avg}) can also be computed by knowing the values of the drag coefficient (C_D) for any arrangement of boulders. In this type of experimental setup, C_D might be the function of obstacle density, obstacle spacing, relative depth, Froude number, Reynolds number, etc. Previous studies have shown that C_D is dependent on relative submergence and Froude number for hemisphere (Flammers et al.1970) and is function of relative submergence and Reynolds number for different arrays of circular cylinders (Cheng 2012). For the hemisphere study by Shamloo (1997) found that C_D is significantly related with relative submergence compared with Froude number. For this particular study, assuming that drag coefficient is only a function of relative submergence (*H/D*), the variation of C_D with *H/D* for all experiments is presented in Figure 4.13, where *Fr*=0.39 to 0.78 and *Re*=63,000 to 192,000. From Figure 4.13, it is apparent that C_D is a function of submergence ratio (*H/D*) with a good agreement of all data points for all experiments. The following power equation may be written to describe the fitted line as:

$$C_D = 1.787\left(\frac{H}{D}\right)^{-2.16} \qquad (R^2=0.96) \qquad (4.10)$$

It is observed that C_D decreases with increasing *H/D*. C_D increases rapidly from 1.2 to 3.0 as submergence ratio decreases from 1.2 to 0.8. For $H/D>1.2$, the drag coefficient decreases at lower rate from 1.2 to 0.7. Stone and Shen (2002) calculated C_D for emergent and submerged cylindrical stems of various sizes and concentrations which varied from 1.10 to 1.93. Cheng (2012) found C_D values greater than 1.0 for arrays of emergent circular cylinders. At $H/D>1.2$, C_D

values are lower than that for arrays of circular cylinders; the probable reasons might be geometric shape effect (Potter and Wiggert 2010) and moderate free surface effect (Flammers et al. 1970). At higher Reynolds number (10^4-10^5), C_D for the single smooth sphere (approximately 0.5) is smaller than that for single smooth cylinder (approximately 1.1) (Potter and Wiggert 2010). In addition, the variation of C_D with H/D for single hemisphere for Fr=0.7 predicted by Flammers et al. (1970) was plotted in this figure. Here the values of C_D within the range of this study having different trend which is expected because obstacle in a cluster could differ from that for a single obstacle (Blevins 1984). Flammer et al (1970) found that for $H/D<1.5$, C_D increases rapidly with decreasing submergence ratio and C_D decreases at smaller rate for $H/D>1.5$, afterward C_D does not vary with H/D. Therefore, the only unknown (C_D) in Eq. (4.8) can be estimated from this relationship (Eq. (4.10)). More experiments are needed in order to obtain family of curves showing the relationship between drag coefficient and submergence ratio for different arrangement of boulders.

The performance of the proposed Eq. (4.9) ($0.8<H/D<1.6$, S_0=1.5-5%) was assessed by comparing the measured and predicted values of flow velocity in Figure 4.14. The results showed very good agreement between measured and predicted velocities. The average absolute prediction error is about 3% having the maximum and minimum values of 7% and less than 1%, respectively. The implication of this equation on steep mountain streams/rivers and flumes with intermediate to large scale roughness was also tested in this figure. The predicted

flow velocities using resistance formulas of Pagliara et al. (2008) for flumes having crushed stones with protruding boulders ($0.26< H/D_{84}<5$, S_0=1-9%), Smart et al. (2002) for natural streams ($0.25<R_v/D_{84}<4.5$), Bathurst (2002) for mountain rivers ($0.37<H/D_{84}<11$, $S_0>0.8\%$), and Bathurst (1985) for mountain rivers ($0.43< H/D_{84}<5.97$, S_0=0.4-4%) were plotted against measured velocity with 10% accuracy limits, where D_{84} is the 84-percentile bed material size and R (hydraulic radius) is replaced by R_v. The results confirmed good similarity where all data points fitted within 10% accuracy limits, except for Bathurst (1985). The semi-logarithmic equation by Bathurst (1985) was developed from the assumption of small scale roughness and could underestimate the flow resistance in boulder-bed rivers (Bathurst 2002).

4.4 Summary and Conclusions

This study investigated the mean flow characteristics generated by a staggered arrangement of boulders in a rock-ramp fishpass in a relation to fish passage. This fishpass increased water depth by about three times compared with the unregulated water depth, and reduced the flow velocity by about 64%. Therefore, it will be beneficial for fish to migrate upstream through this fishpass. The contour maps of water depth revealed that the repetitive pattern of higher and lower water depths formed a relatively deeper pathway through the fishpass. Similarly, the spatial distributions of flow velocity showed that fish might find some preferred paths for migration and resting areas. Based on the literature, the measured average water depth (varied from 44 to 88 cm for a 1:4 undistorted

scale model) can provide adequate depth (large salmon required 15-35 cm and smaller trout 6-10 cm) for fish passage and the maximum velocity magnitude (varied from 1.3 to 2.2 m/s for a 1:4 scale model) will be less than the burst swim velocity of Salmonid fishes (2.3–8.1 m/s).

The water surface profile analysis confirmed that the normalized flow depth is correlated with the relative longitudinal distance along the centre line of the flume. A generalized correlation between the dimensionless discharge *(Q*)* and average water depth (*H/D*) was developed and the correlation followed a linear relationship. Both correlations agree well with all supplementary experimental points, where the boulder size was scaled down, especially for smaller submergence ratios ($H / D \leq 1.2$). The normalized streamwise velocity profiles and velocity vectors along the centre line distinguished three different flow regions: downstream of boulders/wake region (*X/D*=1 to 2), intermediate region (*X/D*=2 to 3), and upstream of boulders (*X/D*=3 to 4.2). In the wake region, the flow accelerated at higher gradients ($du / dx > 3s^{-1}$) and there was no negative velocity near the bed. In the intermediate region, the variation of maximum velocity magnitude over the entire flow depth was relatively small (less than 5 to 20%) and the variation diminished with increasing flow rates as well as with decreasing slopes. Upstream of the boulders, the observed flow started to decelerate as it approached the boulder; also the velocity gradient near the bed was predominantly negative.

A general linear relationship has also been developed between the dimensionless discharge *(Q*)* and dimensionless maximum velocity magnitude *(U_{max}*)* and streamwise average velocity *(u*)*. The relationship for U_{max}* agrees well with large-scale data sets that ensured the applicability of Eq. (4.2) in field-scale. The normalized depth-average streamwise velocity ($\bar{u}/U_{\max}$) along the centre line of the flume was also related with the longitudinal distance (*X/D)*. From those general correlations it is possible to predict the velocity in a rock-ramp fishpass as a function of normalized discharge and streamwise distance. Based on an elementary flow resistance analysis for wake-interference flow regime in a rock-ramp fishpass, a general equation for average velocity has been developed. In this equation, the drag coefficient is a function of submergence ratio and this equation shows good agreement with other equations for steep mountain streams/rivers and flumes for large scale roughness.

It is encouraging to note that all the proposed relationships have been formulated in dimensionless parameters, which enables us to compare with prototype studies. Eqs. (4.1) and (4.2) were tested for smaller boulder size (scaling down) and large-scale data sets, respectively. To examine the reliability of other equations in a rock-ramp fishpass, it would be useful to conduct further studies with field-scale data.

The results presented in this paper are important in understanding the mean flow characteristics with a relationship to fish passage in nature-like fishpasses and

would be useful to both fish biologists and fishpass designers. It is hoped that the outcome of this study will allow us to make improvements for the design and building of successful nature-like fishpasses. These analyses could be developed to some degree for specialized ideal cases in the flume, but yielded little information regarding the general case. Therefore, it would be necessary to pursue additional investigations via field to define the relationships for water depth, velocity, and flow resistance especially for different boulder spacings and arrangements in a rock-ramp fishpass.

4.5 References

Bathurst, J. C. (1985). "Flow resistance estimation in mountain rivers." *Journal of Hydraulic Engineering*, 111(4), 625–643.

Bathurst, J. C. (2002). "At-a-site variation and minimum flow resistance for mountain rivers." *Journal of Hydrology*, 269, 11–26.

Bathurst, J. C., Li, R. M., and Simons, D. B. (1981). "Resistance equation for large scale roughness." *Journal of the Hydraulics Division*, 107(12), 1593-1613.

Blevins, R.D. (1984). "*Applied Fluid Dynamics Handbook*." Van Nostrand Reinhold, N.Y.

Biggs, J. F., Duncan, M. J., Francoeur, S. N., and Meyer, W. D. (1997). "Physical characterization of microform bed cluster refugia in 12 headwater streams, New Zeland." *New Zealand Journal of Marine Freshwater Research,* 13(4), 413–422.

Cheng, N. S. (2012). "Calculation of drag coefficient for arrays of emergent circular cylinders with pseudofluid model." *Journal of Hydraulic Engineering*, 139(1), 602-611.

Crowder, D. W., and Diplas, P. (2000). "Using two-dimensional hydrodynamic models at scales of ecological importance." *Journal of Hydrology*, 230(3-4), 172–191.

Crowder, D. W., and Diplas, P. (2006). "Applying spatial hydraulic principles to quantify stream habitat." *River Research and Applications,* 22(1), 79-89.

DVWK (2002). "*Fish passes-Design, dimensions and monitoring."* Published by the Food and Agriculture Organization of the United Nations in arrangement with German Association for Water Resources and Land Improvement as DVWK-Merkblatt.

Ead, S.A., Katopodis, C., Sikora, G. J., and Rajaratnam, N. (2004). "Flow regimes and structure in pool and fishways." *Journal of Environmental Engineering and Science,* 3, 379–390.

Ferro, V. (2003). Flow resistance in gravel-bed channels with large-scale roughness." *Earth Surface Processes and Landforms,* 28, 1325-1339, DOI: 10.1002/esp.589.

Flammer, G. H., Tullis, J. P., and Mason, E. S. (1970). "Free surface velocity gradient flow past hemisphere." *Journal of the Hydraulic Division*, 96(7), 1485-1502.

Franklin, P.A., and Bartels, B. (2012). "Restoring connectivity for migratory native fish in a New Zealand stream: effectiveness of retrofitting a pipe culvert." *Aquatic Conservation: Marine and Freshwater Ecosyst*ems, 22, 489–497.

Franklin, A. E., Haro, A., Castro-Santos, T., and Noreika, J. (2012). "Evaluation of nature-like and technical fishways for the passage of Alewives at two coastal streams in New England." *Transactions of the American Fisheries Society*, 141, 624-637.

Goring, D.G., and Nikora, V. I. (2002). "Despiking acoustic doppler velocimeter data." *Journal of Hydraulic Engineering,* 128(1), 117–126.

Haro, A., Franklin, A., Castro-Santos, T., and Noreika, J. (2008). "Design and evaluation of nature-like fishways for pasage of Northeastern Diadromous fishes." Final report, Submitted to NOAA National Marine Fisheries Service Office of Habitat Conservation.

Hassan, M. A., and Reid, I. (1990). "The influence of microform bed roughness elements on flow and sediment transport in gravel bed rivers." *Earth Surface Processes and Landforms,* 15, 739-750.

Jordanova, A. A. (2008). "*Low flow hydraulics in rivers for environmental applications in South Africa*." Ph. D. Thesis, Faculty of the Engineering and the Built Environment, University of the Witwatersrand, Johannesburg, South Africa.

Katopodis, C., Kells, J. A., and Acharya, M. (2001). "Nature-like and conventional fishways: alternative concepts?" *Canadian Water Resources Journal*, 26(2), 211-232.

Katopodis, C, and Williams, J. G. (2011). "The development of fish passage research in a historical context." *Ecological Engineering*, 48, 8-18.

Lacey, R. W. J., and Rennie, C. D. (2012). "Laboratory investigation of turbulence flow structure around a bed mounted cube at multiple flow stages." *Journal of Hydraulic Engineering*, 137(1), 71-84.

Lacey, R. W. J., and Roy, A. G. (2008). "The spatial characterization of turbulence around large roughness elements in a gravel-bed river." *Geomorphology,* 102, 542-553.

Liu, M., Rajaratnam, N., and Zhu, D. Z. (2005). "Mean flow and turbulence structure in vertical slot fishways." *Journal of Hydraulic Engineering*, 132(8), 765–777.

Martin, V., Fischer, T. S. R., Millar, R. G., and Quick, M. C. (2002). "ADV data analysis for turbulent flows: Low correlation problem." In: T. L. Wahl (ed.), Proc. Conf. Hydraulic Measurements and Experimental Methods, ASCE, Estes Park, CO, USA.

Martinuzzi, R., and Tropea, C. (1993). "Flow around surface-mounted, prismatic obstacles placed in a fully developed channel flow." *Journal of Fluids Engineering*, 115(1), 85-92.

Morris, Jr. H. M. (1954). "Flow in rough conduits." *Transactions of the American Society of Civil Engineers*, 119, 373–410.

Pagliara, S., Das, R., and Carnacina, I. (2008). "Flow resistance in large-scale roughness condition." *Canadian Journal of Civil Engineering*, 35(9), 1285-1293.

Papanicolaou, A. N., Kramer, C. M., Tsakiris, A. G., Stoesser, T., Bomminayuni, S., and Chen, Z. (2012). "Effects of a fully submerged boulder within a boulder array on the mean and turbulent flow fields: Implications to bedload transport." *Acta Geophysca*, 60(6), 1502-1546.

Parasiewicz, P., Eberstaller, J., Weiss, S., and Schmutz, S (1998). "Conceptual Guidelines for Nature-like Bypass Channels." In: M. Jungwirth, S. Schmutz, and S. Weiss, (eds), *Fish Migration and Fish Bypasses*, Oxford: Fishing News Books, Blackwell Science Ltd, 348-362.

Peterson, D. F., and Mohanty, P. K. (1960). "Flume studies of flow in steep, rough channels." Proceedings of the ASCE, *Journal of the Hydraulic Division*, 86(HY9), 55-76.

Potter, M. C., and Wiggert, D. C. (2010). *"Mechanics of Fluids.*" Third Edition, SI, Cengage Learning, USA.

Powers, P. A., Orsborn, J. F., Bumstead, T. W., Klinger-Kingsley, S., and Mih, W. C. (1986). "Fishways: an assessment of their development and design." Bonneville Power Administration, Project 82–14, Portland, Oregon.

Rajaratnam, N., and Muralidhar, D (1968). "Yaw probe used as Preston tube." *The Aeronautical Journal of the Royal Aeronautical Society*, 72, 1059-1060.

Rajaratnam, N., Van der Vinne, G., and Katopodis, C (1986). "Hydraulics of vertical slot fishways.' *Journal of Hydraulic Engineering*, 112(10), 909–927.

Reiser, D. W., and Bjornn. T. C. (1979). "Habitat requirements of anadromous Salmonids." In: Meehan, W. R., Technical Editor. Influence of forest and rangeland management on anadromous fish habitat in the Western United States and Canada, USDA Forest Service, GTR PNW-96.

Sadeque, M. A. F., Rajaratnam, N., and Loewen, M. R. (2008). "Flow around cylinders in open channels.' *Journal of Engineering Mech*anics, 134(1), 60-71.

Shamloo, H. (1997). "*Hydraulics of simple habitat structures in open channels.*" Ph. D. Thesis, Department of Civil and Environmental Engineering, University of Alberta, Canada.

Shamloo, H., Rajaratnam, N., and Katopodis, C (2001). "Hydraulics of simple habitat structures." *Journal of Hydraulic Res*earch, 39(4), 351–366.

Smart, G. M., Duncan, M. J., and Walsh, J. M. (2002). "Relatively rough flow resistance equations." *Journal of Hydraulic Engineering*, 128(6), 568-578.

SonTek (1997). "*ADV technical documentation."* SonTek.

Stone, B. M., and Shen, H. T. (2002). "Hydraulic resistance of flow in channels with cylindrical roughness." *Journal of Hydraulic Engineering*, 128 (5), 500-506.

Strom, K.B., and Papanicolaou, A. N. (2007). "ADV measurements around a cluster microform in a shallow mountain stream." *Journal of Hydraulic Engineering*, 133(12), 1379-1389.

Thorncraft, G. A., and Harris, J. H. (1996). "Assessment of rock-ramp fishways." NSW Fisheries Research Institute and the Coorperative Research Centre for Freshwater Ecology, Report for NSW Environment Protection Authority.

Tritico, H. M., and Hotchkiss, R. H. (2005). "Unobstructed and obstructed turbulent flow in gravel bed rivers." *Journal of Hydraulic Engineering*, 131(8), 635-645.

U.S.B.R. (2007). "*Rock-ramp Design Guidelines."* U.S. Department of the Interior Bureau of Reclamation Technical Service Center Denver, Colorado, USA.

van Zyll de Jong, M. C., Cowx, I. G., and Scruton, D. A. (1997). "An evaluation of instream habitat restoration techniques on salmonid populations in a Newfoundland stream." *Regulated Rivers: Research & Management*, 13(6), 603-614.

Wang, R.W., and Hartlieb, A. (2011). “Experimental and field approach to the hydraulics of nature-like pool-type fish migration facilities.” *Knowledge and Management of Aquatic Ecosystems*, 400, 05.

Table 4-1 Primary details of the experimental scenarios.

Experiment No.	Channel slope	Discharge (L/s)	Velocimeter	Average water depth *H* (cm)	Submergence ratio *(H/D)*	Reynolds number, *Re*	Froude number, *Fr*
1	5 %	60	ADV	11.74	0.84	63,266	0.50
2		75	ADV	12.92	0.92	80,974	0.55
3		100	ADV	14.17	1.00	105,660	0.64
4		125	Yaw Probe	15.47	1.11	148,340	0.78
5**	3 %	45	-	12.28	0.88	-	
6*		60	Vectrino Plus	13.93	1.00	77,244	0.47
7*		80	Vectrino Plus	15.22	1.09	106,817	0.57
8**		105	-	17.18	1.23	-	
9*		120	Vectrino Plus	17.60	1.26	150,844	0.65
10**	1.5 %	25	-	10.82	0.77	-	
11**		40	-	13.41	0.96	-	
12*		60	Vectrino Plus	15.53	1.11	75,231	0.39
13**		80	-	17.25	1.23	-	
14*		90	Vectrino Plus	18.08	1.29	114,176	0.47
15*		160	Vectrino Plus	22.38	1.60	191,939	0.58

*Water level and instantaneous velocity were measured along the centre line in the detailed measurement area

**Only water level was measured along the centre line in the detailed measurement area

Table 4-2 Details of supplementary experimental scenarios.

Experiment No.	Channel slope	Discharge (L/s)	Average water depth *H* (cm)	Submergence ratio *(H/D)*
A1	2.6 %	1.8	2.33	0.99
A 2	2.6 %	2.6	2.69	1.14
A 3	2.6 %	2.9	2.77	1.18
A 4	2.6 %	3.9	2.87	1.22
A 5	2.6 %	4.5	3.05	1.30
B1	5 %	1.2	1.74	0.74
B2	5 %	2.0	2.08	0.89
B3	5 %	3.0	2.39	1.02
B4	5 %	4.0	2.69	1.14
B5	5 %	5.0	2.91	1.24

Table 4-3 The ratio of regulated and unregulated flow depth and velocity for all experiments.

Expt. No.	Flow (L/s)	Depth (cm)		Increased depth (times) $= H / H_0$	Velocity (m/s)		Velocity Reduction (%) $= \frac{(u_0 - u_{avg})}{u_0} * 100$
		Unregulated* *(H_0)*	Regulated** *(H)*		Unregulated* *(u_0)*	Regulated** *(u_{avg})*	
1	60	3.46	11.75	3.4	1.88	0.54	71
2	75	3.97	12.92	3.3	2.05	0.62	70
3	100	4.75	14.17	3.0	2.28	0.75	67
4	125	5.46	15.47	2.8	2.48	0.96	61
6	60	4.05	13.93	3.4	1.61	0.55	66
7	80	4.84	15.22	3.1	1.79	0.70	61
9	120	6.25	17.60	2.8	2.08	0.86	59
12	60	5.03	15.53	3.1	1.29	0.48	63
14	90	6.5	18.08	2.8	1.50	0.63	58
15	160	9.36	22.38	2.4	1.85	0.86	54

* Using Manning's equation where n=0.012 for smooth steel bottom

**Measured

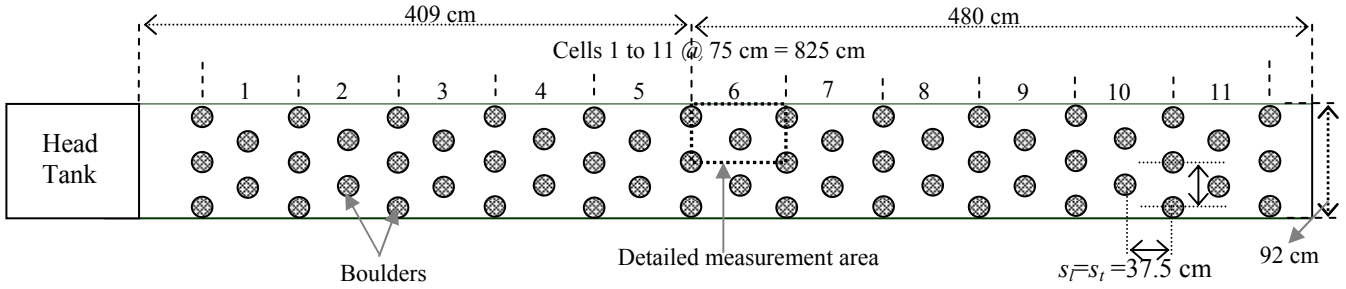

(a) Plan view

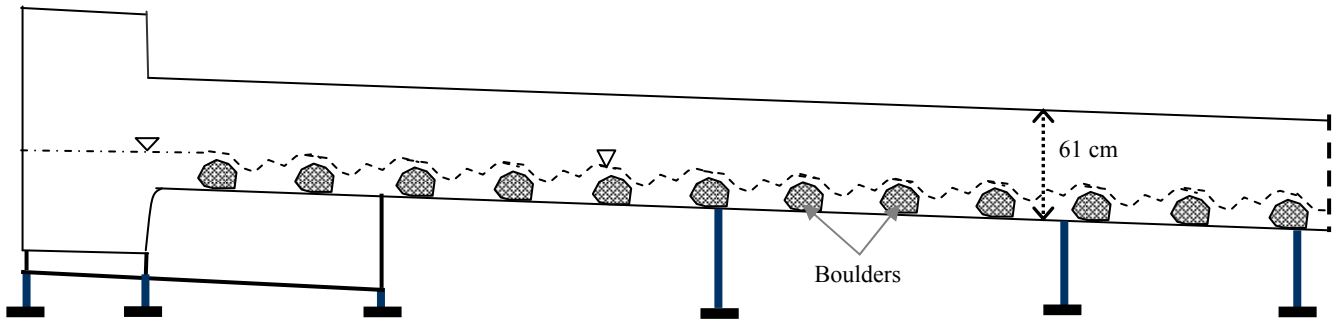

(b) Side view

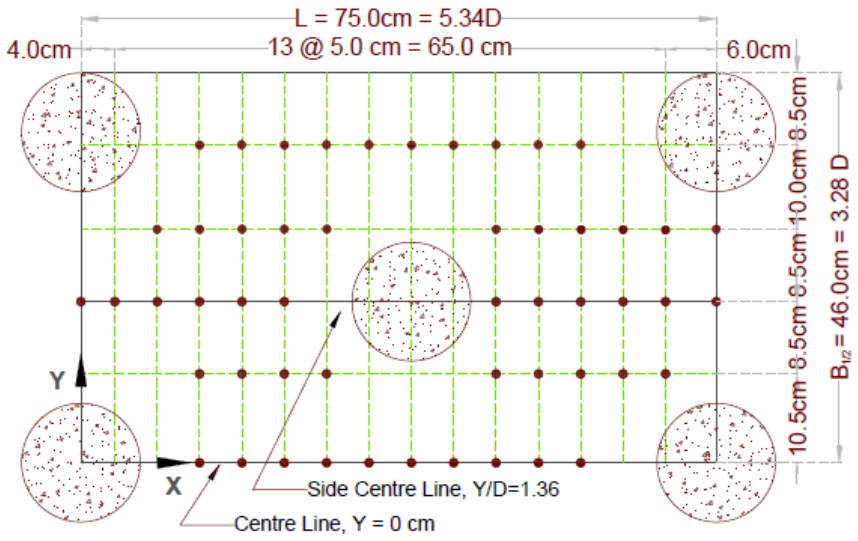

(c) Detailed measurement area

Figure 4.1 (a) Plan view and (b) side view of the experimental setup of rock-ramp nature-like fishpass, (c) reference grid used for detailed measurement.

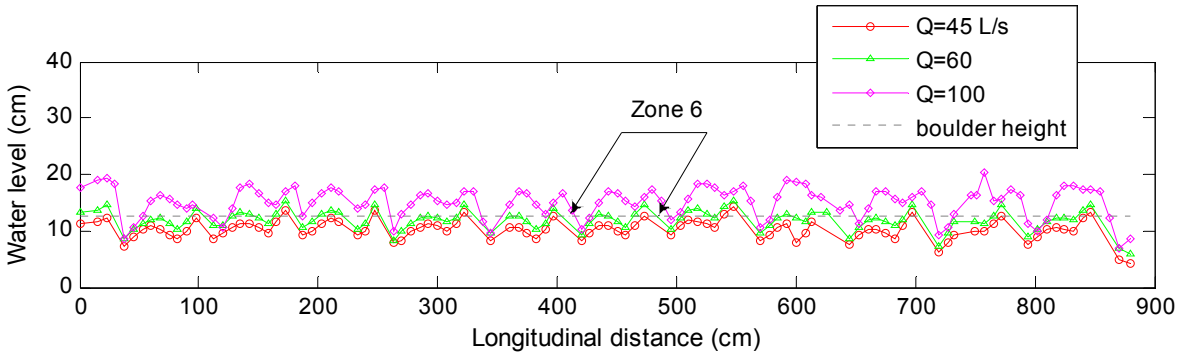

Figure 4.2 Longitudinal water surface profiles along the centre line of the flume for the 5% slope under different flow rates 45, 60, and 100 L/s.

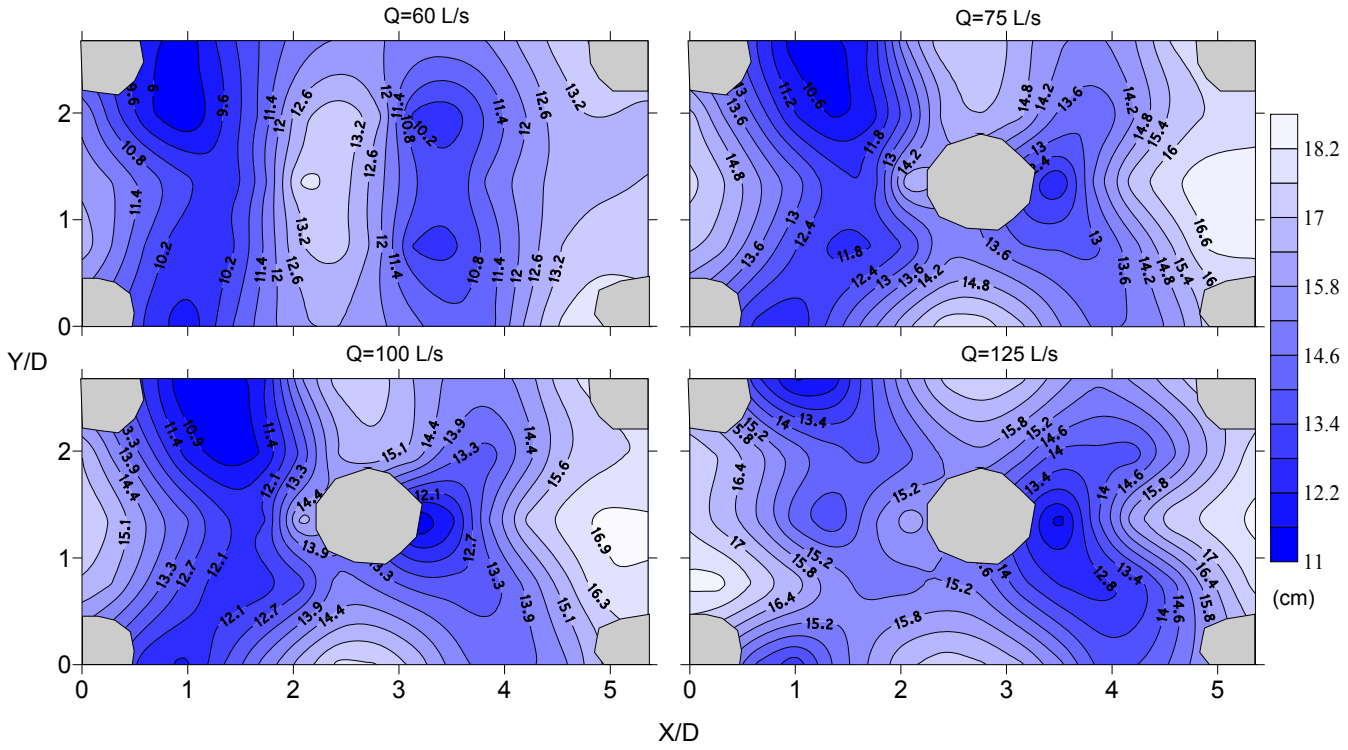

Figure 4.3 Contour maps for water depth in the detailed measurement area for the 5% slope under different flow conditions (boulder dimensions are approximated and are not to scale).

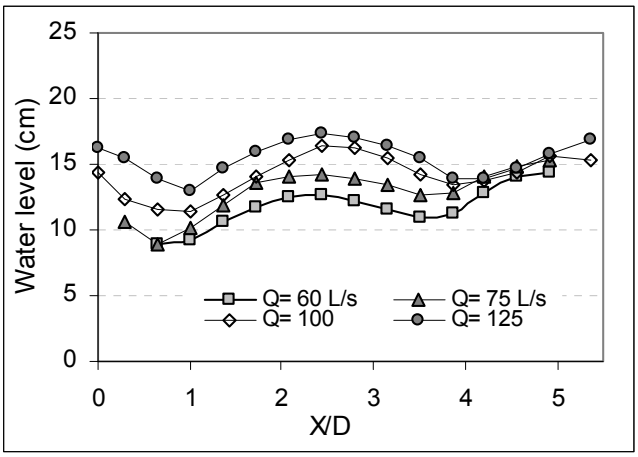

(a)

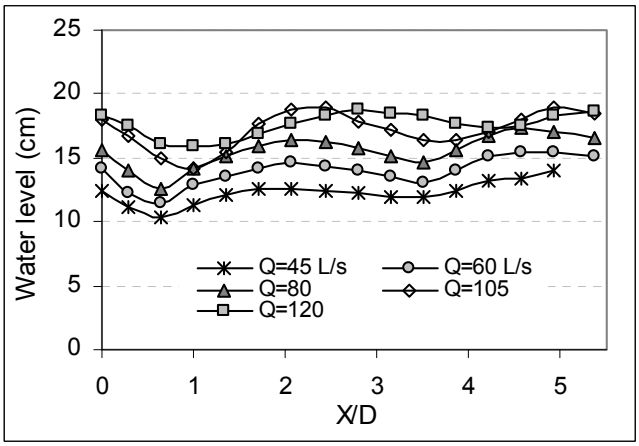

(b)

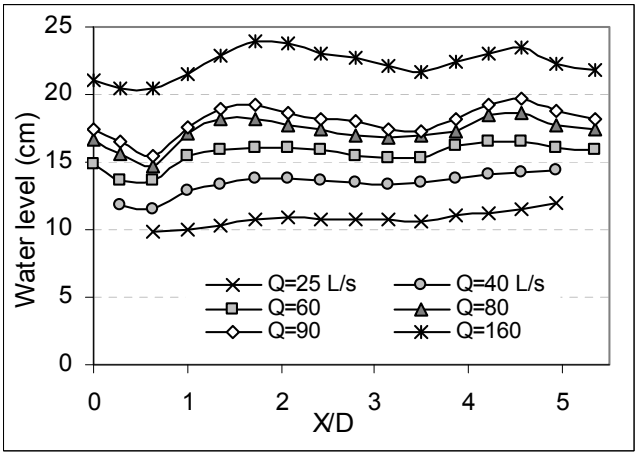

(c)

Figure 4.4 Longitudinal water surface profiles along the centre line of the flume in the detailed measurements area for (a) 5%, (b) 3%, and (c) 1.5% slope under different flow conditions.

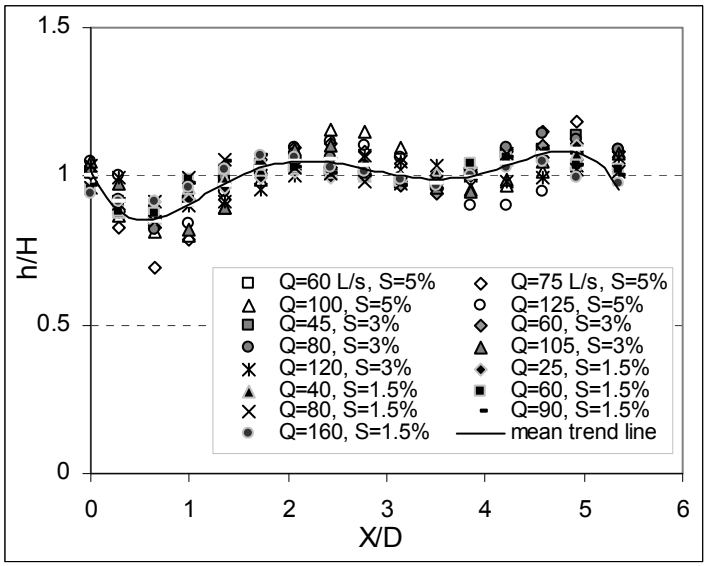

(a)

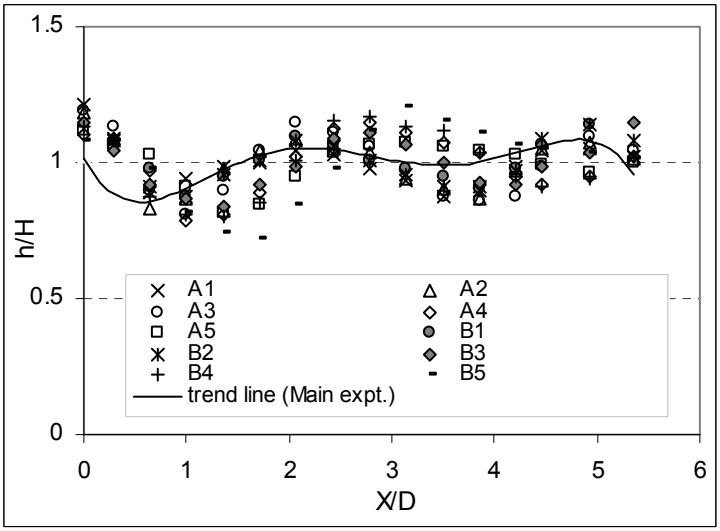

(b)

Figure 4.5 The normalized water surface profiles along the centre line of the flume (a) for all experiments and (b) for all supplementary experiments as series A and B fitted with trend line from (a).

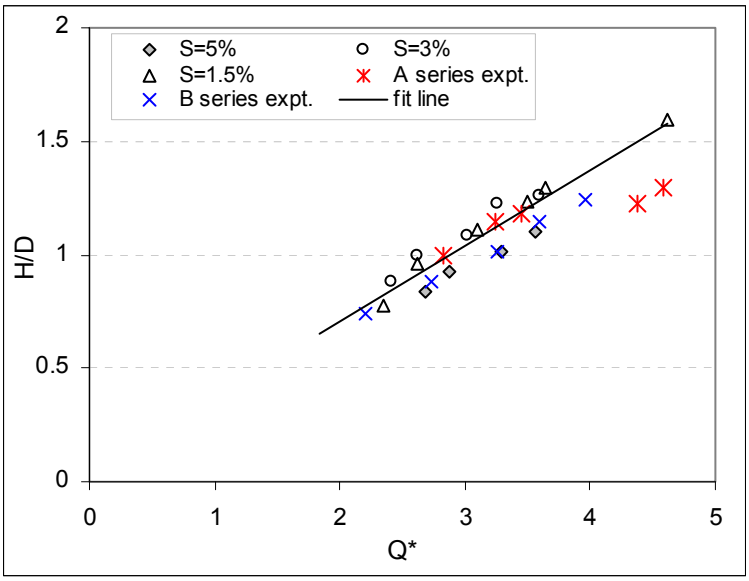

Figure 4.6 The generalized depth–discharge relationship for all experiments. The results of the supplementary experiments are over-plotted as series A and B.

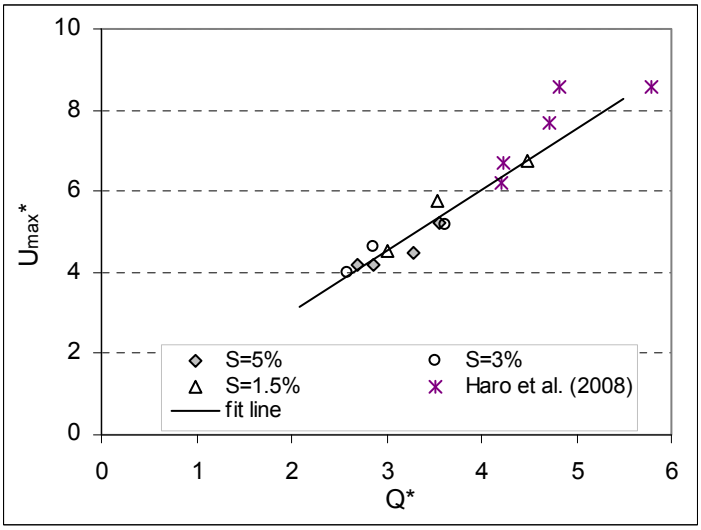

(a)

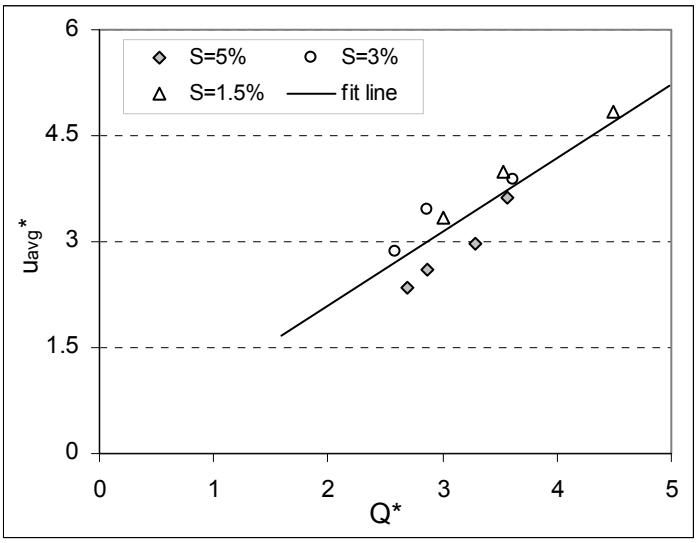

(b)

Figure 4.7 General correlation for normalized discharge versus dimensionless (a) maximum velocity magnitude and (b) streamwise average velocity.

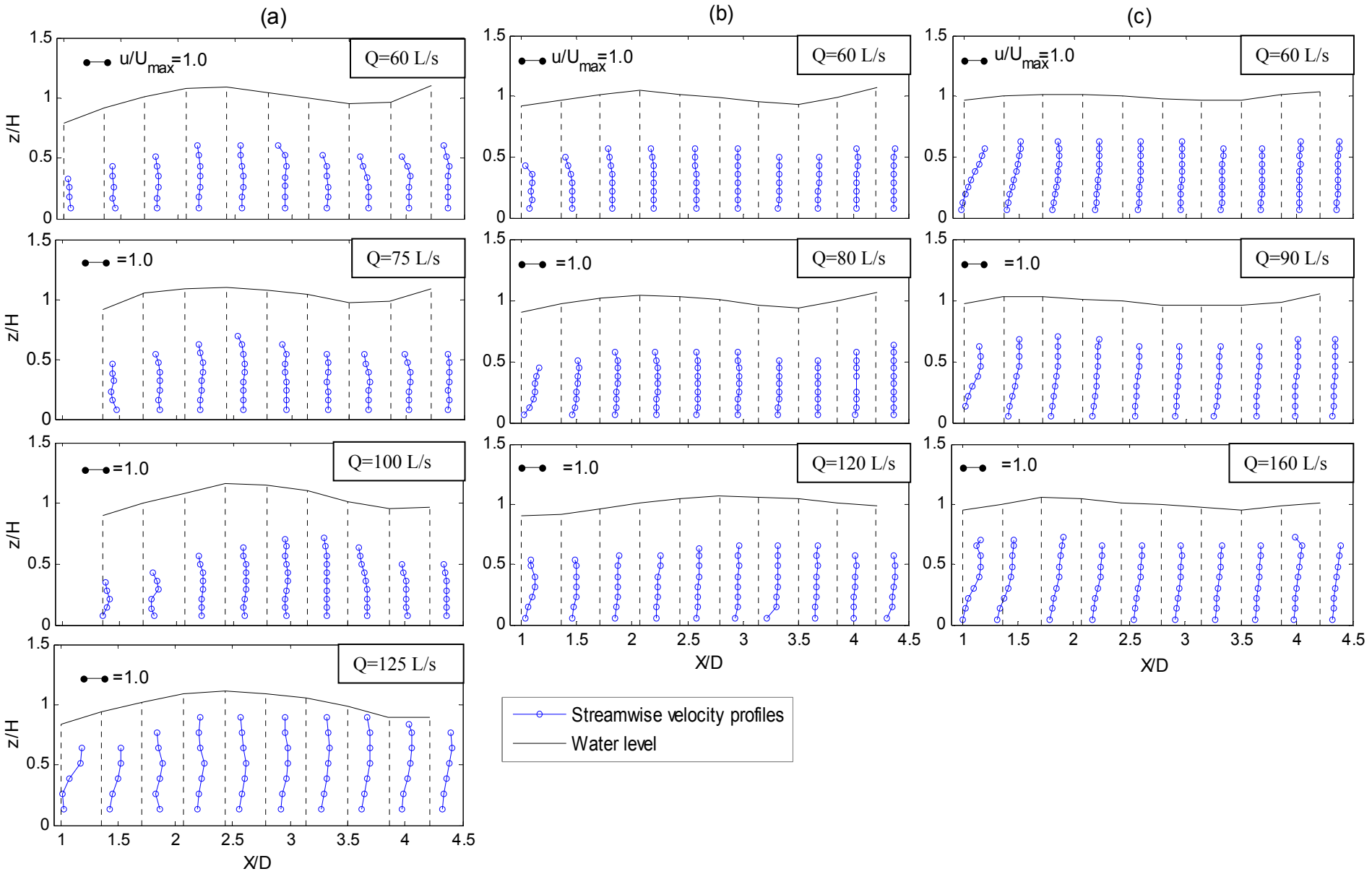

Figure 4.8 Distribution of normalized streamwise mean velocity *(u/U_{max})* along the centre line of the flume in the detailed measurement area for (a) 5%, (b) 3%, and (c) 1.5% slope under different flow conditions.

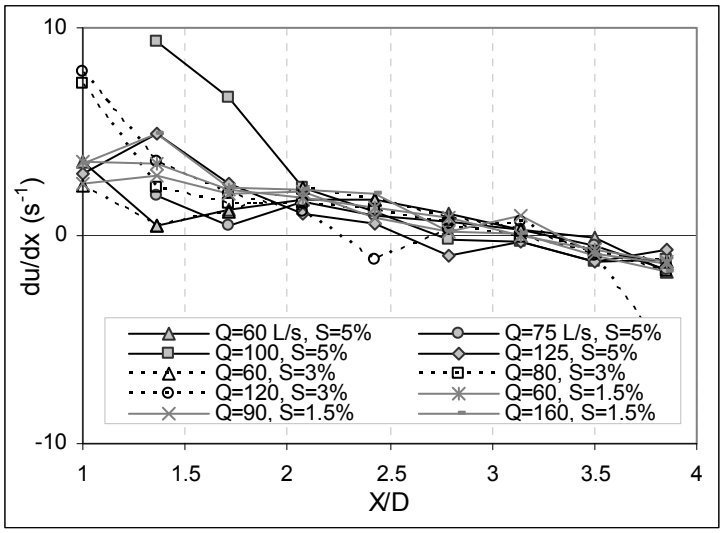

Figure 4.9 The profiles of the streamwise velocity gradient in the streamwise direction (du/dx) near the bed (at z= 1.0 cm) along the centre line along of the flume in the detailed measurement area for all experiments.

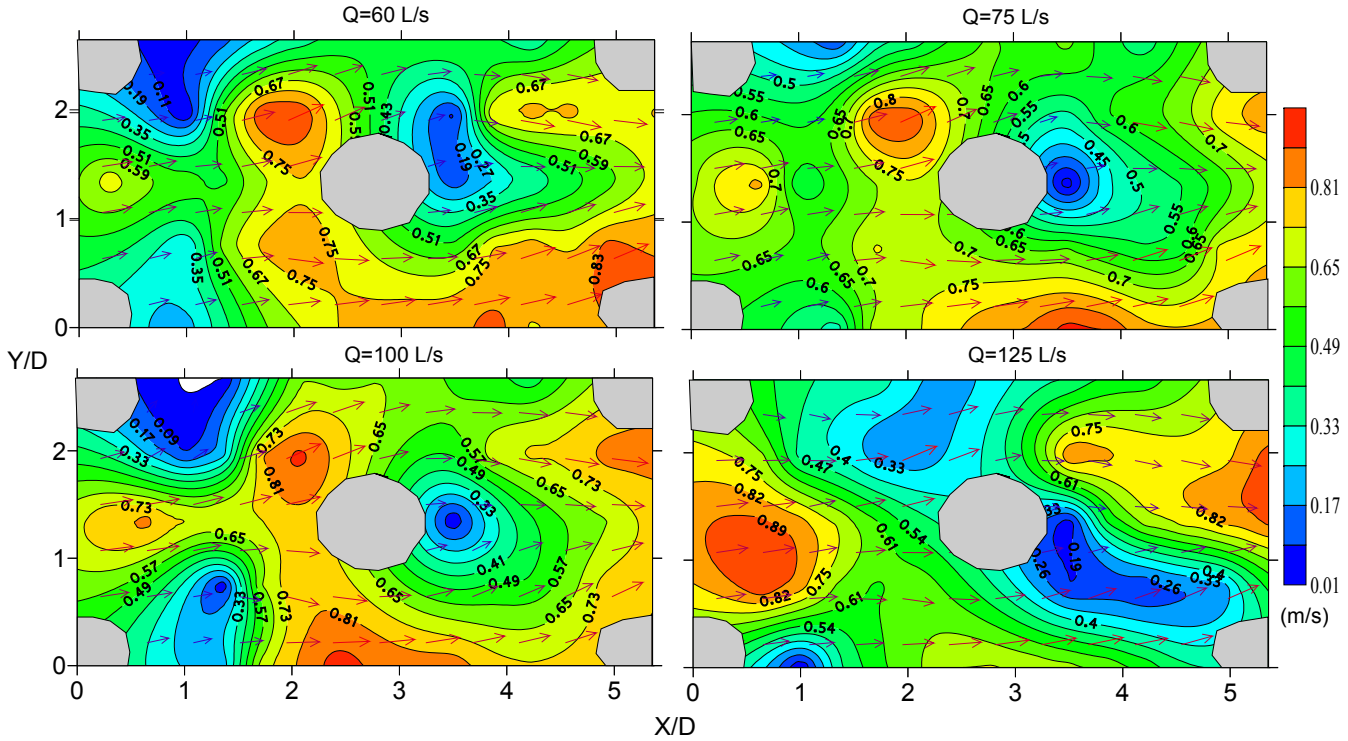

Figure 4.10 Spatial distributions of normalized plane velocity magnitude ($U_{xy}/U_{\max}$) with directions on horizontal plane (XY) at z=4 cm in the detailed measurement area for the 5% slope under different flow conditions (boulder dimensions are approximated and are not to scale).

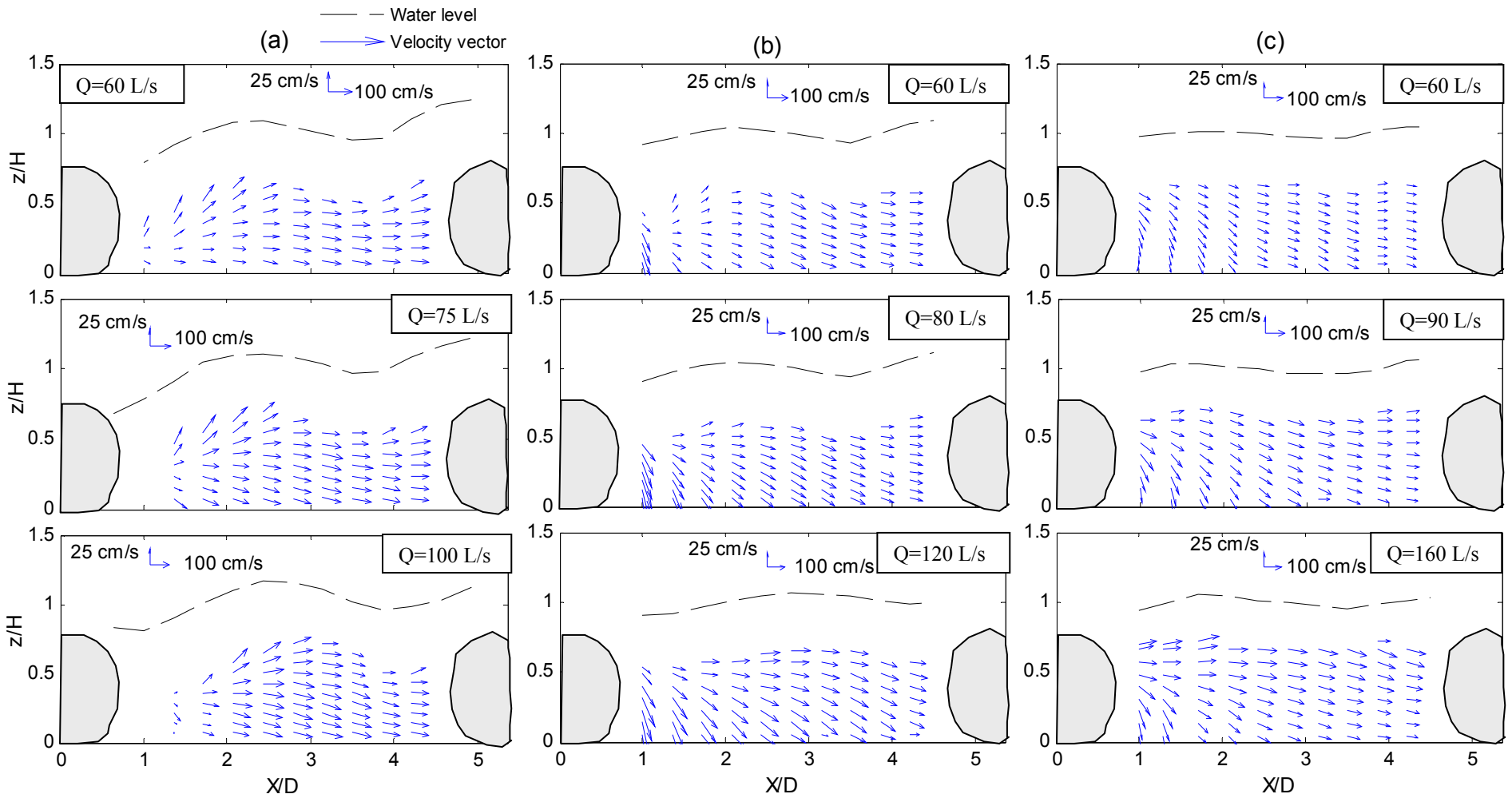

Figure 4.11 Velocity vectors on vertical plane (XZ) along the centre line of the flume in the detailed measurement area for (a) 5%, (b) 3%, and (c) 1.5% slope under different flow conditions (boulder dimensions are approximated and are not to scale).

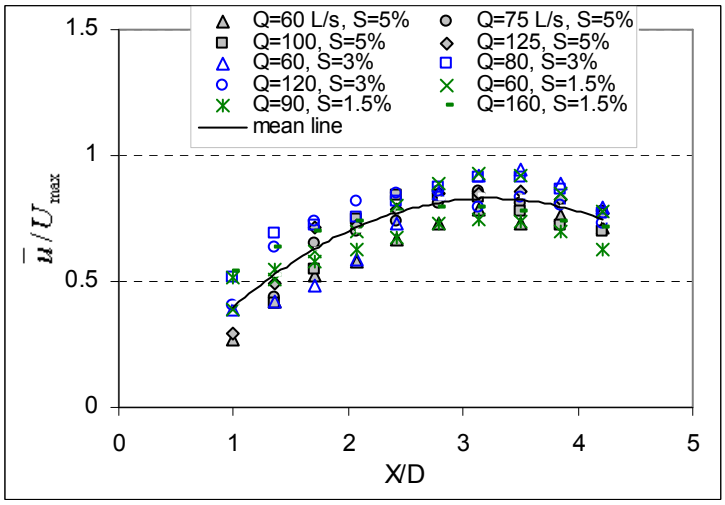

Figure 4.12 Variation of normalized depth-average velocity ($\bar{u}/U_{max}$) with relative downstream distance *X/D* along the centre line of the flume in the detailed measurement area for all experiments.

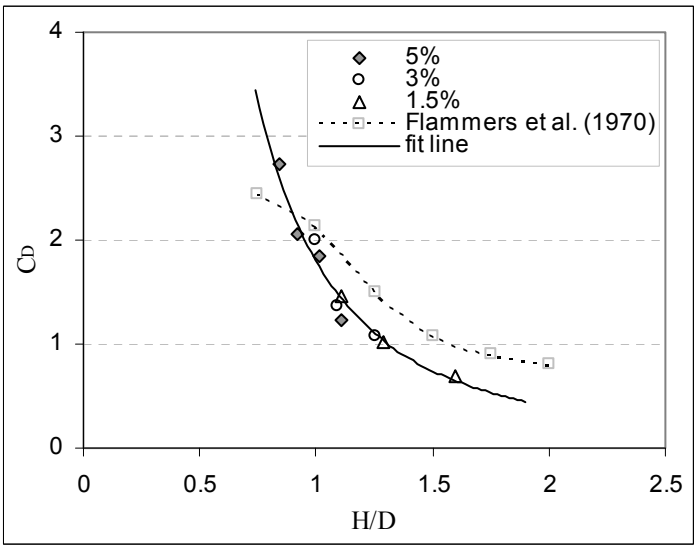

Figure 4.13 Variation of drag coefficient (C_D) with submergence ratio (*H/D*) for all the experiments.

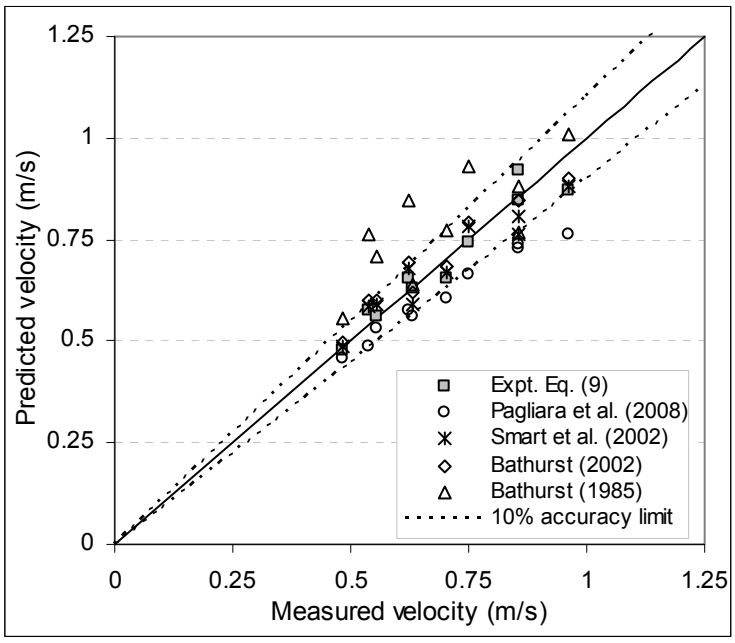

Figure 4.14 Comparison of velocities predicted using Eq. (4.9) with the measurements reported in the literature.

CHAPTER 5

Turbulence Characteristics in a Rock-Ramp Type Fishpass*

5.1 Introduction

An ecosystem approach leading to nature-like fishpasses was advanced in the 1990s (Katopodis and Williams 2011). The principle objective of nature-like fishpass is to provide suitable aquatic habitat for all organisms and biota living in a waterbody (Katopodis et al. 2001). Recently, they have been recognized as economically and ecologically viable alternatives to traditional engineered fishpasses, and have become of considerable interest throughout much of the world. Their patterns are in meandering and cross-sections are of nearby rivers, aiming to generate diverse hydraulic conditions and pathways for fish of various sizes (Katopodis and Williams 2011). Pool–riffle and rock-ramp are the two major types of nature-like fishpasses. The performance of rock-ramp fishpass was previously evaluated through laboratory setup (Haro et al. 2008) and field (Thorncraft and Harris 1996; Franklin et al. 2012) and showed most promising results.

*The content of this chapter has been drafted as a journal manuscript: Baki et al. (2013b). "Turbulence Characteristics in a Rock-Ramp Type Fishpass." *Journal of Hydraulic Engineering, ASCE, (drafted)*.

The turbulence characteristic of nature-like fishpasses is limited in literature. Relevant studies (Nikora and Smart 1997; Nikora et al. 2001; Strom and Papanicolaou 2007; Lacey and Roy 2008; and others) have intensively studied the turbulence structures in gravel bed river flows with large scale roughness. However, studies particularly on simple fish habitat structures, (Tritico and Hotchkiss 2005; Sadeque et al. 2009; Lacey and Rennie 2012) have investigated the turbulent flow characteristics around different bluff bodies and isolated instream pebble cluster. Papanicolaou et al. (2012) studied (experimentally and numerically) mean and turbulent flow fields within an array of fully submerged, isolated, and immobile boulders. Most previous studies have focused on the mean flow field, time-averaged turbulence statistics, and turbulent structures surrounding a single, wall-mounted, and fully submerged boulder. Studies on shear stress and turbulent kinetic energy with fish responses (Enders et al. 2003; Silva et al. 2012) or turbulent eddies including their vorticity and size generated by cylindrical bodies (Webb and Cotel 2010) have provided meaningful biological inputs regarding fish migration.

During the last few decades, the relationships between fish habitat preference and mean velocity, mean flow depth, and substrate size have been the focus of numerous studies. Turbulence is also an imperative physical characteristic of streams. Turbulence characteristics are believed to be harmful to fish at high levels (Silva et al. 2012). Recently, researchers have observed the effect of turbulence on fish density, behavior, and swimming performance. Investigations

of turbulence have revealed a wide range of responses by fishes. Smith and Brannon (2005) showed that trout choose locations with reduced turbulence level. According to Lupandin (2005), "the longer the body of the fish, the higher is the turbulence required to decrease the critical flow velocity". In turbulent environments, fish swimming performance might be troubled (Enders et al. 2003; Silva et al. 2012) or to be unaffected (Nikora et al. 2003). Also, it is interesting to estimate the efficient energy dissipation rate and its effects on fish passage (Papanicolaou and Maxwell 2000). Furthermore, the turbulence scale is a central issue in the study of turbulence (Smith 1975), which may be perceived as eddies as rotating body of fluid.

The present study used instantaneous velocity to investigate the turbulence characteristics of flow generated by a staggered arrangement of boulders in a rock-ramp nature-like fishpass. The goals of this study were (i) to conduct a detailed investigation on turbulence characteristics that have potential importance for fish passage, specifically the relative turbulence intensity, turbulent kinetic energy, Reynolds shear stress, mean turbulent statistics (skewness and kurtosis), energy dissipation rate, and dissipative eddy size (eddy length scales), in a particular cell of the exploratory rock-ramp fishpass; (ii) to develop some general correlations for predicting the average turbulent intensity and turbulent kinetic energy in a rock-ramp fishpass as a function of normalized streamwise distance; and (iii) to distinguish the influence of cluster of boulders (wake interference flow) versus single boulder (isolated roughness flow) on flow fields in the wake

region behind the boulder. Such knowledge is important for the passage of migratory fish through the nature-like fishpasses.

5.2 Experimental Procedures

The experimental setup followed in this study is similar to the study on mean flow characteristics of a rock-ramp nature-like fishpass (Chapter 4). The rock-ramp type design consists of a staggered arrangement of isolated natural boulders of spherical shape that were placed throughout the length of the rectangular flume (width, height, and length being 0.92 m, 0.61 m, 8.89 m, respectively) (*Figure 5.1a*). The detailed measurement plane was the vertical centre plane of the flume in cell 6, having a length L=75 cm (5.36D, where D is the boulder diameter) in the X direction (*Figure 5.1b*). Longitudinally, cell 6 was started at a distance of X= 409 cm from the most upstream section (*Figure 5.1a*) and it was chosen based on uniform flow criteria (discussed in Chapter 4). As recommended by DVWK (2002), the resulted spacing of boulders in this setup established a wake-interference flow (Morris 1954), more details were discussed in Chapter 4.

Total nine sets of experiments were conducted for different flow rates, for the channel slopes of 1.5, 3, and 5%, see in Table 5.1. For the1.5% slope, three sets of experiments were conducted (60, 90, and 160 L/s) and for each set of experiments the measurements were taken at each grid point (*Figure 5.1b*), where the spacing between two points in the streamwise (X) directions was 4 to 6 cm. Therefore, the

grid spacing was about 1/3 times of boulder diameter in X direction. Similarly, for the 3% (60, 80, and 120 L/s) and 5% (60, 75, and 100 L/s) slopes, total six sets of experiments were conducted. For all sets of experiments, the spacing between two measuring points in the vertical (Z) direction varied from 1 to 2 cm depending on flow depths. The submergence ratio *(H/D)*, where *H* was the average water depth along the centre line of the flume, varied from 1.11 to 1.60, 1.0 to 1.26, and 0.84 to 1.0 for the 1.5, 3, and 5 % slopes, respectively (Table 1). The Froude number $(Fr = u_{avg} / \sqrt{gH})$ and Reynolds number $(\mathrm{Re} = u_{avg} H / \upsilon)$, for all experimental runs, (based on average streamwise velocity, u_{avg}, and average flow depth, *H,* along the central plane of the flume) were *Fr*=0.39 to 0.65 and *Re*=63,000 to 192,000 respectively (*Table 5-1*).

For the 1.5 and 3% slopes a Vectrino Plus (Nortek) and for the 5% slope an ADV (SonTek 10MHz) was used to measure the three-dimensional instantaneous velocity fields with 3-D down-looking probe. To ensure the statistical significance of the velocity record, velocity measurements were recorded at a frequency of 100 Hz and 25 Hz for 3 minutes, yielding 18000 and 4500 measurements with Vectrino Plus and ADV, respectively. The average correlation coefficients (COR) varied from 55 to 71% and the average signal-to-noise ratios (SNR) varied from 41 to 61 dB for all experiments. Manufacturers of both NorTek and SonTek ADVs recommend that COR and SNR values should be greater than 70% and 15dB, respectively, for reliable turbulence measurements. The values of COR and SNR can be somewhat subjective since they vary with the flow properties and are

strongly affected by the high-frequency turbulent fluctuations (Wahl 2000; Cea et al. 2007). In relatively high turbulent flow, especially when the signal to noise ratio is high, samples can provide good data having correlation values much less than 70% (Wahl 2000). For flow over rough cobble boundaries, data filtered with a minimum correlation of 40% could be used to measure Reynolds stress if at least 70% of the data were retained after filtering (Martin et al. 2002). The lower correlation values (COR<70%) in highly turbulent flows do not imply that they are erroneous (Cea et al. 2007; Storm and Papanicolaou 2007). Also, a filter criteria (COR>70% and SNR>15dB) for this particular highly turbulent flow would yield significant removal of data. Therefore, the raw data was filtered to eliminate poor signals based on a filtering scheme of SNR≥30 dB and COR ≥55%, and spikes were eliminated using the method of Goring and Nikora (2002) prior to calculation of the instantaneous velocities and turbulence quantities. The filtering process resulted in more than 70% of the original velocity time series data retained after filtering. Similarly, Storm and Papanicolaou (2007) used COR≥50% and SNR≥10dB to examine the turbulent properties of the flow around a cluster microform in a shallow mountain stream.

For the purpose of studying the characteristics of turbulence structures and their significance in a rock-ramp fishpass, three different stations (I, II, and III) were also chosen from cell 6 along the centre line of the flume. The station (I) is located downstream of boulder (in the wake region) at X/D=1.36, (II) is in the intermediate region at X/D=2.79, and (III) is in the upstream of boulder at

X/D=4.21, along the centre line of the flume. Figure 5.1b shows the position of those stations with respect to the central vertical plane. These three regions (downstream of boulders, intermediate, and upstream of boulders) were distinguished from mean velocity characteristics in Chapter 4.

5.3 Results and Discussions

5.3.1 Turbulent Intensity

In turbulent flow, the standard deviation of the velocity fluctuation is referred to as the root-mean-square (rms) values, i.e., turbulence intensity and is defined as $u'_{rms} = \sqrt{\overline{u'^2}}$, where u' is the streamwise fluctuating velocity. The profiles of normalized streamwise turbulent intensity (u'_{rms}/u^*) versus the normalized water depth (z/H) for all experiments at stations (I), (II), and (III) are shown in Figure 5.2. The prediction of u'_{rms}/u^* profile using the universal expression ($u'_{rms}/u^* = 2.3\exp(-z/H)$) by Nezu and Nakagawa (1993) was also included in this figure for comparison purposes. Herein, *z* is the distance from the channel bed and *u** is the friction velocity which is calculated from the measured Reynolds stress following Nezu and Nakagawa (1993). It has been observed that at station (I) the profiles showed maximized deviations from the universal expression by Nezu and Nakagawa (1993), and the deviations decreased with decreasing channel slopes. This is in disagreement with the findings of Sadeque (2008), where the profiles agreed with the universal expression up to *z/H*=0.4, and

Papanicolaou et al. (2012), where the profiles agreed over *z/H*=0.3. At stations (II) and (III), the profiles also deviated from the universal expression, except for the 1.5% slope. For the 1.5% slope, the profiles agreed over *z/H*=0.3, which is in good agreement with Papanicolaou et al. (2012). The magnitude of the profiles decelerated from station (I) to (III) and became more comparable with the universal expression while decreasing channel slopes.

Silva et al. (2012) recommended to consider the magnitude of the turbulent fluctuations (turbulence intensity) while studying upstream movements of fish species. The normalized profiles of streamwise turbulence intensity ($u'_{rms}/U_{\max}$) along the centre line of the flume for the 1.5, 3, and 5% slopes under different flow rates are plotted in Figures 5.3(a-c), respectively. Herein, $U_{\max}$ is the maximum flow velocity magnitude of U for individual flow rate. The magnitude of flow velocity, U, was calculated by $U = \sqrt{u^2 + v^2 + w^2}$ at all measurement points, where u, v, and w are the time-averaged streamwise, lateral and vertical velocities, respectively. It is important to mention that a general correlation has been derived to estimate the value of $U_{\max}$ in this fishpass from the dimensionless discharge in Chapter 4. From these profiles, it could be easily identified three different regions along the centre line: downstream of boulders (wake region, *X/D*=1 to 2), intermediate region (*X/D*=2 to 3), and upstream of boulders (*X/D*=3 to 4.5). In wake the region, increased turbulence intensity was the common observation in all flow conditions. In this region, the maximum values of u'_{rms} were varied from 36 to 42%, 41 to 46%, and 40 to 50% of $U_{\max}$ under

different flow rates for the 1.5, 3, and 5% channel slopes, respectively. It was also common to observe that the turbulence intensities gradually decayed in the downstream direction for all experiments. In contrast, the vertical profiles at intermediate/upstream region were regular and uniform over the flow depth, except near the water surface, for all experiments. Here, the magnitude of u'_{rms} slightly elevated with increasing water depth and the average value was about 20% of $U_{\max}$ for all experiments. Therefore, the magnitude of $(u'_{rms})_{\max}$ in wake region was about 20% (2 times) higher than the average values at intermediate/upstream of boulder regions.

Figure 5.4 shows the variation of normalized depth-average magnitude of streamwise turbulence intensity ($\overline{u'_{rms}}/U_{\max}$) with *X/D* along the centre line of the flume for all experiments. All data points fall together in a narrow band also the width of the band decreased somewhat as the relative longitudinal distance increased approaching the boulder. The following power equation may be written to describe the variation with the fitted line as

$$\frac{\overline{u'_{rms}}}{U_{\max}} = 0.289\left(\frac{X}{D}\right)^{-0.45} \qquad (R^2=0.95) \qquad (5.1)$$

It was found that the highest values of ($\overline{u'_{rms}}$) (about 30% of $U_{\max}$) in the wake region declined gradually in the downstream direction with *X/D* and attained its lowest values (about 15% of $U_{\max}$) at upstream of boulder. The data approximately correlated with a decay exponent of (-0.45), which is dissimilar with a decay exponent of (-1) for maximum streamwise turbulent intensity by the

single cylinder wake (Tennekes and Lumley 1972) and by twin cylinders wake (parallel side-by-side and staggered arrangements) (Nosier et al. 2012). Therefore, the wake-interference flow (generated by a staggered arrangement of boulders) has major effect on the turbulence intensity decay rate, and this rate ensured lower deceleration of turbulence intensity, potentially due to the effect of the neighboring boulders. It is also apparent that the magnitude of $\overline{u'_{rms}}$ increased with increasing slopes.

5.3.2 Turbulent Kinetic Energy

The turbulent kinetic energy *(K)* per unit mass is defined as $K = \frac{1}{2}\left(u'^2_{rms} + v'^2_{rms} + w'^2_{rms}\right)$, where v' and w' are the transverse and vertical fluctuating velocities, respectively. Here, *K* is formulated in dimensionless terms (normalized) using the maximum velocity *(U_{max})* as $k = K^{0.5} / U_{\max}$. Figures 5.5(a-c) shows the spatial distribution of normalized turbulent kinetic energy *(k)* along the centre plane for the 1.5, 3, and 5% slopes under different flow conditions, respectively. From these figures, it is also apparent that increased turbulent kinetic energy in the near wake region was the common observation in all flow conditions. The magnitude of *k* gradually increased vertically towards the water surface with increasing flow rates at upstream of the boulders; similarly at downstream of the boulders it increased vertically towards the flume bottom and extended in the downstream direction with increasing flow rates (Figure 5.5). This

trend of observations is consistent with previous studies by Lacey and Roy (2008) and by Sadeque et al. (2009). For the 1.5, 3, and 5% slopes, the maximum magnitude of k (K for a 1:4 undistorted scale model) varied from 0.37-0.39 (0.28-0.80 m^2/s^2), 0.44-0.53 (0.52-2.0 m^2/s^2), and 0.40-0.46 (0.60-1.04 m^2/s^2) for different flow rates, respectively. Comparatively in conventional fishpasses, maximum K have been measured at 0.11 m^2/s^2 in a single slot pools (Liu et al. 2006), 0.07 m^2/s^2 in pool-type fishpass (Silva et al. 2011), 0.40–1.2 m^2/s^2 in a pool with orifice fishway (Guiny et al., 2005), and 0.60 m^2/s^2 in a culvert retrofitted with baffles for fish passage (Morrison et al. 2008).

It was also common to observe that the magnitude of k gradually decayed in the downstream direction in all flow conditions. A leading fraction of area in the detailed measurement cell along the centre plane having the maximum values of k for all runs was less than 25% of U_{max}. That area with a low value of k would be good for fish passage. Because at sustained swimming levels fish normally avoid entering areas of high turbulence (Bell 1973). Correspondingly, the maximum value of normalized turbulent kinetic energy (k_{max}) was about 33% of mean free-stream longitudinal velocity by Lacey and Roy (2008), about 40% of depth-averaged streamwise velocity (for boulder B) by Tritico and Hotchkiss (2005), and 33% of depth-average centre line velocity by Lacey and Rennie (2012). Therefore, the maximum value of normalized turbulent kinetic energy in this study was higher than previous studies of flow around different isolated bluff bodies and instream pebble cluster.

The variation of normalized depth-average turbulent kinetic energy ($\bar{k}$) with *X/D* for all experiments along the centre line is shown in Figure 5.6. Similar to the variation of ($\overline{u'_{rms}}$), all data points fall together in a narrow band and the width of the band decreased somewhat as the relative longitudinal distance increased approaching the boulder. The variation is fitted with a mean line and the power equation is

$$\bar{k} = 0.33\left(\frac{X}{D}\right)^{-0.44} \qquad (R^2=0.98) \qquad (5.2)$$

Where, the highest values of ($\bar{k}$) (about 35% of U_{max}) in the wake zone decreased gradually in the downstream direction with *X/D* and reached its lowest values (about 15% of U_{max}) upstream of boulder. The magnitude of $\bar{k}$ gradually decayed in the downstream direction with a decay exponent of about -0.44, which is much lower than the average exponent of -0.87 and -0.98 for maximum turbulent kinetic energy on smooth and rough bed found by Sadeque (2008) for bed mounted single cylinder, respectively. Therefore, the increased turbulent kinetic energy in the wake-interference flow decayed slowly compared to a single cylinder. The level of submergence has significant effect on the decay of increased turbulence (Sadeque 2008), which is also apparent in Figure 5.6. At higher flow rates, the increased energy released slowly compared to lower flow rates.

The maximum magnitude of *k* (about 40% of U_{max}) in wake region was about 20% (2 times) higher than the average values (about 20% of U_{max}) at outside of

the wake region. The magnitude of the ratio between maximum turbulent kinetic energy (K_{max}) values in wake region versus outside of wake found by Tritico and Hotchkiss (2005) was 4.5 times, by Lacey and Roy (2008) was 4 times, by Sadeque et al. (2009) was 5 times, and by Lacey and Rennie (2012) was 4 times. Therefore, the discrepancy between the highest and lowest values of *k* in this study was significantly lower than other studies; this ensured that the dispersion of turbulence kinetic energy over the study area was higher than the isolated single boulder.

5.3.3 Reynolds Stress

The Reynolds shear stresses are additional turbulent parameters that have major importance on fish passage studies (Silva et al. 2012). In open channel flows, Reynolds shear stress occurs when two water masses or layers of different velocities are parallel or adjacent to each other due to turbulent fluctuations. Fish moving between two water layers having different velocities or when moving near a solid structure may experience shear stress (see Silva et al. 2012). For the horizontal plane (XY), Reynolds stress is defined by $-\overline{u'v'}$, which can be made dimensionless using U_{max} as $-\overline{u'v'}/U_{max}^2$. Other two dimensionless Reynolds stresses are $-\overline{u'w'}/U_{max}^2$ and $-\overline{v'w'}/U_{max}^2$.

The normalized profiles of primary Reynolds stress ($-\overline{u'w'}/U_{max}^2$), indicative of the vertical gradient of streamwise velocity, is presented in Figure 5.7 for all

experiments. It is apparent that $-\overline{v'w'}/U_{max}^2$ was dominating in the wake region for all experiments. Its values were small (tend towards zero) in the other regions. Their distributions, including its increased magnitude (negative for downward *w* components) towards the bed, are quite similar to that of the *k*. Also, $-\overline{u'w'}/U_{max}^2$ values (positive for upward *w* components) elevated near to water surface. The dominance of $-\overline{u'w'}/U_{max}^2$ occurred in the wake with previous studies of flow around different bluff bodies (Sadeque et al. 2009; Lacey and Rennie 2012) and large roughness elements (Lacey and Roy 2008). For the 1.5, 3, and 5% slopes, the maximum magnitude of $-\overline{u'w'}/U_{max}^2$ varied from 0.014 to 0.049, 0.044 to 0.051, and 0.005 to 0.006 for different flow rates, respectively. In contrast, the maximum value of normalized dominant Reynolds shear stress ($(-\overline{u'w'})_{max}/U_{max}$) was about 0.032 by Lacey and Roy (2008), about 0.034 by Tritico and Hotchkiss (2005), and 0.034 by Lacey and Rennie (2012). Hence, the maximum value of dominant Reynolds shear stress in this study was slightly higher than previous studies of flow around different isolated bluff bodies.

The normalized Reynolds stresses ($-\overline{u'v'}/U_{max}^2$) is a measure of streamwise shear stress along the vertical plane. The spatial distributions of $-\overline{u'v'}/U_{max}^2$ along the central vertical plane (XZ) are presented in Figures 5.8(a-c) for the 1.5, 3, and 5% slopes under different flow rates, respectively. The spatial distribution also demonstrates the dominance of $-\overline{u'v'}/U_{max}^2$ in the wake of the boulders. The

highest magnitude of $-\overline{u'v'}/U_{\max}^2$ was centered behind the boulders, and extends towards the bed. For the 1.5, 3, and 5% slopes, the maximum magnitude of $-\overline{u'v'}/U_{\max}^2$ ($-\rho\overline{u'v'}$ for a 1:4 undistorted scale model) varied from 0.008 to 0.014 (28 to 80 N/m^2), 0.008 to 0.035 (28 to 180 N/m^2), and 0.029 to 0.042 (156 to 300 N/m^2) for different flow rates, respectively, which should be within the tolerable limit for different fishes. Because for maximum values of $-\rho\overline{u'v'}$=73.4 N/m^2, fish damage was not witnessed but fish disorientation and displacement was observed (Odel et al. 2002). Only the maximum values of $-\rho\overline{u'v'} \geq 700$ N/m^2, caused injuries and mortalities of fish (Cada et al. 1999).

The values of $-\overline{u'v'}$ are approximately similar with the maximum magnitude of primary Reynolds stress. Tritico and Hotchkiss (2005) also found that the dominant component of the Reynolds stress switched from $-\overline{u'w'}$ to $-\overline{u'v'}$ in the wake region. The developed recirculation in the wake region enhanced the secondary velocities and $-\overline{u'v'}$ become important. Moreover, the privileged blockage ratio in this study (0.3 to 0.45) based on cross sectional area, compared to <0.1 by Sadeque et al. (2009), 0.044 to 0.067 by Lacey and Rennie (2012), and extremely small in a natural rivers by Lacey and Roy (2008), are responsible for that the dominating role of $-\overline{u'v'}$. The present results suggested that lateral momentum exchange with vertical axis is much stronger than vertical momentum exchange. For fish habitat this is really important (Enders et al. 2003), because

"swimming fish can capture the kinetic energy in vertical axis coherent structures" (Videler et al. 1999).

The variation of normalized depth-average Reynolds shear stress ($(-\overline{\overline{u'v'}}/U_{max}^2)$) against *X/D* for all experiments along the centre line of the flume is shown in Figure 5.9. All data points demonstrated some degree of scatter and fall in a wide band, also the width of the band decreased somewhat as the relative longitudinal distance increased approaching the boulder. The mean line confirmed that the highest value of $-\overline{\overline{u'v'}}/U_{max}^2$ was about 1% of U_{max} in the wake region decreased gradually in the downstream direction with *X/D* and reached its lowest values (about 0.25% of U_{max}) at upstream of boulder. Therefore, the maximum magnitude of $(-\overline{u'v'})_{max}$ (about 2.5% of U_{max}^2) in wake region was about 2.25% (10 times) higher than the average values (about 0.25% of U_{max}^2) at outside of the wake region. On the other hand, Tritico and Hotchkiss (2005) found that the magnitude of the ratio between maximum $(-\overline{u'v'})_{max}$ values in obstructed versus unobstructed flow regions was 14.8 times.

Also, the spatial distribution of normalized Reynolds stresses $-\overline{v'w'}/U_{max}^2$ (cross-stream shear stress along the vertical plane) is presented in Figure 5.10 only for the 5% slope along the centre vertical plane for different flow conditions. It is apparent that $-\overline{v'w'}/U_{max}^2$ values were very small in magnitude and they are relatively identical for different flow rates. Their distributions and increased

magnitude (negative for downward *w* components) occurred towards the bed and also elevated magnitude (positive for upward *w* components) near to water surface.

5.3.4 Higher-order Moments

Third- and higher-order moments of the time series turbulent velocity provide useful statistical information on the temporal distribution of the turbulent fluctuations around the mean velocity. Also, provide complementary results to quadrant analysis for characterizing turbulent events (Lacey and Roy 2008). Here, additional turbulence parameters were determined from third- and fourth-order statistics, including coefficients of skewness *(S_u)* and kurtosis *(K_u)*, respectively. Previously, Nikora and Smart (1997) and Balachandar and Bhuiyan (2007) have carried out these types of investigations in flumes, lowland rivers, steeper rivers, and gravel bed rivers. The vertical profiles of S_u and K_u are qualitatively and quantitatively the same in all these cases, where S_u is positive near the bed/water surface ($0<S_u<1.0$) and negative in the intermediate region ($-1.0<S_u<0$), and K_u varies slightly within the limit ±1.0 (Nikora and Smart 1997). The vertical distributions of S_u and K_u values at stations (I), (II), and (III) for all experiments are shown in Figure 5.11. At station (I), S_u was negative (where the distribution of turbulent fluctuations were skewed) over the entire depth and its values ranged from -1.0 to 0, except 90 and 160 LPS under 1.5% slope. Correspondingly, K_u was mostly positive (distributions had flatter peak) over the entire depth and its

values ranged from 1.0 to 0. Thus, the large negative S_u along with a positive K_u indicates the occurrence of strong ejection events within the velocity signal (Lacey and Roy 2008) in the wake region (I). At stations (II) and (III), S_u was negative over the entire depth and only the band width decreased from (II) to (III), where the band width ranged from -0.75 to 0 and -0.50 to 0, respectively. Similarly, K_u was positive over the entire depth and values ranged from 0.75 to 0 and 0.50 to 0 for stations (II) and (III), respectively. Therefore for all experiments, the negative values of S_u over the entire depth are in disagreement with the data for the gravel bed river, steeper rivers, lowland rivers, and flumes. On the other hand, K_u varied within a narrow band of 0-1.0 in all experiments rather than ± 1.0.

5.3.5 Turbulent Energy Dissipation Rate and Scale

The availability of energy within the water column to enhance the transport of gas and heat across the air-water interface can be guessed from the turbulent kinetic energy dissipation rate (ε) (Melville 1994). Siddiqui and Loewen (2004) demonstrated that using direct method (with the velocity gradients computed from the two-dimensional turbulent velocity field) the values of ε are in good agreement with the values of ε estimated by curve fitting in the inertial subrange method (fitting a power law equation proportional to $w_w^{-5/3}$ to the wave number spectrum of the streamwise velocity in the inertial subrange, where w_w is the wave number). Liu et al. (2003 and 2006) also used the curve fitting in the inertial subrange method to calculate the energy dissipation rate in hydraulic jumps with

low Froude number and in vertical slot fishpass, respectively. The analysis of the power spectra for the streamwise, transverse, and vertical velocity displayed the regions of constant *"-5/3"* slope at higher frequencies and this slope indicates the existence of the inertial subrange from Kolmogorov theory (*Figure 5.12*).

In this method, using an assumption of isotropic, homogeneous turbulence, at least in the inertial range, the dissipation rate can be estimated from the spectrum, $G_u(w_w)$, of the streamwise velocity as (Hinze 1975):

$$G_u(w_w) = M\varepsilon^{2/3} w_w^{-5/3} \tag{5.3}$$

where $G_u(w_w)$ is the power spectra of the streamwise velocity in the domain of wave number, w_w; ε is the kinetic energy dissipation rate; and M is a constant with a value of 0.56 for local isotropic turbulence. Using Taylor's frozen turbulence hypothesis (Hinze 1975), the spectrum can be transferred from the wave number domain to the frequency domain, and the converted Eq. (5.3) can be written as follows (for more details see Liu et al. 2003)

$$G_u(f) = M(2\pi)^{-2/3} u^{2/3} \varepsilon^{2/3} f^{-5/3} \tag{5.4}$$

where $G_u(f)$ is the power spectra of the streamwise velocity in the domain of frequency, f in Hz, and then the kinetic energy dissipation rate could be estimated using Eq. (5.4). The values of energy dissipation rate estimated for all experiments are given in Table 5-2. The average dissipation rates varied from 0.020 to 0.023, 0.039 to 0.046, and 0.013 to 0.016 m^2/s^3 for the 1.5, 3, and 5% slopes under different flow rates, respectively. Correspondingly, the values of the turbulent dissipation rate estimated for the gravel bed river by Nikora and Smart

(1997) were in the order of 0.1 m^2/s^3 near the bottom and 0.01 m^2/s^3 near the surface. Figure 5.13 shows the spatial distributions of normalized energy dissipation rate in the form of $\varepsilon D / U_{max}^3$. It was found that the higher dissipation rates occurred near the wake recirculation region and these rates gradually decelerated in the downstream direction for all experiments. The maximum energy dissipation rate were 0.087 (22), 0.088 (22), and 0.042 (11) m^2/s^3 (W/m^3 for a 1:4 undistorted scale model) for the 1.5, 3, and 5% slopes, respectively. The average energy dissipation is generally considered acceptable if less than 200 W/m^3 for salmonids, and 150 W/m^3 for cyprinids (Larinier 2008; Rodriguez et al. 2006).

The variation of normalized depth-average energy dissipation rate, $\bar{\varepsilon} D / U_{max}^3$, with relative distance *X/D* along the centre line of the flume for all experiments is shown in Figure 5.14. All data points demonstrated some degree of scatter and fall in a wide band. The mean line confirmed that the highest value of $\bar{\varepsilon} D / U_{max}^3$ (about 0.01) in the wake region decreased gradually in the downstream direction with *X/D* and reached its lowest values (about 0.003) at upstream of boulder.

Furthermore, fish in fishpass structures might be affected by eddy size (Papanicolaou and Maxwell 2000). The Kolmogorv's length scale (η) corresponds to dissipative eddies can be calculated from the relation $\eta = (\upsilon^3 / \varepsilon)^{1/4}$. This relationship ($\eta \propto \varepsilon^{-1/4}$) means the accuracy of estimated ε will have less effect on the accuracy of η. The spatial distributions of η for all set

of experiments are given in Figure 5.15. For the 1.5% slope, the dissipative eddy size ranges from 0.15 to 0.06 mm with a mean value of about 0.09 mm. Similarly, for the 3 and 5 % slopes, the size ranging from 0.14 to 0.06 mm and 0.22 to 0.07 mm with a mean value of about 0.07 mm and 0.11 mm, respectively. These values are reasonable having a slightly larger eddy size compared to the results of other researchers for similar flows. Nikora and Smart (1997) found for a gravel bed river flow with Reynolds number of 2×10^6 that the dissipative eddy size varies from 0.05 mm near the bottom to 0.10 mm near the surface. Liu et al. (2003) estimated the dissipative eddy size varied from 0.04 to 0.15 mm for hydraulic jump of low Froude numbers (2.0-3.32). Gibson (1963) found that the dissipative eddy size for a round turbulent jet with Reynolds number of 1.2×10^5 varies from 0.0126 to 0.014 mm.

5.4 Summary and Conclusions

This experimental study reported the investigations of turbulence characteristics generated by a staggered arrangement of boulders in a particular cell of the rock-ramp nature-like fishpass.

Increased turbulence in the wake region was the common observation for all experiments, where u'_{rms}/u^* profiles showed maximized deviations from the universal expression by Nezu and Nakagawa (1993) and the deviations decreased with decreasing channel slopes. It was also apparent that the increased turbulence

decayed more slowly (a decay exponent of about -0.45) in the downstream direction compared to a single cylinder (a decay exponent of about -1.0), and this rate ensured lower deceleration of turbulence, potentially due to the effect of the neighboring boulders. In upstream/intermediate region the profiles ($u'_{rms}/U_{\max}$) were regular over the entire flow depth, and the average values were about 20% of $U_{\max}$ for all experiments. A governing fraction of area in the detailed measurement plane along the centre line having the maximum values of k for all runs was less that 25% of $U_{\max}$, which would be good for fish passage.

The normalized depth-average streamwise turbulence intensity ($\overline{u'_{rms}}/U_{\max}$) and turbulent kinetic energy ($\overline{k}$) along the centre line of the flume was correlated with the relative longitudinal distance, *X/D,* for all sets of experiments. Though the above relations will depend on the spatial arrangement, not just the density, of the boulders, the turbulence in a rock-ramp fishpass as a function of normalized streamwise distance can be predicted using these relationships. The lower discrepancy of the highest and lowest values of turbulence (about 2 times for k and 10 times for $-\overline{u'w'}$) in this study ensured that the dispersion of turbulence over the study area was higher than the previous study around different isolated bluff bodies/instream pebble cluster (about 4-5 times for k and 15 times for $-\overline{u'w'}$).

The maximum value of primary Reynolds shear stress ($-\overline{u'w'}/U_{max}^2$) in this study was slightly higher than previous studies of flow around different isolated bluff bodies and instream pebble cluster. The dominance of the Reynolds shear stress ($-\overline{u'v'}/U_{max}^2$), similar magnitude with primary Reynolds stress $-\overline{u'w'}/U_{max}^2$, in the wake of the boulders ensured lateral momentum exchange with vertical axis which is important for fish habitat. The normalized depth-average Reynolds stress ($(-\overline{\overline{u'v'}}/U_{max}^2$) was also correlated with the relative longitudinal distance, *X/D,* for all experiments with some degree of scatter.

The negative values of skewness *(S_u)* over the entire depth are in disagreement with the data for the gravel bed river, steeper rivers, lowland rivers, and flumes, where S_u is positive near the bed/water surface ($0<S_u<1.0$) and negative in the intermediate region ($-1.0<S_u<0$),. Consequently, kurtosis *(K_u)* varies within a narrow band 1.0 to 0 in all experiments rather than ± 1.0. Thus, the large negative S_u along with a positive K_u indicates the occurrence of strong ejection events in the wake region which may be stressful for fish. The estimated maximum energy dissipation rates, by fitting a power law equation proportional to $w_w^{-5/3}$ to the wave number spectrum of the streamwise velocity in the inertial subrange, varied from 0.042 to 0.087 (11 to 22) m^2/s^3 (W/m^3 for a 1:4 undistorted scale model) for all experiments, which is less than the recommended values of 200 W/m^3 for salmonids, and 150 W/m^3 for cyprinids. The normalized energy dissipation rates were maximum in the near wake recirculation region and these rates gradually decelerated in the downstream direction. By using Kolmogorov theory of local

isotropic turbulence as a first approximation, it was found that the average dissipative eddy size varied from 0.07 to 0.11 mm.

It is hoped that the results from this study will be important in understanding the possible effects of turbulence structures with a relationship to fish passage and will be useful to both fishpass designers and fish biologists. Further studies are required especially for different boulder size, spacing, and arrangement in a rock-ramp fishpass in the development of practical relationships for prediction of turbulence characteristics.

5.5 References

Balachandar, R., and Bhuiyan, F. (2007). "Higher-order moments of velocity fluctuations in an open-channel flow with large bottom roughness." *Journal of Hydraulic Engineering*, 133(1), 77-87.

Bell, M. C. (1973). "*Fisheries handbook of engineering requirements and biological criteria."* U. S. Army Corps of Engineers, North Pacific Division, Portland, Ore.

Cada, G. F., Carlson, T., Ferguson, J., Richmond, M., and Sale, M. (1999). "Exploring the role of shear stress and severe turbulence in downstream fish passage." In: Brookshier, P. A. (Ed.), Proceedings of waterpower'99. Hydro's Future: Technology, Markets, and Policy. American Society of Civil Engineers, Reston, VA, 10 pp.

Cea, L., Puertas, J., and Pena, L. (2007). "Velocity measurements on highly turbulent free surface flow using ADV." *Experiments in Fluids*, 42, 333-3348.

DVWK (2002). "*Fish passes-Design, dimensions and monitoring."* Published by the Food and Agriculture Organization of the United Nations in arrangement with German Association for Water Resources and Land Improvement as DVWK-Merkblatt.

Enders, E. C., Boisclair, D., and Roy, A. G. (2003). "The effect of turbulence on the cost of swimming for juvenile Atlantic salmon (salmo salar)." *Canadian Journal of Fisheries and Aquatic Sciences*, 60(9), 1149–1160.

Franklin, A. E., Haro, A., Castro-Santos, T., and Noreika, J. (2012). "Evaluation of nature-like and technical fishways for the passage of Alewives at two coastal streams in New England." *Transactions of the American Fisheries Society*, 141, 624-637.

Gibson, M. M. (1963). "Spectra of turbulence in a round jet." *Journal of Fluid Mechanics*, 15, 161–173.

Goring, D. G., and Nikora, V. I. (2002). "Despiking acoustic Doppler velocimeter data." *Journal of Hydraulic Engineering,* 128(1), 117–126.

Guiny, E., Ervine, D., and Armstrong, J. (2005). "Hydraulic and biological aspects of fish passes for atlantic salmon." *Journal of Hydraulic Engineerin*g, 131(7), 542-553.

Haro, A., Franklin, A., Castro-Santos, T., and Noreika, J. (2008). "Design and evaluation of nature-like fishways for pasage of Northeastern Diadromous fishes." Final report, Submitted to NOAA National Marine Fisheries Service Office of Habitat Conservation.

Hinze, J. O. (1975). "*Turbulence."* McGraw-Hill, New York.

Katopodis, C., Kells, J. A. and Acharya, M. (2001). "Nature-like and Conventional Fishways: Alternative Concepts?" *Canadian Water Resources Journal,* 26(2), 211–232.

Katopodis, C., and Williams, J. G. (2011). "The development of fish passage research in a historical context." *Ecological Engineering*, 48, 8-18.

Lacey, R. W. J., and Rennie, C. D. (2012). "Laboratory investigation of turbulence flow structure around a bed mounted cube at multiple flow stages." *Journal of Hydraulic Engineering*, 137(1), 71-84.

Lacey, R. W. J., and Roy, A. G. (2008). "Fine-Scale Characterization of the turbulent shear layer of an instream pebble cluster." *Journal of Hydraulic Engineering,* 134(7), 925-936.

Liu, M., Rajaratnam, N., and Zhu, D. Z. (2003). "Turbulence structure of hydraulic jumps of low Froude numbers." *Journal of Hydraulic Engineering,* 130(6), 511–520.

Liu, M., Rajaratnam, N., and Zhu, D. Z. (2006). "Mean flow and turbulence structure in vertical slot fishways." *Journal of Hydraulic Engineering*, 132(8), 765–777.

Larinier, M. (2008). "Fish passage experience at small-scale hydro-electric power plants in France." *Hydrobiologia*, 609, 97-108.

Lupandin, A. I. (2005). "Effect of flow turbulence on swimming speed of fish." *The Biological Bulletin*, 32, 461–466.

Martin, V., Fischer, T. S. R., Millar, R. G., and Quick, M. C. (2002). "ADV data analysis for turbulent flows: Low correlation problem." In: T. L. Wahl (ed.), Proc. Conf. Hydraulic Measurements and Experimental Methods, ASCE, Estes Park, CO, USA.

Melville, W. K. (1994). "Energy dissipation by breaking waves." *Journal of Physical Oceanography*, 24, 2041– 2049.

Morrison, R., Hotchkiss, R., Stone, M., Thurman, D., and Horner-Devine, A. (2008). "Turbulence characteristics of flow in a spiral corrugated culvert fitted with baffles and implications for fish passage." *Ecological Engineering*, 35, 381-392.

Morris, Jr. H. M. (1954). "Flow in rough conduits." *Transactions of the American Society of Civil Engineers*, 119, 373–410.

Nezu, I., and Nakagawa, H. (1993). "*Turbulence in Open-Channel Flows.*" Balkema, Rotterdam, Netherlands.

Nikora, V. I., and Smart, G. M. (1997). "Turbulence characteristics of New Zealand Gravel-bed rivers." *Journal of Hydraulic Engineering,* 123(9), 764-773.

Nikora, V. I., Goring, D., McEwan, I., and Griffiths, G. (2001). "Spatially averaged open-channel flow over rough bed." *Journal of Hydraulic Engineering*, 127(2), 123-133.

Nikora, V. I., Aberle, J., Biggs, B. J. F., Jowett, I. G., and Sykes, J. R. E. (2003). "Effects of fish size, time to fatigue, and turbulence on swimming performance: a case study of Galaxias maculates." *Journal of Fish Biology*, 63:1365–1382.

Nosier, M. A., Elbaz, A. R., Fetouh, T. N. A., and El-Gabry, L. A. (2012). "Characteristics of turbulent wakes generated by twin parallel cilindres." *Journal of Fluids Engineering*, 134, 121201-10.

Odeh, M., Noreika, J. F., Haro, A., Maynard, A., and Castro-Santos, T. (2002). "Evaluation of the Effects of Turbulence on the Behavior of Migratory Fish."

Bonneville Power Administration, Portland, OR, Final Report to the Bonneville Power Administration, Contract 00000022, Project 200005700.

Papanicolaou, A. N., and Maxwell, A. R. (2000). ”Hydraulic performance of fish bypass-pools for irrigation diversion channels.” *Journal of Irrigation and Drainage Engineering,* 126(5), 314–321.

Papanicolaou, A. N., Kramer, C. M., Tsakiris, A. G., Stoesser, T., Bomminayuni, S., and Chen, Z. (2012). “Effects of a fully submerged boulder within a boulder array on the mean and turbulent flow fields: Implications to bedload transport.” *Acta Geophysca*, 60(6), 1502-1546.

Rodriguez, T. T., Agydo, J. P., and Mosquera, L. P. (2006). “Evaluating vertical-slot fishway designs in terms of swimming capabilities.” *Ecological Engineering*, 27, 37-48.

Sadeque, M. A. F. (2008). “*Structure of turbulent flows around bedmounted cylinders in open channels.*” Ph. D. Thesis. University of Alberta, Edmonton, Canada.

Sadeque, M. A. F., Rajaratnam, N., and Loewen, M. R. (2009). “Shallow turbulent wakes behind bedmounted cylinders in open channels.” *Journal of Hydraulic Ressearch,* 47(6), 727-743.

Siddiqui1, M. H. K., and Loewen, M. R. (2004). “Coherent structures beneath wind waves and their influence on air-water gas transfer.” *Journal of Geophysical Research*, 109, C03024.

Silva, A. T., Katopodis, C., Santos, J. M., Ferreira, M. T., and Pinheiro, A. N. (2012). "Cyprinid swimming behaviour in response to turbulent flow." *Ecological Engineering*, 44, 314-328.

Silva, A.T., Santos, J. M., Ferreira, M. T., Pinheiro, A. N., and Katopodis, C. (2011). "Effects of water velocity and turbulence on the behaviour of Iberian barbell (Luciobarbus bocagei, Steindachner 1865) in an experimental pool-type fishway." *River Research Application*, 27, 360-373.

Smith, I. R. (1975). "*Turbulence in Lakes and Rivers."* Freshwater Biological Association, UK.

Smith, D. L., and Brannon, E. L. (2005). "Response of juvenile Rainbow Trout to turbulence produced by prismatoidal shapes." *Transactions of the American Fisheries Soccity*, 134, 741-753.

Strom, K.B., and Papanicolaou, A. N. (2007). "ADV measurements around a cluster microform in a shallow mountain stream." *Journal of Hydraulic Engineering*, 133(12), 1379-1389.

Tennekes, H., and Lumley, J. L. (1972). "*A First Course in Turbulence.*" MIT Press, Cambridge, MA.

Thorncraft, G. A., and Harris, J. H. (1996). "Assessment of rock-ramp fishways." NSW Fisheries Research Institute and the Coorperative Research Centre for Freshwater Ecology, Report for NSW Environment Protection Authority.

Tritico, H. M., and Hotchkiss, R. H. (2005). "Unobstructed and obstructed turbulent flow in gravel bed rivers." *Journal of Hydraulic Engineering*, 131(8), 635-645.

Videler, J. J., Muller, U. K., and Stamhuis, E. J. (1999). "Aquatic vertebrate locomotion: Wakes from body waves." *Journal of Experimental Biology*, 202(23), 3423–3430.

Wahl, T. L. (2000). "Analyzing ADV data using WinADV.' Proceeding, Joint Conference on Water Resources Engineering and Water Resources Planning and Management, ASCE, Minneapolis, MN.

Webb, P.W., and Cotel, A. J. (2010). "Turbulence: does vorticity affect the structure and shape of body and fin propulsors?" *Integrative and Comparative Biology*, 1–12, doi:10.1093/icq020.

Table 5-1 Primary details of the experimental scenarios.

Experiment	Channel slope	Discharge (L/s)	Velocimeter	Average water depth *H* (cm)	Submergence ratio *(D/H)*	Reynolds number, *Re*	Froude number, *Fr*
1	1.5 %	60	Vectrino Plus	15.53	1.11	75,231	0.39
2		90		18.08	1.29	114,176	0.47
3		160		22.38	1.60	191,939	0.58
4	3 %	60	Vectrino Plus	13.93	1.00	77,244	0.47
5		80		15.22	1.09	106,817	0.57
6		120		17.60	1.26	150,844	0.65
7	5 %	60	ADV	11.74	0.84	63,266	0.50
8		75		12.92	0.92	80,974	0.55
9		100		14.17	1.00	105,660	0.64

Table 5-2 Summary of turbulent kinetic energy dissipation rates.

Expt.	Slope	Flow	Dissipation rate		
			Average	Maximum	Minimum
No.	(%)	(L/s)		(m^2/s^3)	
1		60	0.021	0.087	0.0036
2	1.5	90	0.020	0.066	0.0049
3		160	0.023	0.054	0.0018
4		60	0.039	0.064	0.0077
5	3	80	0.039	0.088	0.0079
6		120	0.046	0.078	0.0024
7		60	0.013	0.032	0.0005
8	5	75	0.014	0.038	0.0056
9		100	0.016	0.042	0.0094

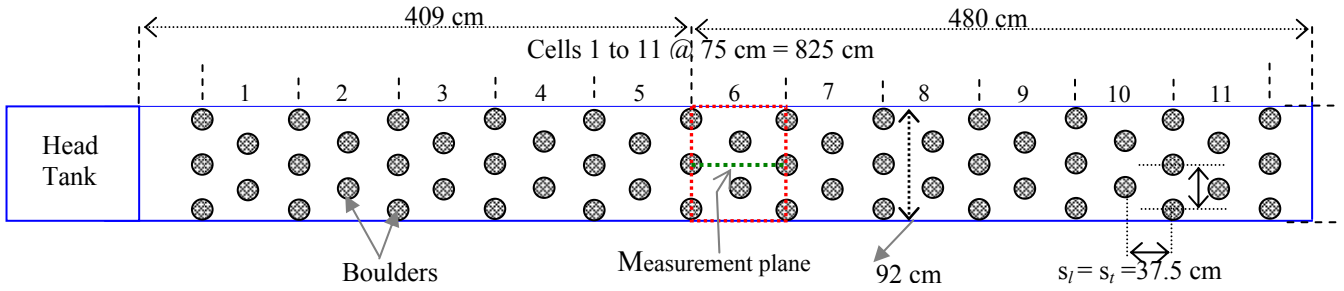

(a) Plan view

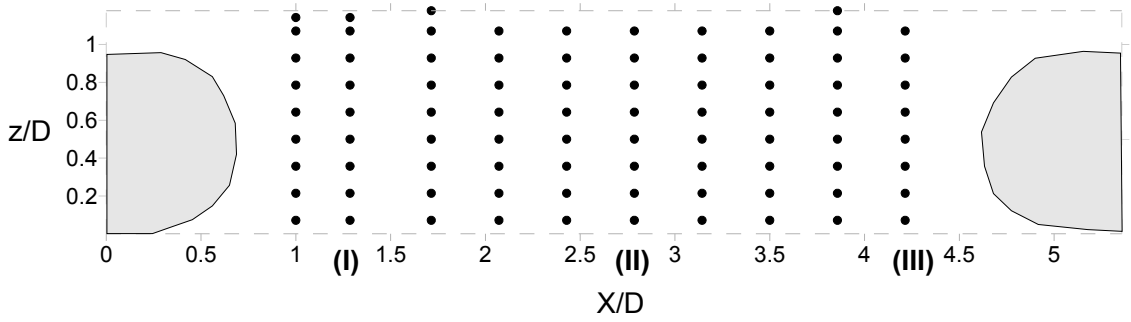

(b) Reference grid

Figure 5.1 (a) Plan view of the experimental setup of rock-ramp type nature-like fishpass and (b) reference grid on vertical plane (XZ) along the centre line of the flume in cell 6 for velocity measurement. Stations (I), (II), and (III) are selected to present some turbulence characteristics.

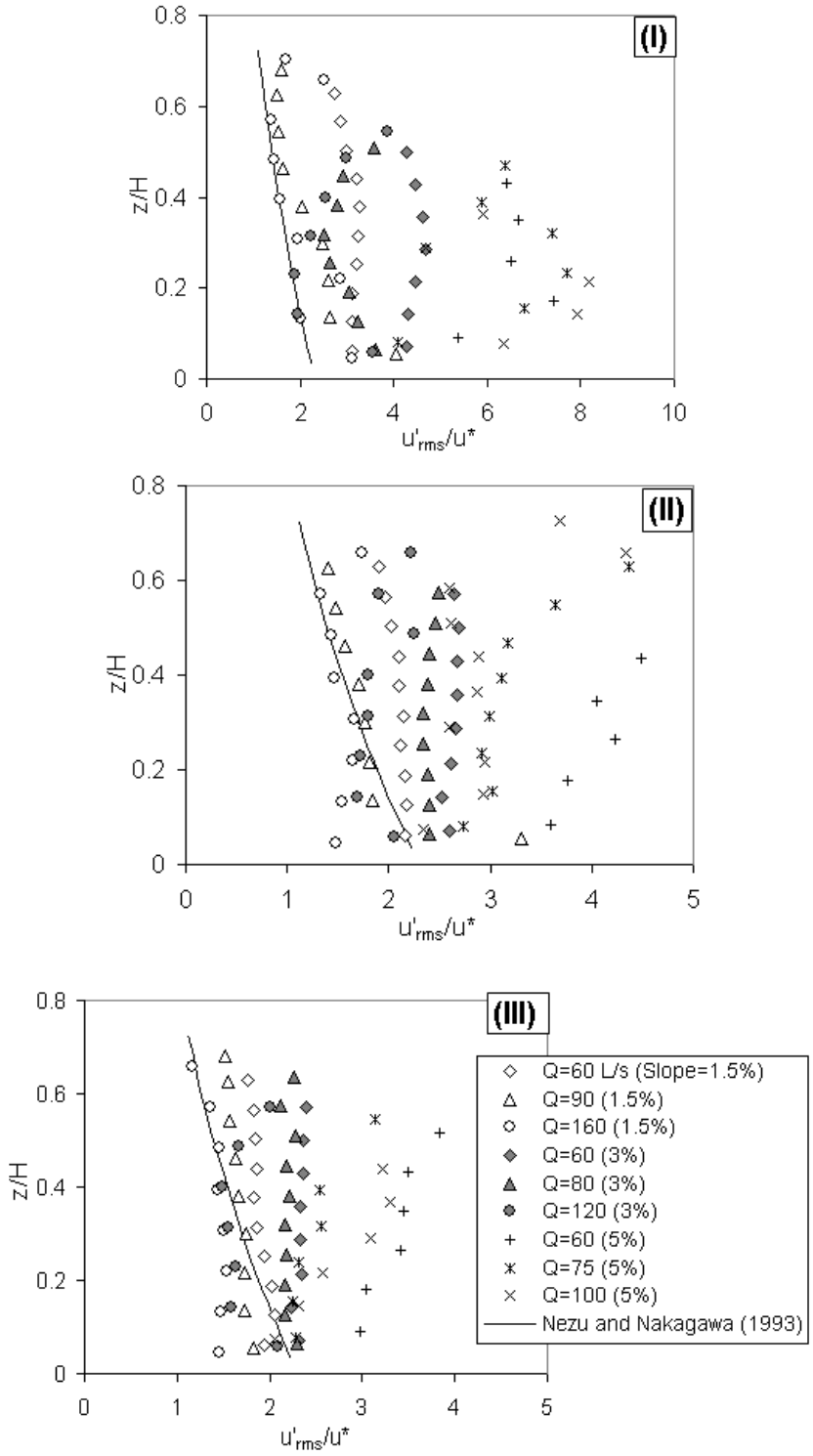

Figure 5.2 Comparison of the normalized streamwise turbulent intensity, $u'_{rms}/u*$, profiles with the universal expression by Nezu and Nakagawa (1993) at stations (I), (II), and (III).

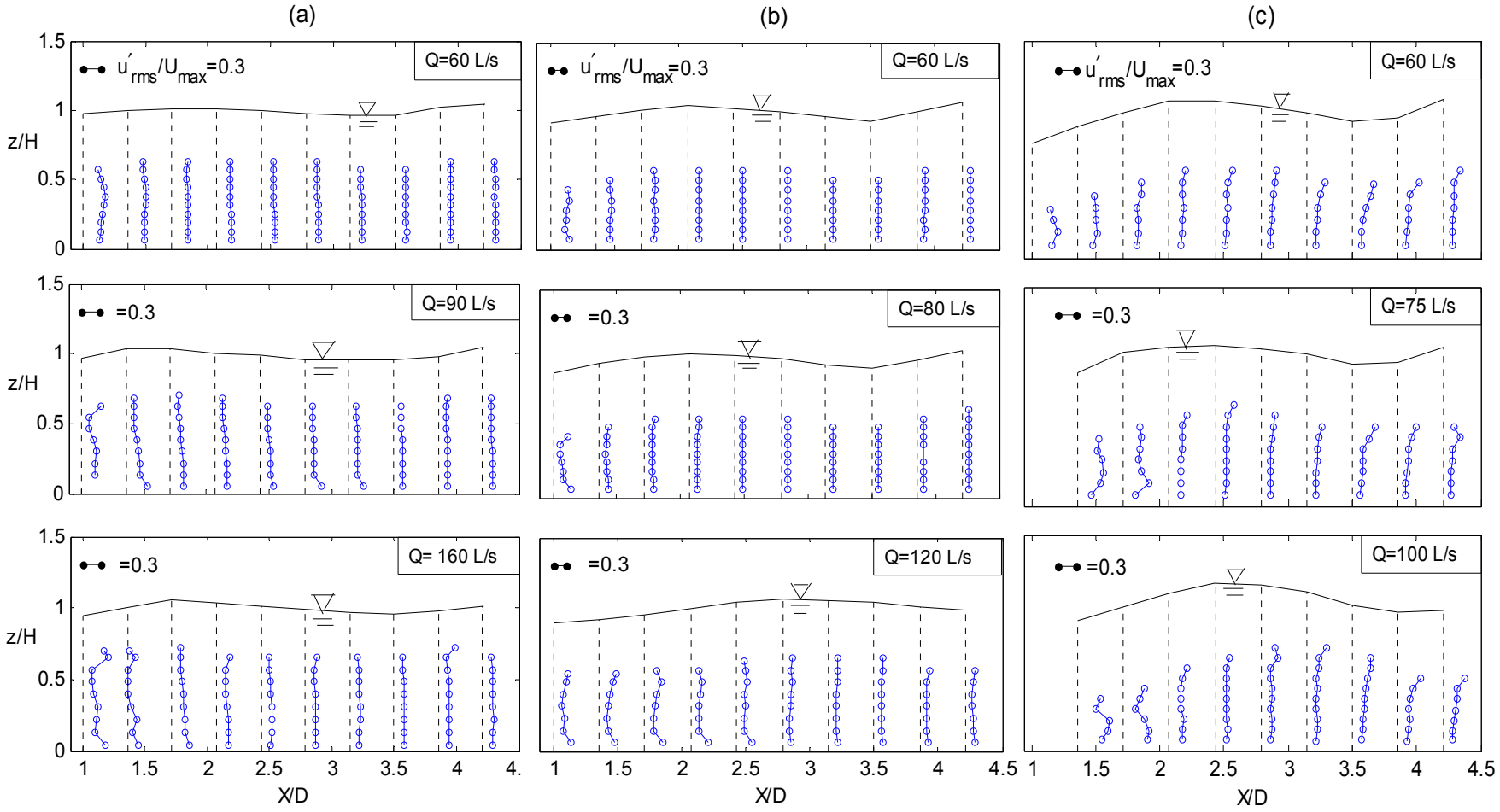

Figure 5.3 Distribution of normalized streamwise turbulence intensities ($u'_{rms}/U_{\max}$) for the (a) 1.5%, (b) 3%, and (c) 5% slopes along the centre line of the flume under different flow conditions.

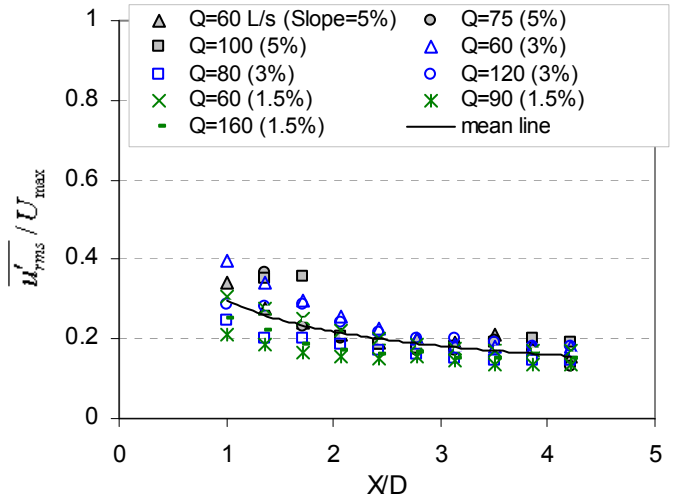

Figure 5.4 Variation of normalized depth-average streamwise turbulence intensities $(\overline{u'_{rms}}/U_{\max})$ with relative distance *X/D* along the centre line of the flume for all experiments.

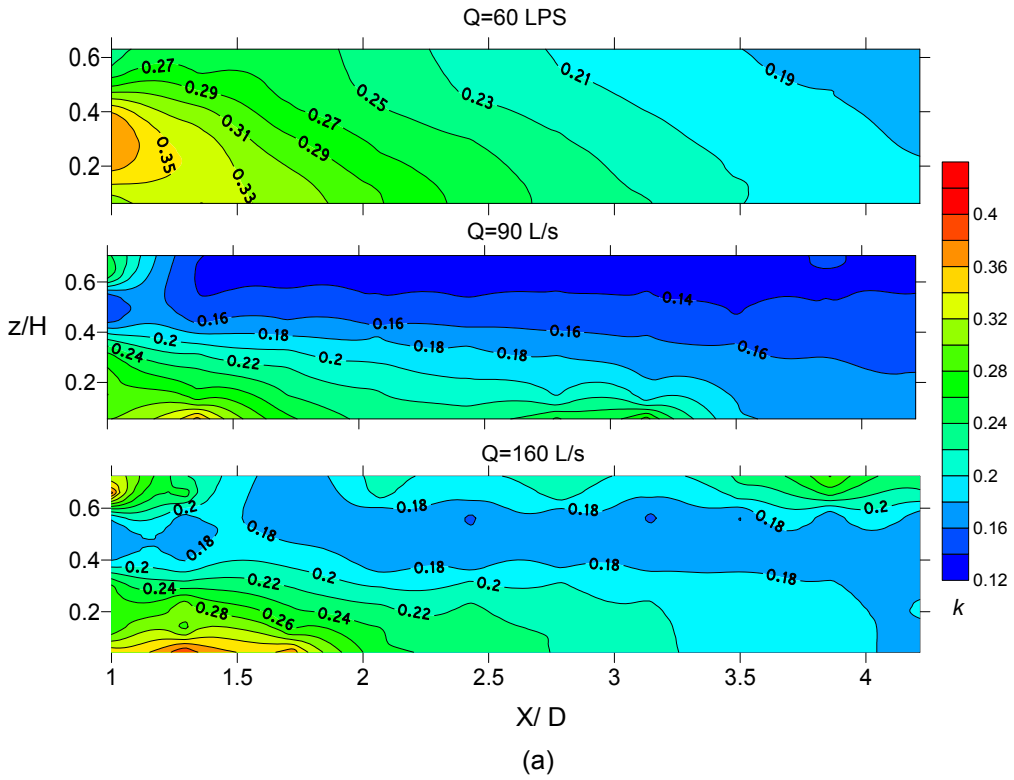

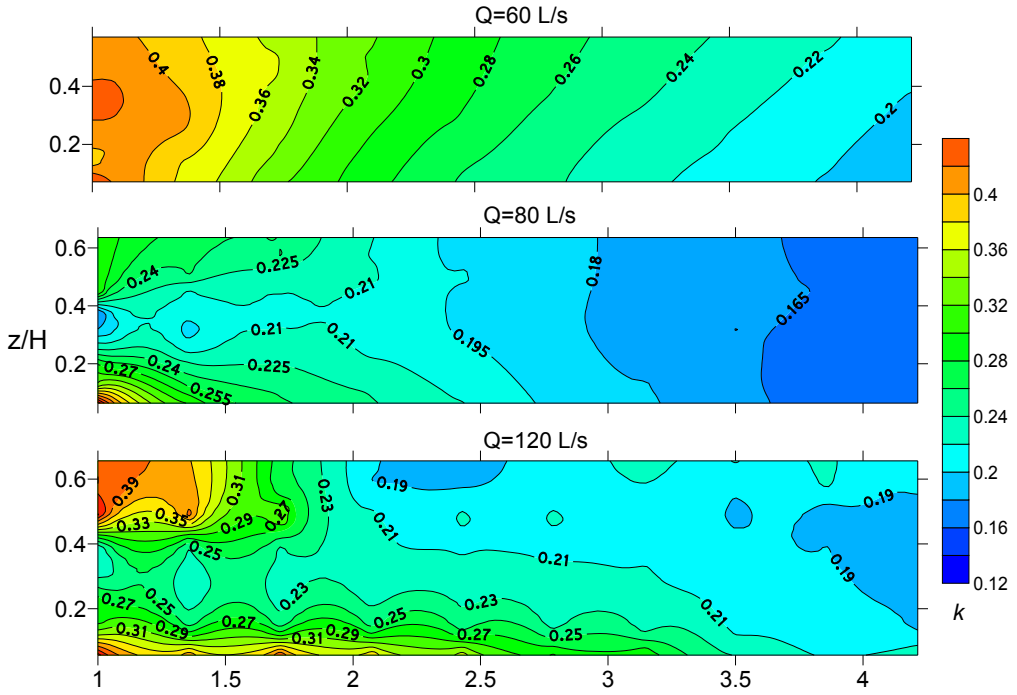

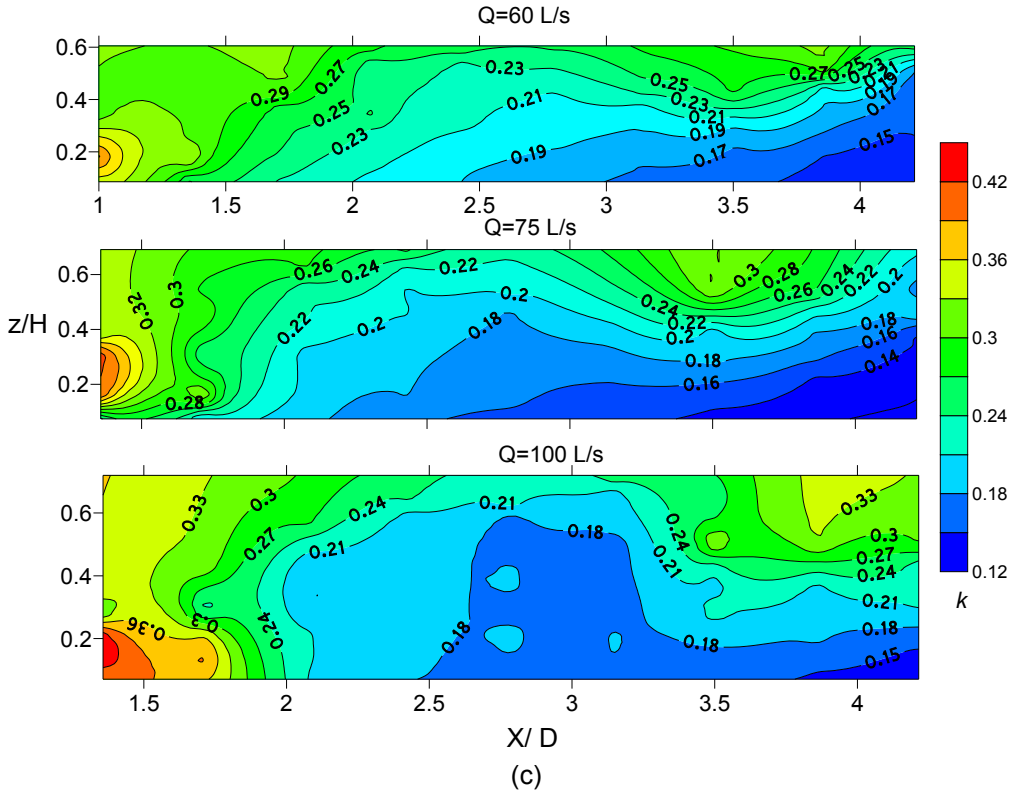

Figure 5.5 The spatial distribution of normalized turbulent kinetic energy (k) for the (a) 1.5%, (b) 3%, and (c) 5% slopes along the central vertical plane (XZ) at cell 6 under different flow rates.

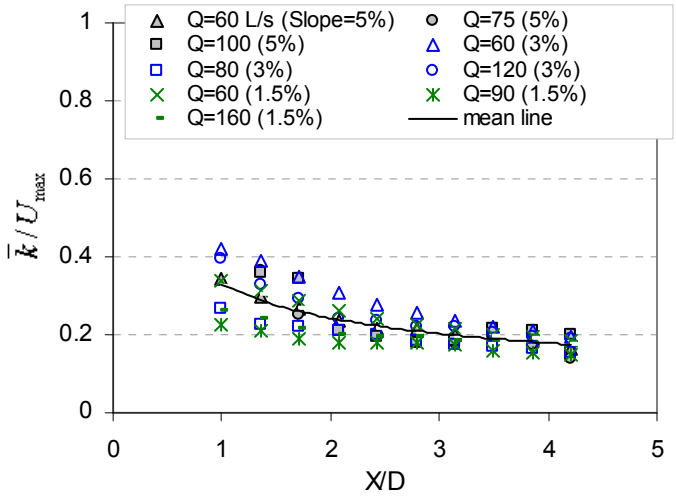

Figure 5.6 Variation of normalized depth-average turbulence kinetic energy, $\bar{k}/U_{max}$, with relative distance *X/D* along the centre line of the flume for all experiments.

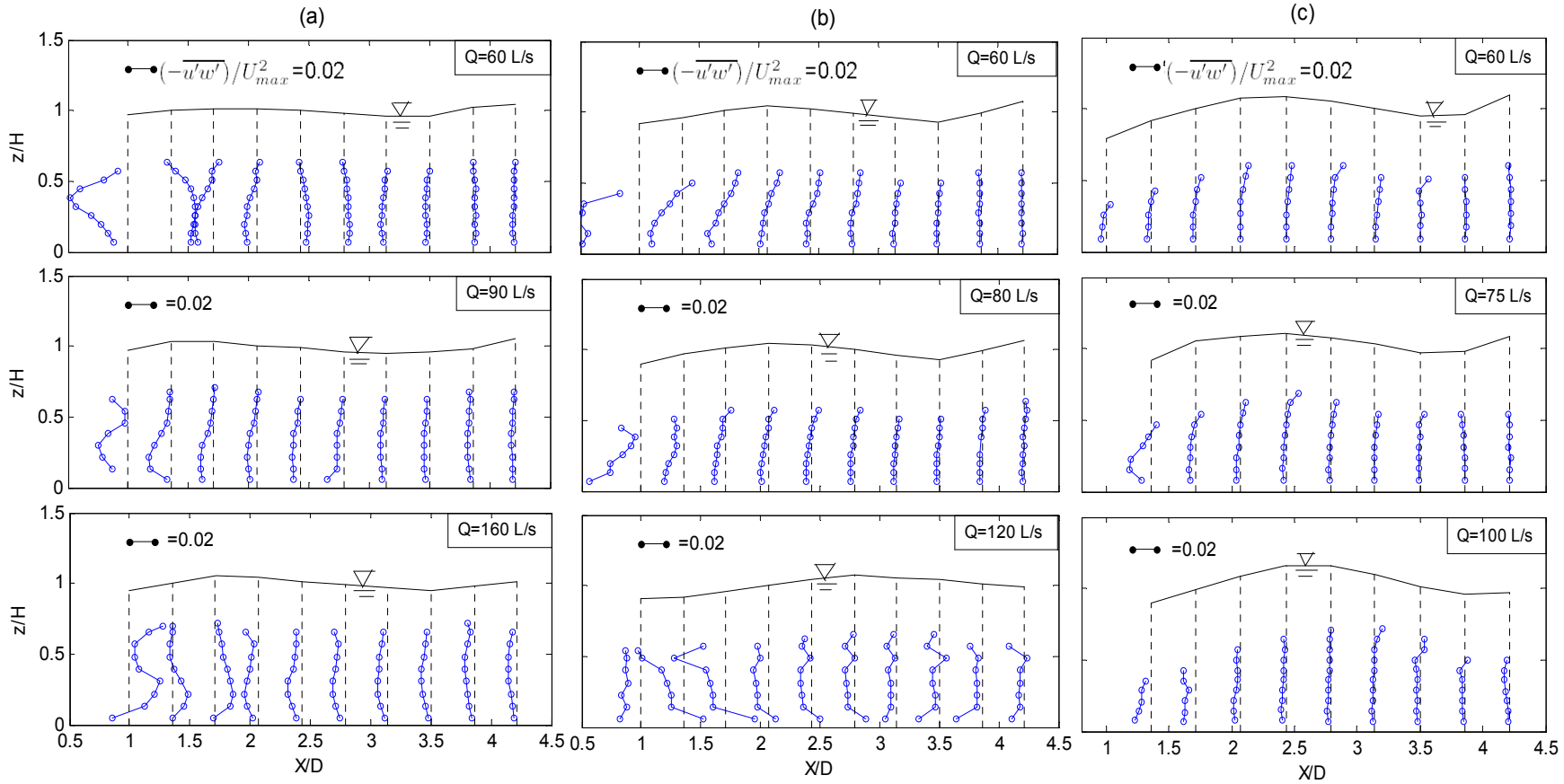

Figure 5.7 Distribution of normalized principal Reynolds shear stress, $-\overline{u'w'}/U_{\max}^2$, for the (a) 1.5%, (b) 3%, and (c) 5% slopes along the centre line of the flume under different flow conditions.

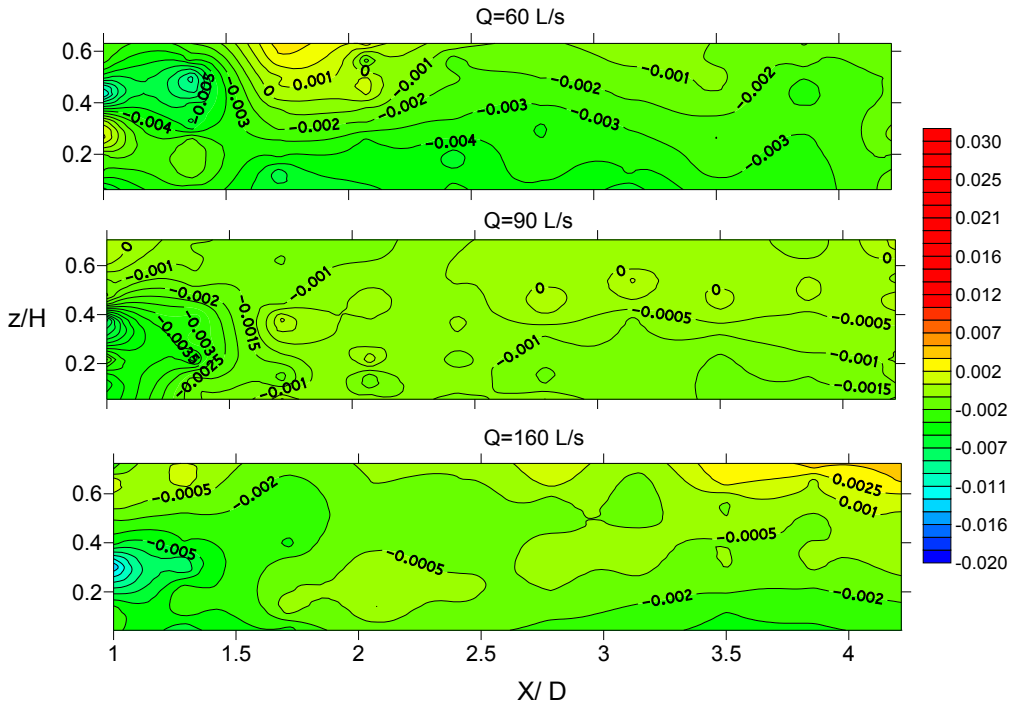
Q=60 L/s
Q=90 L/s
Q=160 L/s
z/H
X/ D
0.6
0.4
0.2
1
1.5
2
2.5
3
3.5
4
0.030
0.025
0.021
0.016
0.012
0.007
0.002
-0.002
-0.007
-0.011
-0.016
-0.020

(a)

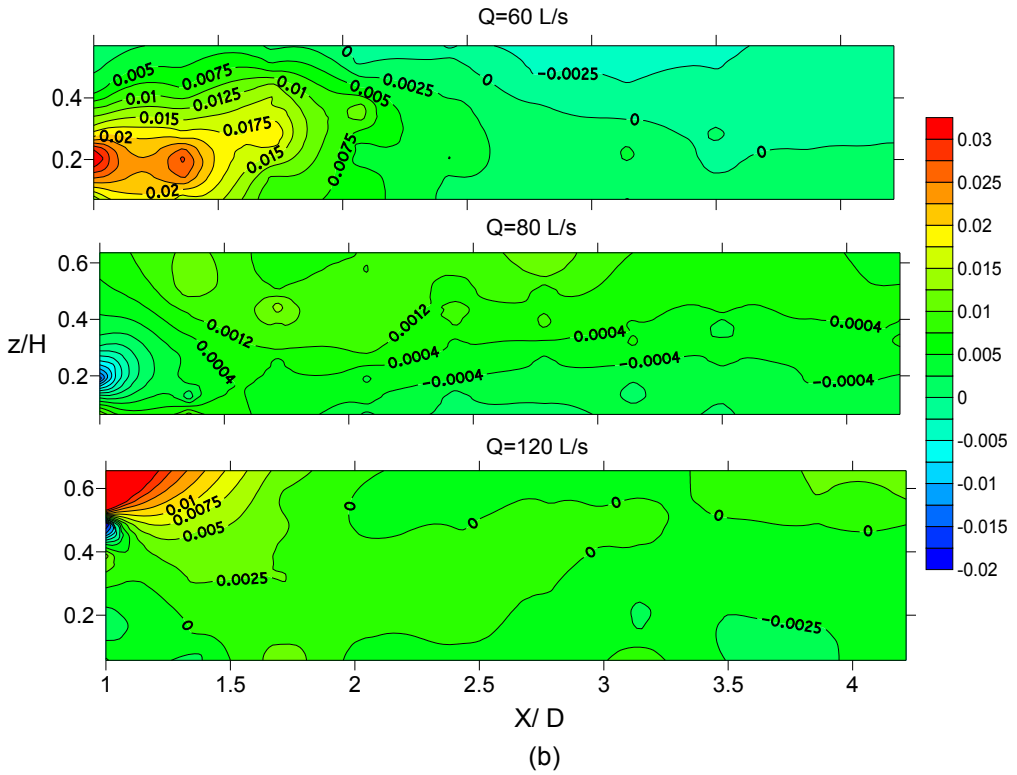
Q=60 L/s
Q=80 L/s
Q=120 L/s
z/H
X/ D
0.6
0.4
0.2
1
1.5
2
2.5
3
3.5
4
0.03
0.025
0.02
0.015
0.01
0.005
0
-0.005
-0.01
-0.015
-0.02

(b)

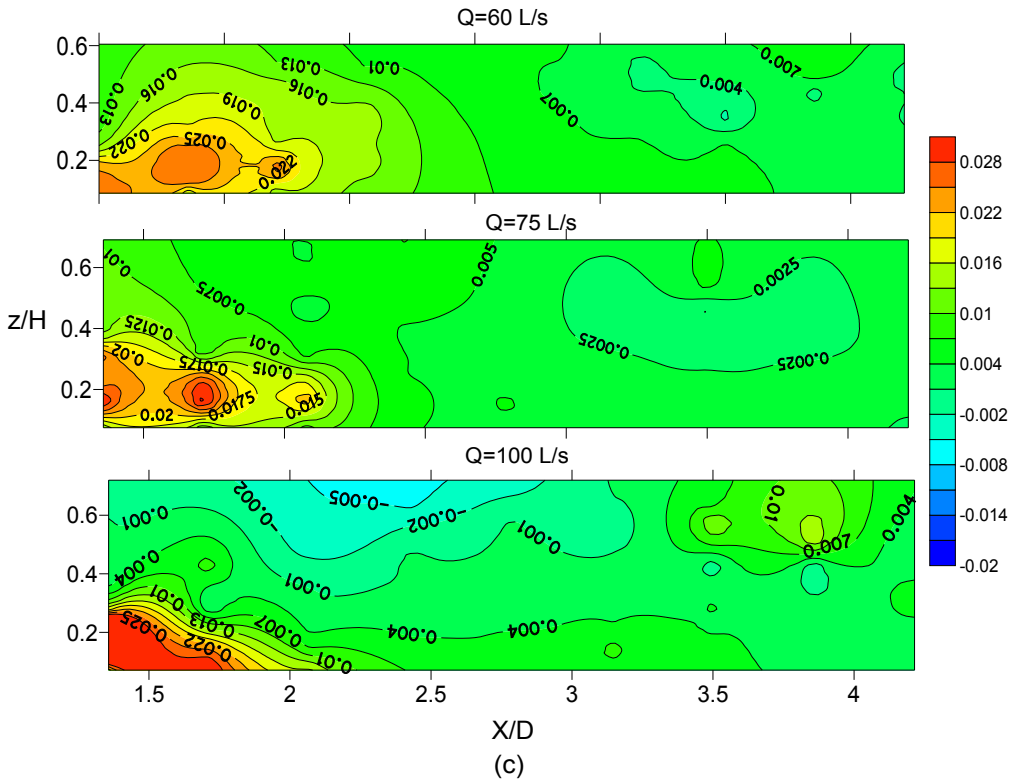

(c)

Figure 5.8 The spatial distribution of normalized Reynolds shear stress ($-\overline{u'v'}/U_{\max}^2$) for the (a) 1.5%, (b) 3%, and (c) 5% slopes along the centre vertical plane (XZ) under different flow conditions.

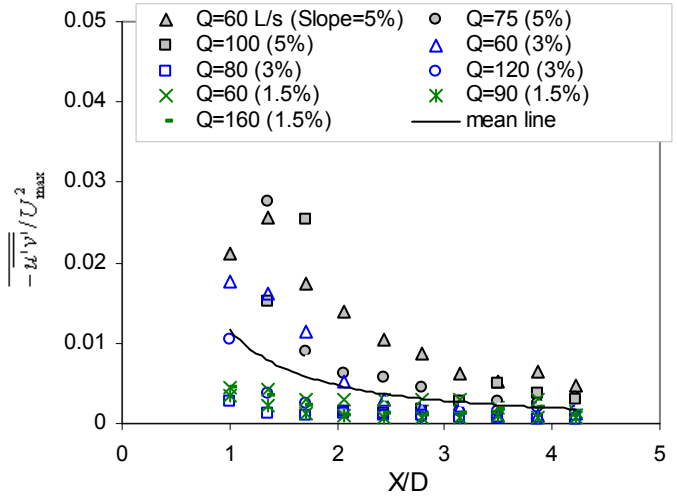

Figure 5.9 Variation of normalized depth-average Reynolds shear stress, $-\overline{\overline{u'v'}}/U_{\max}^2$, with relative distance *X/D* along the centre line of the flume for all experiments.

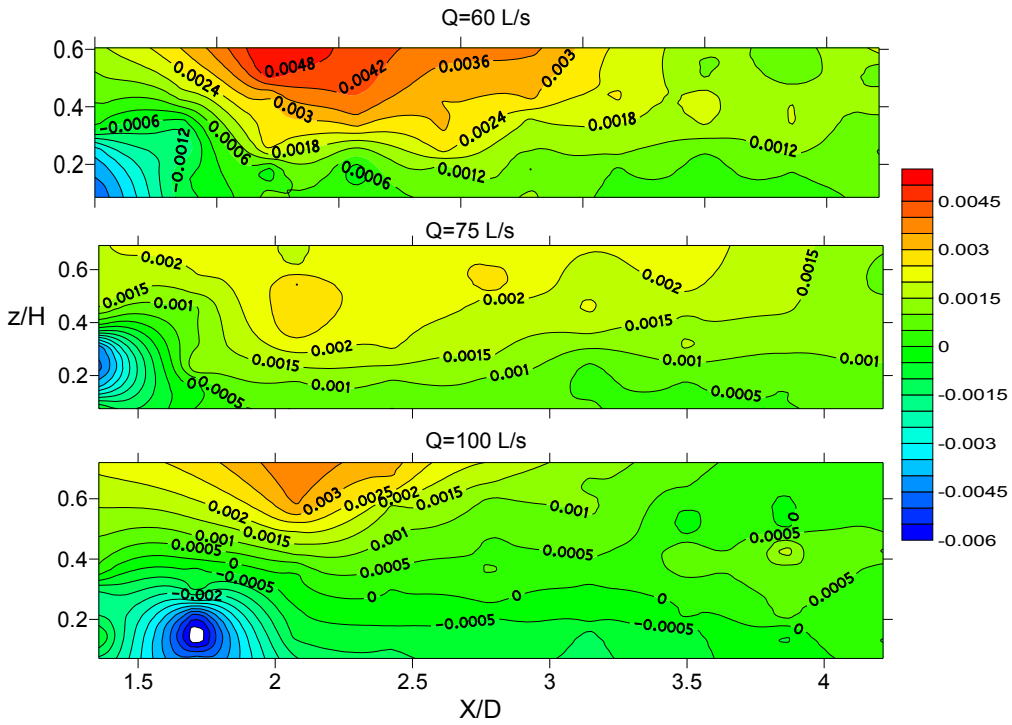

Figure 5.10 The spatial distribution of normalized Reynolds shear stress $-\overline{v'w'}/U_{\max}^2$ for the 5% slope along the centre vertical plane (XZ) under different flow conditions.

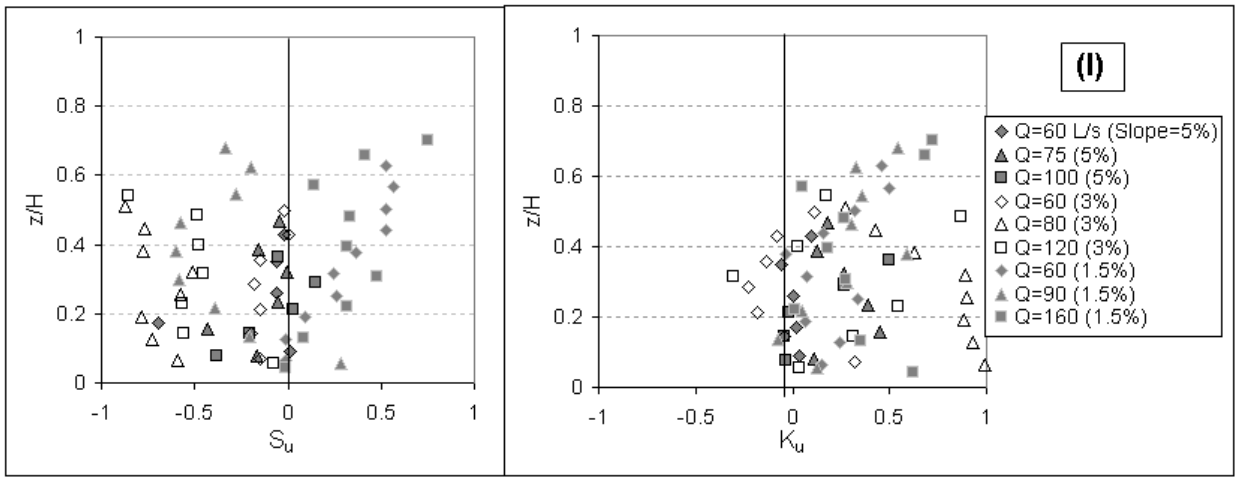

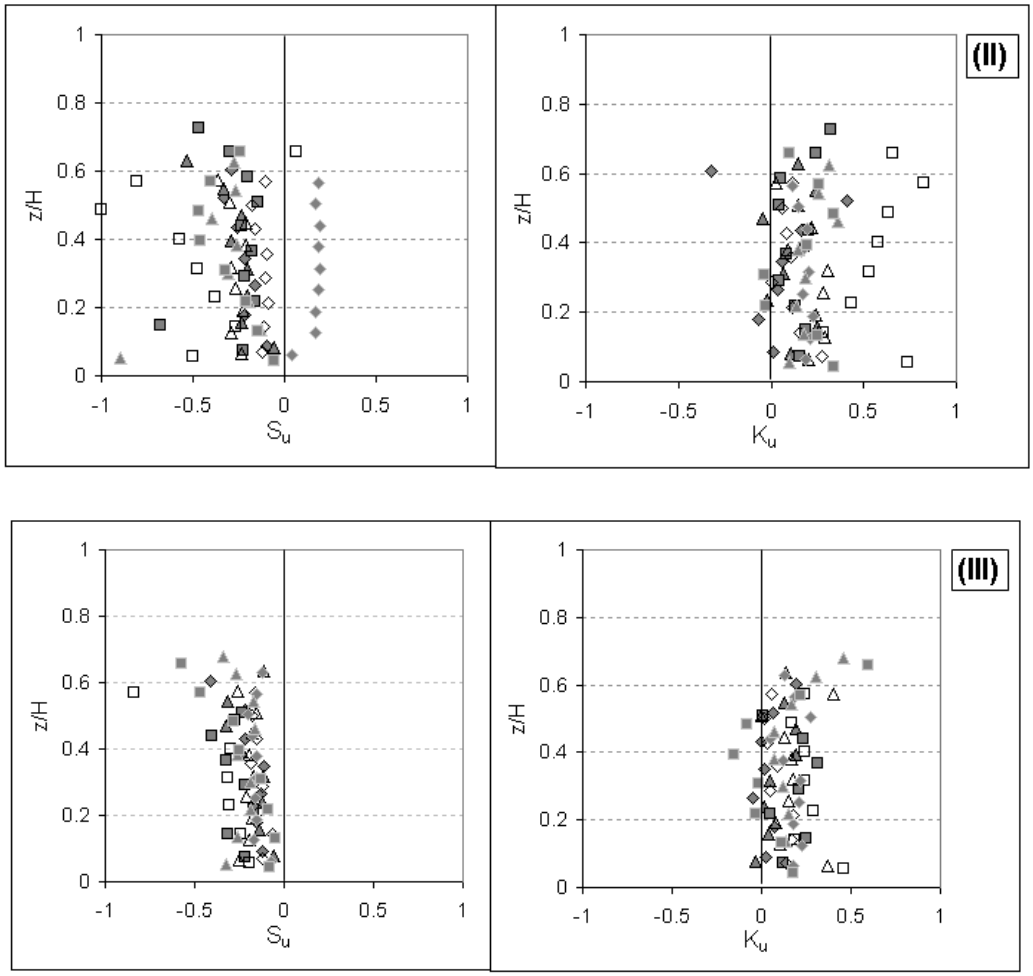

Figure 5.11 Vertical distribution of skewness (S_u) and kurtosis (K_u) at stations (I), (II), and (III).

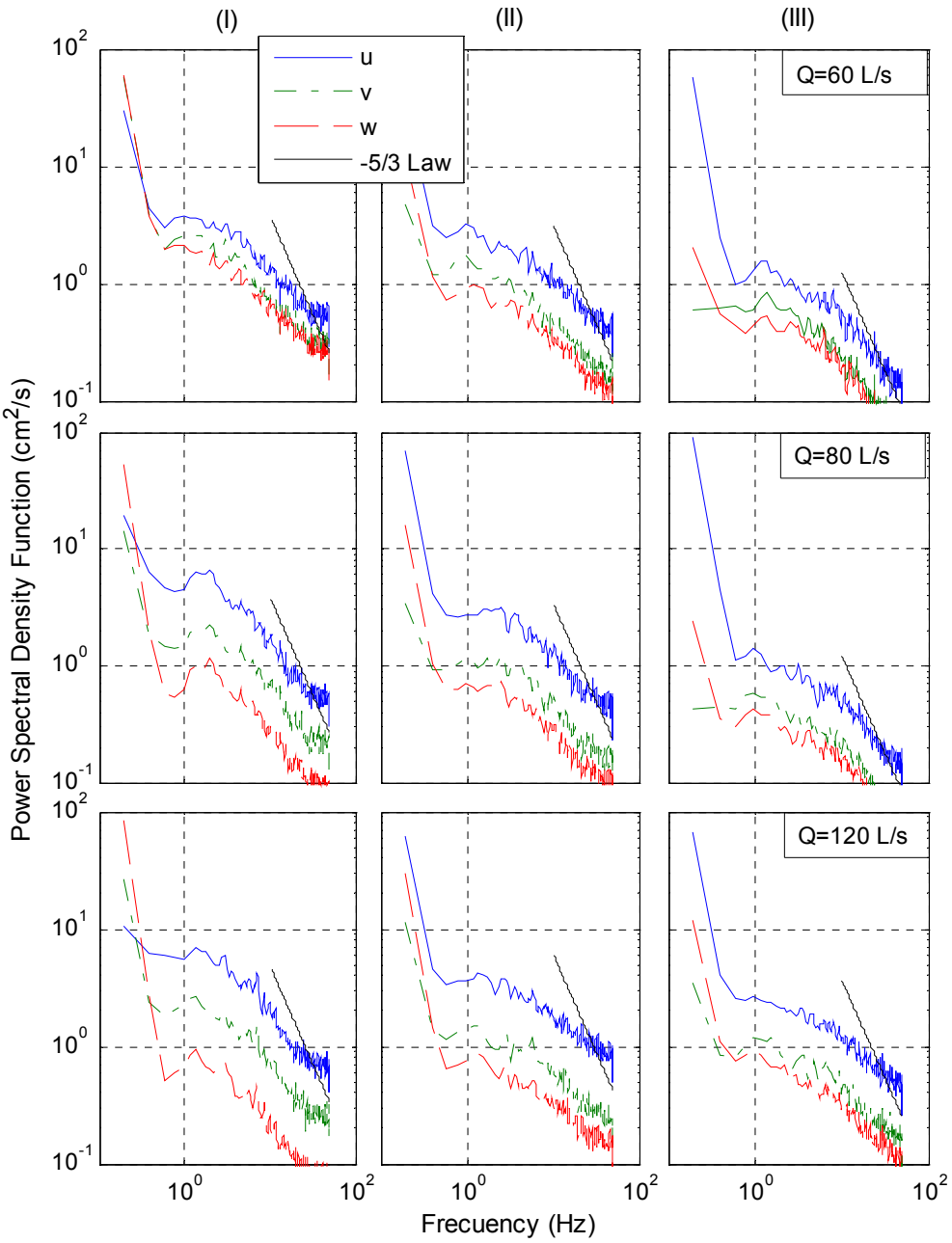

Figure 5.12 Power spectrum of *u, v*, and *w* velocity components for the 3% slope at stations (I), (II), and (III) under different flow rates.

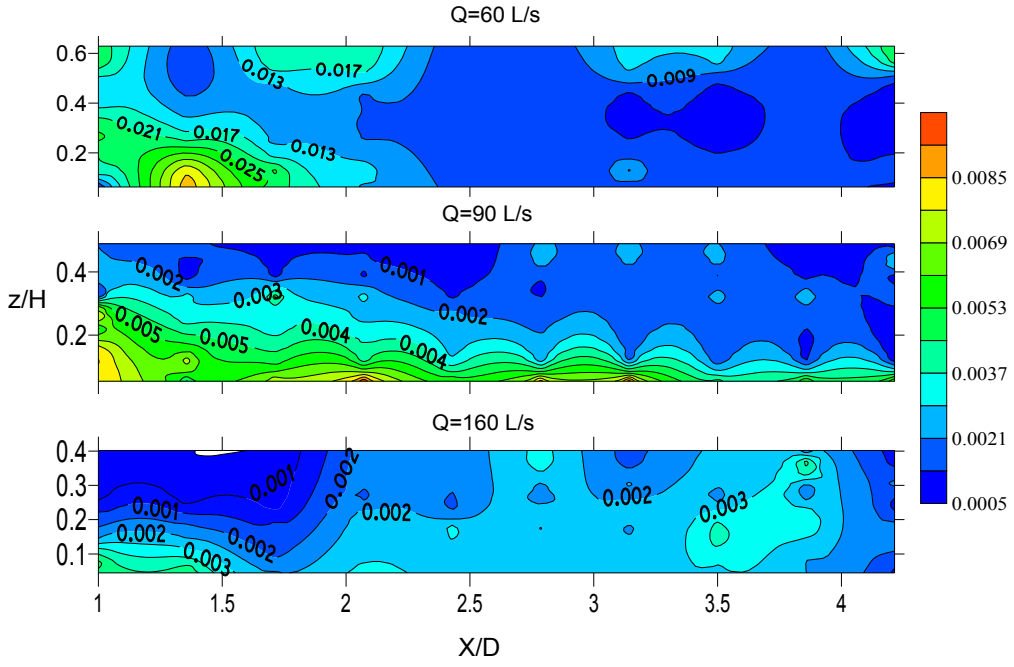
Q=60 L/s
Q=90 L/s
Q=160 L/s
z/H
X/D
0.0085
0.0069
0.0053
0.0037
0.0021
0.0005

(a)

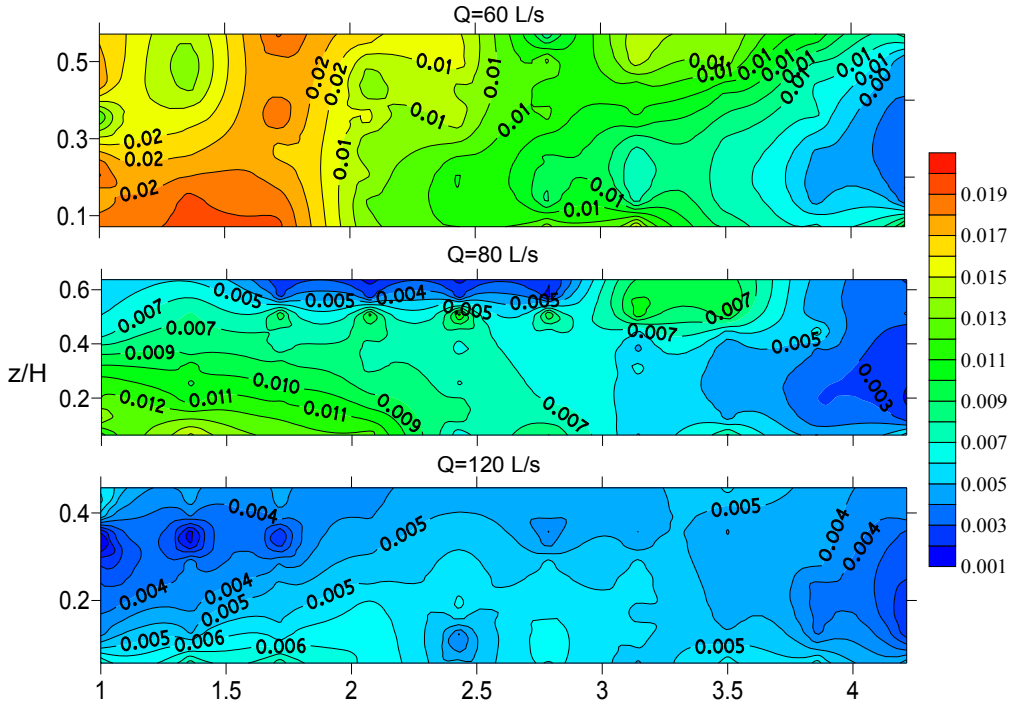
Q=60 L/s
Q=80 L/s
Q=120 L/s
z/H
X/D
0.019
0.017
0.015
0.013
0.011
0.009
0.007
0.005
0.003
0.001

(b)

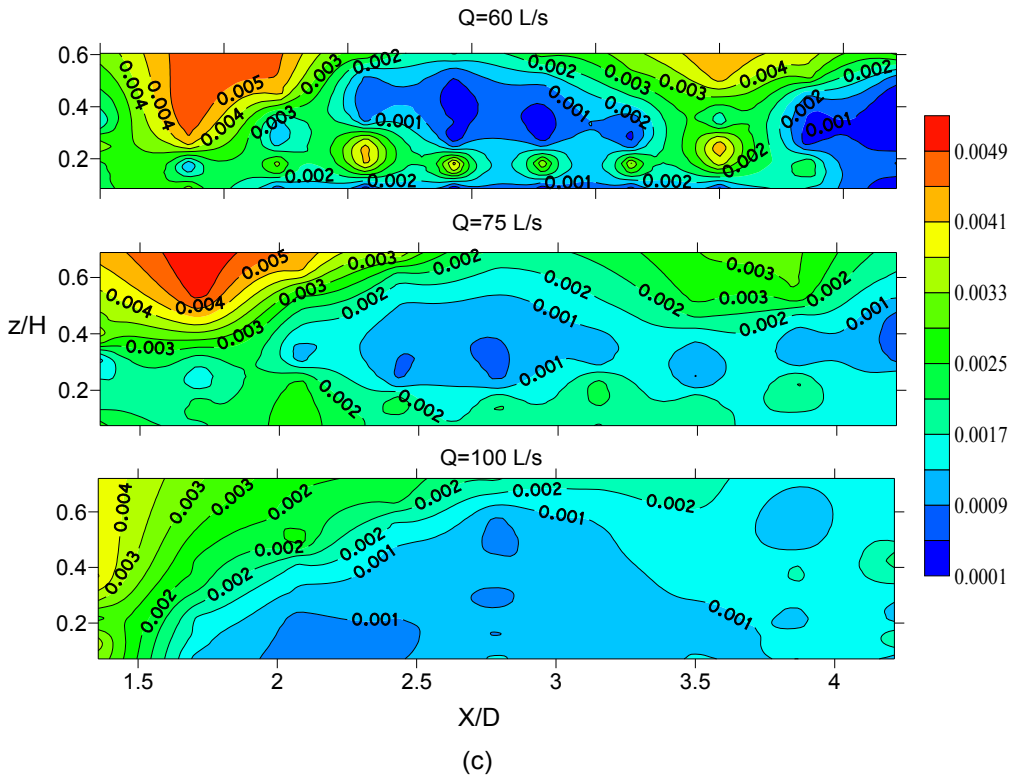

(c)

Figure 5.13 The spatial distribution of normalized energy dissipation rate ($\varepsilon D/U_{\max}^3$) for the (a) 1.5%, (b) 3%, and (c) 5% slopes along the central vertical plane (XZ) under different rates.

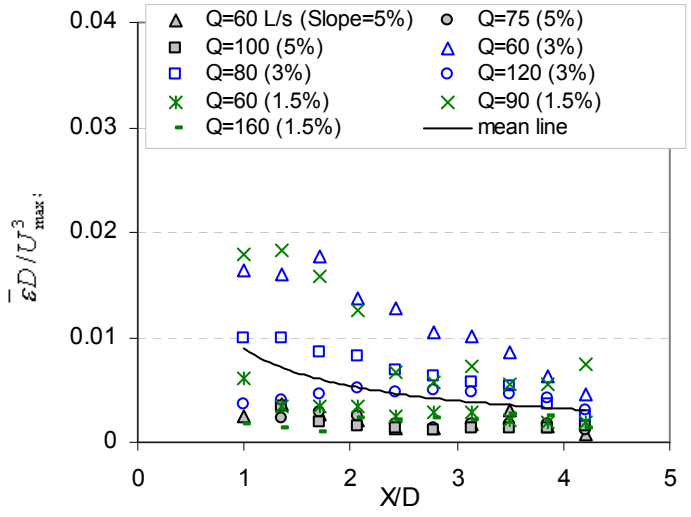

Figure 5.14 Variation of normalized depth-average energy dissipation rate, $\overline{\varepsilon D}/U_{\max}^3$, with relative distance *X/D* along the centre line of the flume for all experiments.

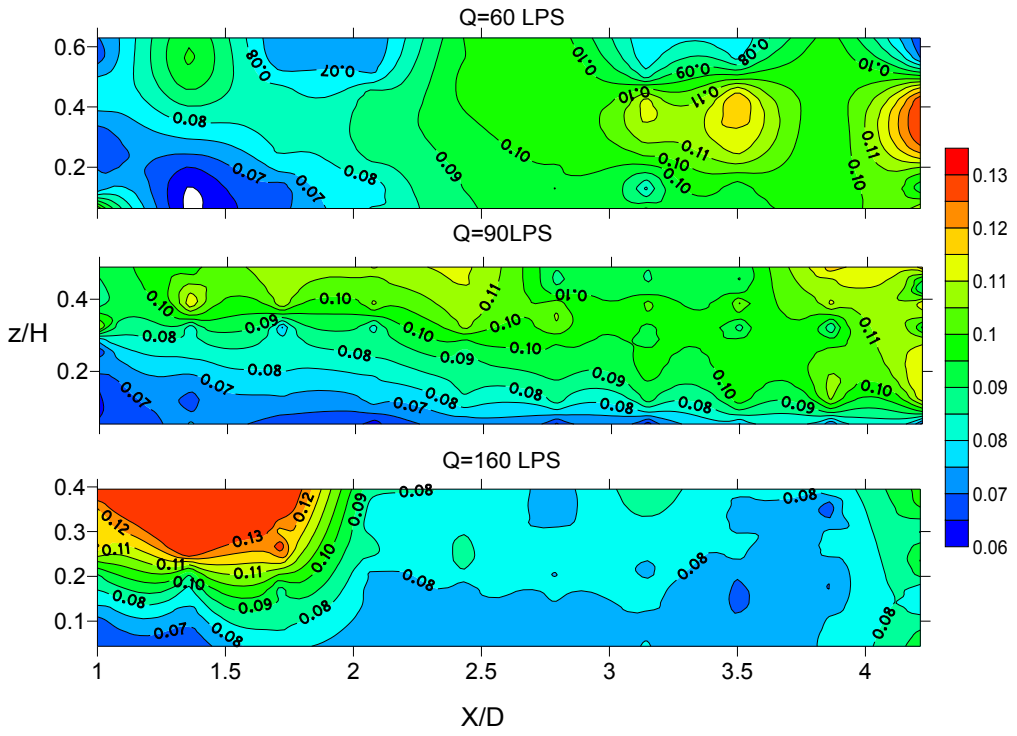
Q=60 LPS
Q=90LPS
Q=160 LPS
z/H
X/D
0.6
0.4
0.2
0.3
0.1
1
1.5
2
2.5
3
3.5
4
0.13
0.12
0.11
0.1
0.09
0.08
0.07
0.06

(a)

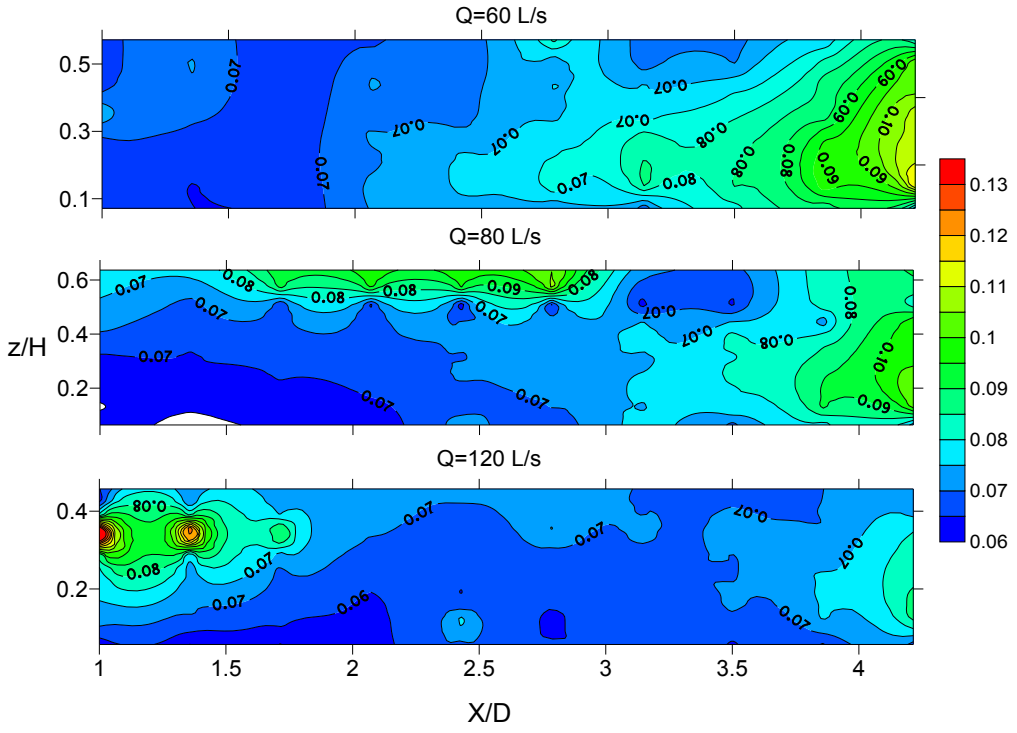
Q=60 L/s
Q=80 L/s
Q=120 L/s
z/H
X/D
0.5
0.3
0.1
0.6
0.4
0.2
1
1.5
2
2.5
3
3.5
4
0.13
0.12
0.11
0.1
0.09
0.08
0.07
0.06

(b)

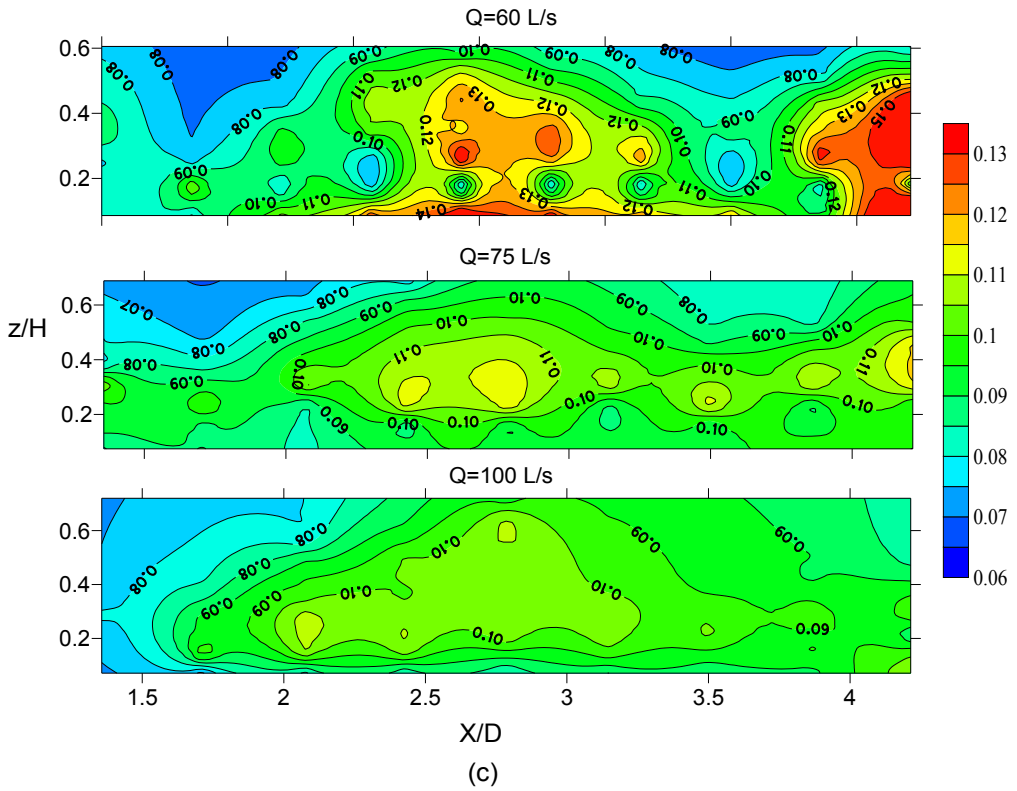

Figure 5.15 Speatial distribution of Kolmogorov's eddy length scale (in mm) for the (a) 1.5%, (b) 3%, and (c) 5% slopes along the central vertical plane (XZ) under different rates.

CHAPTER 6

Computational Fluid Dynamics Modeling of Flow in a Rock-Ramp Type Nature-like Fishpass*

6.1 Introduction

Nature-like fishpasses have been designed, in response to concerns with technical fishpasses, to provide passage for all species occurring in a system (Katopodis 1995) and a growing desire to reestablish stream continuity (Eberstaller et al. 1998). The goal of a nature-like fishpass is to dissipate energy and reduce channel velocities while mimicking the habitat conditions found within the river (Franklin et al. 2012). The design is site-specific, and examples are bypass channels around dams and roughened rock-ramps constructed either immediately downstream of a dam or in association with a partially removed dam (Parasiewicz et al. 1998). The rock-ramp fishpass consists of a long sloping channel with interspersed boulders providing resting places for fish swimming upstream. The performance of rock-ramp fishpass was previously evaluated through laboratory setup (Haro et al. 2008) and field (Franklin et al. 2012; Franklin and Bartels 2012) and showed most promising results.

*The content of this chapter has been drafted as a journal manuscript: Baki et al. (2013c). "Computational Fluid Dynamics Modeling of Flow in a Rock-Ramp Type Nature-like Fishpass." *Journal of Hydraulic Research, IAHR, (drafted)*.

Limited investigations, via field and experimental, on flow characteristics in nature-like fishpasses have been carried out. For instance, DVWK (2002), Parasiewicz et al. (1998), and USBR (2007) provided some practical guidelines based on critical velocity criteria for rock-ramp and bypass type nature like fishpasses. Haro et al. (2008) conducted several experiments with field-scale laboratory setup for a nature-like fishpass in a perturbation boulder design. In addition, Wang and Hartlieb (2011) examined the hydraulics of nature-like pool-type fishpasses via experimental and field investigations. Since, the flow characteristics in a rock-ramp will differ for different geometric conditions especially for boulder arrangements and spacing, additional studies are required to investigate all unknown hydraulics more systematically. The recent advances in numerical modeling can provide an outstanding opportunity to explore those unknown hydraulic features in nature-like fishpasses and, hopefully, with more accuracy and understanding.

In the past ten to fifteen years, much attention has been directed to the development of numerical models as tools to facilitate eco-hydraulic studies (Crowder and Diplas 2000 and Guay et al. 2000). A typical example is the development of the Physical Habitat Simulation Method (PHABSIM, see Bovee et al. 1998), and River2D (see Steffler et al. 2002). In recent years, research in the use of CFD model for assessing the flow characteristics in fish habitat structures and fishpasses has increased tremendously. Haltigin et al. (2007) conducted a 3-D numerical simulation of flow around stream deflectors using the experimental

results of Biron et al. (2005) with the computational fluid dynamics software PHOENICS; Shen and Diplas (2008) used 2-D and 3-D hydrodynamic model, ANSYS-CFX, to validate against published experimental results by Shamloo et al. (2001) and investigated the impact of boulders on local flow patterns. Reviews of recent 3-D CFD models without free surfaces can be found in Lai et al. (2003) and Khan et al. (2004). Free surface flows involve immiscible fluids (air and water) separated by sharp interfaces and such type of 3-D CFD models was done by Khan (2006) in a vertical slot fishpass. This study did not verify the accuracy of the model; rather it referenced other studies designed to validate CFD models using similar mathematics. Therefore, furthering the validation of CFD at predicting complex velocity patterns, and simply characterizing 3-D flow patterns and turbulence are extremely important areas of research (Hotchkiss and Frei 2007). Following CFD model validation, Salaheldin et al. (2004) and Naghavi et al. (2011) simulated flow field around circular piers and weirs, respectively, using free surface interface.

The above modeling studies have demonstrated that there is great potential in using computational fluid dynamics (CFD) for representing the detailed flow field in the nature-like fishpasses. In the present study, a CFD model simulating free surface flow in a rock-ramp nature-like fishpass is presented. The performance of this model is first validated against the experimental measurements. Next, the flow fields in a rock-ramp fishpass for different flow conditions and geometric variables were analyzed. Therefore, the primary objective of this study is to carry

out a systematic investigation on the effects of flow rates, channel slopes, boulder diameters, boulder spacing, and boulder arrangements on water level, flow velocity, and flow resistance in a rock-ramp fishpass to optimize the design. Results from this study could play an important role in advancing our knowledge about the effect of geometric variables on mean flow characteristics in a rock-ramp fishpass and would be useful to both fishpass designers and fish biologists. Moreover, this study can persuade the researchers to use CFD model to explore all unknown hydraulics in nature-like fishpasses.

6.2 Experimental Setup

The study was conducted in an exploratory rock-ramp nature-like fishpass, installed in a rectangular flume. The width, height, and length of the flume were 0.92 m, 0.61 m, 8.89 m, respectively (*Figure 6.1*). The rock-ramp design consists of a staggered arrangement of isolated boulders that were placed throughout the length of the flume (*Figure 6.1*). The boulders were glued to the ramp bottom with silicone. A total of fifty-eight boulders, D=14 cm in an equivalent diameter and 12 cm in average height from the bed, were used in this experiment. Isolated boulders were arranged in 23 rows alternating between two and three boulders, and resulting in a total of 11 cells, as shown in Figure 6.1. In X direction, the longitudinal distance of each cell is 75 cm, and this length is considered as x=75 cm. The centre to centre distance between two boulders in longitudinal (s_l) and transverse (s_t) directions was approximately 37.5 cm (2.7D) followed the

recommendation by DVWK (2002). The water level and streamwise velocity at various longitudinal distances along the centre line of the flume in cell 6 were measured. A point-gauge was used to measure the fluctuating water level. For the velocity, an Acoustic Doppler Velocimeter (SonTek 10MHz ADV and Nortek Vectrino Plus) were used. Because of the ADV sampling volume and fluctuating water level, there is zone near the water surface where no measurements are available. In addition, a Yaw probe (Rajaranam and Muralidhar 1968) was used to measure the velocity especially for that upper region. Further details on the experimental setup, measurements, and data processing procedure are provided in Chapter 4.

6.3 Numerical Model Description

6.3.1 Governing Equations

A numerical model of the fluid flow through rock-ramp fishpass was developed using ANSYS-CFX. The model solves three-dimensional Reynolds averaged Navier Stokes (RANS) equation using the finite volume approach. ANSYS-CFX uses a multiphase model, with air and water representing the two phases of fluid, to model the "free-surface". The free surface representing the interface between air and water was modeled using the Volume of Fluid (VOF) method (VOF; introduced by Hirt and Nichols 1981). VOF solves a single set of momentum equations throughout the domain, while keeping track of the volume of phases in

each computational cell. The continuity and the momentum equations solved by the CFX solver (ANSYS-CFX) are as follows (in tensor form),

$$\frac{\partial \rho}{\partial t} + \frac{\partial \rho u_j}{\partial x_j} = 0$$

$$\frac{\partial \rho u_i}{\partial t} + \frac{\partial \rho u_j u_i}{\partial x_j} = -\frac{\partial p}{\partial x_i} + \frac{\partial}{\partial x_j}\left\{(\mu + \mu_t)\left(\frac{\partial u_i}{\partial x_j} + \frac{\partial u_j}{\partial x_i}\right) - \frac{2}{3}\rho k \delta_{ij}\right\} + (\rho - \rho_a) g_i \quad (6.1)$$

where, ρ is the fluid density, ρ_a is the density of air, p is the static pressure, g is the gravitational force, k is the turbulent kinetic energy, δ_{ij} is the Kronecker delta, μ is the molecular viscosity of fluid, and μ_t is the turbulent viscosity of fluid. For closure of the governing equations, the standard $k-\varepsilon$ turbulence model was used in order to determine the turbulent viscosity. Although, both the standard and the RNG $k-\varepsilon$ models were found to have performed satisfactorily in reproducing the measured velocity profiles around the circular piers (Salaheldin et al. 2004), further study needs to finalize the best turbulence model especially for the strong turbulent flow fields in a rock-ramp fishpass.

Equation (1) involves the volume fractions of both phases that enter through the physical properties of the phases such as density and viscosity. Accordingly, the phase-averaged properties are given as

$$\rho = \alpha_w \rho_w + \alpha_a \rho_a$$

$$\mu = \alpha_w \mu_w + \alpha_a \mu_a \quad (6.2)$$

where, α is the volume fractions and the subscripts, *w* and *a*, correspond to the phases, water and air, respectively. In modeling the free surface between water and air, a transport equation can be considered for the water phase:

$$\frac{\partial \alpha_w}{\partial t} + u_j \frac{\partial \alpha_w}{\partial x_j} = 0 \tag{6.3}$$

In this case, as the volume fraction for air phase can be inferred from the constraint, the transport equation should only be solved:

$$\alpha_a = 1 - \alpha_w \tag{6.4}$$

This equation is solved in the entire domain and volume fraction computed for all cells. The tracking of the interface is done in the cells where the volume fraction is different from 0 to 1. If a cell is completely filled with water, the volume fraction of that phase in the cell is equal to unity ($\alpha_w = 1$), and the cell is considered to be in the main flow region of that phase. A cell is considered to be on the free surface when the value of volume fraction is between 0 and 1($0 < \alpha_w < 1$).

In the homogeneous model, the mass transfer terms between the immiscible water and air phases are neglected (Fernandes et al. 2009). The VOF model, however, accounts for the effect of surface tension along the interface between the phases. The surface tension model used in these simulations is the continuum surface force (CSF) model that was proposed by Brackbill et al. (1992). The CSF models the surface tension force as a volume force concentrated at the interface, rather than a surface force.

6.3.2 Variables and Design Modifications

The model layout of the rock-ramp fishpass domain matches the dimensions of the original experimental setup as shown in Figure 6.1 having a length of only X=3.5 m and considering simply 3 cells (5, 6, and 7) (*Figure 6.2*). In the domain, the boulders were placed in two different patterns: (I) a staggered arrangement of isolated boulders which is exactly similar to the original geometry and (II) a modified staggered arrangement of boulders as shown in Figure 6.2. In pattern (II), the longitudinal distance between two subsequent rows alternating two and three boulders is constant and s_l=1.5*D*. For both patterns, the centre point of each boulder (*D*=14 cm) is 5 cm from the channel bottom resulting 2 cm embedded in the channel bed and 12 cm boulder height from the channel bed. All the variables considering flow, boulder diameter, channel slope, boulders spacing, and boulder arrangement for each numerical domain are listed in Table 6-1. Series A varies flow rate; series B varies channel slope; series C varies boulder diameter; series D varies boulder spacing in longitudinal direction in (I); series E varies boulder spacing in transverse direction in (I); and F varies boulder spacing in longitudinal direction in (II). Series A to C followed the boulder arrangement pattern (I) having s_l=s_t=*2.7D*. In series D, s_l varied from 2.7*D* to 1.6*D,* 2.0*D,* 3.4*D,* and 3.8*D* and in series E, s_t from 3.7*D* to 3.0*D,* 3.5*D,* 4.0*D,* and 4.5*D*. For series E, s_l were 3.0*D,* 3.5*D,* 4.0*D,* 4.5*D,* and 5.0*D* in pattern (II).

6.3.3 Boundary Conditions and Mesh

Boundary conditions were applied to all sides or faces of the domain. The mass flow rate was specified at the upstream inlet boundary of the channel, which is uniformly distributed over the water and air phases. The VOF technique allows air flow through the channel above water. If no air is allowed to enter through the inlet (or air flow rate is too small), then large recirculating regions of air may occur above the water that may cause computational instabilities (Ma et al. 2002). The turbulence intensity (*I*) of the fluid flow at the upstream boundary was specified as medium (5%). Ma et al. (2002) for upland urban river noted that the predicted velocities are graphically indistinguishable for 5, 10, and 20% turbulence intensity. The solver uses the following expression to compute *k* and ε at the inlet from the given value of intensity (CFX 2009),

$$k_{in} = \frac{3}{2} I^2 u_{in}^2 \quad \text{and} \quad \varepsilon_{in} = \rho C_\mu \frac{k^2}{100 I \mu_t} \tag{6.5}$$

where, C_μ is the $k-\varepsilon$ turbulence model constant (0.09). Zero static pressure was applied at the downstream boundary and no-slip boundaries (indicates water flow is zero at the boundaries) were applied at all sidewalls, channel floor, and all boulder surfaces. The channel floor was assumed as rough and the roughness height was set as 0.0008 m equivalent to the Manning's roughness coefficient for smooth steel bottom. The top surface was specified as an opening boundary and this is a pressure boundary which allows both inflow and outflow.

The initial conditions for the fluid flow field may be specified in an arbitrary way. The initials values of velocities were provided as zero in inlet boundary and the initial pressure was assumed as hydrostatic for the water region and zero for the air region in outlet boundary. In addition to the fluid velocities and hydrostatic pressure, the water level at the inlet and outlet needs to be given to specify the water volume fraction at the boundary. This water level should be consistent with the water flow rate through the channel. For saving computational time, the experimental water level for a steady discharge was used as initial water level at inlet and outlet. Even, for any initial water level, it is assumed that the steady water level in the computational domain should be produced as time progresses. Moreover, the sensitivity of the initial water level at inlet/outlet was tested for the simulated water level and it was graphically identical (*Figure 6.3*). Therefore, the same water level at inlet and outlet, equivalent to the experiment, was used as the initial boundary conditions for other simulations.

The upwind scheme was used as the advection scheme. Unstructured tetrahedral mesh was used in the solution domain. The fluids are assumed to be Newtonian, isothermal, and incompressible; therefore, their properties are kept constant. Typically, the relative error between two successive iterations is specified using a convergence criterion of 0.0001 for each scaled residual component. The computations are conducted under the steady state condition. The model was found to converge to steady state in less than 600 iterations.

A mesh independence study was conducted for assessing the grid sensitivity of the results for the simulation A2. Three mesh systems, Mesh 1 (coarse), Mesh 2 (medium), and Mesh 3 (fine) were used to examine the effect of the mesh size on the accuracy of the numerical results. The basic properties of the three computational meshes are summarized in Table 6-2. Figure 6.4 compares the simulated streamwise velocity profiles for three different mesh sizes at x= 29, 39, and 49 cm (in cell 6) along the centerline of the flume. At these three locations, the average differences from each other in streamwise velocity profiles varied from 4-5%, 1.5-2%, and 1-2% cm/s, respectively. Hereafter, Mesh 3 has been used for all simulations. The development of flow field through the domain was checked for the simulation A2 by comparing the streamwise velocity profiles at cell 5 (X=72.5 cm), cell 6 (X=147.5 cm), and cell 7 (X=222.5 cm) in Figure 6.5. It is apparent that the average differences in streamwise velocities from cell 5 to cell 6/7 is about 2.5%, where this difference in between cell 6 to cell 7 is less than 0.2%. Therefore, this consequence ensured that the flow fully developed from cell 6 and no sensitivity was observed.

6.3.4 Model Validation

Experimental results related to water surface profiles and streamwise velocity distributions were used to validate the numerical simulation predictions. For the simulations A2 (Q=60 L/s, S_0=5%) and B2 (Q=60 L/s, S_0=3%), the simulated water surface and streamwise velocity profiles in cell 6 at various longitudinal distances (x=75 cm) along the centre line of the flume were compared with

experimental results. Figure 6.6(a&b), comparison of simulated and experimental results, shows that the overall agreement between CFD predictions and experimental measurements is good. Downstream of the boulder (x=0 to 29 cm or *2D*), considerable discrepancy existed between simulations and measurements due to strong flow re-circulation and the form roughness which is expected to dominate in the boulder vicinity (Papanicolaou et al. 2012). The adverse pressure gradient encountered in the flow behind the boulder is expected to create a recirculation region dominated by vortices and reverse flow, which could extend several boulder diameters downstream of the boulder (Munson et al. 1990). Similar deviation between numerical results and laboratory measurements in the wake region was reported by Salaheldin et al. (2004) and Shen and Diplas (2008). This discrepancy minimized while approaching downstream direction. At locations further away from the boulder, the simulated stremwise velocities were very close to the measured values, where the flow circulations vanished and the form roughness attenuated (Papanicolaou et al. 2012).

The correlation coefficient for water level between the numerical and experimental results is found to be 0.98 and 0.90 for the simulations of A2 and B2, respectively. The corresponding correlation coefficient for velocity using ADV was 0.88 and 0.96, respectively. The Mean Absolute Percentage Error (MAPE) for water level was about 1.5 and 2.5% for A2 and B2, respectively. Naghavi et al. (2011) also found a good agreement between CFD predictions and experimental results for water surface profiles over a cylindrical weir, where the

maximum difference was about 2.5%. The Mean Absolute Error (MAE) for velocity was about 0.05 and 0.03 m/s for A2 and B2; and the Mean Absolute Percentage Error (MAPE) was about 10 and 8 %, respectively. This percentage of error between experimental and CFD results might be attributed from the measurement inaccuracy in the laboratory due to strong turbulent flow field and small variations in the numerical model.

6.4 Results and Discussions

6.4.1 Water Depth

The normalized water surface profiles (*h/H* versus *x/D*) for all simulations are plotted in Figure 6.7 along the centre line of the channel at cell 6 with the experimental mean tend line from Chapter 4, where, *h* and *H* are the water depth and average water depth, respectively. In general, it was observed that a drop in water level occurred in the wake region due to expansion of flow area and an occurrence of maximum water depth immediately upstream of boulder due to the obstruction. In each cell, the water surface rises and falls as flow approaches upstream and downstream of the boulders, which generated two complete cycles. The profiles for different flow rates (series A, *Figure 6.7a*), channel slopes (series B, *Figure 6.7b*), boulder diameters (series C, *Figure 6.7c*), and boulder transverse spacings (series E, *Figure 6.7e*) followed the experimental mean tend line with some degree of scatter. In contrast, the water surface profiles for series D and F (*Figure 6.7d&f*) deviated from the experimental mean tend line. The peaks and

drops in water surface profiles shifted upwards or downwards from the corresponding peaks and drops of the trend line due to the variation of boulder longitudinal spacing.

To investigate the effect of flow rates, channel slopes, boulder diameters, boulder spacings, and boulder arrangements on average water depth in a rock-ramp fishpass, the generalized discharge ($Q^* = Q/\sqrt{gS_0 R_v^{\,3} B^2}$) and average water depth (H/D) for all simulations are plotted in Figure 6.8. Herein, g is the acceleration due to gravity, S_0 is the channel slope, B is the channel width, and R_v is the volumetric hydraulic radius. R_v is defined for a wide channel as the volume of overlying water per unit plan area of the bed (Smart et al., 2002) (for more details see in Chapter 4). Here, the volumetric hydraulic radius was preferred essentially for minimizing the integrated effect of boulder diameter and arrangement (spacing and density). It has been found that the average water depth for different flow rates, channel slopes, and boulder diameters followed the experimentally established depth-discharge linear equation ($H/D = 0.345Q^*$) from Chapter 4, where all data points fitted within 90% confidence limit. Subsequently, data points for the corresponding water depth simulated for series D, E, and F partially agreed with that linear relationship. In series D, the data points for s_l=2.7-3.4D fitted within 90% confidence limit, for $s_l \geq 2.0D$ and $\leq 3.8D$ fitted within 75% confidence limit, and for $s_l \leq 1.6D$ plotted outside of 75% confidence limit. In series E, the data points for s_l=2.7-3.0D fitted within 90% confidence limit, for $s_l \leq 3.5D$ fitted within 75% confidence limit, and for $s_l \geq$4-

4.5D plotted outside of 75% confidence limit. Finally, in series F all data points for s_l=3.0-5.0D fitted within 90% confidence limit. Therefore, the depth-discharge relationship is valid for s_l=2.0-3.8D and s_t=2.7-3.5D in boulder arrangement pattern (I) and for s_l=3.0-5.0D in pattern (II) having 75% confidence limit.

At lower longitudinal distance (s_l<2.0D) the flow skimming over the tops of the boulders resulting in higher water depth due to the higher boulder concentration (Ferro 2003) and dominated shear friction resistance over the form roughness (Ferro 2003). However, at higher longitudinal or transverse distance (s_l or s_t>4.0D) the flow pattern performed as isolated roughness flow resulting smaller water depth due to the lower boulder concentration (Morris 1954) and dominated individual form roughness (Ferro 2003).

6.4.2 Velocity

The variation of the normalized discharge, Q*, versus the normalized time averaged maximum velocity, $U_{\max}* = U_{\max} / \sqrt{gS_0R_v}$, and the streamwise average velocity, $u_{avg}* = u_{avg} / \sqrt{gS_0R_v}$, for all simulations are plotted in Figure 6.9 (a) and (b), respectively. Herein, $U_{\max}$ is the time averaged maximum velocity and u_{avg} is the streamwise average velocity along the centre line. In Figure 6.9(a), the effect of flow rates, channel slopes, boulder diameters, boulder spacings, and boulder arrangements on experimentally established linear relationship, $U_{\max}* = 1.504Q*$, from Chapter 4 was investigated. It was apparent that the time-averaged

maximum velocity corresponding to the series A to F simulations provided an excellent fit with that experimental linear relationship where all data points fitted within 75% confidence limit. It is important to state that this relationship was validated with field-scale data sets in Chapter 4. In series A, B, C, and D, the data points fitted within 90% confidence limit. In series E, the data points for s_l=2.7-3.5D fitted within 90% confidence limit and for s_l≥4-4.5D fitted within 75% confidence limit. In series F, data points for s_l=3.0-4.0D fitted within 90% confidence limit and for s_l≥4.5-5.0D fitted within 75% confidence limit.

Similarly, the experimentally established linear relationship, $u_{avg}^* = 1.047Q^*$, from Chapter 4 was also investigated in Figure 6.9 (b). Form this figure, it was apparent that most of all data points plotted outside of 90% confidence limit but fitted within 75% confidence limit, except the simulation D1. For D1, s_l≤1.6D plotted outside of 75% confidence limit. Most of all simulated streamwise average velocity was under-predicted from the experimental relationship. The possible reason is that the streamwise average velocity in CFD included the velocity zones near the water surface, that was excluded in experiments due to the ADV limitations (mention above).

From CFX model simulations, the spatial distributions of time-averaged velocity magnitude with directions along the centre vertical plane of the flume in cell 6 are presented in Figure 6.10. From these figures, it is clearly apparent several velocity zones having different magnitude. Downstream of the boulder, in wake region,

the distributions of the velocity were more complex having the minimum magnitude. The flows in the wake gradually overcome the disturbance caused by the boulders. Moving further downstream and away from the wake region, the velocity distributions started to develop and the velocity reached their maximum values. The approach velocity towards the boulders started to decelerate due to considerable increase in water level. For all simulations, some preferred path for upstream migration (with velocity ranging from 0 to 0.60 m/s) and resting areas at downstream of the boulders (with velocity less than 0.40 m/s) may be found by fish.

For A series simulations the maximum velocity magnitude varied from 0.8-1.4 m/s, and for B series it varied from 0.8-1.3 m/s, where the maximum values increased with increasing flow rates and channel slopes. The preferred path and resting areas diminished while increasing flow rates and channel slopes. For series C the maximum velocity magnitude (0.8 to 1.1 m/s) decreased and preferred path/resting areas increased with increasing boulder diameter. However, for series D and E the maximum velocity magnitude (0.8 to 1.3 m/s) increased and preferred path/resting areas decreased for increasing boulder longitudinal and transverse distances. Moreover, series F provided better preferred path for upstream migration and extended low velocity area for resting than other series, where the maximum velocity magnitude (0.8 to 1.1 m/s) increased and preferred path/resting areas decreased for increasing boulder longitudinal distances. Considering the maximum velocity magnitude and the extend of low velocity areas for fish

preferred path/resting during ascension, the simulations A1, A2, B1, B2, C3, C4, D1, F1, and F2 are identified as the most hydraulically suitable to fish passage and are recommended for further study.

6.4.3 Flow Resistance

The results from all simulations were used to analyse the influence of various flow rates, channel slopes, boulder diameters, boulder spacings (density), and boulder arrangements on overall flow resistance. The predicted flow resistance by the equation, $\sqrt{\frac{8}{f}} = \frac{u_{avg}}{\sqrt{gR_v S_0}}$, in terms of the f values against submergence ratios (H/D) is plotted in Figure 6.11, where f is the Darcy-Weisbach friction factor and R (hydraulic radius) is replaced by R_v. Two different trend lines between f and H/D were observed. For the series B, D, E, and F, f values increased with increasing H/D (*Figure 6.11a*) and for the series A and C f values increased with decreasing H/D (*Figure 6.11b*). In general, the flow resistance is maximum at $H/D=1.0$, it decreases rapidly for $H/D>1.0$ and decreases gradually for $H/D<1.0$ (Jordanova 2008). For A and C series simulations, f values decreased with increasing flow rates and boulder diameters, where H/D varied from 0.79 to 1.11. For B series simulations, f values decreased with increasing channel slopes, because higher flow resistance for mild slopes than for steeper ones (Jordanova 2008). The f values decreased with increasing boulder longitudinal and transverse spacing (decreasing boulder density) under D and E series simulations. Finally, for boulder arrangements pattern (II) in the series F, f values decreased with

increasing boulder longitudinal spacing (decreasing boulder density). Similarly, Jordanova (2008) concluded that the flow resistance increases with increasing density up to 30%, thereafter overall resistance decreases with increasing density.

Based on an elementary flow resistance analysis for wake-interference flow regime in a rock-ramp fishpass, a general equation for average velocity has been proposed in Chapter 4 as follows:

$$u_{avg} = \sqrt{\frac{2g}{C_D N A_p}} \sqrt{S_0} \sqrt{R_v} \qquad (6.6)$$

where, A_p is the projected cross-sectional area of each individual boulder, C_D is the drag coefficient, and N is the number of boulders, for more details see in Chapter 4. The performance of this equation was evaluated in Chapter 4 and showed good agreement with other equations for steep mountain streams/rivers and flumes with large scale roughness. In this equation, the only unknown drag coefficient is a function of submergence ratio ($C_D = 1.787(H/D)^{-2.16}$). Figure 6.12 shows the variation of drag coefficient (C_D) with submergence ratio (H/D) for all simulations. It is apparent that the values of C_D for different flow rates, channel slopes, boulder diameters, boulder spacings, and boulder arrangements in this study (H/D varied from 1.11 to 0.73)) are within the range of experimental power equation with some degree of scatter. Here the C_D values have different trend which is expected because obstacle in a cluster with different spacings and arrangements could differ from that for a particular arrangement. More simulations are needed especially for 0.73>H/D>1.11, in order to obtain family of

curves showing the relationship between drag coefficient and submergence ratio for different boulder spacings and arrangement. Generally, C_D decreases with increasing *H/D*. It is also important to note that in Chapter 4 the values of C_D were compared with that for the emergent and submerged cylindrical stems, for arrays of emergent circular cylinders, and for the single smooth sphere (Flammers et al. 1970; Stone and Shen 2002; Cheng 2012; Potter and Wiggert 2010).

6.5 Summary and Conclusions

The numerical study analyzed the effects of different flow rates, channel slopes, boulder diameters, boulder spacings, and boulder arrangements on water level, flow velocity, and flow resistance in a rock-ramp type nature-like fishpass. Numerical results were validated with experimental data which showed satisfactory agreement, also confirmed the CFD capability in prediction of flow field in a rock-ramp fishpass.

The simulated normalized water surface profiles for A, B, and C series simulations followed the experimental mean tend line with some degree of scatter. Subsequently, the profiles for D, E, and F series simulations declined that trend line due to the variation of boulder to boulders spacing. The simulated average water depths ensured that the experimentally proposed depth-discharge relationship ($H/D = 0.345Q^*$) is valid for s_l=2.0-3.8D and s_t=2.7-3.5D in

boulder arrangement pattern (I) and for s_l=3.0-5.0D in pattern (II) having 75% confidence limit.

The simulated time-averaged maximum velocity for all simulations provided an excellent fit with the experimentally proposed velocity-discharge linear relationship ($U_{\max}* = 1.504Q*$). In contrast, the proposed relationship, $u_{avg}* = 1.047Q*$, is valid for s$_l$=2.0-3.8D and s_t=2.7-4.5D in boulder arrangement pattern (I) and for s_l=3.0-5.0D in pattern (II) having 75% confidence limit. Considering the maximum velocity magnitude, the extent of areas having low velocity, and the validity with experimental relationships (for water depth and velocity), several simulations (A1, A2, B1, B2, C3, C4, F1, and F2) could be identified as the most hydraulically suitable to fish passage and are recommended for further study.

The overall flow resistance analysis, in terms of Darcy-Weisbach f and submergence ratios (H/D), confirmed two different trend lines. For the series B, D, E, and F, f values increased with increasing H/D and for the series A and C this relation is reversed. The results also confirmed that f values decreased with increasing flow rates, boulder diameters, channel slopes, and boulder longitudinal and transverse spacing (decreasing boulder density).The simulated results also evidenced that the drag coefficient followed the experimental power equation ($C_D = 1.787(H/D)^{-2.16}$) with some degree of scatter.

These investigations demonstrate that CFD model could play an important role in advancing our knowledge about nature-like fishpasses hydrodynamics.

6.6 References

Biron, P. M., Robson, C., Lapointe, M. F., Gaskin, S. J. (2005). "Three dimensional flow dynamics around deflectors." *River Research and Applications*, 21, 961-975.

Bovee, K. D., Lamb, B. L., Bartholow, J. M., Stalnaker, C. B., Taylor, J., Henriksen, J. (1998). "*Stream habitat analysis using the instream flow incremental methodology*." US Geological Survey, Biological Resources Division Information and Technology Report USGS/BRD, 1998-0004.

Brackbill, J. U., Kothe, D. B., Zemach, C. (1992). "A continuum method for modeling surface tension." *Journal of Computational Physics*, 100, 335-354.

CFX (2009). ANSYS CFX Solver Theory Guide, Release 12.0. ANSYS Inc., PA 15317.

Cheng, N. S. (2012). "Calculation of drag coefficient for arrays of emergent circular cylinders with pseudofluid model." *Journal of Hydraulic Engineering*, 139(1), 602-611.

Crowder, D. W., Diplas, P. (2000). "Using two-dimensional hydrodynamic models at scales of ecological importance." *Journal of Hydrology*, 230, 172–191.

DVWK (2002). "*Fish passes-Design, dimensions and monitoring."* Published by the Food and Agriculture Organization of the United Nations in arrangement with German Association for Water Resources and Land Improvement as DVWK-Merkblatt.

Eberstaller, J., Hinterhofer, M., Parasiewicz, P. (1998). "The effectiveness of two nature-like bypass channels in an upland Austrian river." In: Jungwirth, M., S. Schmutz, and S. Weiss, editors. *Fish Migration and Fish Bypasses*. Fishing News Books, Oxford.

Fernandes, J., Lisboa, P. F., Simoes, P. C., Mota, J. P. B., Saatdjian, E. (2009). "Application of CFD in the study of supercritical fluid extraction with structured packing: wet pressure drop calculations." *Journal of Supercritical Fluids*, 50(1), 61–68.

Ferro, V. (2003). "Flow resistance in gravel-bed channels with large-scale roughness." *Earth Surface Processes and Landforms,* 28, 1325-1339.

Flammer, G. H., Tullis, J. P., and Mason, E. S. (1970). "Free surface velocity gradient flow past hemisphere." *Journal of the Hydraulic Division*, 96(7), 1485-1502.

Franklin, P.A., and Bartels, B. (2012). "Restoring connectivity for migratory native fish in a New Zealand stream: effectiveness of retrofitting a pipe culvert." *Aquatic Conservation: Marine and Freshwater Ecosyst*ems, 22, 489–497.

Franklin, A. E., Haro, A., Castro-Santos, T., Noreika, J. (2012). "Evaluation of nature-like and technical fishways for the passage of Alewives at two coastal streams in New England." *Transactions of the American Fisheries Society*, 141, 624-637.

Guay, J. C., Boisclair, D., Rioux, D., Leclerc, M., Lapointe, M., Legendre, P. (2000). "Development and validation of numerical habitat models for

juveniles of Atlantic Salmon." *Canadian Journal of Fisheries and Aquatic Sciences*, 57, 2065–2075.

Haro, A., Franklin, A., Castro-Santos, T., and Noreika, J. (2008). "Design and evaluation of nature-like fishways for pasage of Northeastern Diadromous fishes." Final report, Submitted to NOAA National Marine Fisheries Service Office of Habitat Conservation.

Haltigin, T. W., Biron, P. M., Lapointe, M. F. (2007). "Three-dimensional numerical simulation of flow around stream deflectors: The effect of obstruction angle and length." *Journal Hydraulic Research*, 45(2), 227-238.

Hirt, C. W., Nichols, B. D. (1981). "Volume of fluid (VOF) method of the dynamics of free boundaries." *Journal of Computational Physics*, 39, 201–225.

Hotchkiss, R. H., Frei, C. M. (2007). "*Design for fish passage at roadway-stream crossings: synthesis report."* FHWA-HIF-07-033. Mclean, VA.

Jordanova, A. A. (2008). "*Low flow hydraulics in rivers for environmental applications in South Africa*." Ph. D. Thesis, Faculty of the Engineering and the Built Environment, University of the Witwatersrand, Johannesburg, South Africa.

Katopodis, C. (1995). "Riverine fish habitat: mitigation and restoration approaches." International conference on ecological system enhancement technology for aquatic environments, Tokyo, Oct. 29 - Nov. 3, 356-360.

Katopodis, C., Williams, J. G. (2011). "The development of fish passage research in a historical context." *Ecological Engineering*, 48, 8-18.

Parasiewicz, P., Eberstaller, J., Weiss, S., Schmutz, S. (1998). "Conceptual guidelines for nature-like bypass channels." In: M. Jungwirth, S. Schmutz, and S. Weiss, (eds), *Fish Migration and Fish Bypasses*, Oxford: Fishing News Books, Blackwell Science Ltd, 348-362.

Khan, L. A. (2006). "A three-dimensional computational fluid dynamics (CFD) model analysis of free surface hydrodynamics and fish passage energetics in a vertical-slot fishway." *North American Journal of Fisheries Management*, 26, 255–267.

Khan, L. A., Wicklein, E. A., Rashid, M., Ebner, L. L., Richards, N. A. (2004). "Computational fluid dynamics modeling of turbine intake hydraulics at a hydropower plant." *Journal of Hydraulic Research*, 42, 61–69.

Lai, Y. G., Weber, L. J., Patel, V. C. (2003). "Nonhydrostatic three-dimensional model for hydraulic flow simulation, I. formulation and verification." *Journal of Hydraulic Engineering*, 129, 196–205.

Ma, L., Ashorth, P. I., Best, J. L., Elliott, L., Ingham, D. B., and Whitcombe, L. J. (2002). "Computational fluid dynamics and the physical modelling of an upland urban river." *Geomorphology,* 44, 375-391.

Morris, Jr. H. M. (1954). "Flow in rough conduits." *Transactions of the American Society of Civil Engineers*, 119, 373–410.

Munson, B. R., Young, D. F., Okiishi, T. H. (1990). "*Fundamentals of fluid mechanics*." 2nd edition, John Wiley and Sons Inc., New York.

Naghavi, B., Esmaili, K., Yazdi, J., Vahid, F. K. (2011). "An experimental and numerical study on hydraulic characteristics and theoretical equations of circular weirs." *Canadian Journal of Civil Engineering*, 38, 1327-1334.

Papanicolaou, A. N., Kramer, C. M., Tsakiris, A. G., Stoesser, T., Bomminayuni, S., and Chen, Z. (2012). "Effects of a fully submerged boulder within a boulder array on the mean and turbulent flow fields: Implications to bedload transport." *Acta Geophysca*, 60(6), 1502-1546.

Potter, M. C., and Wiggert, D. C. (2010). "*Mechanics of Fluid."* Third Edition, SI, Cengage Learning, USA.

Rajaratnam, N., Muralidhar, D. (1968). "Yaw probe used as Preston tube." *The Aeronautical Journal of the Royal Aeronautical Society*, 72, 1059-1060.

Salaheldin, T. M., Imran, J. I., Chaudhry, M. H. (2003). "Numerical modeling of three-dimensional flow field around circular piers." *Journal of Hydraulic Engineering*, 130 (2), 91-100.

Shamloo, H., Rajaratnam, N., Katopodis, C. (2001). "Hydraulics of simple habitat structures." *Journal of Hydraulic Research*, 39, 351-366.

Shen, Y., Diplas, P. (2008). "Application of two- and three-dimensional computational fluid dynamics models to complex ecological stream flows." *Journal of Hydrology*, 348, 195-214.

Smart, G. M., Duncan, M. J., Walsh, J. M. (2002). "Relatively rough flow resistance equations." *Journal of Hydraulic Engineering*, 128(6), 568-578.

Stone, B. M., and Shen, H. T. (2002). "Hydraulic resistance of flow in channels with cylindrical roughness." *Journal of Hydraulic Engineering*, 128 (5), 500-506.

Steffler, P., Ghanem, A., Blackburn, J. (2002). "*River2D Version 0.90*." University of Alberta, Fisheries and Oceans, Canada, and United States Geological Survey.

USBR (2007). "*Rock-ramp Design Guidelines."* U.S. Department of the Interior Bureau of Reclamation Technical Service Center Denver, Colorado, USA.

Wang, R.W., Hartlieb, A. (2011). "Experimental and field approach to the hydraulics of nature-like pool-type fish migration facilities." *Knowledge and Management of Aquatic Ecosystems*, 400, 05.

Table 6-1 Descriptions of all simulations.

Simulation	Varying Parameter	Flow (L/s)	Slope (%)	Boulder diameter (cm)	Longitudinal Spacing s_l	Transverse Spacing s_t	Area concentration by boulders (%)	Boulder Arrangement Pattern
A1	Flow	45	5	14	2.7D	2.7D	12	I
*A2		60	5	14			12	I
A3		75	5	14			12	I
A4		100	5	14			12	I
A5		125	5	14			12	I
B1	Channel Slope	60	2	14	2.7D	2.7D	12	I
*B2		60	3	14			12	I
B3		60	4	14			12	I
B4		60	6	14			12	I
C1	Boulder Diameter	60	5	10	2.7D	2.7D	6	I
C2		60	5	12			9	I
C3		60	5	16			15	I
C4		60	5	18			20	I
D1	Boulder Longitudinal Spacing	60	5	14	1.6D	2.7D	20	I
D2		60	5	14	2.0D		16	I
D3		60	5	14	3.4D		10	I
D4		60	5	14	3.8D		8	I
E1	Boulder Transverse Spacing	60	5	14	2.7D	3.0D	11	I
E2		60	5	14		3.5D	8	I
E3		60	5	14		4.0D	6	I
E4		60	5	14		4.5D	6	I
F1	Boulder Longitudinal Spacing	60	5	14	3.0D	2.7D	13	II
F2		60	5	14	3.5D		12	II
F3		60	5	14	4.0D		11	II
F4		60	5	14	4.5D		10	II
F5		60	5	14	5.0D		9	II

* validated by the experimental data

Table 6-2 Details of three mesh sizes used for computations.

Mesh	1	2	3
Size (cm)	1.75	1.5	1.35
Nodes	199,341	307,053	410,598
Elements	1,061,574	1,662,760	2,254,500

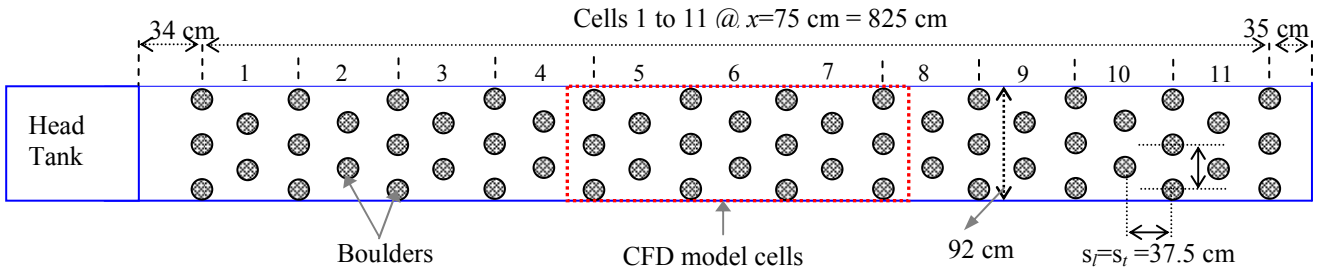

Figure 6.1 Experimental setup of rock-ramp nature-like fishpass (adapted from Chapter 4).

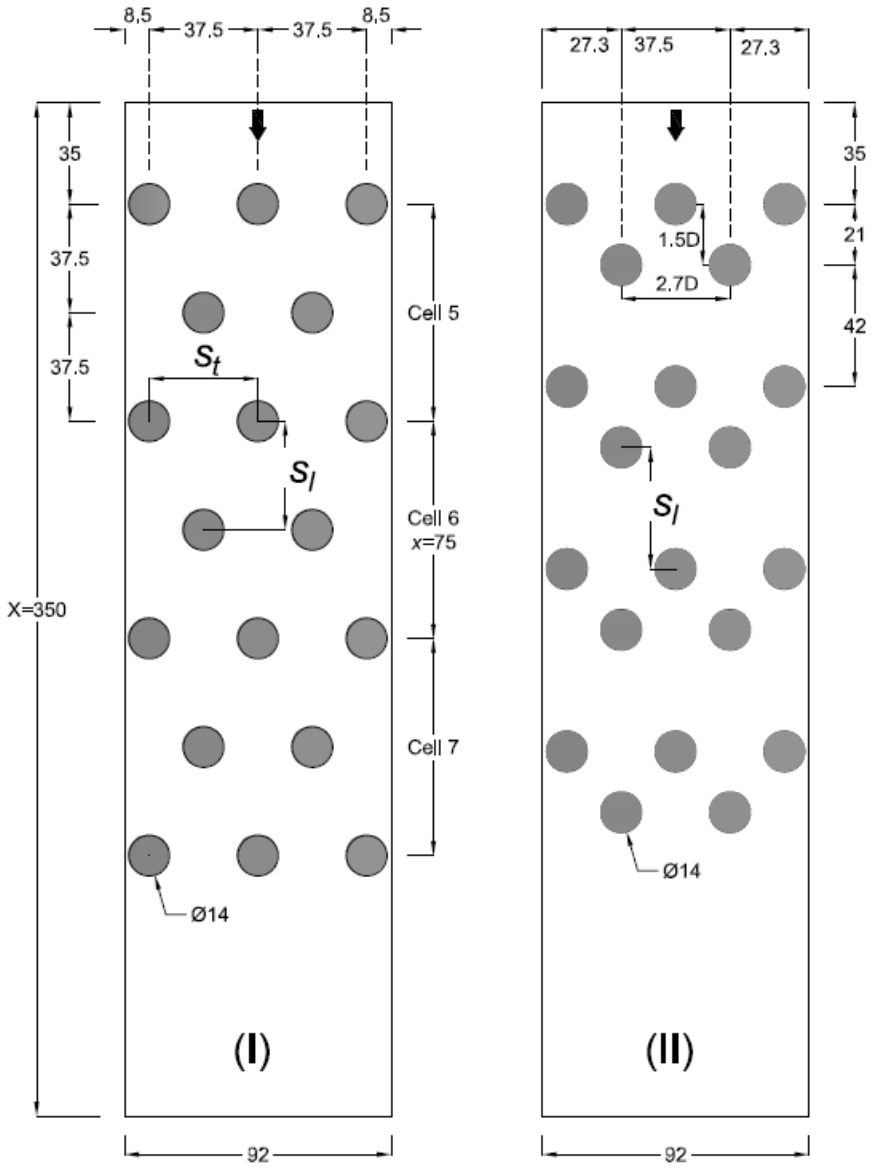

Figure 6.2 Boulder arrangement pattern (I) and (II) for CFD modelling (all scales are in cm).

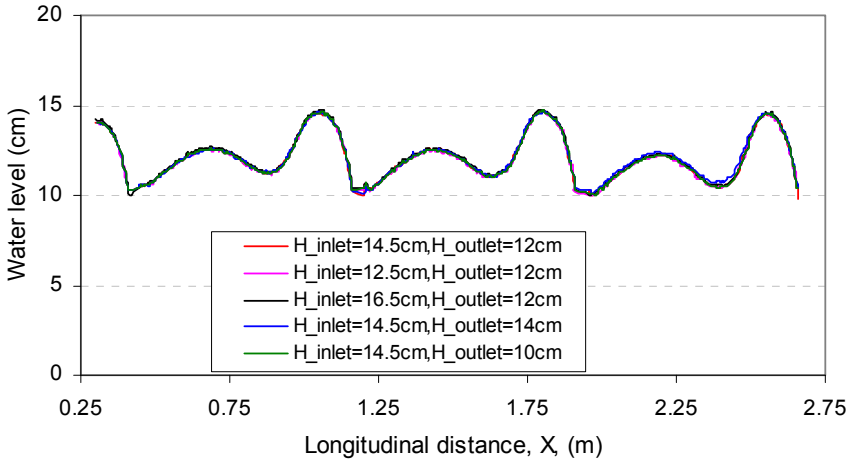

Figure 6.3 Comparison of the simulated water surface profiles over three cells along the centerline of the flume due to different initial boundary (inlet and outlet) conditions.

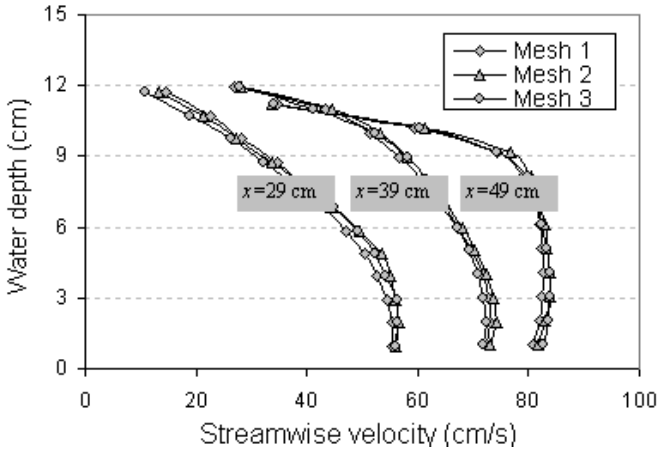

Figure 6.4 Comparison of the simulated streamwise velocity profiles for three different mesh sizes at various locations along the centerline at cell 6.

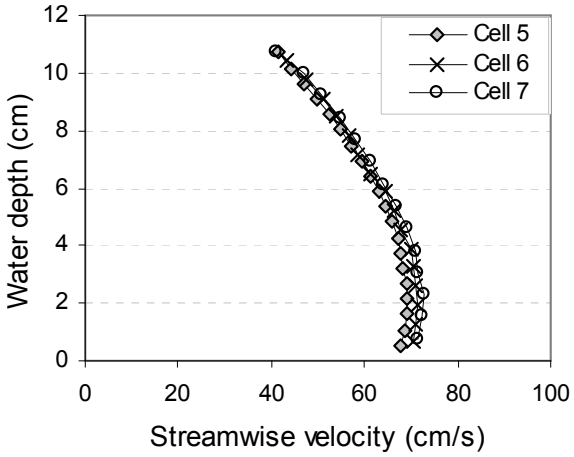

Figure 6.5 Comparison of the simulated streamwise velocity profiles at mid-point of cells 5, 6, and 7 along the centerline of the flume.

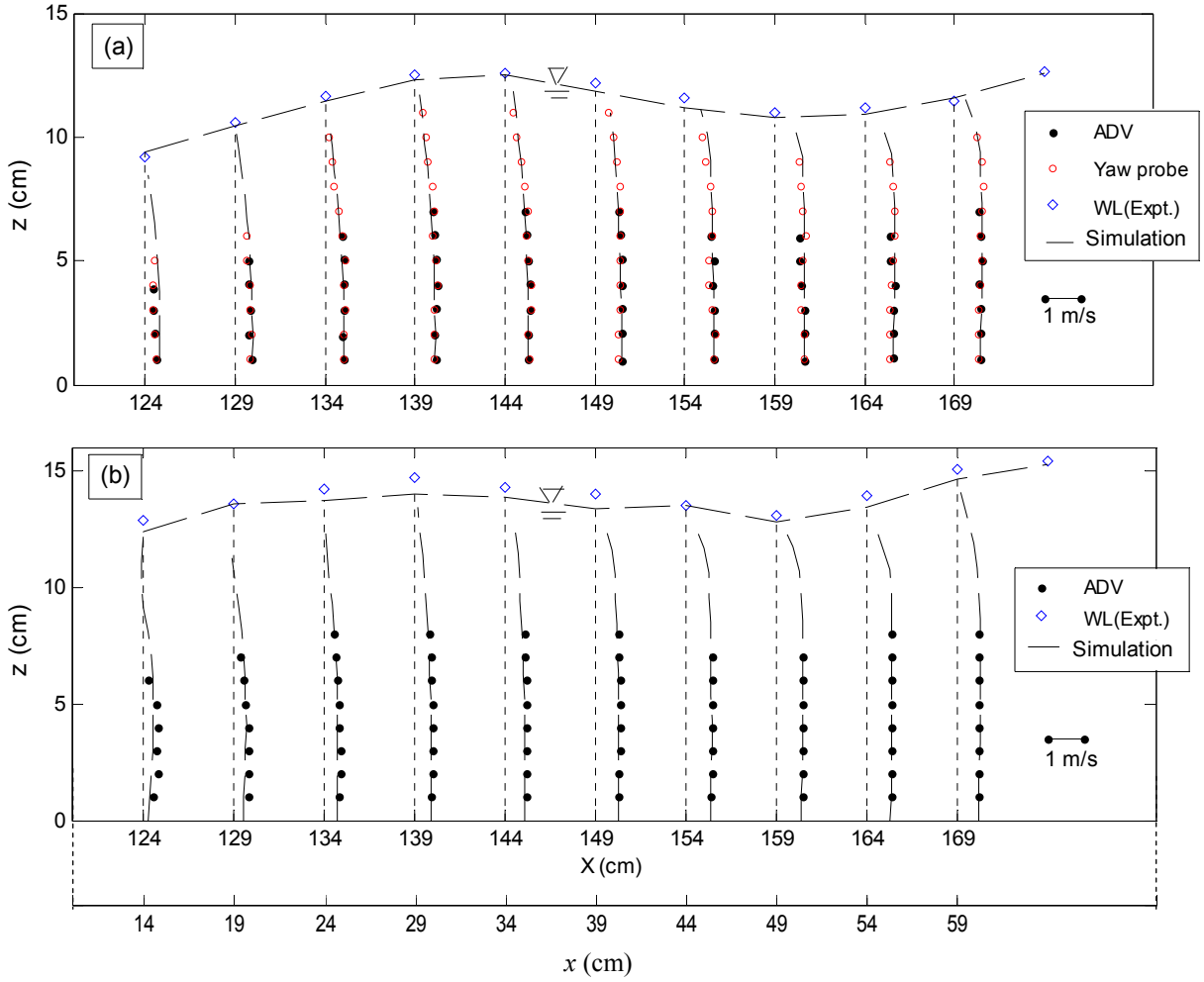

Figure 6.6 Comparison of streamwise velocity profiles between numerical simulation and experimental measurements along the central vertical plane at cell 6 for the simulations of (a) A2 and (b) B2.

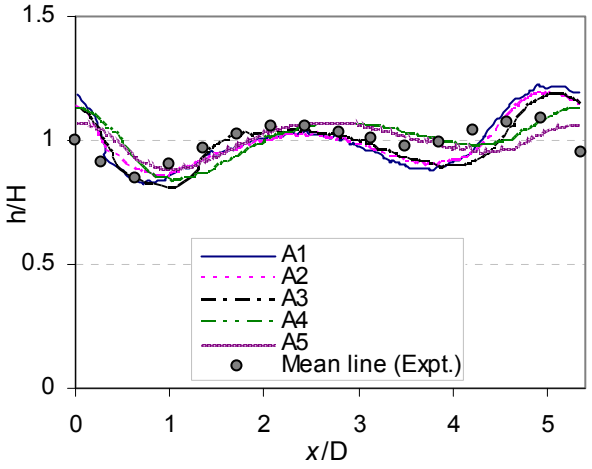
1.5
1
0.5
0
h/H
0
1
2
3
4
5
x/D
A1
A2
A3
A4
A5
Mean line (Expt.)

(a)

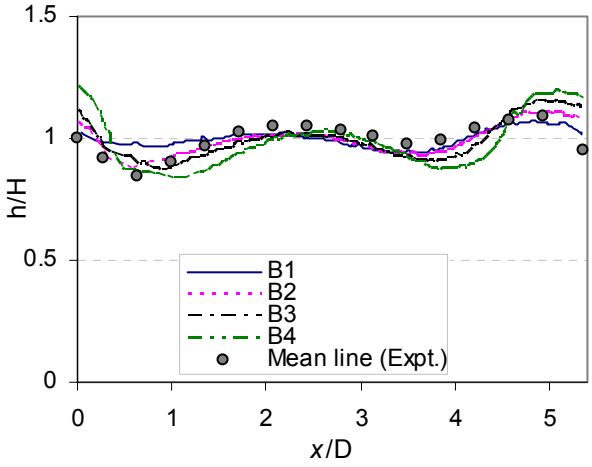
1.5
1
0.5
0
h/H
0
1
2
3
4
5
x/D
B1
B2
B3
B4
Mean line (Expt.)

(b)

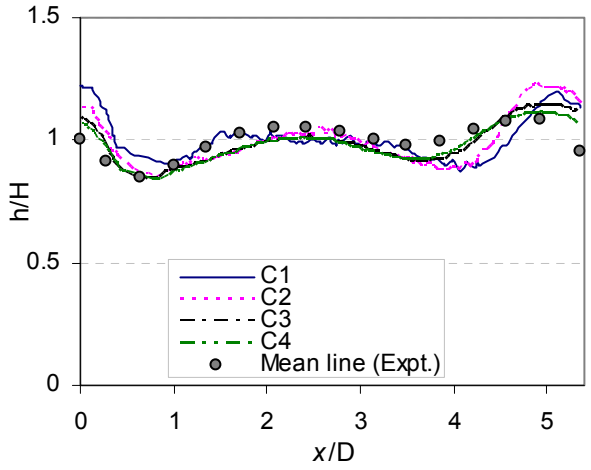
1.5
1
0.5
0
h/H
0
1
2
3
4
5
x/D
C1
C2
C3
C4
Mean line (Expt.)

(c)

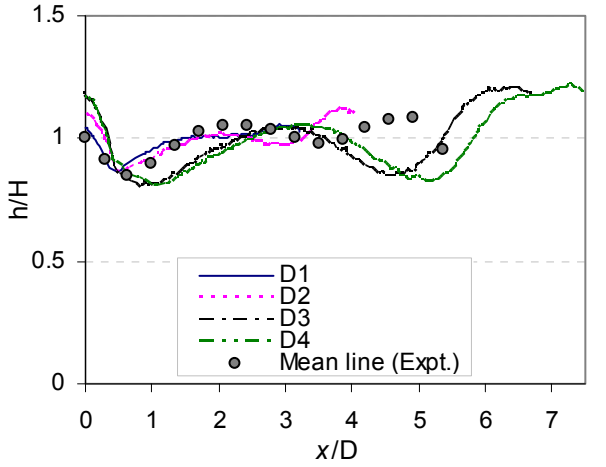

(d)

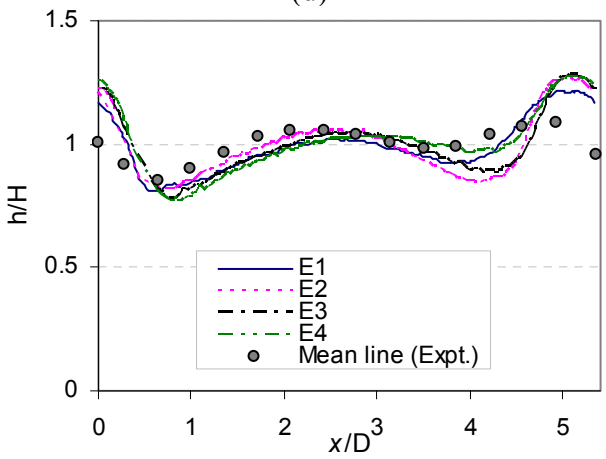

(e)

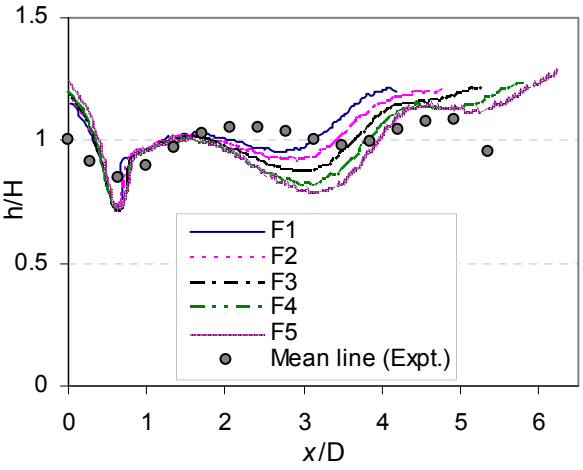

(f)

Figure 6.7 The normalized water surface profiles along the centre line of the flume at cell 6 for the simulations of series (a) A, (b) B, (c) C, (d) D, (e) E, and (f) F (here Mean line (Expt.) is the experimental mean tend line from Chapter 4).

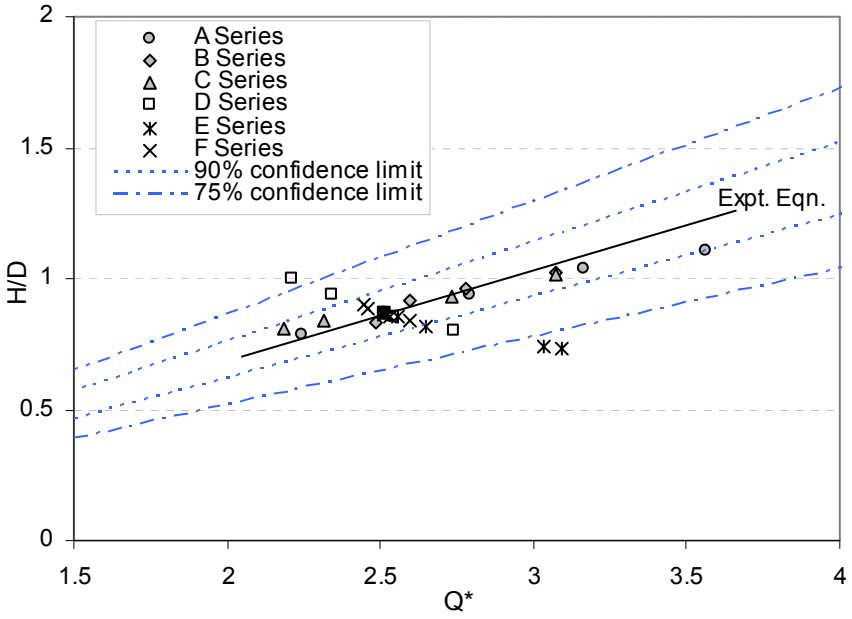

Figure 6.8 The normalized depth-discharge relationship for all simulations (here Expt. Eqn. corresponding to the linear equation ($H/D = 0.345Q*$) in Chapter 4).

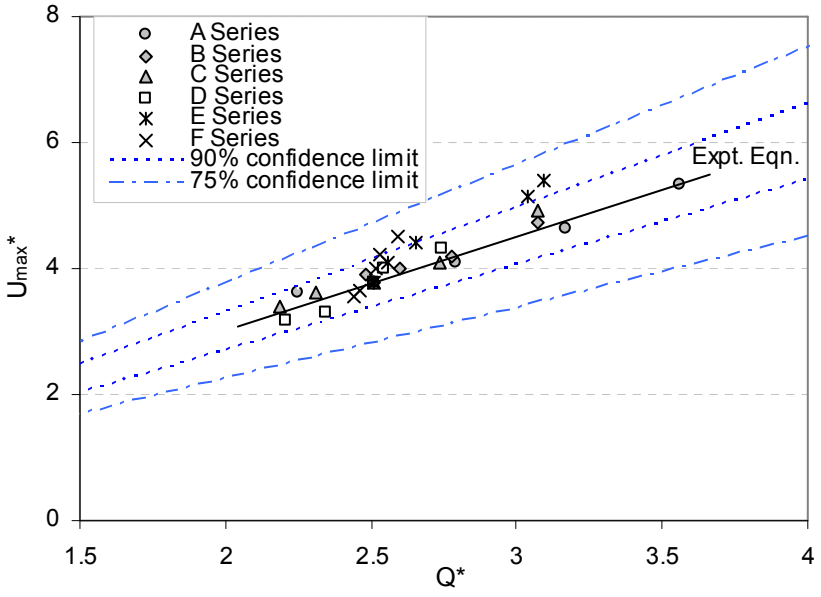

(a)

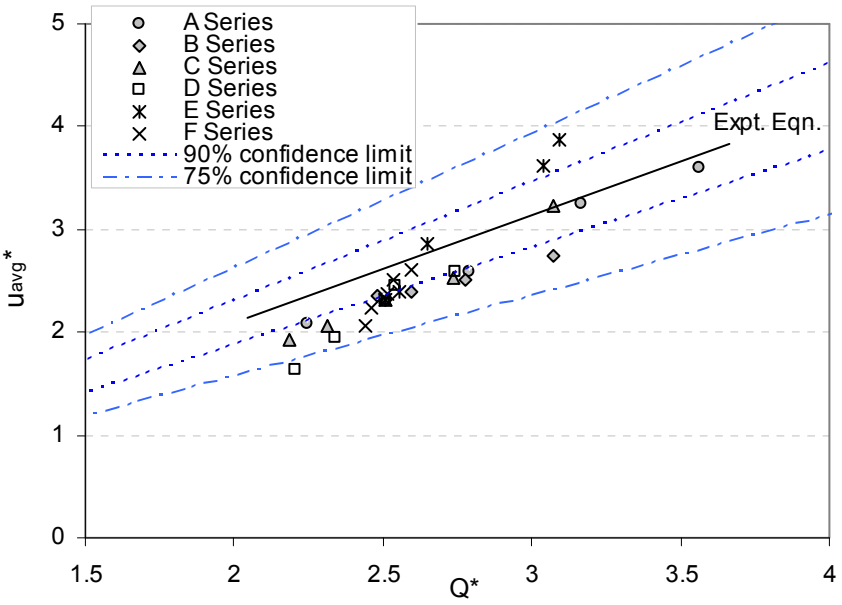

(b)

Figure 6.9 The normalized velocity-discharge relationships for (a) time-averaged maximum velocity and (b) average streamwise velocity for all simulations (here Expt. Eqn. corresponding to the liner equation ($U_{\max}* = 1.504Q*$) in (a) and $u_{avg}* = 1.047Q*$ in (b) in Chapter 4).

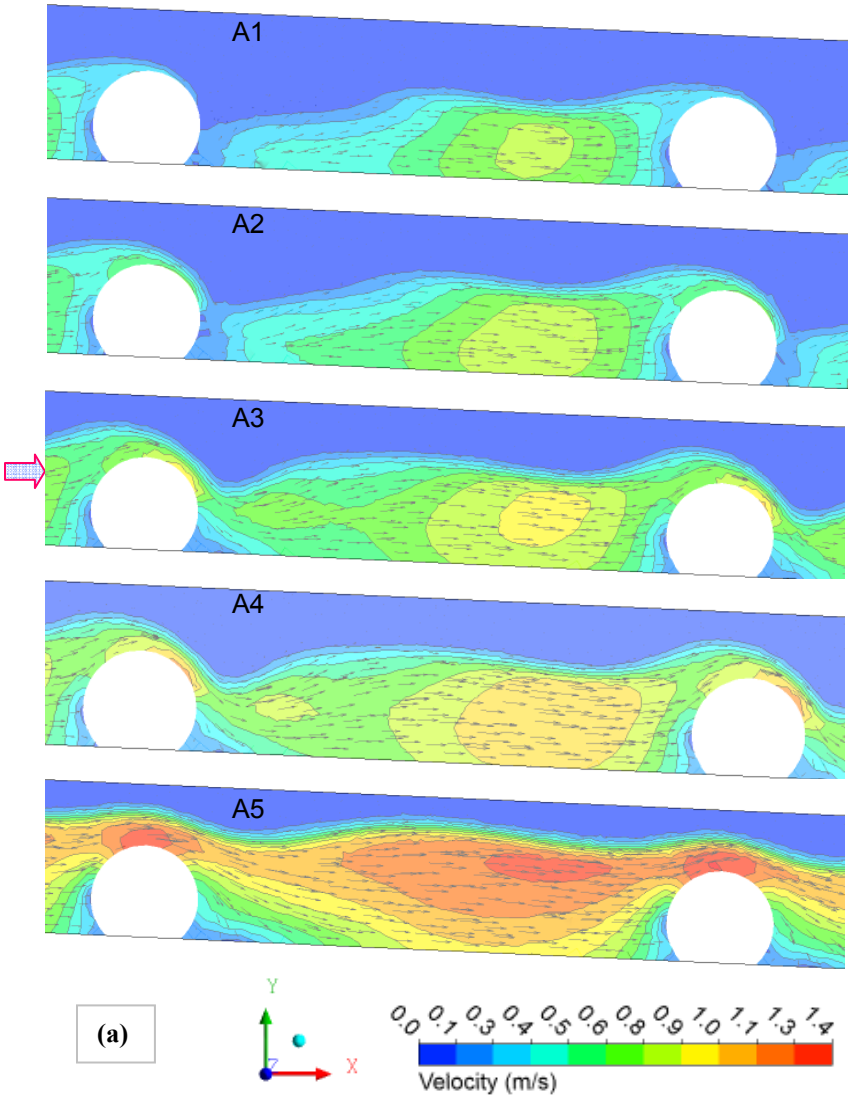
A1
A2
A3
A4
A5
(a)
Y
X
0.0 0.1 0.3 0.4 0.5 0.6 0.8 0.9 1.0 1.1 1.3 1.4
Velocity (m/s)

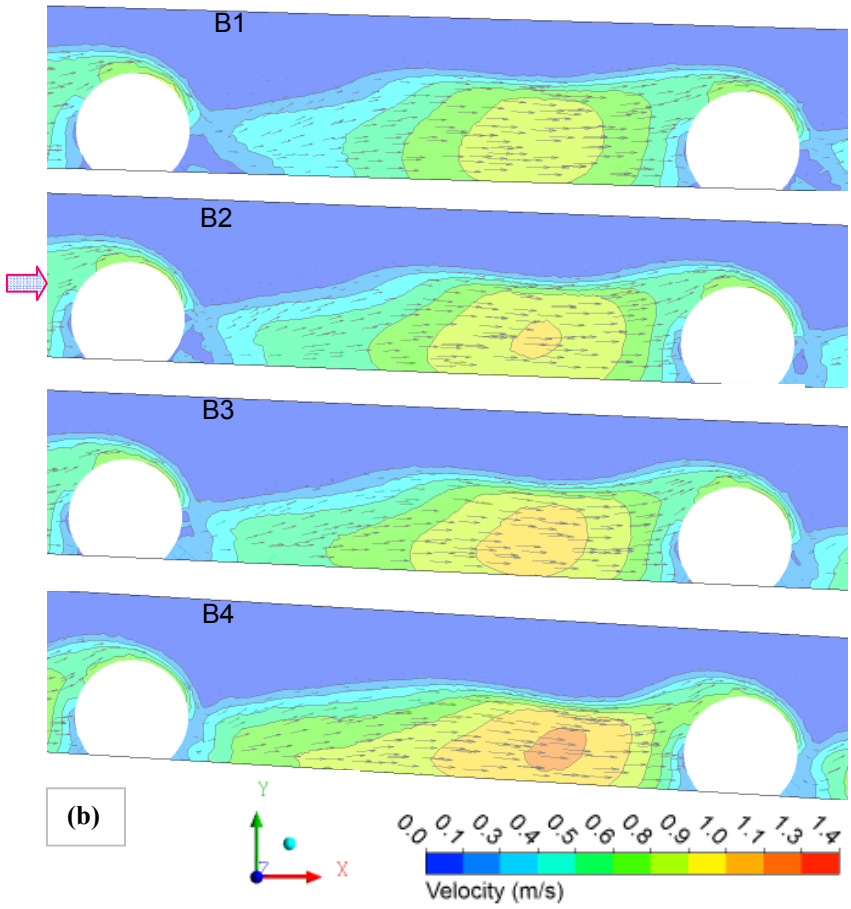
B1
B2
B3
B4
(b)
Y
X
Z
0.0 0.1 0.3 0.4 0.5 0.6 0.8 0.9 1.0 1.1 1.3 1.4
Velocity (m/s)

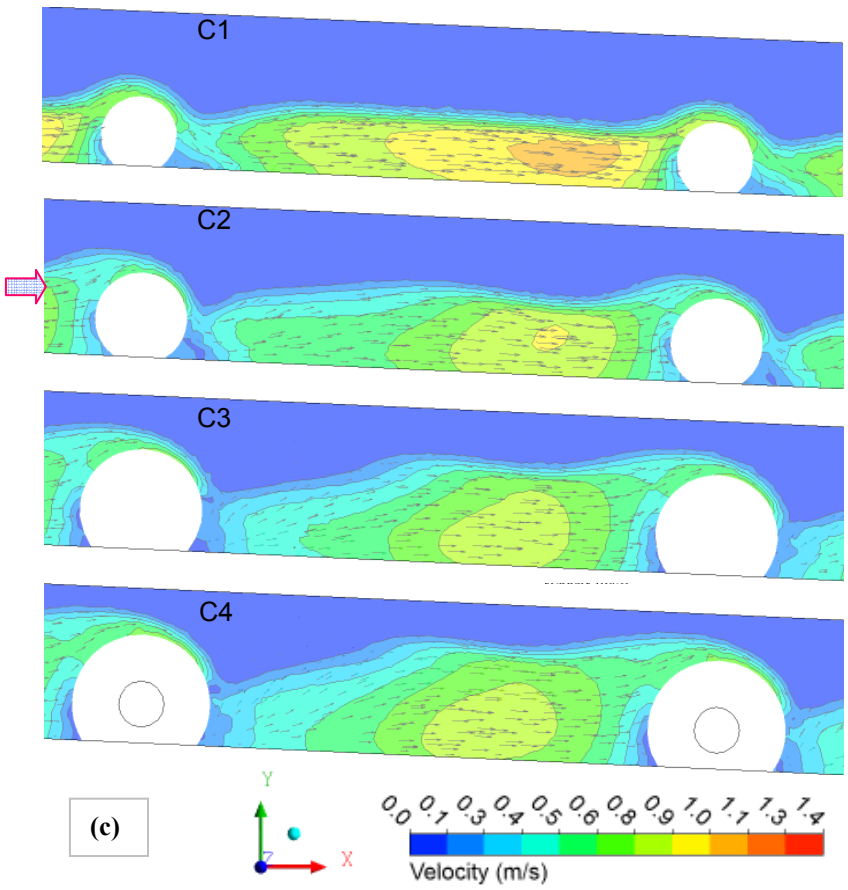
C1
C2
C3
C4
(c)
Y
X
Z
0.0 0.1 0.3 0.4 0.5 0.6 0.8 0.9 1.0 1.1 1.3 1.4
Velocity (m/s)

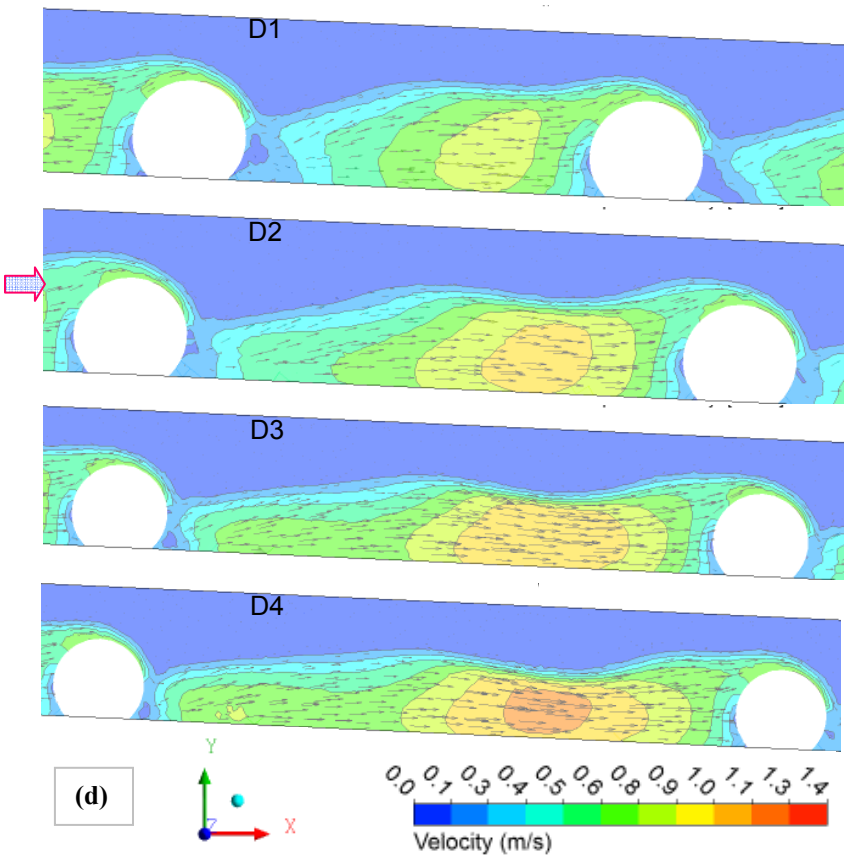
D1
D2
D3
D4
(d)
Y
X
0.0 0.1 0.3 0.4 0.5 0.6 0.8 0.9 1.0 1.1 1.3 1.4
Velocity (m/s)

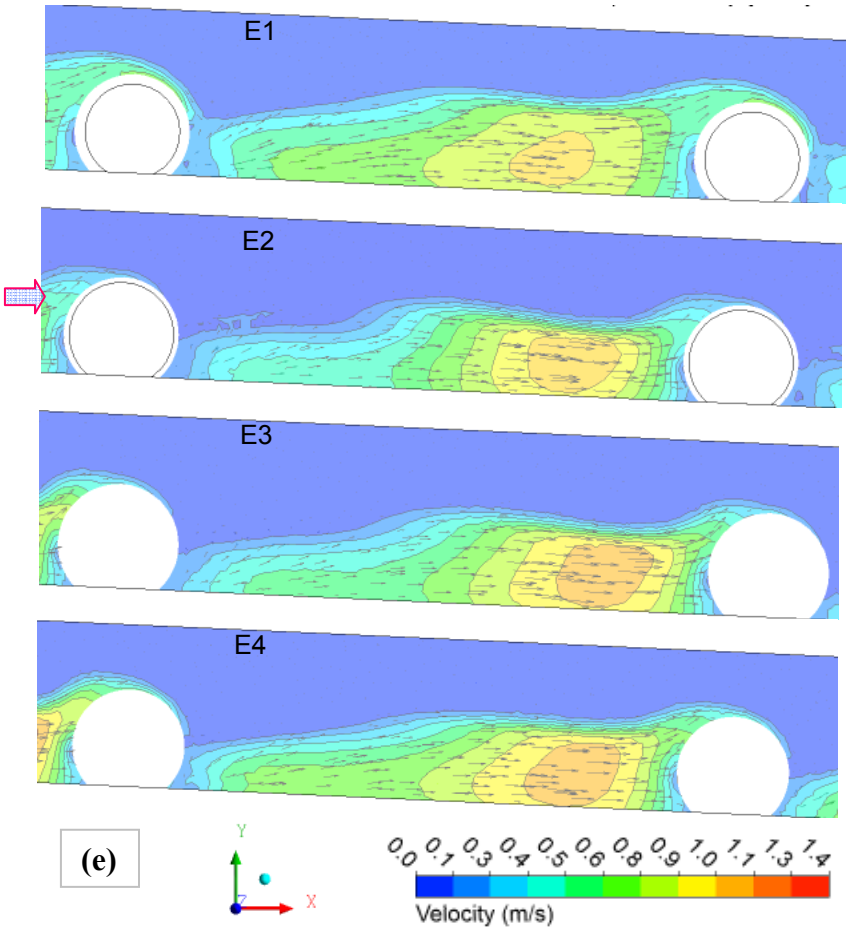
E1
E2
E3
E4
(e)
Y
X
0.0 0.1 0.3 0.4 0.5 0.6 0.8 0.9 1.0 1.1 1.3 1.4
Velocity (m/s)

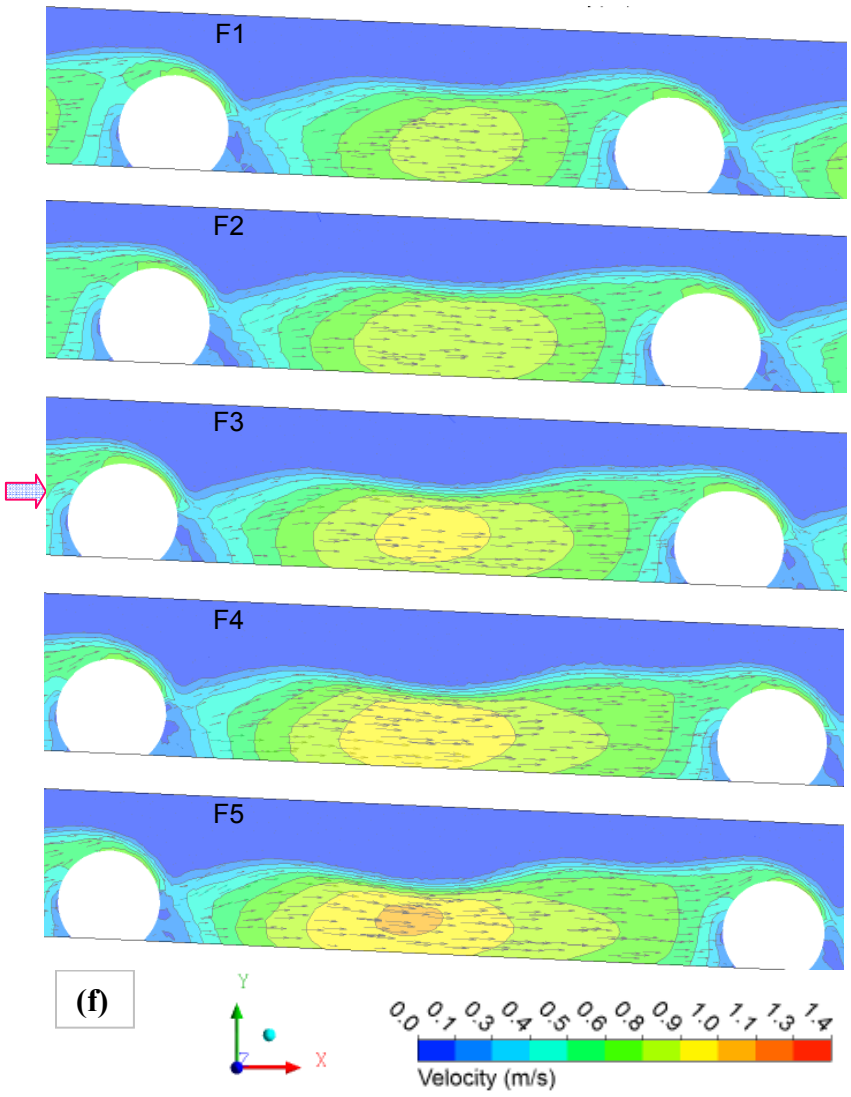

Figure 6.10 Spatial distributions of time-averaged velocity magnitude with directions on central vertical plane at cell 6 for all simulations: (a) A series, (b) B series, (c) C series, (d) D series, (e) E series, and (f) F series.

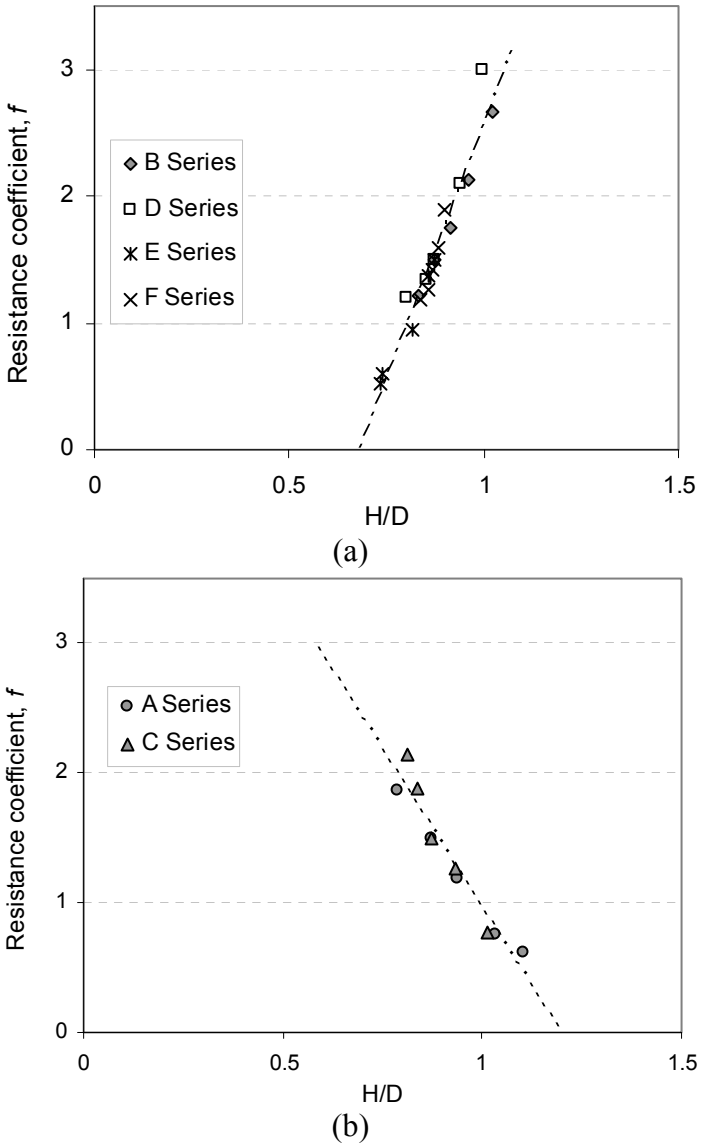

Figure 6.11 The variation of flow resistance in the form of Darcy-Weisbach *f* with submergence ratio (*H/D*) for the simulations of series (a) B, D, E, and F and (b) of series A and C.

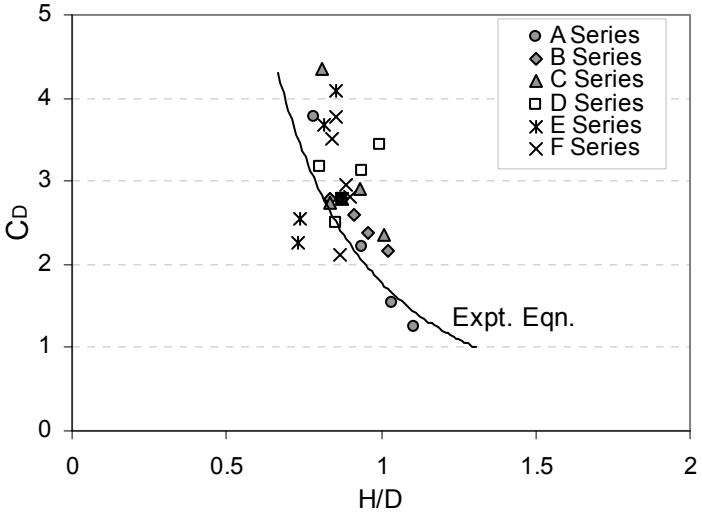

Figure 6.12 The variation of drag coefficient (C_D) with submergence ratio (H/D) for all simulations (here Expt. Eqn. corresponding to the power equation ($C_D = 1.787(H/D)^{-2.16}$) in Chapter 4).

CHAPTER 7

Conclusions and Recommendations

7.1 General Conclusions

This paper based thesis is primarily concerned with investigating the flow characteristics in the small northern streams and nature-like fishpasses. The general conclusions are summarized as follows:

- Chapter 2 investigated the hydrological characteristics and fish suitability of an Arctic stream within an integrated framework of lake-stream connectivity. The results indicated that the lake can be recharged by runoff from the catchment, but summer evaporation, combined with groundwater loss, caused draw down of lake level below the outflow threshold. Summer rainfall in this semi-arid environment was insufficient to overcome storage deficits to re-establish flow connectivity between lakes. Some sections of the study stream for certain durations of the study period (entire June) appeared to naturally provide suitable habitat for select stages of YOY Arctic grayling, while other sections could provide suitable habitat after certain modifications (creating a defined channel with consistent slope and fishpass structures) and additional outlet flow arrangements or by controlling the stream outlet (discharges

are minimized while flow depth and storage retention is maximized) are achieved through the fish habitat compensation project.

- Chapter 3 investigated the at-a-station hydraulic geometry and resistance to flow for head-water streams in the Northwest Territories of Canada. Power functions described at-a-station hydraulic geometry relationships very well, where the velocity exponent (*l*) exceeded the width exponent (*b*) and mean depth exponent (*t*) at all sections and is greater than the sum of *b* and *t* in 7 out of 9 study cross sections demonstrating the dominant role of velocity in accommodating changing discharge in headwater streams. The mean values of width, depth, and velocity exponents (0.14, 0.17, and 0.65, respectively) in our sites are lower, much lower, and higher than those typically reported in the literature (which varied from 0.20 to 0.49, 0.20 to 0.41, and 0.13 to 0.55) for the braided rivers, mountain, and steep-pool streams, respectively. Darcy–Weisbach resistance factor (f) and Manning's n individually vary over three orders of magnitude, (1.0–267) and (0·085–1.37), respectively. Despite large ranges, hydraulic relations are described effectively through power equations and Keulegan function curves fitted for each section.

- Chapter 4 investigated the mean flow characteristics generated by a staggered arrangement of boulders in a rock-ramp type nature-like

fishpass. The results showed that this type of fishpass can produce adequate water depth (varied from 44 to 88 cm for a 1:4 undistorted scale model) and favorable flow velocity (varied from 1.3 to 2.2 m/s for a 1:4 scale model) suitable for fish passage. Three different characteristic velocity regions were identified: downstream of boulders (wake region), intermediate region, and upstream of boulders. Some general correlations were developed for predicting the flow depth and velocity in a rock-ramp fishpass as a function of normalized discharge and streamwise distance. The relationships for average water depth ($H/D = 0.345Q^*$) and maximum velocity magnitude ($U_{\max}{}^* = U_{\max}/\sqrt{gS_0R_v}$) were tested for smaller boulder size (scaling down) and field-scale data sets, respectively, that ensured the applicability of those relationships. Moreover, a flow resistance analysis based on basic concepts for wake-interference flow regime in this fishpass has resulted in a general equation for the average velocity. In this equation, the drag coefficient is a function of submergence ratio and this equation shows good agreement with other equations for steep mountain streams/rivers and flumes for large scale roughness.

- Chapter 5 investigated the turbulence flow characteristics in a rock-ramp type nature-like fishpass with a relationship to fish passage. The study showed some major discrepancies between cluster of boulders (wake interference flow) and single boulder (isolated roughness flow) through

the decay rate of turbulence and the range of turbulence magnitude. The lower discrepancy of the highest and lowest values of turbulence (about 2 times for k and 10 times for $-\overline{u'w'}$) in this study ensured that the dispersion of turbulence over the study area was higher than the previous study around different isolated bluff bodies/instream pebble cluster (about 4-5 times for k and 15 times for $-\overline{u'w'}$). General correlation was obtained for predicting the turbulent intensity and turbulent kinetic energy in a rock-ramp fishpass as a function of normalized streamwise distance. The negative values of skewness *(S_u)* over the entire depth are in disagreement with the data for the gravel bed river, steeper rivers, lowland rivers, and flumes, where S_u is positive near the bed/water surface ($0<S_u<1.0$) and negative in the intermediate region ($-1.0<S_u<0$). Consequently, kurtosis (K_u) varies within a narrow band 1.0 to 0 in all experiments rather than ±1.0. The estimated maximum energy dissipation rates, by fitting a power law equation proportional to $w_w^{-5/3}$ to the wave number spectrum of the streamwise velocity in the inertial subrange, varied from 0.042 to 0.087 (11 to 22) m^2/s^3 (W/m^3 for a 1:4 undistorted scale model) for all experiments, which is less than the recommended values of 200 W/m^3 for salmonids, and 150 W/m^3 for cyprinids. The normalized energy dissipation rates were maximum in the near wake recirculation region and these rates gradually decelerated in the downstream direction. By using Kolmogorov theory of local isotropic

turbulence as a first approximation, it was found that the average dissipative eddy size varied from 0.07 to 0.11 mm.

- Chapter 6 investigated the fishpass hydrodynamics by developing a three-dimensional Computational Fluid Dynamics (CFD) model with a free surface flow for different flow rates, channel slopes, boulder diameters, boulder spacings, and boulder arrangements in a rock-ramp type nature-like fishpass. Numerical results were validated with experimental data which showed satisfactory agreement, also confirmed the CFD capability in prediction of flow field in a rock-ramp fishpass. The simulated time-averaged maximum velocity magnitude for all simulations provided an excellent fit with the experimentally proposed velocity-discharge linear relationship ($U_{\max}* = 1.504Q*$). Subsequently, the simulated average water depths and velocity ensured that the experimentally proposed depth-discharge relationship ($H/D = 0.345Q*$) and velocity-discharge relationship ($u_{avg}* = 1.047Q*$) are valid for s_l=2.0-3.8D and s_t=2.7-3.5D in a staggered arrangement of boulders and for s_l=3.0-5.0D in a modified staggered arrangement of boulders having 75% confidence limit, respectively. Herein, s_l and s_t are the centre to centre distance between two boulders in longitudinal and transverse directions, respectively. The flow resistance analysis, in terms of Darcy-Weisbach f and submergence ratios (H/D), confirmed that f values decreased with increasing flow

rates, boulder diameters, channel slopes, and boulder longitudinal and transverse spacing (decreasing boulder density).The simulated results also indicated that the drag coefficient followed the experimental power equation ($C_D = 1.787(H/D)^{-2.16}$) with some degree of scatter. Considering the maximum velocity magnitude, the extent of areas having low velocity, and the validity with experimental relationships (for water depth and velocity), several simulations (A1, A2, B1, B2, C3, C4, F1, and F2) could be identified as the most hydraulically suitable to fish passage and are recommended for further study.

7.2 Recommendations for Future Research

Research on stream eco-hydraulics and -hydrology in northern Canada is extremely scarce and challenging. The nature-like fishpasses have recently become a common type of fish migration facilities over conventional fishpasses. Fundamental research can increase our ability to predict and understand the eco-hydrological/hydraulic behaviors of Arctic head-water streams and enhance our current understanding of the unknown hydraulics of nature-like fishpasses. Immense opportunities are available to extend the ideas developed in these studies. Future research in this area can be classified in the following three categories:

Field Study:

- Long-term monitoring of lake-stream hydrology, hydraulics, and fish populations can increase our ability to predict and understand the eco-

hydrological and -hydraulics behaviors of head-water streams in the Northwest Territories, Canada.

- Using hydrological data from locally available meteorological stations, an accurate hydrological model can be proposed to estimate the stream flow from snowmelt for small Arctic watersheds.
- A River2D model can be developed for the study stream to identify the fish habitat suitability and stream flow requirements for habitat protection.
- A good correlation between the Arctic stream hydraulics and instream flow requirements for fish habitat can be developed in future.
- The current study streams and cross sections are limited in numbers to develop a definitive conclusion on eco-hydraulics, hydraulic geometry, and flow resistance for Arctic region, hence further study is required to validate the current results with additional streams and cross-sectional measurements.

Lab Study:

- Additional study can be undertaken to investigate the effect of boulder spacing and arrangement on detailed flow characteristics in a rock-ramp type fishpass.
- It would be useful to conduct further investigation through lab and field study that is required to functionalize the proposed relationships for mean and turbulence flows in a rock-ramp type fishpass.

- Further study on the evaluation of the performance of different fish species with hydraulic investigation in situ can be conducted to identify appropriate criteria on assessment of fish free passage through rock-ramp type nature-like fishpasses.

Numerical Study:

- Future CFD study can be undertaken to investigate the turbulence characteristics in a rock-ramp type fishpass under different flow conditions and geometric variables.
- Future research is necessary to find the best turbulence model to quantify the complex flow pattern in a rock-ramp type fishpass to develop spatial hydraulic metrics that can be better linked to fish habitat.

However, the research conducted here in terms of exploratory lab measurements and CFD modeling to explore the detailed flow characteristics systematically in a rock-ramp nature like fishpass to retrofit small streams for habitat connectivity and compensation. To further advance the science of nature-like fish passage design, particularly for a rock-ramp fishpass, it is necessary to construct and field test the hydraulics and fish passage performance of the recommended designs outlined in this study. Additional research on the biological and hydraulic aspects of rock-ramp fishpass is needed to improve guidelines and inform future designs.

APPENDIX A

Boulder Stability under Hydrodynamic Forces

The size of a boulder in a rock-ramp type nature-like fishpass must be large enough to simultaneously resist movement as well as create the desired hydraulic conditions. Incipient motion can determine the likely flow required to move a boulder. Critical shear stress, Shields parameter, or stream power methods provide an empirical approach to sizing the boulders. Figure A.1 shows a principle sketch of a boulder located randomly on a bed inclined with the angle α, against horizontal. The forces acting on this boulder are:

- the force due to gravity *G*, acting in the vertical direction,
- the buoyancy *B*, acting perpendicular to the streamlines and the free surface,
- the hydrodynamic drag force F_D, acting parallel to the channel bed, and
- the hydrodynamic lift force F_L, acting perpendicular to the channel bed.

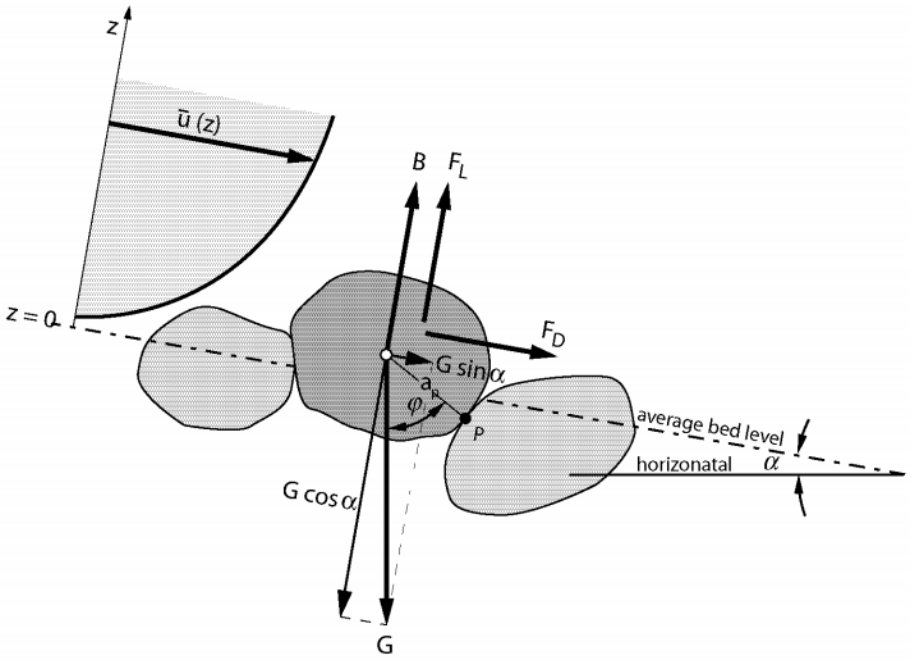

Figure A.1 Forces acting on a single boulder (adapted from Bezzola 2002)

A boulder will be entrained in the flow when the drag and lift forces acting on that boulder exceed the forces of resistance (F_R). Resistance is a function of the boulder mass, shape, and pre-transport position minus the buoyancy of the water covering a submerged boulder. This can be expressed by the following equation:

$$(F_D + F_L) > F_R\text{-}B \qquad \text{(a.1)}$$

Besides these forces, the incipient motion criteria developed on the bedding conditions of the boulder, which can be described by the pivoting angle φ. This angle is defined between the vertical and the connection line between the centroid of the boulder and the contact point *P*, of the downstream neighboring grain (Figure A.1).

In order to determine the general conditions for the incipient motion of the boulder, one has to distinguish between two different entrainment mechanisms: rolling and sliding. The question what mechanism dominates mainly depends on the particle shape and the bed configuration (Li and Komar 1986). Referring to the considerations of Bezzola (2002), the critical condition in case of rolling can be derived from the equilibrium of moments around the pivot point *P* as follows:

$$\Theta_c = \frac{2k_1 \cos\alpha(\tan(\varphi+\alpha) - \frac{s^*}{s^*-1}\tan\alpha)}{C^2 k_2 C_D(1 + k_4 \frac{D^*}{\alpha_P \cos(\varphi+\alpha)}) + k_3 C_L(\tan(\varphi+\alpha) + k_5 \frac{D^*}{\alpha_P \cos(\varphi+\alpha)})} \qquad \text{(a.2)}$$

Within this equation, Θ_c is the critical dimensionless shear stress, D^* denotes the diameter of a sphere with the same mass as the boulder under consideration, α_P denotes the distance between the pivot point *P* and the centre of gravity,

$s^* = \rho_s / \rho$ is the specific gravity, C is the Chézy-coefficient, that takes into account the near-bed flow conditions, and C_D and C_L are thr drag and lift coefficients respectively. Besides the geometry parameters defined in Figure 1.1, the factors k considered as:

- k_1: the influence of the grain shape, $V_s=k_1D^3$, with V_s denoting the boulder volume, and D is an imaginary boulder diameter (sphere diameter with the same mass as the considered boulder).
- k_2 and k_3: the ratio between the projected area of the boulder (A_P) against the direction of flow to the base area of the boulder, $A_P /(D^*)^2$,
- k_4 and k_5: the influence of the location where the hydrodynamic forces act on the boulder. If the hydrodynamic forces apply at the centroid these factors become zero. For more details see Bezzola (2002).

A.1 References

Bezzola, G. (2002). *"Fliesswiderstand und Sohlenstabilität natürlicher Gerinne."* Mitteilungen der Versuchsanstalt für Wasserbau, Hydrologie und Glaziologie (VAW). ETH Zürich. Nr. 173.

Li, Z. and Komar, P. D. (1986). *"*Laboratory measurements of pivoting angles for applications to selective entrainment of gravel in a current." *Sedimentology*, 33(3):413-423.